

Small molecule stabilisation of the glucocorticoid receptor and 14-3-3 protein-protein interaction

Citation for published version (APA):

Munier, C. C. (2020). *Small molecule stabilisation of the glucocorticoid receptor and 14-3-3 protein-protein interaction*. [Phd Thesis 1 (Research TU/e / Graduation TU/e), Biomedical Engineering]. Technische Universiteit Eindhoven.

Document status and date:

Published: 23/10/2020

Document Version:

Publisher's PDF, also known as Version of Record (includes final page, issue and volume numbers)

Please check the document version of this publication:

- A submitted manuscript is the version of the article upon submission and before peer-review. There can be important differences between the submitted version and the official published version of record. People interested in the research are advised to contact the author for the final version of the publication, or visit the DOI to the publisher's website.
- The final author version and the galley proof are versions of the publication after peer review.
- The final published version features the final layout of the paper including the volume, issue and page numbers.

[Link to publication](#)

General rights

Copyright and moral rights for the publications made accessible in the public portal are retained by the authors and/or other copyright owners and it is a condition of accessing publications that users recognise and abide by the legal requirements associated with these rights.

- Users may download and print one copy of any publication from the public portal for the purpose of private study or research.
- You may not further distribute the material or use it for any profit-making activity or commercial gain
- You may freely distribute the URL identifying the publication in the public portal.

If the publication is distributed under the terms of Article 25fa of the Dutch Copyright Act, indicated by the "Taverne" license above, please follow below link for the End User Agreement:

www.tue.nl/taverne

Take down policy

If you believe that this document breaches copyright please contact us at:

openaccess@tue.nl

providing details and we will investigate your claim.

Small Molecule Stabilisation of the Glucocorticoid Receptor and 14-3-3 Protein- Protein Interaction

PROEFSCHRIFT

ter verkrijging van de graad van doctor aan de Technische Universiteit
Eindhoven, op gezag van de rector magnificus prof.dr.ir. F.P.T. Baaijens,
voor een commissie aangewezen door het College voor Promoties, in het
openbaar te verdedigen op vrijdag 23 oktober 2020 om 13:30 uur

door

Claire Caroline Munier

geboren te Mont Saint Aignan, Frankrijk

Dit proefschrift is goedgekeurd door de promotoren en de samenstelling van de promotiecommissie is als volgt:

voorzitter:	prof.dr. M. Merx
1e promotor:	dr.rer.nat. C. Ottmann
2e promotor:	prof.dr.ir. L. Brunsveld
copromotor:	dr. M. Perry (AstraZeneca)
leden:	prof.dr.dr. P.Y.W. Dankers prof.dr. W.T. Zwart (The Netherlands Cancer Institute) prof.dr. O.C. Meijer (LUMC)
adviseur:	dr. K. Amrein (Roche)

Het onderzoek dat in dit proefschrift wordt beschreven is uitgevoerd in overeenstemming met de TU/e Gedragscode Wetenschapsbeoefening.

Munier, C.M. ©

Cover design: Xerox Sverige AB
Printing: Xerox Sverige AB

A catalogue record is available from the Eindhoven University of Technology Library

ISBN: 978-90-386-5151-4

This research has been financially supported by the Initial Training Network TASPPi, funded by the H2020 Marie Skłodowska-Curie Actions of the European Commission under Grant Agreement 675179.

Table of Contents

List of Abbreviations	i
Chapter 1	1
14-3-3 Modulation of the Inflammatory Response	1
Abstract.....	1
1.1. Introduction	2
1.2. Modulation by 14-3-3 binding of the inflammatory response at the genetic level....	4
1.2.1. 14-3-3 role within the NF- κ B signalling pathway	4
1.2.2. 14-3-3 role within the JAK-STAT signalling pathway.....	6
1.2.3. 14-3-3 role within PPAR signalling pathway	8
1.2.4. 14-3-3 role on GR transcriptional activity.....	10
1.3. Modulation by 14-3-3 binding at the molecular level	12
1.3.1. 14-3-3 modulation of pattern recognition receptors	12
1.3.2. 14-3-3-mediated modulation of other receptors involved in inflammation: the protease-activated receptors (PARs)	15
1.3.3. Direct modulation of the inflammatory cytokine level.....	16
1.4. Modulation by 14-3-3 binding at the cellular level.....	17
1.4.1. T lymphocytes.....	17
1.4.2. B lymphocytes.....	18
1.4.3. Other immune cells.....	19
1.5. 14-3-3 and its function in chronic inflammatory disorders	20
1.5.1. Autoimmune diseases.....	20
1.5.2. Respiratory diseases	21
1.6. Conclusion.....	22
1.7. Aim and outline of this thesis	23
1.8. References	26
Chapter 2	37
Phosphopeptide Investigation for the Characterisation of the Glucocorticoid Receptor–14-3-3 Protein-Protein Interaction.....	37
Abstract.....	37
2.1. Introduction	38
2.2. Results.....	39
2.2.1. 14-3-3 Binding to phosphopeptides, centred on putative 14-3-3 binding sites of GR	39
2.2.2. Interaction of 14-3-3 with a dimeric peptide: GR_pT524-pS617	42

2.2.3. Identification of GR_pT524-pS617 binding hotspots by mutation and alanine scan.....	43
2.2.4. Crystallization of GR_pT524-pS617, GR_pT524 and GR_pS617 with 14-3-3ζ....	45
2.2.5. GR_pT524-pS617 orientation in the crystal structure with 14-3-3ζ.....	48
2.3. Discussion	54
2.4. Conclusion.....	55
2.5. Acknowledgements	56
2.6. Materials and methods.....	56
2.7. References	70

Chapter 3 75

Activation of MINK1 Induces 14-3-3 Regulation of Glucocorticoid Receptor Through Protein-Protein Interaction.....75

Abstract.....	75
3.1. Introduction	76
3.2. Results.....	77
3.2.1. Posttranslational phosphorylation of GR LBD by chemical synthesis.....	78
3.2.2. Assessment of the GR LBD phosphorylation profile by kinase screening.....	80
3.2.3. MINK1 phosphorylates GR LBD driving the interaction with 14-3-3	92
3.2.4. Interaction between full-length GR and 14-3-3.....	94
3.3. Discussion	97
3.4. Conclusion.....	99
3.5. Acknowledgements	99
3.6. Materials and methods.....	99
3.7. References	107

Chapter 4 111

Identification of Small Molecule Stabilisers of the Glucocorticoid Receptor 14-3-3 Protein-Protein Interaction.....111

Abstract.....	111
4.1. Introduction	112
4.2. Results.....	113
4.2.1. Ligandability of the GR–14-3-3 PPI interface	113
4.2.2. Screening of 8K compounds to identify plausible stabilisers of GR–14-3-3 PPI	114
4.2.3. Confirmation of the identified hits	118
4.2.4. Assessment of the structure activity relationship of the identified hits.....	130
4.3. Discussion and conclusion	137
4.4. Acknowledgements	138
4.5. Materials and methods.....	138
4.6. References	144

Chapter 5	147
-----------------	-----

Early Exploration of the Structure Activity Relationship of Small Molecule Stabilisers of the Glucocorticoid Receptor 14-3-3 Protein-Protein Interaction147

Abstract.....	147
5.1. Introduction	148
5.2. Results.....	149
5.2.1. Destabilisation of the GR–14-3-3 PPI by Fusicoccin A	149
5.2.2. Mizoribine: a non-specific binder	152
5.2.3. Stabilisation of GR–14-3-3 PPI by pyrrolidone1.....	153
5.2.4. Contribution of the nitro benzyl and the salicylic acid moiety in the stabilisation of the GR–14-3-3 PPI.....	153
5.2.5. Increased stabilisation with para substitution of the benzo ketone	157
5.2.6. Co-crystallization of 7.10 with GR peptide and 14-3-3ζ.....	161
5.3. Discussion	162
5.4. Conclusion.....	164
5.5. Acknowledgements	164
5.6. Materials and methods.....	164
5.7. References	169

Chapter 6	171
-----------------	-----

Epilogue: Towards the Modulation of GR Activity Beyond Ligand Binding.....171

6.1. Introduction	172
6.2. Quantitative characterisation of the GR–14-3-3 PPI	172
6.3. Biological relevance of the GR–14-3-3 PPI.....	175
6.4. Insight into 14-3-3 regulation of GR though the use of small molecule stabilisers	178
6.5. Modulation of GR activity in drug discovery for the regulation of inflammation...	180
6.6. Conclusion.....	181
6.7. Acknowledgements	182
6.8. Materials and methods.....	182
6.9. References	184

Summary	187
----------------------	------------

List of publications.....	191
----------------------------------	------------

Curriculum Vitae.....	193
------------------------------	------------

Acknowledgement.....	194
-----------------------------	------------

List of Abbreviations

ACN	Acetonitrile
AID	Activation-induced cytidine deaminase
AMPK	AMP-activated protein kinase
AMPK	Adenosine 5 monophosphate-activated protein kinase
ASK1	Apoptosis signal-regulating kinase 1
CaIA	Calyculin A
CaMKK2	Calcium/calmodulin dependent protein kinase kinase 2
CDK	Cyclin-dependent kinase
CEBPB	CCAAT/enhancer-binding protein β
CFTR	Cystic fibrosis transmembrane conductance regulator
Co-IP	Co-immunoprecipitation
cPGI ₂	Carbaprostacyclin
CSR	Class-switch recombination
DAMP	Damage-associated molecular pattern
DBD	DNA binding domain
DHA	Dehydroalanine
DIG	Digoxigenin
DIPEA	N,N-Diisopropylethylamine
DMEM	Dulbecco's Modified Eagle Medium
DPBS	Dulbecco's Phosphate-Buffered Saline
EDT	1,2-Ethanedithiol
ER	Endoplasmic reticulum
ERR γ	Estrogen-related receptor γ
ER α	Estrogen receptor α
FBS	Fetal bovine serum
FC-A	Fusicoccin-A
FITC	Fluorescein isothiocyanate
FMF	Familial Mediterranean fever
FP	Fluorescence polarization
FSK	Forskolin
G6Pase	Glucose 6-phosphatase
GCK	Germinal center kinase
GCs	Glucocorticoids
GFP	Green fluorescent protein
GPIb-IX	Glycoprotein Ib-IX
GR	Glucocorticoid receptor
GSK	Glycogen synthase kinases
HATU	1-[bis(dimethylamino)methylene]-1H-1,2,3-triazolo[4,5-b]pyridinium 3-oxid hexafluorophosphate
HCC	Hepatocellular carcinoma
HDAC	Histone deacetylase
HIDS	Hyper-IgD syndrome
HR	Hinge region
HTS	High-throughput screening
ID	Intrinsically disordered
IgH	Immunoglobulin H

List of Abbreviations

IKK	I κ B kinase
IL-1 β	Interleukin-1 β
IL-6	Interleukin-6
IMiD	Immunomodulatory imide drug
IPA	Isopropanol
IRAK4	Interleukin-1 receptor-associated kinase 4
iRhom	Inactive Rhomboid proteases
ITC	Isothermal titration calorimetry
JAK-STAT	Janus kinase-signal transducer and activator of transcription protein
JNK	c-Jun N-terminal kinase
LBD	Ligand binding domain
LPS	Lipopolysaccharide
MAPK	Mitogen-activated kinase
MDA5	Melanoma differentiation association gene 5
MDS	Myelodysplastic syndrome
MEKK3	Mitogen-activated protein kinase kinase kinase 3
MINK1	Misshapen-like kinase 1
MMP-1	Matrix metalloproteinase-1
MyD88	Myeloid differentiation factor 88
NF- κ B	Nuclear factor kappa-light-chain-enhancer of activated B cells
NMP	N-Methyl-2-pyrrolidone
NN	Near neighbours
NS3	Non-structural protein 3
NTD	N-Terminal domain
p53	Tumour protein 53
PAAND	Pyrin-associated autoinflammation with neutrophilic dermatosis
PAMP	Pathogen-associated molecular pattern
PAR	Protease-activated receptors
PDA	Photodiode array
PDB	Protein Data Bank
PEI	Polyethylenimine
PEPCK	Phosphoenolpyruvate carboxykinase
PKA	Protein kinase A
PKB	Protein kinase B
PMA2	Plasma membrane ATPase 2
PPAR	Peroxisome proliferator-activated receptor
PPI	Protein-protein interaction
PPM1B	Protein phosphatase 1B
PRGC1	Peroxisome proliferator-activated receptor gamma coactivator 1
PRR	Pattern recognition receptor
PS	Penicillin-Streptomycin
PTM	Posttranslational modification
PVDF	Polyvinylidene difluoride
PXR	Pregnane X receptor
RIG-I	Retinoic-acid inducible gene I
RIPA	Radioimmunoprecipitation assay
RIPOR2	Rho family-interacting cell polarization regulator 2
RLR	Retinoic acid-inducible gene-I-like receptor
ROCK1	Rho-associated protein kinase1
RP	Reversed-phase

RT-PCR	Real-time reverse transcription polymerase chain reaction
RXR	Retinoid X receptor
SAR	Structure activity relationship
SEDIGRAMs	Selective dimer GR agonists and modulators
SEGRAMs	Selective glucocorticoid receptor agonists and modulators
SEMOGRAMs	Selective monomer GR agonists and modulators
Sly1	SH3-domain protein expressed in Lymphocytes 1
SPPS	Solid phase peptide synthesis
SPR	Surface plasmon resonance
SUMO-1	Small ubiquitin-related modifier-1
T-bet	T-box-containing protein expressed in T cells
TACE	Tumour necrosis factor alpha converting enzyme
TAK1	Transforming growth factor beta-activated kinase 1
TEA	Triethylamine
TFA	Trifluoroacetic acid
TGF- β 1	Transforming growth factor- β 1
THP	Tris(hydroxypropyl)phosphine
TIS	Triisopropylsilane
TLR	Toll-like receptor
TNF- α	Tumour necrosis factor- α
TRIF	Toll/IL-1 resistance-domain-containing adapter-inducing interferon- β
TRIM25	Tripartite motif-containing 25
TTP	Tristetraprolin
VCD	Vibrational circular dichroism
wt	Wild type

Chapter 1

14-3-3 Modulation of the Inflammatory Response

Abstract

Regulation of inflammation is a central part of the maintenance of homeostasis by the immune system. One important class of regulatory protein that has been shown to have effects on the inflammatory process are the 14-3-3 proteins. Herein are described the roles, that have been identified for 14-3-3 in regulation of the inflammatory response. These roles encompass regulation of the response that affect inflammation at the genetic, molecular and cellular levels. At a genetic level 14-3-3 is involved in the regulation of multiple transcription factors and affects the transcription of key effectors of the immune response. At a molecular level many of the constituent parts of the inflammatory process, such as pattern recognition receptors, protease activated receptors and cytokines are regulated through phosphorylation and recognition by 14-3-3 whilst disruption of the recognition processes has been observed to result in clinical syndromes. 14-3-3 is also involved in the regulation of cell proliferation and differentiation, this has been shown to affect the immune system, particularly T- and B-cells. Finally, abnormal levels of 14-3-3 are discussed and how they contribute to undesirable immune responses and chronic inflammatory conditions.

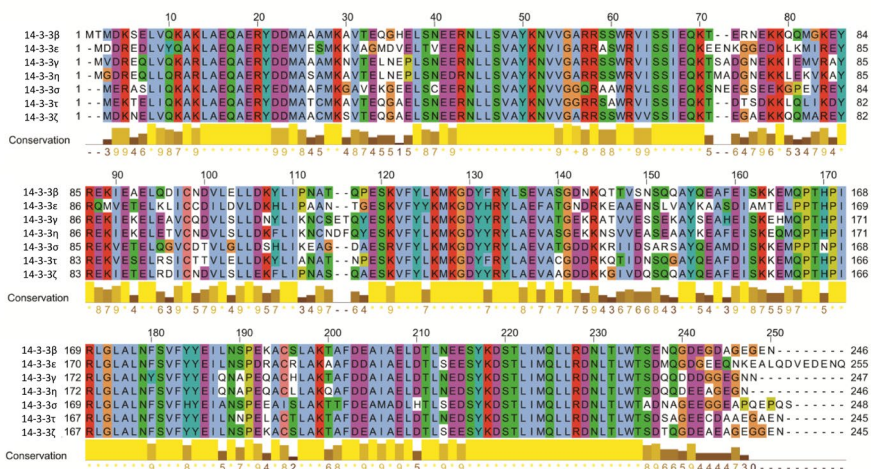
1.1. Introduction

Inflammation is a multicomponent biological response to adverse stimuli and conditions. Controlled intermittent inflammation is a protective response from the host, fundamental for defence against infection, for tissue repair, tissue remodelling and restoration of homeostasis. The complexity of the inflammatory response necessitates a tissue, cell, signal and gene specific regulation at multiple levels. The innate immune response comes into play immediately as a first line of defence and includes the recognition by immune cell receptors of specific molecular motifs carried by viruses and microbes, the secretion of inflammatory mediators, such as cytokines, and the migration of monocytes and granulocytes to the affected site. If the innate immune response is insufficient, dendritic cells within the innate immune system become activated upon recognition of pathogenic material, migrate to lymph nodes and present fragments of peptides from the pathogenic agents on their surface that, in turn, activate naïve T- and B-lymphocytes. Regulation of the inflammatory response is also achieved *via* activation of signalling pathways and alteration of gene expression¹. The beneficial role of the inflammatory response can, however, turn into chronic inflammatory disorders in case of dysregulation of these complex mechanisms². Recently, chronic inflammatory disorders have been recognised as the most significant cause of death in the world and more than 50% of all deaths have been attributed to inflammation-related diseases³. Considerable progress has been made in understanding the mechanisms underpinning the inflammatory response¹. Progress has, however, revealed the great complexity of the processes and further work is required to fully unravel the causes and the mechanisms associated with chronic inflammation for efficient disease prevention, early diagnosis and the treatment of inflammation-related conditions.

14-3-3 was discovered in 1967 by Moore and Perez in bovine brain tissue. 14-3-3s form a family of regulatory proteins and consist, in mammals, of seven isoforms β , ϵ , γ , η , σ , τ and ζ , which are highly conserved across species⁴. A high sequence similarity between the 14-3-3 isoforms was observed, notably in the amphipathic binding groove, whereas the outer surface bears more variations (Fig. 1.1)⁵. Overlaps between their functions have been identified, and at first, the 14-3-3 isoforms were thought to be redundant. Further studies, however, revealed specific roles and some differential tissue expression levels^{6,7}. 14-3-3 proteins act as dimers (principally heterodimers) and recognize phosphorylated serine/threonine residues, thus forming part of a regulatory system with kinases and phosphatases⁸. Tremendous efforts have been made to identify 14-3-3 partners and the roles of the 14-3-3 protein-protein interactions. Indeed, more than 200 structurally and functionally diverse 14-3-3 protein clients have been identified⁹ and 14-3-3 proteins were found to be involved in regulating a wide range of cellular processes, such as cell cycle progression, apoptosis, intracellular

protein trafficking and signal transduction. Accumulated evidence has started to delineate the role of 14-3-3 in the inflammatory response^{10–19} and recent studies have indicated a link between alteration of 14-3-3 protein levels and chronic inflammatory disorders^{20–24}. Together these results suggest 14-3-3 as a potential target for future therapeutic intervention, representing an, as yet unrealized, opportunity in the field of inflammation. In this review, the 14-3-3 mediated modulation of the inflammatory response will be discussed at a genetic, molecular and cellular level, before focussing on the role of 14-3-3 in chronic inflammation, including autoimmune and respiratory diseases. The 14-3-3 isoforms will be clearly reported in this chapter whenever identified in the cited studies, otherwise the generic 14-3-3 term will be used. Ultimately, the question is: does 14-3-3 provide an interaction node to therapeutically intervene with inflammatory disorders?

A



B

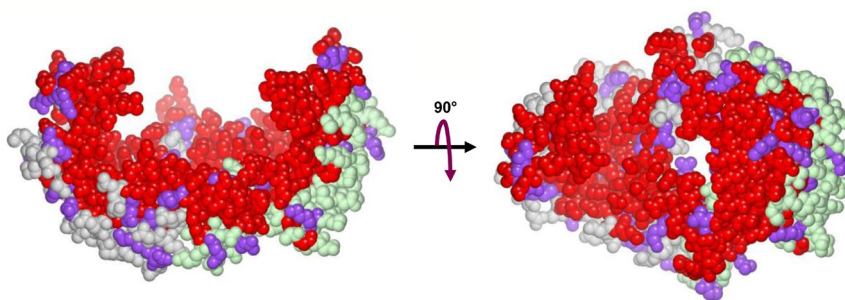


Figure 1.1. Homology between 14-3-3 isoforms. (A) Homology data from Clustal showing the very high degree of homology across all seven human isoforms. The residues are coloured following the Clustal X colouring. **(B)** and **(C)**

Two views of the bovine 14-3-3ζ dimer (PDB:1A4O) coloured by homology with residues with total identity across all isoforms in red and residues with very high homology coloured in purple. Other residues are coloured pale grey for monomer A and pale green for monomer B. Note how the homology is highest on the inner faces of the 14-3-3 dimer around the binding clefts.

1.2. Modulation by 14-3-3 binding of the inflammatory response at the genetic level

One group of proteins regulated through phosphorylation and 14-3-3 recognition are transcription factors involved in the inflammatory response, such as the nuclear factor kappa-light-chain-enhancer of activated B cells (NF-κB), the Janus kinase-signal transducer and activator of transcription protein (JAK-STAT), the peroxisome proliferator-activated receptor (PPAR) and the glucocorticoid receptor (GR).

1.2.1. 14-3-3 role within the NF-κB signalling pathway

NF-κB proteins form a family of heterodimeric inducible transcription factors which play a crucial role in various physiological and pathological processes, mainly immune response and inflammation. These proteins and their roles have been studied extensively. Activation of NF-κB notably results in the expression of inflammatory mediators such as cytokines, chemokines, and adhesion molecules²⁵. One of the major signalling pathways mediating NF-κB activation is the canonical pathway. Here, the activated, serine-specific IκB kinase (IKK) complex, consisting of two kinase subunits, IKKα and IKKβ and a regulatory subunit IKKγ, phosphorylates the inhibitor of nuclear factor kappa B α (IκBα) proteins. Phosphorylated IκBα proteins are subsequently ubiquitinated and degraded by the 26S proteasome releasing the NF-κB complex which then translocates to the nucleus²⁶. Once in the nucleus, NF-κB forms complexes with coactivators and corepressors resulting in the transcription of a plethora of target genes²⁵.

The participation of 14-3-3 proteins in the regulation of NF-κB signalling pathway has been reported by multiple studies (Fig. 1.2). For example, a role of 14-3-3γ in preventing lipopolysaccharide (LPS)-induced inflammatory responses was identified in bovine mammary epithelial cells. Overexpression of 14-3-3γ in LPS-induced cells correlated with decreased levels of the mRNA expression of pro-inflammatory cytokines, such as tumour necrosis factor-α (TNF-α), interleukin-6 (IL-6), and interleukin-1β (IL-1β)¹¹. This 14-3-3 mediated inhibition of the inflammatory response was shown to occur through the NF-κB pathway since 14-3-3γ decreased the level of phosphorylated IκB and NF-κB translocation to the nucleus¹¹. *In vivo* dual-tagging quantitative proteomic analysis, validated by coimmunoprecipitation and colocalization experiments, profiled the interacting partners of 14-3-3ε following TNFα stimulation of 293T cells. 14-3-3ε was shown to interact with key elements of the NF-κB signalling pathway: the transforming growth factor beta-activated kinase 1 (TAK1) and

its interacting protein, protein phosphatase 1B (PPM1B)¹⁰. TAK1 and PPM1B are part of the mitogen-activated protein kinase signalling module localized immediately upstream of NF- κ B and activate or repress NF- κ B, respectively²⁷⁻²⁹. Interactions between 14-3-3 ϵ with each of TAK1 and PPM1B have been shown to be dynamic and to modulate the transcriptional activity of NF- κ B¹⁰. At initial cellular stress, using TNF- α stimulation, 14-3-3 was found to bind both TAK1 and PPM1B and high-levels of NF- κ B activity were observed. Hence, 14-3-3 was suggested to disrupt the TAK1/PPM1B interaction, activating TAK1 and thus the NF- κ B pathway. Prolonged cellular stress, however, showed dissociation of 14-3-3 from TAK1 and PPM1B, respectively, together with lower NF- κ B activity. This dissociation of 14-3-3 was postulated to promote the inhibitory dephosphorylation of TAK1^{6,30}. Further analysis will be necessary to get to a deeper understanding of the mechanism at a molecular level. IKK functions as a central node at the interface of the pro-survival NF- κ B signalling pathway and the cellular stress response and apoptosis pathway by promoting the interaction between the apoptosis signal-regulating kinase 1 (ASK1) and 14-3-3. IKK interacts with ASK1 and, together with protein kinase B (PKB, also named AKT), leads to phosphorylation of ASK1. Upon phosphorylation, ASK1 interacts with 14-3-3 and the ASK1-14-3-3 protein-protein interaction (PPI) was found to be correlated with a decrease of ASK1 activity, modulating the downstream ASK1/JNK axis^{6,31}.

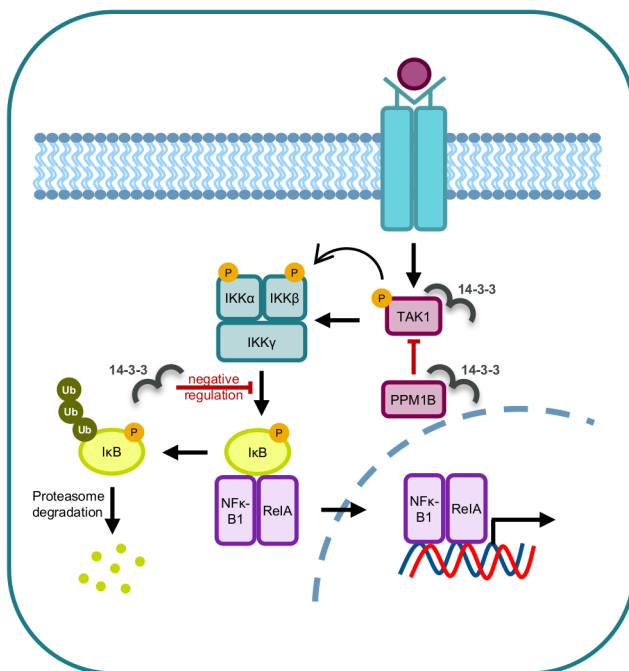


Figure 1.2. Modulation by 14-3-3 of the NF- κ B canonical pathway. 14-3-3 was found to interact with TAK1 and PPM1B modulating NF- κ B transcriptional activity and to impair I κ B phosphorylation and NF- κ B translocation to the nucleus. Note that the regulatory role of 14-3-3 is stated whenever it has been clearly reported.

1.2.2. 14-3-3 role within the JAK-STAT signalling pathway

The JAK-STAT signalling pathway plays a major part in mediating the immune response. It was originally discovered during investigation of the anti-viral activity of interferons³² and has been extensively studied in recent years. Upon activation of the cytokine membrane receptors of the JAK-STAT pathway, JAK kinases phosphorylate STAT tyrosines which triggers STAT dimerization, resulting in STAT translocation to the nucleus where they bind specific DNA elements to modulate the transcription of their target genes^{33–35}.

14-3-3 has been found to exercise both positive and negative effects on the JAK-STAT signalling pathway, depending on interactions with different members. A negative effect of 14-3-3 on the JAK-STAT pathway was identified upon 14-3-3 binding to JAK kinases whereas a positive effect was reported upon 14-3-3 binding to STAT (Fig. 1.3). 14-3-3 binding of JAK1 has been hypothesized to downregulate JAK-STAT signalling and to inhibit STAT mediated transcription. JAK1 25-mer peptides phosphorylated at Ser515 or Ser518 interacted with 14-3-3. Simultaneous phosphorylation at these two residues, however, impaired the binding to 14-3-3, most probably due to steric hindrance and/or

electrostatic repulsion between the peptide and 14-3-3. The 14-3-3–JAK1 PPI was further investigated in cells, confirming the role of phosphorylated Ser515 or Ser518, within the JAK1 SH2 like domain, in the 14-3-3 binding, mediated by adenosine 5 monophosphate-activated protein kinase (AMPK)^{36,37}. AMPK activation in cells also suggested that JAK1 phosphorylation and subsequent binding to 14-3-3 inhibits STAT1 and STAT3 tyrosine phosphorylation and subsequent activation in vascular endothelial cells and fibroblasts³⁷.

Further evidence indicates another layer of STAT regulation through posttranslational modifications that influence STAT activity, such as phosphorylation of Ser727. This phosphorylation has been shown to up-regulate STAT3 activity^{12,35,38}. A systematic proteomic analysis (QUICK³⁹) identified 14-3-3 ζ as a protein partner of STAT3. Using several biochemical approaches, the physical interaction of 14-3-3 ζ with STAT3 was further confirmed in multiple myeloma cells¹², glioblastoma cells⁴⁰ and lung cancer cells⁴¹. The role of Ser727 in the C terminus of STAT3 appeared to be vital for 14-3-3 ζ interaction since S727A mutation abrogated the 14-3-3 ζ –STAT3 PPI¹². Binding by 14-3-3 ζ stabilises phospho Ser727 of STAT3 by preventing dephosphorylation by phosphatases¹² whilst specific 14-3-3 ζ knockdown reduced pSer727 STAT3 levels⁴⁰. In lung cancer cells, 14-3-3 ζ overexpression increased the levels of phosphorylated STAT3 at Ser727 but also at Tyr705, the residue through which STAT3 dimerization occurs; 14-3-3 ζ knockdown displayed the reverse effect⁴¹. Evidence suggests that 14-3-3 binding to STAT proteins maximizes STAT transcription. Indeed, upon binding to 14-3-3 ζ , STAT3 translocation to the nucleus is enhanced, as is binding to DNA and subsequent transcriptional activity¹². Macrophages in which 14-3-3 ζ has been knocked down by siRNA have significantly reduced levels of phosphorylation of STAT3 following LPS stimulation; this translates further into a reduced immune response. Conversely, overexpression of 14-3-3 ζ in the absence of any stimulus enhanced STAT3 phosphorylation and activation⁴². The up-regulatory effect of 14-3-3 on the JAK-STAT signalling pathway by binding to STAT3 exemplifies the chaperone role of 14-3-3. For example, in glioblastoma cells, 14-3-3 ζ interaction with STAT3 increases STAT3 solubility, preventing STAT3 from aggregation, as observed by confocal immunofluorescence images analysis. This data was able to explain the subsequent STAT3 activation⁴⁰.

The downregulation of 14-3-3–STAT3 signalling has also been demonstrated to play a role in tumour progression⁴⁰. By binding to phosphorylated STAT3, 14-3-3 ζ drives the transcription of HIF-1 α , a crucial component in the regulation of angiogenesis in cancer¹³. In brief, 14-3-3 ζ enhanced STAT3 transcriptional activity resulting in HIF1 α expression⁴¹. A study reported that the activation of angiogenesis by HIF1 α could be counteracted by miR-206, a short non-coding RNA that acts as a

tumour suppressor in lung cancer. Mechanistically, MiR-206 binds the 3'-UTR of 14-3-3 ζ mRNA, decreasing the endogenous expression of 14-3-3 ζ , and inhibiting the cascade STAT3/HIF1 α ⁴¹.

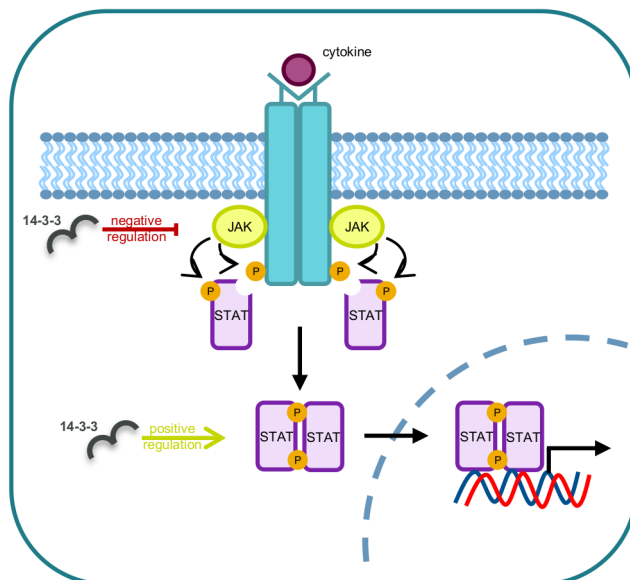


Figure 1.3. Modulation by 14-3-3 of the JAK/STAT signalling pathway 14-3-3 was found to interact with JAK, impairing STAT tyrosine phosphorylation and with STAT, enhancing STAT translocation.. Note that the regulatory role of 14-3-3 is stated whenever it has been clearly reported.

1.2.3. 14-3-3 role within PPAR signalling pathway

PPARs form a family of three nuclear receptors, PPAR α , PPAR β or δ , and PPAR γ , which act as ligand dependent transcription factors having an anti-inflammatory role. In the absence of stimulation, the complex of PPAR and retinoid X receptor (RXR) is bound to co-repressive factors and histone deacetylases. Binding of endogenous or synthetic ligands to PPAR leads to a conformational change that activates PPAR/RXR and subsequent binding to specific DNA response elements for the regulation of PPAR target gene transcription^{43,44}.

All PPAR isoforms modulate 14-3-3 expression (Fig. 1.4). Ligand interaction with PPAR δ results in binding to the promoter of 14-3-3 ϵ and upregulation of 14-3-3 ϵ protein expression. Similarly, 14-3-3 ϵ protein levels can be reduced *via* inhibition of PPAR δ -mediated 14-3-3 ϵ transcription by using PPAR δ siRNA, by treatment of endothelial cells with nonsteroidal anti-inflammatory drugs, such as sulindac sulfide, or by deletion of 14-3-3 ϵ PPAR promoter regions^{45–48}. PPAR binding to the 14-3-3 ϵ gene and subsequent 14-3-3 expression triggered anti-apoptotic effects in human endothelial cells^{45–}

⁴⁷, colon cancer cells⁴⁹ and vascular smooth muscle cells⁴⁸. Various drugs target the PPAR/14-3-3 ϵ promoter interaction, such as nonsteroidal anti-inflammatory drugs or, for example, the PPAR γ agonist rosiglitazone¹⁴. PPAR γ agonists mediate the PPAR γ binding to 14-3-3 ϵ promoter and 14-3-3 ϵ expression⁴⁹. Indeed, *in silico* analysis of transcription factors involved in adipogenesis identified two PPAR γ binding sequences in the 14-3-3 γ promoter region as well as one in 14-3-3 β and one in 14-3-3 ϵ . None were found for the 14-3-3 isoforms η , θ , ζ and σ ⁵⁰. Anti-apoptotic effects of PPAR α have been hypothesized to occur using the same mechanism as for the other two isoforms PPAR δ and PPAR γ , through the interaction between ligand activated PPAR α and 14-3-3 ϵ promoter and further expression of 14-3-3¹⁴. Surprisingly, treatment of vascular smooth muscle cells with PPAR α agonists upregulated mainly 14-3-3 β and only to a much smaller extent 14-3-3 ϵ ⁴⁸.

14-3-3 proteins were also reported to modulate PPAR activity (Fig. 1.4). Research on the regulation of lactation in dairy cow mammary epithelial cells identified a 14-3-3 γ mediated anti-inflammatory effect through 14-3-3 modulation of the PPAR γ expression, suggesting a downregulation of inflammatory mediators *via* the modulation of PPAR expression beyond the inactivation of NF- κ B¹¹. Through the use of a functional genomics approach, 14-3-3 ϵ was found to interact with PPAR β and γ ²⁴. Another study reported competitive and direct interactions of 14-3-3 β and γ with PPAR γ depending on PPAR γ Ser273 phosphorylation. 14-3-3 β and γ showed antagonistic regulatory roles on PPAR γ transcriptional activity⁵¹.

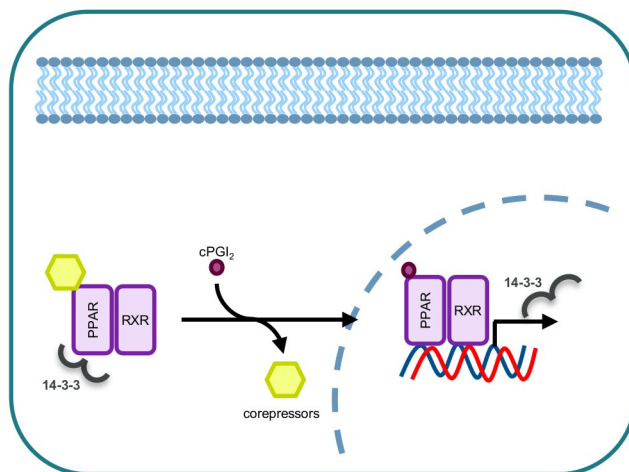


Figure 1.4. Modulation by 14-3-3 of the PPAR signalling pathway. 14-3-3 was found to be upregulated by PPAR and to bind PPAR to modulate PPAR activity. Note that the regulatory role of 14-3-3 is stated whenever it has been clearly reported.

1.2.4. 14-3-3 role on GR transcriptional activity

GR is a ligand-dependent transcription factor which belongs to the superfamily of nuclear hormone receptors, a highly conserved protein family. GR plays a major role in controlling inflammation and immune responses, and its activity is mediated by glucocorticoids, steroid hormones produced by the cortex of the adrenal gland. In the resting state GR is found in an immunophilin/heat shock protein inhibitory complex. Upon binding of glucocorticoids to GR, the GR is released from the inhibitory complex and translocates to the nucleus, where it binds specific DNA sequences to modulate the transcriptional activity of its target genes⁵².

The first evidence for binding between 14-3-3 and GR emerged when a yeast two-hybrid system isolated complementary DNA encoding proteins that interact with the human ligand binding domain (LBD) of GR⁵³. 14-3-3 was further identified as a GR binding protein by immunoaffinity chromatographic purification of rat liver cytosol⁵⁴. The 14-3-3 isoforms η and σ were found to interact with GR LBD^{53,55} while the GR β isoform, which shares the same N-terminal and DNA binding domain but contains a different LBD, did not^{15,55}. 14-3-3 was also reported to interact with phosphorylated GR Ser134 which matches the mode 1 binding motif, RSX-pS/T-XP where X is any amino acid (cysteine excluded) and pS/T is a phosphorylated serine or threonine⁵⁶. Some groups focused on 14-3-3 ζ and showed that GR Ser134 phosphorylation, in a p38 mitogen-activated kinase (MAPK)-dependent manner, was crucial for the interaction⁵⁶. Other groups were interested in 14-3-3 σ and utilized AKT1 to phosphorylate GR Ser134 triggering the interaction with this 14-3-3 isoform¹⁵. Interestingly, 14-3-3 σ could be shown to bind to two different regions of GR: GR Ser134 but also GR LBD¹⁵.

Research work from various groups suggests that 14-3-3 has differential regulatory activities on the biological role of GR depending on the 14-3-3 isoform (Fig. 1.5). 14-3-3 β , γ , ϵ , ζ , η , and θ have been shown to upregulate GR transcriptional activity to different extents^{53,57}. For example, 14-3-3 β and γ are suspected to play a role in hepatic gluconeogenesis since both enhanced the expression of phosphoenolpyruvate carboxykinase (PEPCK) and glucose 6-phosphatase (G6Pase) by binding DNA in the PEPCK promoter⁵⁷. Phosphorylation of Ser134 leads to the regulation of different sets of genes, notably genes associated with endocrine disorders, metabolic diseases and the inflammatory response, such as the histone deacetylase 1 (HDAC1), the tumour protein 53 (p53), and CCAAT/enhancer-binding protein beta (CEBPB), suggesting a function in pathological inflammatory disorders⁵⁶. Conversely, 14-3-3 σ proteins repress GR transcriptional activity, by enhancing GR localisation to the cytoplasm thanks to the 14-3-3 σ nuclear export sequence⁵⁵. Other evidence suggested dual effects of 14-3-3 σ , mediated by AKT1, on the GR activity and a role of the GR-14-3-3 PPI in some cancers¹⁵.

GR biological activity is not only controlled by hormone binding and post-translational modifications but also through interactions with cofactors, highlighting the extensive crosstalk which occurs between GR and other signalling pathways. GR was found to bind various cofactors. As a scaffolding protein, it could be envisioned that 14-3-3 takes part in the formation or the regulation of these coactivator complexes. For example, C-Raf co-precipitated with 14-3-3⁵⁴ while a 14-3-3 σ E182K mutant abolished the interaction with C-Raf by changing the phosphopeptide-binding pocket⁵⁵. Phosphorylation of the GR corepressor RIP140 leads to interaction with 14-3-3, which drives RIP140 relocalisation from the nucleus to the cytoplasm⁵⁸. It has been proposed that there is a synergistic enhancement of GR transcriptional activation by 14-3-3 η through repression of the function of the corepressor RIP140 and through increasing the nuclear level of GR proteins⁵⁹. Annexin-A1 has been shown to have a role in mediating glucocorticoid signalling by negatively affecting the up-regulation of GR induced by 14-3-3 η ⁶⁰.

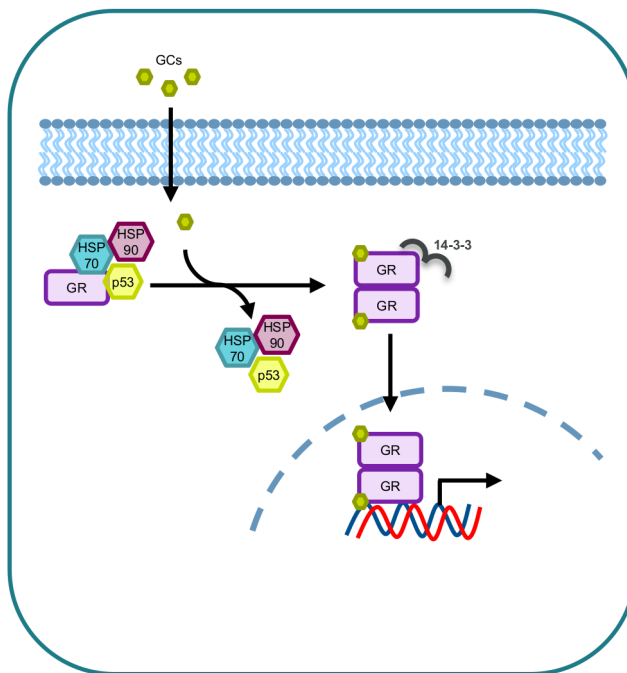


Figure 1.5. Modulation by 14-3-3 of the GR signalling pathway. 14-3-3 was found to interact with GR and to modulate GR translocation and transcriptional activity. Note that the regulatory role of 14-3-3 is stated whenever it has been clearly reported.

1.3. Modulation by 14-3-3 binding at the molecular level

Many of the constituent parts of the innate immune response are regulated through phosphorylation and 14-3-3 recognition and notably the receptors involved in inflammation which alter signal transduction.

1.3.1. 14-3-3 modulation of pattern recognition receptors

Pattern recognition receptors (PRRs) constitute the first line of defence against pathogen infection by recognising specific molecular motifs carried by viruses and microbes, known as pathogen-associated molecular patterns (PAMPs), and host derived molecules from damaged cells, called damage-associated molecular patterns (DAMPs). Upon ligand recognition, PRRs trigger an immune and inflammatory response from the host organism by upregulating the transcription of specific genes. PRRs are grouped in families, such as Toll-like receptors (TLRs) that are transmembrane proteins recognising extracellular or endosomal PAMPs and DAMPs, retinoic acid-inducible gene-I-like receptors (RLRs) localised in the cytoplasm where they control viral infection and pyrin that forms an inflammasome in response to bacterial toxins^{61,62}.

TLRs are transmembrane proteins, upon recognition of extracellular or endosomal PAMPs and DAMPs, myeloid differentiation factor 88 (MyD88) and/or Toll/IL-1 resistance-domain-containing adapter-inducing interferon- β (TRIF) are recruited, activating the MyD88 signalling pathway and/or the MyD88 independent pathway respectively⁶³. The role of 14-3-3 in the signalling of different TLRs, has been proposed to be ambivalent, contributing to the distinct outcome of NF- κ B activation (Fig. 1.6)¹⁶. Upon stimulation of TLR2, 14-3-3 θ was found as a part of the TLR2 signal transduction pathway and 14-3-3 ϵ as a part of the signalling complex involving MyD88¹⁶. Overexpression of 14-3-3 θ downregulated TLR2-induced NF- κ B activation in cells treated with TLR2 ligands. Conversely, LPS stimulation of cells overexpressing 14-3-3 θ led to upregulation of TLR4-mediated NF- κ B activation, probably due to the TLR4 alternative pathway *via* the adapter TRIF¹⁶. 14-3-3 θ has been coprecipitated with other members of the TLR signalling pathway, such as interleukin-1 receptor-associated kinase 4 (IRAK4)¹⁶, TAK1¹⁰ and mitogen-activated protein kinase kinase kinase 3 (MEKK3)⁶⁴. Indeed, phosphorylation of MEKK3 Thr294 upon LPS and TNF α stimulation has been shown to lead to interaction with 14-3-3, resulting in its downregulation and inhibition of NF- κ B activation⁶⁴.

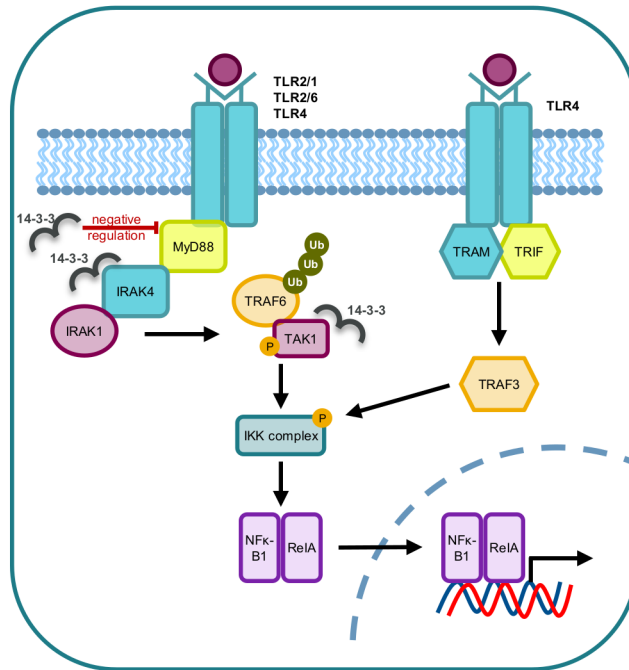


Figure 1.6. TLR mediated signal transduction and its modulation by 14-3-3. 14-3-3 was found to bind MyD88, IRAK4 and TAK1 and to negatively regulate the MyD88 signalling pathway. Note that the regulatory role of 14-3-3 is stated whenever it has been clearly reported.

RLRs are localised in the cytoplasm where they control viral infection. Dysregulation of the RLR-induced signalling cascade can lead to autoimmune diseases, such as type 1 diabetes, systemic lupus erythematosus, psoriasis, and colitis⁶⁵. 14-3-3 proteins were shown to interact with two members of the RLR family following immunostimulation: retinoic-acid inducible gene I (RIG-I) and melanoma differentiation association gene 5 (MDA5), as well as the tripartite motif-containing 25 (TRIM25), an E3 ubiquitin ligase that ubiquitinates RIG-I (Fig. 1.7)^{66–69}. 14-3-3 ϵ was found to be part of the large multimeric protein complex that is formed in response to acute virus infection and includes 14-3-3 ϵ , RIG-I and TRIM25. RIG-I translocation from the cytosol to the mitochondrial membrane was impaired in 14-3-3 ϵ -knockdown cells, suggesting a role of 14-3-3 ϵ in the redistribution of the complex to the mitochondrial membrane and a role in immune response upon RNA virus infection⁶⁷. Similarly, disruption of the RIG-I–14-3-3 ϵ interaction, by non-structural protein 3 (NS3) of dengue virus, abolished RIG-I redistribution and inhibited the innate immune response⁷⁰. 14-3-3 γ , 14-3-3 η and 14-3-3 θ have been shown to interact with MDA5 following immunostimulatory treatment, but only 14-3-3 η could upregulate type I interferon production *via* MDA5⁶⁶. Dephosphorylation of MDA5 at Ser88

activates it and leads to interaction with 14-3-3 η , promoting MDA5 aggregation and redistribution to the mitochondrion-associated membrane^{66,71}.

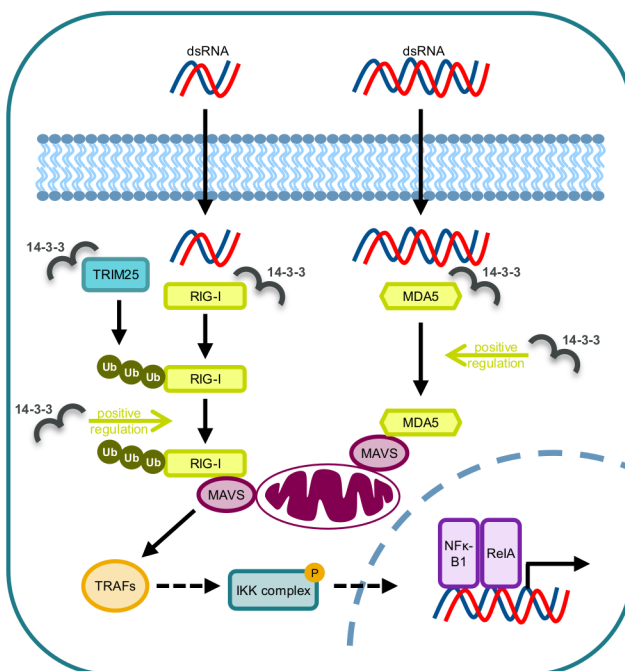


Figure 1.7. RLR mediated signal transduction and its modulation by 14-3-3. 14-3-3 was found to bind RIG-I, TRIM25 and MDA5 and to enhance RIG-I and MDA5 redistribution to the mitochondrial membrane. Note that the regulatory role of 14-3-3 is stated whenever it has been clearly reported.

Pyrin, mainly present in immune cells such as neutrophils, monocytes and dendritic cells, belongs to the group of PRRs, with a major role in the inflammation response⁷². Pyrin proteins do not directly recognize PAMPs or DAMPs but are sensitive to the infection-mediated loss of cellular homeostasis known as homeostasis-altering molecular processes^{20,73}. 14-3-3 ϵ and 14-3-3 τ have been shown to interact with pyrin with an important role of pyrin phosphorylated at Ser208, Ser209 or Ser242 (Fig. 1.8)¹⁷. The disruption of the 14-3-3–pyrin PPI, for example by alanine mutation of Ser208 and Ser242, activated the formation of the inflammasome^{20,74,75}. Dysregulations of pyrin have been identified in certain autoinflammatory diseases such as familial Mediterranean fever (FMF), pyrin-associated autoinflammation with neutrophilic dermatosis (PAAND) and hyper-IgD syndrome (HIDS). FMF and PAAND are driven by mutations of the pyrin encoding *MEFV* gene and the subsequent mutation in pyrin sequence. HIDS is driven by mutations of the *MVK* gene, decreasing pyrin

phosphorylation⁷⁵⁻⁷⁷. These pyrin mutations or the lack of pyrin phosphorylation prevent pyrin from interacting with its inhibitory partner 14-3-3 and activate the formation of the pyrin inflammasome⁷⁵⁻⁷⁷.

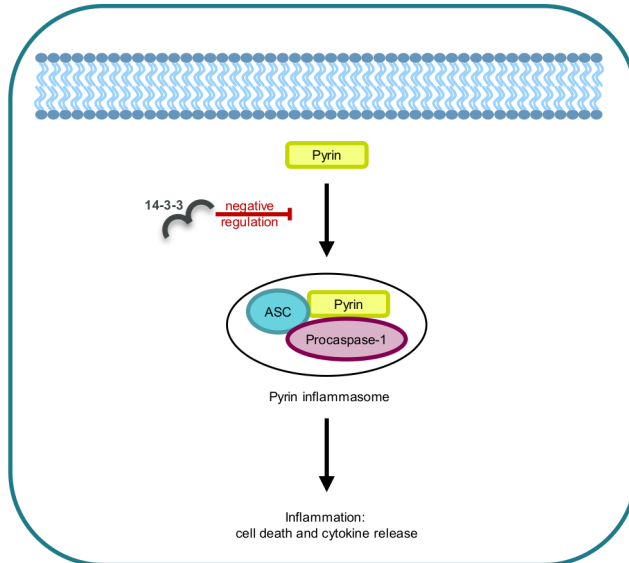


Figure 1.8. Pyrin mediated signal transduction and its modulation by 14-3-3. 14-3-3 was found to bind pyrin and to impair the formation of the pyrin inflammasome. Note that the regulatory role of 14-3-3 is stated whenever it has been clearly reported.

1.3.2. 14-3-3-mediated modulation of other receptors involved in inflammation: the protease-activated receptors (PARs)

PARs are GPCRs that play a role in various conditions such as inflammation in the cardiovascular, respiratory and digestive system⁷⁸, in rheumatic disease⁷⁸ and multiple cancers⁷⁹. PARs share a unique feature by being irreversibly activated. To maintain a response under PAR agonist stimulation, limited by internalisation and proteolytic desensitisation, new receptors need to translocate to the cell membrane to be activated in turn. PAR4 has been found to be retained in the endoplasmic reticulum (ER) bound to the coat protein complexes (β -COP1). The PAR4 sequence contains an ER retention motif which is recognized and masked upon binding to 14-3-3, acting as a chaperone protein. To escape from the ER and localise to the surface, PAR4 heterodimerizes with PAR2 whereupon the dimer undergoes a ligand exchange from β -COP1 to 14-3-3 ζ (Fig. 1.9)^{80,81}. PAR receptors have the ability to interact with other members of the PAR family as previously mentioned, but they can also interact with other receptors, such as the membrane thrombin receptor

glycoprotein Ib-IX (GPIb-IX)^{82,83}. PARs and GPIb-IX cooperatively promote platelet response in low-dose thrombin conditions, relevant in laser-induced arteriolar thrombosis, and the signal transduction requires binding of thrombin and interaction of 14-3-3 protein with GPIIb α unit⁸²⁻⁸⁵.

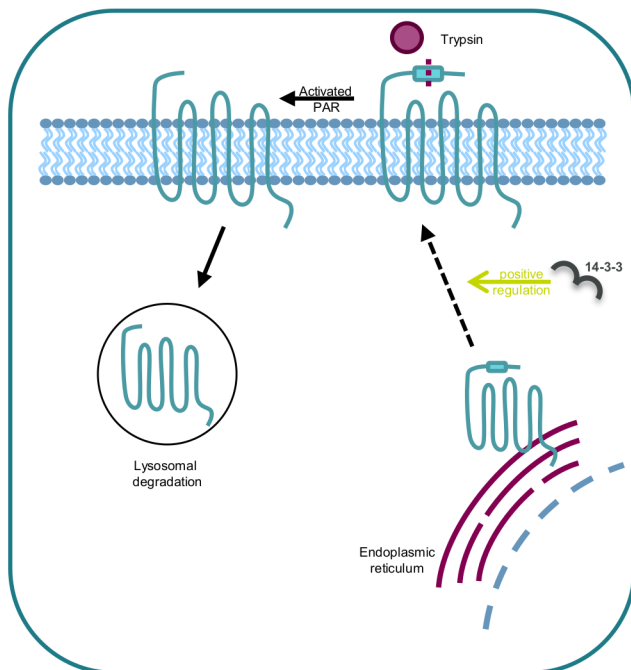


Figure 1.9. PAR mediated signal transduction and its modulation by 14-3-3. 14-3-3 was found to bind PAR4, heterodimerized with PAR2, and to enhance PAR4 translocation to the cell membrane. Note that the regulatory role of 14-3-3 is stated whenever it has been clearly reported.

1.3.3. Direct modulation of the inflammatory cytokine level

As previously described, 14-3-3 proteins modulate the production and thus the level of inflammatory mediators by, for example, binding to transcription factors or interacting with pattern recognition receptors and other receptors involved in inflammation to alter signal transduction. 14-3-3 proteins have also been observed to modulate the level of inflammatory mediators in a more direct manner. Recent evidence points to an effect of 14-3-3 in the regulation of inactive rhomboid proteases (iRhom) which regulate the maturation and the trafficking of the tumour necrosis factor alpha converting enzyme (TACE)⁸⁶⁻⁹⁰. TACE is a multidomain type I transmembrane zinc metalloproteinase which acts as an ectodomain shedding proteinase of membrane-tethered proteins and transmembrane receptors, for example TACE cleaves the soluble form of TNF- α from

transmembrane TNF- α but also the TNF- α receptors tumour necrosis factor alpha receptor 1 and 2⁹¹. TACE-activating stimulation led to the phosphorylation of the intrinsically disordered N-terminus of iRhom2 and proteomic analysis identified all 14-3-3 isoforms, except from 14-3-3 β , complexed to iRhom2⁸⁸⁻⁹⁰. Binding of 14-3-3 was significantly decreased for an iRhom2 S83A mutant, revealing the importance of this residue^{87,90}. Further experiments pinpointed the role of MAP kinase activity in the phosphorylation of iRhom2, its subsequent interaction with 14-3-3 and upregulation of TACE through the release of cytokines. Conversely MEK1/2 and p38 inhibition blocked iRhom2 phosphorylation and weakened the interaction with 14-3-3^{89,90}.

Tristetraprolin (TTP) performs a posttranscriptional modulation of gene expression by destabilising mRNA. Phosphorylation of TTP at Ser52 and Ser178 promotes a PPI with 14-3-3^{92,93}. This interaction prevents the binding of TTP to TNF α mRNA, and enhances TNF expression^{94,95}. Interestingly, immunofluorescence microscopy assays revealed that TTP phosphorylated at Ser52 and Ser178 was redistributed from the nucleus to the cytoplasm in murine macrophages, raising the question of the role of 14-3-3 in this trafficking⁹³. Similarly, phosphorylation of Zfp3611, a member of the TTP family, has been found to trigger the interaction of Zfp3611 with 14-3-3, acting as an inhibitor of Zfp3611 and increasing the mRNA half life^{92,96}.

1.4. Modulation by 14-3-3 binding at the cellular level

14-3-3 proteins are involved in the regulation of cell proliferation and differentiation. These effects have been shown to be of considerable significance for T and B-cells as well as more widely in haemopoietic cells (Fig. 1.10).

1.4.1. T lymphocytes

T cells are critical for efficient cellular immune responses and host defence. They are necessary for the retention of the immune response as part of the adaptive immunity. Hence, T cells play a major role in immune homeostasis and the loss of this equilibrium can lead to inflammatory and autoimmune conditions. One of the defining features of 14-3-3 proteins is their ability to regulate cell proliferation and apoptosis. For example, 14-3-3 ζ has been found to reduce the proliferation of tumour-infiltrating T lymphocytes. 14-3-3 ζ was overexpressed in tumour-infiltrating T lymphocytes from mice with an inflammation-related hepatocellular carcinoma (HCC) and similarly from HCC patients. This high 14-3-3 ζ level correlated with a lower ability of these T lymphocytes to proliferate¹⁸. Another study focused on the role of 14-3-3 in natural recovery from sepsis. A significantly higher expression of 14-3-3 θ was found in regulatory T cells from the spleens of rats that had survived sepsis than from the control group; pathway analysis associates this differential expression with the

upregulation of signalling pathways to balance cell apoptosis and proliferation⁹⁷. 14-3-3 proteins play a scaffolding role in the interaction between RIPOR2 (Rho family-interacting cell polarization regulator 2, also known as FAM65B) and histone deacetylase 6 (HDAC6), with a role in the T cell proliferation arrest^{98–100}. Indeed, upon formation of a complex, FAM65B has been found to trigger a T cell growth arrest in mitosis⁹⁸. Another paper reported on the possible 14-3-3 regulation of T cell proliferation in mice upon infection by pathogenic bacteria. 14-3-3 was found to interact with phosphorylated SH3-domain protein expressed in Lymphocytes 1 (Sly1), exported from the nucleus to the cytoplasm¹⁰¹. Once in the cytoplasm, Sly1/14-3-3 has been suggested to bind FOXO 1, preventing FOXO 1 to be degraded or dephosphorylated and to enable cell cycle progression and T cell proliferation¹⁰¹.

14-3-3 has been shown to impact the differentiation of T cells. Stimulated naïve T cells overexpressing 14-3-3 ζ displayed a distinct pattern of T cell polarization, namely a significant decrease of differentiation into effector T cells and an increase into regulatory T cells¹⁸. 14-3-3 ζ was also suspected to play a role in the differentiation of naïve CD8+ T cells into Tc2 cells under type 2 polarizing conditions. SiRNA-mediated depletion of 14-3-3 ζ , during the priming of CD4+ and CD8+ T cells under type 2 culture conditions, reduced the level of IL-13 production in Tc2 but not Th2 cells²¹. Investigation of the molecular mechanism underlying the decrease of IL-13 production in the absence of 14-3-3 in the case of scleroderma, identified the role of 14-3-3 ζ -T-box-containing protein expressed in T cells (T-bet) interaction and suggested that a similar mechanism operates in Tc2 cell polarization²¹.

14-3-3 modulation of T cell activity and function has also been reported. For example, the level of 14-3-3 ζ correlates with the level of anti-inflammatory cytokines and inversely correlates with the level of inflammatory cytokines produced by tumour-infiltrating T lymphocytes¹⁸. 14-3-3 ζ has been previously mentioned as a modulator of T cell activity by impacting IL-13 production²¹. In addition, high levels of 14-3-3 ζ led to a significantly higher level of T cell exhaustion markers, thus resulting in T cell dysfunction¹⁸. Phosphorylation of the K2P5.1 channel in T lymphocytes has been shown to lead to interaction with 14-3-3 and result in maximisation of the effector T cell functions. Indeed, disruption of the K2P5.1–14-3-3 PPI resulted in reduced CD8+ T cell proliferation, reduced cytokine production and reduced expression of T cell activation markers¹⁰².

1.4.2. B lymphocytes

B cells play a key role in the adaptive immune response by secreting antibodies and cytokines, and by presenting antigen. Their dysfunction gives rise to autoimmune disorders including systemic lupus erythematosus, rheumatoid arthritis, and multiple sclerosis¹⁰³. The 14-3-3 isoform σ has been shown to contribute to B cell survival, proliferation and homeostatic expansion¹⁹. For example, stimulation of B-cell antigen receptor-signalling, inducing cell death, led to an increase of

apoptosis in 14-3-3 σ -deficient splenic B-cells compared to wild-type B-cells whilst enhanced apoptosis of peripheral B cells was observed in 14-3-3 σ -deficient mice. Mice with systemic 14-3-3 σ knockout had poorer survival from a vesicular stomatitis virus infection in comparison to controls¹⁹. Differentiation of B cells can occur through class-switch recombination (CSR), crucial for maturation of the antibody response. Under a specific activation signal, immunoglobulins IgD and IgM from the naïve B cells are changed into IgG, IgA, or IgE, leading to the subsequent increase in B cells with different functions¹⁰³. A transgenic overexpression strategy provided insight into some of the actors involved in CSR; 14-3-3 was one of those identified²³. Overexpression of miR-146a, a microRNA with central role in immune responses, in B cells and in a murine asthma model, promoted the CSR, increasing the secretion of IgE by upregulating 14-3-3 σ ²³. Factors of the CSR were found to interact with 14-3-3 including Activation-induced cytidine deaminase (AID) and protein kinase A (PKA). 14-3-3 interaction, notably with AID, revealed the scaffolding role of 14-3-3 in the assembly of the nucleus of CSR complexes^{104,105}. 14-3-3s bind to the 5'-AGCT-3' repeats contained in the immunoglobulin H (IgH) switch regions together with AID in germinal centres, in which B cells undergo CSR. Impairing this interaction by blocking 14-3-3, using mice lacking 14-3-3 γ or using dominant-negative 14-3-3 σ mutants correlates with a reduced binding of AID, PKA, or both, to the switch region and reduced CSR¹⁰⁵.

1.4.3. Other immune cells

14-3-3 has been found to be part of the regulation of other immune cells such as macrophages and neutrophils. Interaction between the MEK-1/2 kinase TPL-2 and 14-3-3 was found to be responsible for TLR activation of ERK-1/2 MAP kinases in macrophages, which is indispensable for TNF secretion during inflammation¹⁰⁶. Neutrophil migration towards targets located in the site of infection or inflammation has been suspected to be mediated notably by 14-3-3 and its known partner miR-451, a microRNA regulating cell proliferation, invasion, and apoptosis in tumours¹⁰⁷.

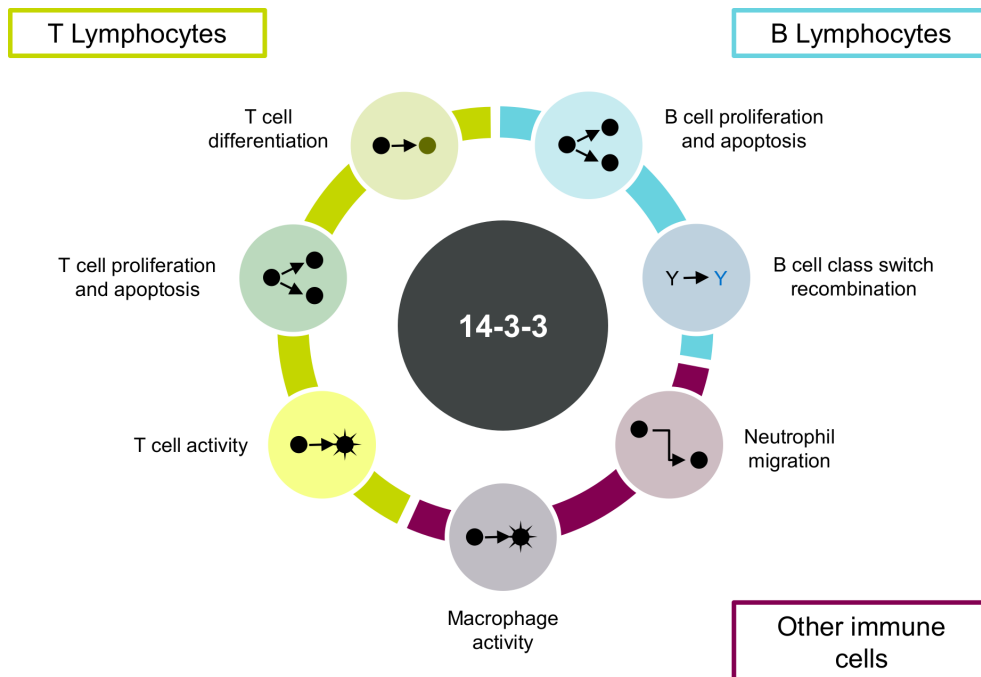


Figure 1.10. Differing levels of 14-3-3 has been shown to have a considerable significance in haemopoietic cells.

1.5. 14-3-3 and its function in chronic inflammatory disorders

Aberrant expression of 14-3-3 proteins have been implicated in chronic inflammatory disorders including autoimmune diseases and respiratory diseases.

1.5.1. Autoimmune diseases

Autoinflammatory diseases are characterised by apparently unprovoked inflammation. More specifically, they are defined by the immune system lacking the ability to tolerate self-antigens and attacking host tissues. Therapeutic strategies to treat autoimmune conditions target inflammatory cytokines and their intracellular signalling pathways, including interleukins and TNF. Scleroderma are a group of autoimmune diseases that result in hardening and tightening of the skin and connective tissues, with cutaneous fibrosis as the most characteristic feature. Investigation of the molecular mechanism of the overproduction of IL-13 by CD8+ T cells isolated from the blood and lesioned skin of patients with scleroderma and cutaneous fibrosis highlighted the role of 14-3-3 ζ . Mechanistically, upon 14-3-3 ζ interaction with the transcription factor T-bet, T-bet is retained in the cytoplasm, impairing its association with GATA-3 in the nucleus. GATA-3 can then bind to the IL-13 promoter and induce IL-13 production and overexpression²¹. As discussed earlier, 14-3-3 plays a role in autoimmune pyrin associated disorders such as FMF, PAAND and HIDS. Gene mutations can

decrease 14-3-3 interaction with pyrin, leading to a constitutive activation of the pyrin inflammasome^{20,108}. I previously mentioned in this chapter the role of 14-3-3 in the K_{2p}5.1 channel trafficking by interacting with phosphorylated K_{2p}5.1 channel, and enhancing the number of wild-type channels in the plasma membrane¹⁰². K_{2p}5.1 channels are upregulated on peripheral and central T lymphocytes of multiple sclerosis patients and provoke enhanced T-cell effector functions. Inhibition of this interaction could represent a novel therapeutic strategy for T-cell related neurodegenerative diseases. In autoimmune demyelination, 14-3-3 γ protein may act as a protective factor; 14-3-3 γ deficiency was found to increase oligodendrocyte demyelination and apoptosis. Higher expression levels of 14-3-3 γ were monitored in the spinal cord of a murine model mimicking inflammatory features and neurodegenerative aspects of multiple sclerosis; the autoimmune demyelination was more severe in 14-3-3 γ knockout mice in comparison to the control group¹⁰⁹. 14-3-3 was identified as a biomarker associated with acute transverse myelitis, an inflammation-induced damage of nervous tissues, by measuring serum tissue destruction biomarkers in the central nervous system¹¹⁰.

Rheumatoid arthritis is a chronic inflammatory disease which can generate severe joint damage and disability. 14-3-3 η proteins were identified as a plausible biomarker of rheumatoid arthritis¹¹¹. Indeed elevated serum 14-3-3 η protein has been identified in patients with this autoimmune condition, as has up-regulation of proinflammatory cytokines and cell damage^{111,112}. Clinical variables, serum and radiographs of the hands and feet to measure joint space narrowing and erosions were collected from several hundred patients over a period of 5 years to investigate the relationship between serum 14-3-3 η protein and joint damage progression. Results highlighted a correlation between higher level of 14-3-3 η with lower likelihoods of rheumatoid arthritis remission and higher joint damage progression. Similarly, elevated levels of 14-3-3 η during follow-up predicted higher subsequent disease progression, even for patients in remission.

1.5.2. Respiratory diseases

Asthma is the most common inflammatory lung disease¹¹³ and several works have reported on the putative role of 14-3-3 in this respiratory condition. For example, through the use of an asthma mouse model, 14-3-3 associated with miR-146a was suspected to play a significant role in allergic asthma, inflammation in asthma and other IgE-mediated inflammatory conditions²³. 14-3-3 associated with the collagen degrading protease matrix metalloproteinase-1 (MMP-1) was suspected to modulate tissue remodelling in asthma¹¹⁴. Indeed, extracellular 14-3-3 from primary lung epithelial cells correlated with the production of MMP-1 by lung fibroblasts. 14-3-3 induced MMP-1 production was not inhibited by transforming growth factor- β 1 (TGF- β 1) a pro-inflammatory cytokine known for impairing MMP-1 expression by fibroblasts. Lung epithelial cell derived 14-3-3 may represent a potent

MMP-1-inducing factor in lung fibroblasts, which is of a particular interest since excessive transcription of MMP has been proposed to be key in airway remodelling in asthma, enhancing collagenase expression in lung fibroblasts¹¹⁴. Proteomic based mapping of the protein expression profiles of complex biological samples has contributed to a better understanding of the biological processes underlying inflammation-related respiratory conditions. For example, quantitative proteomic profiling in the lung of murine eosinophilic and neutrophilic asthma models identified markers for a more comprehensive and specific diagnosis. 14-3-3 ϵ was found to display significant changes between the two asthma phenotypes and the control groups and positively correlated with inflammatory cells such as macrophages¹¹⁵. Proteomic analyses of lung-derived specimens from patients with asthma, patients with allergic rhinitis and from pulmonary sarcoidosis patients with chronic persistent pulmonary disease revealed a significant upregulation of 14-3-3 in comparison to the control group^{22,24}. Another example has come from the proteomic profiling of human bronchial epithelial cells from cystic fibrosis patients which highlighted a differential protein expression in the 14-3-3 signalling pathway. This was the most significant pathway identified, in comparison to a CFTR-complemented isogenic cell line. Notably, the 14-3-3 isoforms ζ and ϵ were found to be upregulated¹¹⁶. Cystic fibrosis is caused by mutation of the cystic fibrosis transmembrane conductance regulator (CFTR) gene and dysfunction of the encoded chloride channel resulting in thickened lung mucus leading to chronic airway inflammation¹¹⁷. Interestingly, 14-3-3 has been shown to interact with CFTR and to increase CFTR trafficking to the plasma membrane^{118,119}.

1.6. Conclusion

Enormous progress has been made since the discovery of 14-3-3 proteins on the identification of client partners and of the functions of this regulatory protein family, in particular in the field of inflammation. The role of 14-3-3 in the innate and adaptative immune responses has been found to be multifaceted, by modulating gene expression, signal transduction, inflammatory mediator level and immune cell activity. This large range of regulation together with the ubiquitous 14-3-3 expression means that pan inhibition of 14-3-3 interactions is unlikely to be clinically useful. Target specific 14-3-3 PPI modulation, however, may provide opportunities for therapeutic intervention. The studies described have contributed to a deeper insight into the role of 14-3-3 in disease. Despite the need of further experiments and in-depth analysis, these studies have started to outline a role for 14-3-3 in inflammatory conditions, such as autoimmune disorders and respiratory diseases. These results suggest that 14-3-3 may be a useful biomarker and that individual 14-3-3 PPI could be targets for therapeutic modulation, providing a novel and promising approach for pharmacological intervention.

A number of 14-3-3 PPI modulators have been reported; molecules that act as inhibitors or stabilisers of the interaction have both been described¹²⁰. Peptidic and non-peptidic inhibitors have been developed including the R18 peptide¹²¹, phosphonate-containing small molecules¹²² and non-phosphate inhibitors such as BV02 and BV101¹²³. 14-3-3 PPI stabilisers have received particular attention. The advantages of stabilisation over inhibition as a modality is due to the non-competitive nature and the potential capacity to achieve higher specificity by binding to a pocket composed by 14-3-3 and its client protein. The first reported stabiliser of a 14-3-3 PPI was Fusicoccin-A (FC-A), a natural product of the diterpene glycoside class of fusicoccanes. Fusicoccin-A has been shown to stabilise a number of 14-3-3 interactions with 14-3-3 protein partners¹²⁰. Additional 14-3-3 PPI stabilisers have been identified from nature but also from synthetic molecules. For example, pyrrolidone1 was selected from a high-throughput screen and was shown to stabilise the interaction between 14-3-3 and the plasma membrane ATPase 2 (PMA2)¹²⁴. Another example is the supramolecular structures which were designed to stabilise 14-3-3 PPIs and were recently shown to stabilise the 14-3-3 ζ -ER α interaction¹²⁵.

The 14-3-3 family consists of seven isoforms and their diversity was thought, first, to secure 14-3-3 protein presence in all cell types where their function was needed^{126,127}. More recently, 14-3-3 isoforms have been reported to bind specific protein partners, have distinct *in vivo* effects on targets and, whilst they are ubiquitous, differences in localization suggest tissue specificities^{7,128,129}. 14-3-3 isoforms are conserved within and across the species with about 50 percent sequence homology. The high sequence homology is notably observed in the amphipathic binding groove⁵ which might be a challenge for the design of 14-3-3 isoform specific modulators.

To conclude, though much progress has been made there are still significant unexplored areas and gaps in our knowledge of the 14-3-3 interactome. Beyond these knowledge gaps the field of therapeutic modulation of the interactions is in its infancy. However, 14-3-3 PPI modulators represent a novel opportunity towards a new approach for the treatment of inflammatory disorders.

1.7. Aim and outline of this thesis

The regulatory family of 14-3-3 proteins is placed at the centre of a signalling network, involved in numerous biological processes such as signal transduction, protein localisation, cell cycle progression and cell apoptosis. The wide spectrum of regulation attributed to 14-3-3 can be explained by the large number of structurally and functionally diverse 14-3-3 protein partners. Aberrant 14-3-3 protein expression has also been correlated to multiple conditions such as cancer and neurodegenerative disorders which prompts the need to better delineate, at a molecular level, the

mechanism underlying 14-3-3 mediated regulation. 14-3-3 proteins act as dimers and recognize and bind phosphorylated consensus motifs, through their highly conserved amphipathic groove. Hence, modulation of these PPIs, either *via* inhibition or stabilisation, could provide the potential to address conditions that are not adequately treated by current therapeutics. In this thesis, I focus on the role of 14-3-3 in the modulation of the inflammatory response. In particular the GR transcription factor and its interaction with 14-3-3 will be investigated to ultimately identify small molecule stabilisers of this PPI.

This introductory chapter highlights 14-3-3 proteins as a potential, yet not realized, opportunity to identify new targets for future therapeutic intervention in inflammatory disorders. Indeed, 14-3-3 proteins play a role at all levels of inflammation. At a genetic level, transcription factors, such as NF- κ B, JAK-STAT, PPAR and GR, are regulated by 14-3-3 upon phosphorylation and subsequent binding to 14-3-3. At a molecular level, 14-3-3 proteins have been reported to recognise and interact with receptors involved in inflammation and to alter signal transduction. These receptors include pattern recognition receptors such as TLRs, RLRs and pyrin, and PARs. At a cellular level, 14-3-3 proteins were found to play a role in the regulation of various immune cells, for example T cell and B cell proliferation and apoptosis, T cell activity, B cell differentiation through class-switch recombination, macrophage activity and neutrophil migration. At a clinical level, 14-3-3 has been implicated in chronic inflammatory disorders notably autoimmune and respiratory diseases.

The regulation of the clinically important transcription factor GR by phosphorylation and subsequent binding to 14-3-3 proteins has been explored. GR regulates a large range of fundamental processes including inflammation and its interaction with 14-3-3 has been suspected to play a role in pathological inflammatory disorders and cancer. Multiple potential phosphorylation sites on GR have been reported that have been claimed to affect the activity of GR, however, the picture has remained unclear. Thus, in chapter 2, the GR–14-3-3 PPI has been investigated at a molecular level. The affinity toward 14-3-3 of GR phosphopeptides, centred on phosphosites identified from literature reports and by use of a prediction webserver, was determined. Two sites in the GR LBD exhibiting the strongest interaction with 14-3-3 were identified. Further investigation of the interactions from these sites was carried out by an alanine scan and X-ray crystallography.

Chapter 3 presents the more in-depth study of the characterisation of the GR–14-3-3 PPI. The two identified GR sites, T524 and S617, are situated within the GR LBD. The kinase(s) responsible for phosphorylation of GR LBD have not been reported yet. Thus, I started investigating the posttranslational phosphorylation of GR LBD by chemical synthesis to site-selectively phosphorylate the two residues of interest. Kinase screen enabled the identification of the relevant kinase(s) and the

binding affinity of *in vitro* phosphorylated full-length GR LBD with 14-3-3 has been tested. MINK1 was found to phosphorylate T524 and to trigger the GR LBD–14-3-3 interaction. In addition, I demonstrated that, in a cellular system, this kinase is required for most of the binding of GR to 14-3-3.

The results obtained in chapter 2 and chapter 3 enable future work on 14-3-3 modulation of GR to proceed from a clearly define molecular understanding. Chapter 4 describes the screening workflow which led to the identification of the first stabilisers of the GR–14-3-3 PPI. From a screen of 8,000 AstraZeneca compounds, 6 hits were found to stabilise the interaction between the GR-derived phosphopeptide centred on the previously identified residues and 14-3-3. These 6 hits were further investigated to build confidence in their stabilising effect using biophysical assays, 1D and 2D NMR spectroscopy, and by analysing near neighbours to outline a structure activity relationship (SAR). At least two compounds were found to be promising and provide starting points for future development into tool compounds.

In chapter 5, I took a particular interest in known 14-3-3 PPI stabilisers. Notably, pyrrolidone1 was identified as an opportunity to develop selective and non-ligand binding pocket modulators of GR activity as an alternative to steroid hormone agonists. In addition to the previously reported stabilisation of the PMA2, estrogen receptor α (ER α) and calcium/calmodulin dependent protein kinase kinase 2 (CaMKK2) PPIs, the pyrrolidone scaffold was found to stabilise the GR PPI. A focused compound library of pyrrolidone1 analogues was evaluated and through the systematic investigation of the stabilisation activity of these structurally related compounds with GR and 14-3-3 followed by crystallization of the most promising hit with the GR–14-3-3 complex, structural differences were identified that point towards the possibility of achieving target selectivity.

The epilogue summarizes the main findings in this process to identify small molecules to stabilise the GR–14-3-3 PPI and proposes suggestions for future investigations. This chapter illustrates the experiments which could be performed to further characterise the GR–14-3-3 PPI and notably to determine the biological relevance of the 14-3-3 binding sites of GR. Additionally, it presents the effort which can be made to get a deeper insight into the 14-3-3 regulation of GR using the identified hit stabilisers and to develop them further into tool compounds. Finally, the impact of such stabilisers are discussed for use in drug discovery and the resolution of inflammation.

1.8. References

1. Netea, M. G. *et al.* A guiding map for inflammation. *Nat. Immunol.* **18**, 826–831 (2017).
2. Schett, G. & Neurath, M. F. Resolution of chronic inflammatory disease: universal and tissue-specific concepts. *Nat. Commun.* **9**, (2018).
3. Furman, D. *et al.* Chronic inflammation in the etiology of disease across the life span. *Nat. Med.* **25**, 1822–1832 (2019).
4. Wang, W. & Shakes, D. C. Molecular evolution of the 14-3-3 protein family. *J. Mol. Evol.* **43**, 384–398 (1996).
5. Bartel, M., Schäfer, A., Stevers, L. M. & Ottmann, C. Small molecules, peptides and natural products: Getting a grip on 14-3-3 protein-protein modulation. *Future Med. Chem.* **6**, 903–921 (2014).
6. Pennington, K., Chan, T., Torres, M. & Andersen, J. The dynamic and stress-adaptive signaling hub of 14-3-3: emerging mechanisms of regulation and context-dependent protein–protein interactions. *Oncogene* **37**, 5587–5604 (2018).
7. Aghazadeh, Y. & Papadopoulos, V. The role of the 14-3-3 protein family in health, disease, and drug development. *Drug Discov. Today* **21**, 278–287 (2016).
8. Johnson, C. *et al.* Bioinformatic and experimental survey of 14-3-3-binding sites. *Biochem. J.* **427**, 69–78 (2010).
9. Rubio, M. P. *et al.* 14-3-3-affinity purification of over 200 human phosphoproteins reveals new links to regulation of cellular metabolism, proliferation and trafficking. *Biochem. J.* **379**, 395–408 (2004).
10. Xue, Y. *et al.* 14-3-3 Epsilon Dynamically Interacts with Key Components of Mitogen-Activated Protein Kinase Signal Module for Selective Modulation of the TNF- α -Induced Time Course-Dependent NF- κ B Activity. *J. Proteome Res.* **9**, 3465–3478 (2010).
11. Gao, X. *et al.* 14-3-3 γ Regulates Lipopolysaccharide-Induced Inflammatory Responses and Lactation in Dairy Cow Mammary Epithelial Cells by Inhibiting NF- κ B and MAPKs and Up-Regulating mTOR Signaling. *Int. J. Mol. Sci.* **16**, 16622–16641 (2015).
12. Zhang, J. *et al.* 14-3-3 ζ interacts with Stat3 and regulates its constitutive activation in multiple myeloma cells. *PLoS One* **7**, 1–12 (2012).
13. Dodd, K. M., Yang, J., Shen, M. H., Sampson, J. R. & Tee, A. R. mTORC1 drives HIF-1 α and VEGF-A signalling via multiple mechanisms involving 4E-BP1, S6K1 and STAT3. *Oncogene* **34**, 2239–2250 (2015).
14. Wu, K. K. Peroxisome proliferator-activated receptors protect against apoptosis via 14-3-3.

- PPAR Res.* **2010**, (2010).
15. Habib, T. *et al.* AKT1 has dual actions on the glucocorticoid receptor by cooperating with 14-3-3. *Mol. Cell. Endocrinol.* **439**, 431–443 (2017).
 16. Ahmad-Nejad, P., Findeisen, P., Neumaier, M., Schuster, T. B. & Costina, V. Identification and Functional Characterization of 14-3-3 in TLR2 Signaling. *J. Proteome Res.* **10**, 4661–4670 (2011).
 17. Jéru, I. *et al.* Interaction of pypin with 14.3.3 in an isoform-specific and phosphorylation-dependent manner regulates its translocation to the nucleus. *Arthritis Rheum.* **52**, 1848–1857 (2005).
 18. Wang, X. *et al.* 14-3-3 ζ delivered by hepatocellular carcinoma-derived exosomes impaired anti-tumor function of tumor-infiltrating T lymphocytes article. *Cell Death Dis.* **9**, (2018).
 19. Su, Y. W. *et al.* 14-3-3 σ regulates B-cell homeostasis through stabilization of FOXO1. *PNAS* **108**, 1555–1560 (2011).
 20. Oda, H. & Kastner, D. L. Genomics, Biology, and Human Illness: Advances in the Monogenic Autoinflammatory Diseases. *Rheum. Dis. Clin. North Am.* **43**, 327–345 (2017).
 21. Cascio, S. *et al.* 14-3-3 ζ sequesters cytosolic T-bet, upregulating IL-13 levels in T C 2 and CD8 + lymphocytes from patients with scleroderma. *J. Allergy Clin. Immunol.* **142**, 109-119.e6 (2018).
 22. Suojalehto, H. *et al.* Level of fatty acid binding protein 5 (FABP5) is increased in sputum of allergic asthmatics and links to airway remodeling and inflammation. *PLoS One* **10**, 1–18 (2015).
 23. Li, F. *et al.* MicroRNA-146a promotes IgE class switch in B cells via upregulating 14-3-3 σ expression. *Mol. Immunol.* **92**, 180–189 (2017).
 24. Landi, C. *et al.* A functional proteomics approach to the comprehension of sarcoidosis. *J. Proteomics* **128**, 375–387 (2015).
 25. Miraghazadeh, B. & Cook, M. C. Nuclear factor-kappaB in autoimmunity: Man and mouse. *Front. Immunol.* **9**, (2018).
 26. Chen, J. & Chen, Z. J. Regulation of NF- κ B by ubiquitination. *Curr. Opin. Immunol.* **25**, 4–12 (2013).
 27. Zhang, Q., Lenardo, M. J. & Baltimore, D. 30 Years of NF- κ B: A Blossoming of Relevance to Human Pathobiology. *Cell* **168**, 37–57 (2017).
 28. Sun, W. *et al.* PPM1A and PPM1B act as IKK β phosphatases to terminate TNF α - induced IKK β -NF- κ B activation. *Cell Signal* **21**, 95–102 (2009).

29. Hanada, M. *et al.* Regulation of the TAK1 Signaling Pathway by Protein Phosphatase 2C. *J. Biol. Chem.* **276**, 5753–5759 (2001).
30. Tang, S. *et al.* 14-3-3 ϵ Mediates the Cell Fate Decision-Making Pathways in Response of Hepatocellular Carcinoma to Bleomycin-Induced DNA Damage. *PLoS One* **8**, (2013).
31. Lin, A. *et al.* Integration of Apoptosis Signal-Regulating Kinase 1-Mediated Stress Signaling with the Akt/Protein Kinase B-I B Kinase Cascade. *Mol. Cell. Biol.* **33**, 2252–2259 (2013).
32. Levy, D. E., Kessler, D. S., Pine, R., Reich, N. & Darnell, J. E. Interferon-induced nuclear factors that bind a shared promoter element correlate with positive and negative transcriptional control. *Genes Dev.* **2**, 383–393 (1988).
33. Seif, F. *et al.* The role of JAK-STAT signaling pathway and its regulators in the fate of T helper cells. *Cell Commun. Signal.* **15**, 1–13 (2017).
34. Villarino, A. V., Kanno, Y. & O’Shea, J. J. Mechanisms and consequences of Jak-STAT signaling in the immune system. *Nat. Immunol.* **18**, 374–384 (2017).
35. Villarino, A. V., Kanno, Y. & Shea, J. J. O. Mechanism of JAK/STAT signaling in immunity disease. *J Immunol* **194**, 21–27 (2016).
36. Zhu, Y. P., Brown, J. R., Sag, D., Zhang, L. & Suttles, J. Adenosine 5’-Monophosphate–Activated Protein Kinase Regulates IL-10–Mediated Anti-Inflammatory Signaling Pathways in Macrophages. *J. Immunol.* **194**, 584–594 (2015).
37. Baillie, G. S. *et al.* Phosphorylation of Janus kinase 1 (JAK1) by AMP-activated protein kinase (AMPK) links energy sensing to anti-inflammatory signaling. *Sci. Signal.* **9**, ra109–ra109 (2016).
38. Lufei, C., Koh, T. H., Uchida, T. & Cao, X. Pin1 is required for the Ser727 phosphorylation-dependent Stat3 activity. *Oncogene* **26**, 7656–7664 (2007).
39. Ge, F. *et al.* Identification of novel 14-3-3X interacting proteins by quantitative immunoprecipitation combined with knockdown (QUICK). *J. Proteome Res.* **9**, 5848–5858 (2010).
40. Lee, J. J. *et al.* BIS targeting induces cellular senescence through the regulation of 14-3-3 zeta/STAT3/SKP2/p27 in glioblastoma cells. *Cell Death Dis.* **5**, e1537-12 (2014).
41. Xue, D. *et al.* MicroRNA-206 attenuates the growth and angiogenesis in non- small cell lung cancer cells by blocking the 14-3-3z/STAT3/HIF- 1a/VEGF signaling. *Oncotarget* **7**, 79805–79813 (2016).
42. Lu, M. *et al.* The Attenuation of 14-3-3 ζ is Involved in the Caffeic Acid-Blocked Lipopolysaccharide-Stimulated Inflammatory Response in RAW264.7 Macrophages.

- Inflammation* **40**, 1753–1760 (2017).
43. Liu, Y. *et al.* The Role of PPAR- δ in Metabolism, Inflammation, and Cancer: Many Characters of a Critical Transcription Factor. *Int. J. Mol. Sci.* **19**, (2018).
 44. Dubois, V., Eeckhoutte, J., Lefebvre, P. & Staels, B. Distinct but complementary contributions of PPAR isotypes to energy homeostasis. *J. Clin. Invest.* **127**, 1202–1214 (2017).
 45. Liou, J. Y., Lee, S., Ghelani, D., Matijevic-Aleksic, N. & Wu, K. K. Protection of endothelial survival by peroxisome proliferator-activated receptor- δ mediated 14-3-3 upregulation. *Arterioscler. Thromb. Vasc. Biol.* **26**, 1481–1487 (2006).
 46. Liou, J.-Y., Wu, C.-C., Chen, B.-R., Yen, L. B. & Wu, K. K. Nonsteroidal Anti-Inflammatory Drugs Induced Endothelial Apoptosis by Perturbing Peroxisome Proliferator-Activated Receptor- Transcriptional Pathway. *Mol. Pharmacol.* **74**, 1399–1406 (2008).
 47. Brunelli, L., Cieslik, K. A., Alcorn, J. L., Vatta, M. & Baldini, A. Peroxisome proliferator-activated receptor- δ upregulates 14-3-3 ϵ in human endothelial cells via CCAAT/enhancer binding protein- β . *Circ. Res.* **100**, (2007).
 48. Chu, L. Y., Liou, J. Y. & Wu, K. K. Prostacyclin protects vascular integrity via PPAR/14-3-3 pathway. *Prostaglandins Other Lipid Mediat.* **118–119**, 19–27 (2015).
 49. Wu, K. K. & Lio, J.-Y. Cyclooxygenase Inhibitors Induce Colon Cancer Cell Apoptosis Via PPAR δ \rightarrow 14-3-3 ϵ Pathway. *Encycl. Immunobiol.* **512**, 295–307 (2009).
 50. Gojanovich, A. D., Bustos, D. M. & Uhart, M. Differential expression and accumulation of 14-3-3 paralogs in 3T3-L1 preadipocytes and differentiated cells. *Biochem. Biophys. Reports* **7**, 106–112 (2016).
 51. Park, S. *et al.* 14-3-3B and Γ Differentially Regulate Peroxisome Proliferator Activated Receptor Γ 2 Transactivation and Hepatic Lipid Metabolism. *Biochim. Biophys. Acta - Gene Regul. Mech.* **1849**, 1237–1247 (2015).
 52. Kino, T. GR-regulating Serine/Threonine Kinases: New Physiologic and Pathologic Implications. *Trends Endocrinol. Metab.* **29**, 260–270 (2018).
 53. Wakui, H., Wright, A. P. H., Gustafsson, J. & Zilliacus, J. Interaction of the Ligand-activated Glucocorticoid Receptor with the 14-3-3 η Protein. *J. Biol. Chem.* **272**, 8153–8156 (1997).
 54. Widén, C., Zilliacus, J., Gustafsson, J. Å. & Wikström, A. C. Glucocorticoid Receptor Interaction with 14-3-3 and Raf-1, a Proposed Mechanism for Cross-Talk of Two Signal Transduction Pathways. *J. Biol. Chem.* **275**, 39296–39301 (2000).
 55. Kino, T. *et al.* Protein 14-3-3 σ Interacts With and Favors Cytoplasmic Subcellular Localization of the Glucocorticoid Receptor, Acting as a Negative Regulator of the

- Glucocorticoid Signaling Pathway. *J. Biol. Chem.* **278**, 25651–25656 (2003).
56. Galliher-Beckley, A. J., Williams, J. G. & Cidlowski, J. A. Ligand-Independent Phosphorylation of the Glucocorticoid Receptor Integrates Cellular Stress Pathways with Nuclear Receptor Signaling. *Mol. Cell. Biol.* **31**, 4663–4675 (2011).
 57. Hwang, Y., An, H. T., Kang, M. & Ko, J. Roles of 14-3-3 β and γ in regulation of the glucocorticoid receptor transcriptional activation and hepatic gluconeogenesis. *Biochem. Biophys. Res. Commun.* **501**, 800–806 (2018).
 58. Zilliacus, J. *et al.* Regulation of Glucocorticoid Receptor Activity by 14-3-3-Dependent Intracellular Relocalization of the Corepressor RIP140. *Mol. Endocrinol.* **15**, 501–511 (2001).
 59. Kim, Y. S. *et al.* Role of 14-3-3 η as a Positive Regulator of the Glucocorticoid Receptor Transcriptional Activation. *Endocrinology* **146**, 3133–3140 (2005).
 60. Sung, H. J. *et al.* Negative regulatory role of annexin-A1 in 14-3-3 β -mediated glucocorticoid receptor transcriptional activation. *Biochem. Biophys. Res. Commun.* **339**, 1208–1211 (2006).
 61. Reikine, S., Nguyen, J. B. & Modis, Y. Pattern recognition and signaling mechanisms of RIG-I and MDA5. *Front. Immunol.* **5**, 1–7 (2014).
 62. Kawasaki, T. & Kawai, T. Toll-like receptor signaling pathways. *Front. Immunol.* **5**, (2014).
 63. Vidya, M. K. *et al.* Toll-like receptors: Significance, ligands, signaling pathways, and functions in mammals. *Int. Rev. Immunol.* **37**, 20–36 (2018).
 64. Matitau, A. E. & Scheid, M. P. Phosphorylation of MEKK3 at threonine 294 promotes 14-3-3 association to inhibit nuclear factor κ B activation. *J. Biol. Chem.* **283**, 13261–13268 (2008).
 65. Chow, K. T., Gale, M. & Loo, Y.-M. RIG-I and Other RNA Sensors in Antiviral Immunity. *Annu. Rev. Immunol.* **36**, 667–694 (2018).
 66. Lin, J. P., Fan, Y. K. & Liu, H. M. The 14-3-3 η chaperone protein promotes antiviral innate immunity via facilitating MDA5 oligomerization and intracellular redistribution. *PLoS Pathog.* **15**, 1–19 (2019).
 67. Liu, H. M. *et al.* The mitochondrial targeting chaperone 14-3-3 ϵ regulates a RIG-I translocon that mediates membrane-association and innate antiviral immunity. *Cell Host Microbe* **11**, 528–537 (2012).
 68. Zhang, D. & Zhang, D.-E. Interferon-Stimulated Gene 15 and the Protein ISGylation System. *J. Interf. Cytokine Res.* **31**, 119–130 (2011).
 69. Zou, W. & Zhang, D. E. The interferon-inducible ubiquitin-protein isopeptide ligase (E3) EFP also functions as an ISG15 E3 ligase. *J. Biol. Chem.* **281**, 3989–3994 (2006).

70. Chan, Y. K. & Gack, M. U. A phosphomimetic-based mechanism of dengue virus to antagonize innate immunity. *Nat. Immunol.* **17**, 523–530 (2016).
71. Wies, E. *et al.* Dephosphorylation of the RNA Sensors RIG-I and MDA5 by the Phosphatase PP1 Is Essential for Innate Immune Signaling. *Immunity* **38**, 437–449 (2013).
72. Vanaja, S. K., Rathinam, V. A. K. & Fitzgerald, K. A. Mechanisms of inflammasome activation: Recent advances and novel insights. *Trends Cell Biol.* **25**, 308–315 (2015).
73. Heilig, R. & Broz, P. Function and mechanism of the pyrin inflammasome. *Eur. J. Immunol.* **48**, 230–238 (2018).
74. Gao, W., Yang, J., Liu, W., Wang, Y. & Shao, F. Site-specific phosphorylation and microtubule dynamics control Pyrin inflammasome activation. *Proc. Natl. Acad. Sci. U. S. A.* **113**, E4857–E4866 (2016).
75. Park, Y. H., Wood, G., Kastner, D. L. & Chae, J. J. Pyrin inflammasome activation and RhoA signaling in the autoinflammatory diseases FMF and HIDS. *Nat. Immunol.* **17**, 914–921 (2016).
76. Özen, S., Batu, E. D. & Demir, S. Familial mediterranean fever: Recent developments in pathogenesis and new recommendations for management. *Front. Immunol.* **8**, (2017).
77. Masters, S. L. *et al.* Familial autoinflammation with neutrophilic dermatosis reveals a regulatory mechanism of pyrin activation. *Sci. Transl. Med.* **8**, 1–10 (2016).
78. Heuberger, D. M. & Schuepbach, R. A. Protease-activated receptors (PARs): Mechanisms of action and potential therapeutic modulators in PAR-driven inflammatory diseases. *Thromb. J.* **17**, 1–24 (2019).
79. Liu, X., Yu, J., Song, S., Yue, X. & Li, Q. Protease-activated receptor-1 (PAR-1): a promising molecular target for cancer. *Oncotarget* **8**, 107334–107345 (2017).
80. Cunningham, M. R. *et al.* Novel role for proteinase-activated receptor 2 (PAR2) in membrane trafficking of proteinase-activated receptor 4 (PAR4). *J. Biol. Chem.* **287**, 16656–16669 (2012).
81. Shikano, S., Coblitz, B., Wu, M. & Li, M. 14-3-3 Proteins: Regulation of Endoplasmic Reticulum Localization and Surface Expression of Membrane Proteins. *Trends Cell Biol.* **16**, 370–375 (2006).
82. Chen, Y., Ruggeri, Z. M. & Du, X. 14-3-3 proteins in platelet biology and glycoprotein Ib-IX signaling. *Blood* **131**, 2436–2448 (2018).
83. Estevez, B. *et al.* Signaling-mediated cooperativity between glycoprotein Ib-IX and protease-Activated receptors in thrombin-induced platelet activation. *Blood* **127**, 626–636 (2016).

84. Gu, M. *et al.* Analysis of the Roles of 14-3-3 in the Platelet Glycoprotein Ib-IX-mediated Activation of Integrin α IIb β 3 Using a Reconstituted Mammalian Cell Expression Model. *Cell* **147**, 1085–1096 (1999).
85. Mangin, P. *et al.* Identification of a novel 14-3-3 ζ binding site within the cytoplasmic tail of platelet glycoprotein Ib α . *Blood* **104**, 420–427 (2004).
86. Lee, M. Y., Nam, K. H. & Choi, K. C. iRhoms; Its functions and essential roles. *Biomol. Ther.* **24**, 109–114 (2016).
87. Dulloo, I., Muliylil, S. & Freeman, M. The molecular, cellular and pathophysiological roles of iRhom pseudoproteases. *Open Biol.* **9**, (2019).
88. Künzel, U. *et al.* FRMD8 promotes inflammatory and growth factor signalling by stabilising the iRhom/ADAM17 sheddase complex. *Elife* **7**, 1–33 (2018).
89. Grieve, A. G. *et al.* Phosphorylation of iRhom2 at the plasma membrane controls mammalian TACE-dependent inflammatory and growth factor signalling. *Elife* **6**, 1–22 (2017).
90. Cavadas, M. *et al.* Phosphorylation of iRhom2 Controls Stimulated Proteolytic Shedding by the Metalloprotease ADAM17/TACE. *Cell Rep.* **21**, 745–757 (2017).
91. Chemaly, M. *et al.* Role of tumour necrosis factor alpha converting enzyme (TACE/ADAM17) and associated proteins in coronary artery disease and cardiac events. *Arch. Cardiovasc. Dis.* **110**, 700–711 (2017).
92. Maitra, S. *et al.* The AU-rich element mRNA decay-promoting activity of BRF1 is regulated by mitogen-activated protein kinase-activated protein kinase 2. *RNA* **14**, 950–959 (2008).
93. Brook, M. *et al.* Posttranslational Regulation of Tristetraprolin Subcellular Localization and Protein Stability by p38 Mitogen-Activated Protein Kinase and Extracellular Signal-Regulated Kinase Pathways. *Mol. Cell. Biol.* **26**, 2408–2418 (2006).
94. Ray, A. *et al.* MK2: a novel molecular target for anti-inflammatory therapy. *Expert Opin. Ther. Targets* **12**, 921–936 (2008).
95. Gaestel, M. MAPKAP kinases - MKs - Two's company, three's a crowd. *Nat. Rev. Mol. Cell Biol.* **7**, 120–130 (2006).
96. Wang, K. T. *et al.* Functional regulation of Zfp361 and Zfp3612 in response to lipopolysaccharide in mouse RAW264.7 macrophages. *J. Inflamm. (United Kingdom)* **12**, 1–13 (2015).
97. Jiao, Y., Tan, S. & Xiong, J. Proteomic changes of CD4+/CD25+/forkhead box p3+ regulatory T cells in a 30-day rat model of sepsis survival. *Exp. Ther. Med.* **14**, 5619–5628 (2017).

98. Froehlich, J. *et al.* FAM65B controls the proliferation of transformed and primary T cells. *Oncotarget* **7**, 63215–63225 (2016).
99. Gao, K. *et al.* Front-signal-dependent accumulation of the RHOA inhibitor FAM65B at leading edges polarizes neut. *J. Cell Sci.* **128**, 992–1000 (2015).
100. Mortenson, J. B. *et al.* Histone deacetylase 6 (HDAC6) promotes the pro-survival activity of 14-3-3 ζ via deacetylation of lysines within the 14-3-3 ζ binding pocket. *J. Biol. Chem.* **290**, 12487–12496 (2015).
101. Schäll, D., Schmitt, F., Reis, B., Brandt, S. & Beer-Hammer, S. SLY1 regulates T-cell proliferation during *Listeria monocytogenes* infection in a Foxo1-dependent manner. *Eur. J. Immunol.* **45**, 3087–3097 (2015).
102. Fernández-Orth, J. *et al.* 14-3-3 Proteins regulate K2P5.1 surface expression on T lymphocytes. *Traffic* **18**, 29–43 (2017).
103. Hofmann, K., Clauder, A. K. & Manz, R. A. Targeting B cells and plasma cells in autoimmune diseases. *Frontiers in Immunology* **9**, (2018).
104. Lam, T. *et al.* Scaffold functions of 14-3-3 adaptors in B cell immunoglobulin class switch DNA recombination. *PLoS One* **8**, (2013).
105. Xu, Z. *et al.* 14-3-3 adaptor proteins recruit AID to 5'-AGCT-3'-rich switch regions for class switch recombination. *Nat. Struct. Mol. Biol.* **17**, 1124–1135 (2010).
106. Kjaer, S. *et al.* I B kinase-induced interaction of TPL-2 kinase with 14-3-3 is essential for Toll-like receptor activation of ERK-1 and -2 MAP kinases. *Proc. Natl. Acad. Sci.* **111**, E2394–E2403 (2014).
107. Murata, K. *et al.* MicroRNA-451 Down-Regulates Neutrophil Chemotaxis via p38 MAPK. *Arthritis Rheumatol.* **66**, 549–559 (2014).
108. Auerbuch, V. The Type III Secretion System Cleans up Its Act(in). *Cell Host Microbe* **20**, 275–276 (2016).
109. Lee, D. H. *et al.* Role of glial 14-3-3 gamma protein in autoimmune demyelination. *J. Neuroinflammation* **12**, 1–11 (2015).
110. Pittock, S. J. & Lucchinetti, C. F. Inflammatory transverse myelitis: Evolving concepts. *Curr. Opin. Neurol.* **19**, 362–368 (2006).
111. Maksymowych, W. P. & Marotta, A. 14-3-3 η : A novel biomarker platform for rheumatoid arthritis. *Clin. Exp. Rheumatol.* **32**, S35–S39 (2014).
112. Kilani, R. T. *et al.* Detection of high levels of 2 specific isoforms of 14-3-3 proteins in synovial fluid from patients with joint inflammation. *J. Rheumatol.* **34**, 1650–1657 (2007).

113. Papi, A., Brightling, C., Pedersen, S. E. & Reddel, H. K. Asthma. *Lancet* **391**, 783–800 (2018).
114. Asdaghi, N. *et al.* Extracellular 14-3-3 from human lung epithelial cells enhances MMP-1 expression. *Mol. Cell. Biochem.* **360**, 261–270 (2012).
115. Bergquist, M., Jonasson, S., Hjoberg, J., Hedenstierna, G. & Hanrieder, J. Comprehensive multiplexed protein quantitation delineates eosinophilic and neutrophilic experimental asthma. *BMC Pulm. Med.* **14**, 1–12 (2014).
116. Battistoni, A. *et al.* Proteomic and ionic profiling reveals significant alterations of protein expression and calcium homeostasis in cystic fibrosis cells. *Mol. Biosyst.* **9**, 1117 (2013).
117. Elborn, J. S. Cystic fibrosis. *Lancet* **388**, 2519–2531 (2016).
118. Stevers, L. M. *et al.* Characterization and small-molecule stabilization of the multisite tandem binding between 14-3-3 and the R domain of CFTR. *Proc. Natl. Acad. Sci. U. S. A.* **113**, E1152–E1161 (2016).
119. Liang, X. *et al.* Phosphorylation-dependent 14-3-3 protein interactions regulate CFTR biogenesis. *Mol. Biol. Cell* **23**, 996–1009 (2012).
120. Ballone, A., Centorrino, F. & Ottmann, C. 14-3-3: A Case Study in PPI Modulation. *Molecules* **23**, 1–14 (2018).
121. Wang, B. *et al.* Isolation of high-affinity peptide antagonists of 14-3-3 proteins by phage display. *Biochemistry* **38**, 12499–12504 (1999).
122. Iralde-lorente, L. *et al.* Identification of Phosphate-Containing Compounds as New Inhibitors of 14-3-3/c-Abl Protein–Protein Interaction. *ACS Chem. Biol.* **15**, 1026–1035 (2020).
123. Corradi, V. *et al.* Computational techniques are valuable tools for the discovery of protein-protein interaction inhibitors: The 14-3-3 σ case. *Bioorganic Med. Chem. Lett.* **21**, 6867–6871 (2011).
124. Rose, R. *et al.* Identification and structure of small-molecule stabilizers of 14-3-3 protein-protein interactions. *Angew. Chemie - Int. Ed.* **49**, 4129–4132 (2010).
125. Gigante, A. *et al.* A Supramolecular Stabilizer of the 14-3-3 ζ /ER α Protein-Protein Interaction with a Synergistic Mode of Action. *Angew. Chemie - Int. Ed.* 1–6 (2020).
doi:10.1002/anie.201914517
126. Van Heusden, G. P. H., Van Der Zanden, a. L., Ferl, R. J. & Steensma, H. Y. Four Arabidopsis thaliana 14-3-3 protein isoforms can complement the lethal yeast *bmh1 bmh2* double disruption. *FEBS Lett.* **391**, 252–256 (1996).
127. Gelperin, D. *et al.* 4-3-3 proteins: Potential roles in vesicular transport and Ras signaling in *Saccharomyces cerevisiae* The 14-3-3 proteins comprise a family of highly related acidic.

- Cell Biol.* **92**, 11539–11543 (1995).
128. Benzinger, A. *et al.* The crystal structure of the non-liganded 14-3-3 σ protein: Insights into determinants of isoform specific ligand binding and dimerization. *Cell Res.* **15**, 219–227 (2005).
129. Wilkert, E. W., Grant, R. A., Artim, S. C. & Yaffe, M. B. A structural basis for 14-3-3 σ functional specificity. *J. Biol. Chem.* **280**, 18891–18898 (2005)

Chapter 2

Phosphopeptide Investigation for the Characterisation of the Glucocorticoid Receptor– 14-3-3 Protein-Protein Interaction

Abstract

GR is a ligand dependent transcription factor that plays a central role in inflammation. Part of a complex cellular network, GR activity is further modulated via PPIs. The regulation of GR by 14-3-3 proteins has been previously reported, though with differing sites of phosphorylation identified and variable consequences assigned. Hence, I sought to examine this PPI. Phosphopeptides corresponding to claimed recognition sites have been investigated and they were found to be only weakly bound to 14-3-3 at best. In contrast, peptides corresponding to other sites, within the ligand binding domain of GR and not previously identified, T524 and S617, showed much stronger binding. Alanine scanning enabled a deeper understanding of the GR interaction with 14-3-3, and peptides centred on the newly identified key residues were co-crystallized with 14-3-3 to determine their structures by X-ray analysis and rationalise the binding mode.

2.1. Introduction

GR is a ligand dependent transcription factor which belongs to the superfamily of nuclear hormone receptors, a highly conserved ligandable protein family. Ubiquitously expressed throughout the human body, GR regulates the expression of many genes that control a wide range of fundamental processes¹. The role of GR is to mediate the actions of glucocorticoids, steroid hormones produced by the adrenal cortex and under tight regulation by the hypothalamic-pituitary-adrenal axis². GR Agonists are widely prescribed drugs used in the treatment of inflammatory and immunological conditions as well as the treatment of some cancers. By their nature in affecting the transcription of many genes, GR agonists are associated with multiple effects, both beneficial and undesired, thus understanding the underlying signalling network of GR is of great importance²⁻⁴.

GR is divided into three major domains: the N-terminal domain (NTD), the DNA binding domain (DBD) and the C-terminal LBD with a short hinge region (HR) between the DBD and LBD. Upon translocation to the nucleus, GR binds to GR binding DNA sequences and, as a scaffolding protein, brings different cofactors and other transcription factors together to build a transcriptional complex that regulates gene expression^{1,5,6}. Additionally, GR can take part in nongenomic signaling^{5,6}, adding another layer of complexity, whilst GR turnover is regulated by the ubiquitin-proteasome pathway⁷.

14-3-3 proteins form a family of eukaryotic regulatory proteins that act as dimers, principally heterodimers, which recognize and bind to specific pairs of phosphorylated serine/threonine residues, thus forming part of a regulatory system with kinases and phosphatases^{8,9}. 14-3-3 proteins are involved in regulating a large number of cellular processes, such as cell cycle progression, apoptosis, intracellular protein trafficking and signal transduction⁸. More than 200 structurally and functionally diverse 14-3-3 protein partners have been identified¹⁰. 14-3-3 has been, for example, reported to interact with numerous nuclear hormone receptors to modulate their activity, including ER α ¹¹, estrogen-related receptor γ (ERR γ)¹² and pregnane X receptor (PXR)¹³.

Early evidence for the interaction between 14-3-3 and GR came from yeast two-hybrid studies¹⁴ and immunoaffinity chromatographic studies on rat liver cytosol¹⁵. The 14-3-3 isoform η has been reported to bind the GR LBD and increase GR transcriptional activity through blocking the ubiquitin-proteasome GR degradation pathway^{14,16}. The 14-3-3 β and γ isoforms have been found to bind full length GR and to up-regulate GR activity in a ligand dependent manner¹⁷. GR transcriptional activity was, however, repressed by phosphorylation of S134 in a p38 MAPK-dependent manner, driving GR interaction with 14-3-3 ζ ¹⁸. Interestingly, 14-3-3 σ has been reported to bind two different portions of GR: GR S134 or GR LBD and to antagonize GR transcriptional activity^{17,19,20}. The interaction

between 14-3-3 and GR has been suspected to play a role in pathological inflammatory disorders¹⁸ and cancer²⁰.

Given this background I wanted to explore the role of the GR–14-3-3 PPI using a bottom-up molecular approach, since information on this level is virtually absent. Identification of the GR residues, whose phosphorylation is recognized by 14-3-3, is crucial to gain this molecular-level insight into the mechanism underlying the 14-3-3 mediated GR regulation. Herein I explore for the first time this molecular mechanism and report on the phosphosites of GR that are recognized by 14-3-3. T524 of GR was found to be the most important phosphosite, particularly in association with S617. This work thus contributes to unravelling the long-standing question on the 14-3-3 regulation of GR signalling pathways, assessing the GR–14-3-3 PPI implication in disease state and the GR–14-3-3 axis as potential targets for future therapeutic intervention.

2.2. Results

2.2.1. 14-3-3 Binding to phosphopeptides, centred on putative 14-3-3 binding sites of GR

Although 14-3-3 proteins can recognize some unphosphorylated sequences in pathophysiological contexts, such as ChREBP and exoenzyme S^{21,22}, the normal recognition elements in binding with 14-3-3 are phosphoserines and phosphothreonines⁹. Potential phosphosites on GR for recognition by 14-3-3 proteins were identified from literature reports and by use of the 14-3-3-Pred webserver (www.compbio.dundee.ac.uk/1433pred)²³ (Fig. **2.1a**). I synthesized 13-mer peptides centred on each of these residues and measured their affinity to 14-3-3 ζ and σ by both fluorescence polarization (FP) and surface plasmon resonance (SPR).

Multiple potential phosphosites on GR have been reported in the literature including T8, S45, S113, S134, S203, S211, S226, S234, S267 and S404^{6,24}. All are all part of the NTD and, apart from T8 and S404, they are located within the transactivation domain activation function 1, suggesting a role in the modulation of GR transcriptional activity^{6,24}. Surprisingly, only one of these phosphosites, GR S134, was identified as a putative 14-3-3 binding site by the prediction algorithm. The 13-mer peptide centred on GR S134 was the only phosphopeptide, from this set, to show an interaction with 14-3-3 ($K_d=90$ and $110 \mu\text{M}$ with 14-3-3 ζ and 14-3-3 σ respectively) (Fig. **2.1b** and Fig. **2.2a**).

Seven putative GR phosphorylation sites were identified by the algorithm as candidates for recognition by 14-3-3 proteins: S83, S134, T493, T524, T561, S617 and T635. Six of these 13-mer GR peptides showed binding with 14-3-3 ζ and σ , the exception being pT493. Peptides centred on the GR

residues pT524 and pS617 were found to be the strongest binders with K_d s in the low micromolar range (Fig. 2.1b-f and Fig. 2.2). Of note, these two sites belong to the GR LBD.

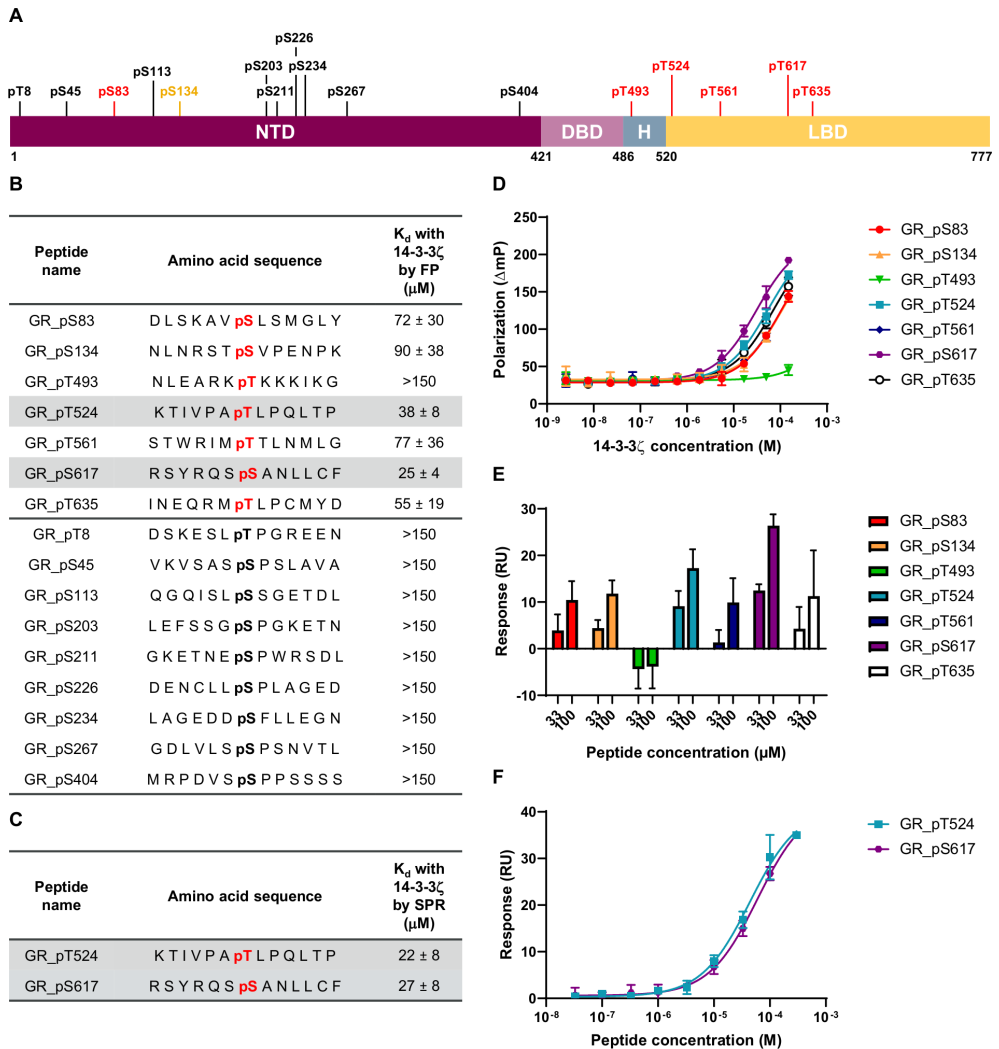


Figure 2.1. Interaction of GR mono phosphopeptides with 14-3-3 ζ . (A) Putative 14-3-3 binding sites of GR from the literature (black), prediction (red) or both (yellow). (B) Amino acid sequences of the monophosphorylated GR peptides centred on the key residues and their binding affinity (K_d) measured by FP. Binding sites of GR from the literature are depicted in bold black and prediction in bold red. The most potent GR peptides are highlighted in grey. (C) K_d of the two most potent monophosphorylated GR peptides measured by SPR. (D) Concentration-response curves of FP assays of seven peptides centred on predicted 14-3-3 binding sites with 14-3-3 ζ . (E) Affinity of monophosphorylated GR peptides with 14-3-3 ζ measured by SPR at two different peptide concentrations (33 and

Phosphopeptide Investigation for the Characterisation of the Glucocorticoid Receptor–14-3-3 Protein-Protein Interaction

100 μM). (F) Concentration-response curves of SPR assays of the two most potent peptides with 14-3-3 ζ . All measurements were performed as triplicates and the error bars represent the standard deviation of these three independent experiments.

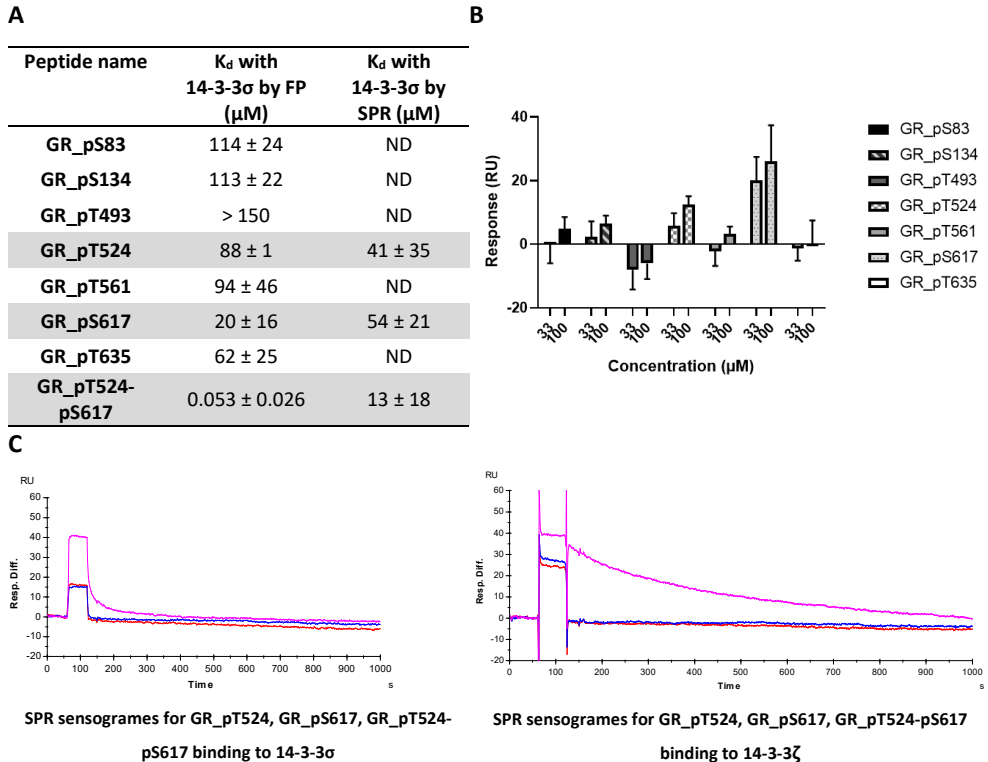


Figure 2.2. Interaction of GR peptides with 14-3-3 σ . (A) Binding affinity of the monophosphorylated GR peptides centred on the key residue and GR_pT524-pS617 measured by FP and binding affinity of GR_pT524, GR_pS617 and GR_pT524-pS617 measured by SPR. (B) Affinity of monophosphorylated GR peptides with 14-3-3 ζ measured by SPR at two different peptide concentrations (33 and 100 μM). (C) Residence time comparison of GR peptides with 14-3-3 σ and 14-3-3 ζ . GR_T524-S617, depicted in magenta, showed a prolonged residence time which drives better potency as compared to GR_T524 and GR_S617, depicted in blue and red respectively. The GR_T524-S617 kinetics on 14-3-3 σ suggest two populations which may explain the observed Hill slope (much smaller than one), the difference in the binding affinity between GR_T524-S617 and the σ and ζ isoforms of 14-3-3 measured by SPR and the binding affinity of GR_T524-S617 with 14-3-3 σ determined by FP and SPR (53 nM and 13 μM respectively). Measurements were performed as triplicates and the error bars represent the standard deviation of these three independent experiments. ND means not determined.

2.2.2. Interaction of 14-3-3 with a dimeric peptide: GR_pT524-pS617

14-3-3s act as a dimer and thus effectively provide 2 amphipathic binding grooves⁸. Many 14-3-3 targets (PKC, C-Raf, CFTR, Gab2) have been shown to interact through tandem phosphosites simultaneously, greatly increasing their binding affinity with 14-3-3^{25–28}. Hence, a dimeric peptide, GR_pT524-pS617, consisting of the two 13-mers GR_pT524, GR_pS617 identified above, linked by a pentaglycine moiety to permit flexibility²⁵, was synthesized and tested for binding to 14-3-3 ζ . The dimeric peptide displayed a remarkable avidity effect, with a 1000-fold improvement of its binding affinity with 14-3-3 ζ , compared to the individual monomers, and a K_d of 18 nM, one of the highest affinities reported for a 14-3-3 motif^{25–28} (Fig. 2.2 and Fig. 2.3).

Previous work has reported 14-3-3 to interact with phosphosites from different domains of its partner proteins²⁹. Hence, the phosphosites from GR NTD and GR LBD could also be envisioned to interact simultaneously with a 14-3-3 dimer. Two potential 14-3-3 binding sites in the NTD had been identified from the bioinformatic analysis: S83 and S134. To test this hypothesis, similar 31-mer peptides containing pentaglycine linked 13-mers, GR_pS83-pT524, GR_pS134-pT524 and GR_pS83-pS134, were synthesized. These peptides also showed significantly increased binding affinity with 14-3-3 ζ compared to the monomers, but were least 15-fold weaker than GR_pT524-pS617 (Fig. 2.3).

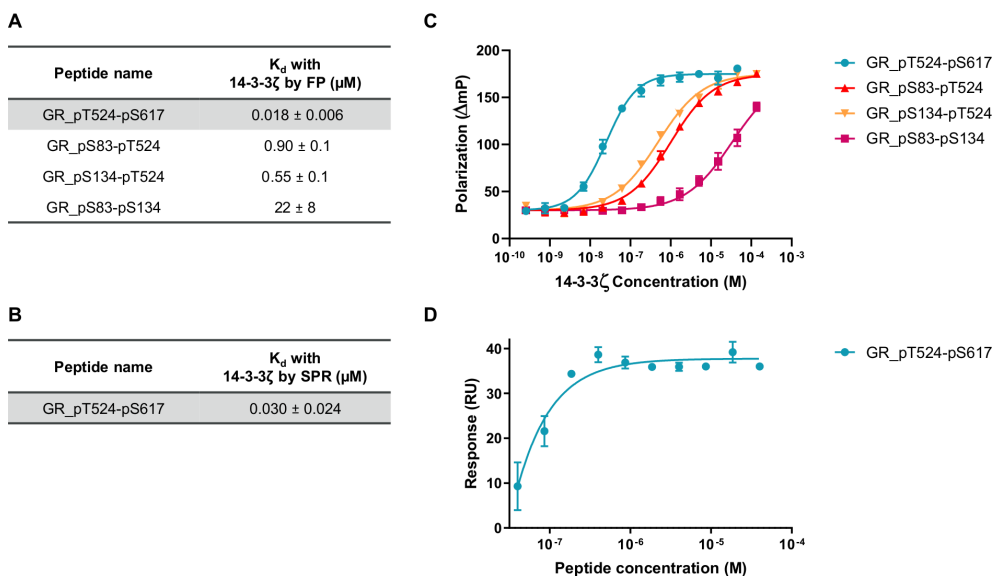


Figure 2.3. Interaction of GR doubly phosphorylated peptides with 14-3-3 ζ . (A) Binding affinity (K_d) of the diphosphorylated GR peptides measured by FP. The most potent GR peptide is highlighted in grey. (B) Binding affinity (K_d) of GR_pT524-pS617 measured by SPR. (C) Concentration-response curves of FP assays of the four diphosphorylated GR peptides with 14-3-3 ζ . (D) Concentration-response curve of SPR assays of GR_pT524-pS617

with 14-3-3 ζ . Measurements were performed as triplicates and the error bars represent the standard deviation of these three independent experiments.

2.2.3. Identification of GR_pT524-pS617 binding hotspots by mutation and alanine scan

I synthesized 24 peptides where each amino acid of the 31-mer GR_pT524-pS617, except the pentaglycine section, was replaced in turn by alanine. Upon replacement of the phosphothreonine pT524 the binding to 14-3-3 decreased by 6700-fold, from $K_d=18$ nM to $K_d=120$ μ M. Mutation of the phosphoserine pS617 had a less marked effect and led to a 72-fold loss in potency resulting in a K_d of 1.3 μ M. The two phosphoresidues are, as expected, the key residues in the binding by 14-3-3 to that doubly-phosphorylated peptide. P526 proved to be the most important non-phosphorylated residue with mutation of P526 resulting in the same effect as for the mutation of pS617, with an almost 70-fold decrease in potency ($K_d=1.2$ μ M). Smaller effects were observed for R614 and K518, resulting in a 12- ($K_d=220$ nM) and 6-fold ($K_d=110$ nM) reduction in binding affinity, respectively (Table 2.1).

To further understand the role of pT524, a diphosphoserine analogue (GR_pS524-pS617) was synthesized. This peptide showed an 8-fold reduction in potency ($K_d=140$ nM) revealing the importance of the singular methyl group of T524. Even so, the affinity drop for pS524 to A524 was still more than an order of magnitude larger than the drop for the pS617 to A617 substitution, highlighting the unexpected relative importance of pT524 versus pS617. This is particularly surprising given the similar affinities for the two individual 13-mers but suggests that the artificial boundary conditions of the linked peptides influence one site more than the other. The potent binding of a diphosphorylated GR peptide with 14-3-3 is in line with the thermodynamic model for multivalency in 14-3-3 protein–protein interactions³⁰. The effect of the individual phosphosites on the strength of GR_pT524-pS617 binding could thus be simulated, assuming an average effective molarity value of 10 mM (Equation 2.1). Indeed this equation allows the estimation of the binding affinity of singly phosphorylated peptides knowing the binding affinity of the corresponding doubly phosphorylated peptide and the effective molarity, and thus can estimate the contribution of the different phosphosites in the overall binding. The effective molarity has been reported to be between 1 and 26 mM with an average value of 10 mM for doubly phosphorylated CFTR and LRRK2 peptides bound to 14-3-3³⁰ and can be assumed to be similar for doubly phosphorylated GR peptides with 14-3-3.

Table 2.1. Binding affinity of the GR peptides from the alanine scan and mutations with 14-3-3 ζ measured by FP

Peptide name	Sequence	pK _d with 14-3-3 ζ	K _d with 14-3-3 ζ (μ M)
GR_pT524-pS617	KTIVPA pT LPQLTPGGGGGRSYRQS pS ANLLCF	7.7	0.018 \pm 0.006
GR_K518A	A TIVPA pT LPQLTPGGGGGRSYRQS pS ANLLCF	7.0	0.107 \pm 0.034
GR_T519A	KAIVPA pT LPQLTPGGGGGRSYRQS pS ANLLCF	7.2	0.067 \pm 0.005
GR_I520A	KTAVPA pT LPQLTPGGGGGRSYRQS pS ANLLCF	7.3	0.051 \pm 0.012
GR_V521A	KTIAPA pT LPQLTPGGGGGRSYRQS pS ANLLCF	7.4	0.043 \pm 0.002
GR_P522A	KTIVAA pT LPQLTPGGGGGRSYRQS pS ANLLCF	7.2	0.065 \pm 0.020
GR_T524A-pS617	KTIVPAAALPQLTPGGGGGRSYRQS pS ANLLCF	3.9	119 \pm 32
GR_L525A	KTIVPA pT APQLTPGGGGGRSYRQS pS ANLLCF	7.2	0.060 \pm 0.011
GR_P526A	KTIVPA pT LAQLTPGGGGGRSYRQS pS ANLLCF	5.9	1.2 \pm 0.1
GR_Q527A	KTIVPA pT LPALTPGGGGGRSYRQS pS ANLLCF	7.5	0.031 \pm 0.005
GR_L528A	KTIVPA pT LPQATPGGGGGRSYRQS pS ANLLCF	7.3	0.046 \pm 0.009
GR_T529A	KTIVPA pT LPQLAPGGGGGRSYRQS pS ANLLCF	7.3	0.042 \pm 0.008
GR_P530A	KTIVPA pT LPQLTAGGGGGGRSYRQS pS ANLLCF	7.5	0.029 \pm 0.008
GR_R611A	KTIVPA pT LPQLTPGGGGGASYSRQS pS ANLLCF	7.3	0.052 \pm 0.009
GR_S612A	KTIVPA pT LPQLTPGGGGGRAYRQS pS ANLLCF	7.5	0.033 \pm 0.008
GR_Y613A	KTIVPA pT LPQLTPGGGGGRSARQS pS ANLLCF	7.1	0.084 \pm 0.002
GR_R614A	KTIVPA pT LPQLTPGGGGGRSYAQS pS ANLLCF	6.7	0.221 \pm 0.017
GR_Q615A	KTIVPA pT LPQLTPGGGGGRSYRAS pS ANLLCF	7.4	0.042 \pm 0.014
GR_S616A	KTIVPA pT LPQLTPGGGGGRSYRQA pS ANLLCF	7.2	0.061 \pm 0.002
GR_pT524-S617A	KTIVPA pT LPQLTPGGGGGRSYRQSAANLLCF	5.9	1.3 \pm 0.3
GR_N619A	KTIVPA pT LPQLTPGGGGGRSYRQS pS AALLCF	7.4	0.039 \pm 0.002
GR_L620A	KTIVPA pT LPQLTPGGGGGRSYRQS pS ANALCF	7.3	0.054 \pm 0.005
GR_L621A	KTIVPA pT LPQLTPGGGGGRSYRQS pS ANLACF	7.4	0.037 \pm 0.005
GR_C622A	KTIVPA pT LPQLTPGGGGGRSYRQS pS ANLLAF	7.2	0.067 \pm 0.003
GR_F623A	KTIVPA pT LPQLTPGGGGGRSYRQS pS ANLLCA	7.3	0.049 \pm 0.007
GR_pS524-pS617	KTIVPA pS LPQLTPGGGGGRSYRQS pS ANLLCF	6.9	0.136 \pm 0.005

Binding affinity (pK_d and K_d) of GR_pT524-pS617, peptides from the alanine scan and GR_pS524-pS617. The residues mutated into alanine are depicted in bold black and the phosphorylated sites in bold red. Measurements were performed as triplicates.

Equation 2.1: Model description of a heterodivalent, noncooperative 1:1 ditopic host–guest system

$$K_{dimer} = 2 * K_{monomer 1} * K_{monomer 2} * EM$$

K_{dimer} is the affinity constant of the doubly phosphorylated peptide, K_{monomer 1} and K_{monomer 2} are the affinity constants of the single phosphorylated peptides and EM is the effective molarity.

2.2.4. Crystallization of GR_pT524-pS617, GR_pT524 and GR_pS617 with 14-3-3ζ

The mechanistic details of the GR–14-3-3 interaction were further resolved by determining the crystal structures of 14-3-3ζ in complex with GR_pT524, GR_pS617, and GR_pT524-pS617. GR_pT524 was co-crystallized with 14-3-3ζ and the crystal structure was solved to a resolution of 2.09Å [Protein Data Bank (PDB) code 6Y08]. This high-resolution crystal structure allowed us to assign 12 out of 13 amino acids of the GR peptide. Two GR_pT524 peptides were found to bind the two respective central binding channels of one 14-3-3 dimer in an extended conformation. Details of the interaction showed that electrostatic effects dominated, with pT524 bound in the positively charged pocket of the 14-3-3 monomer made from K49, R56 and R127. Other polar contacts were observed between the peptide backbone and 14-3-3 residues, such as N173 and N224 (Fig. 2.4a).

The structure of GR_pS617 with 14-3-3ζ was solved to a resolution of 2.01Å (PDB code 6YMO). Similar to GR_pT524, two GR_pS617 peptides were observed to interact with one 14-3-3 dimer and pS617 made tight electrostatic contacts with the positively charged pocket of 14-3-3. Interestingly the electron density allowed us to assign only 6 out of 13 amino acids (Fig. 2.4b).

GR_pT524-pS617 was co-crystallized with 14-3-3ζ and the complex was solved to a resolution of 2.75Å (PDB code 6YOS). One diphosphorylated GR peptide was bound to one 14-3-3ζ dimer. The electron density allowed the assignment of 18 amino acid residues out of 31. Despite the lower resolution, more amino acids surrounding pS617 could be assigned than in the X-ray structure of GR_pS617. The pentaglycine moiety was not visible in the electron density because of its flexibility. However, the distance between L528 and Y613, about 22Å, is sufficient to be bridged by 9 residues (Fig. 2.5a), supported by computational modelling of the pentaglycine linker (chapter 2.2.5). The crystal structure of GR_pT524-pS617 interacting with 14-3-3ζ was consistent with the structures of GR_T524 and GR_S617 co-crystallized with 14-3-3ζ. The main interactions between the phosphorylated residues and 14-3-3 were in line with the GR_pT524-pS617 alanine scan results and previous published crystal structures of phosphopeptides interacting with 14-3-3^{25,26}. Many residues pointed their side-chains away from 14-3-3, consistent with the observation from the alanine scan where mutation had a relatively small impact on the binding affinity with 14-3-3 (Fig. 2.5b and Fig. 2.6). A proline at position +2 relative to the phosphorylated serine/threonine residue, such as P526, is a common feature of 14-3-3 binding motifs 1 and 2 and this amino acid produces a sharp change in

chain direction⁹. P526 of GR_pT524-pS617 adopts a cis-conformation. On one side, it allows the carbonyl oxygen of L525 at the position +1 to form a hydrogen bond with the amino groups of K120 and N173. On the other side, P526 induces the peptide exit from the binding groove and avoids a clash of the remaining portion of the peptide with S45 and K49. The role of the proline in the structure was supported by the alanine scan. This turn creates a new pocket at the interface of the GR peptide and 14-3-3. Similarly, a second pocket is formed between GR residues 618-621 and the second 14-3-3 unit (Fig. 2.5). Of note, an alternative orientation of GR_pT524-pS617 in the crystal structure with 14-3-3 ζ could not be totally excluded and is described in the next section.

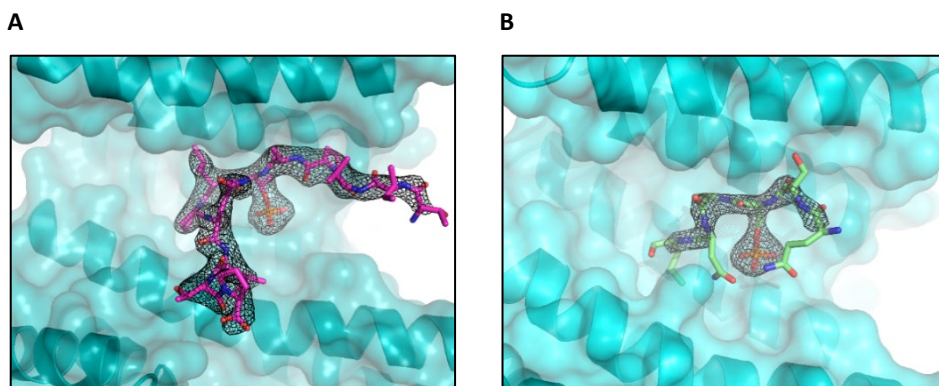


Figure 2.4. GR_pT524 and GR_pS617 co-crystallized with 14-3-3 ζ . (A) Electron density map of GR_pT524 (magenta, red and blue sticks) bound to 14-3-3 ζ (aquamarine ribbons) ($2F_o-F_c$, contoured at 1σ). (B) Electron density map of GR_pS617 (green, red and blue sticks) bound to 14-3-3 ζ (aquamarine ribbons) ($2F_o-F_c$, contoured at 1σ).

Phosphopeptide Investigation for the Characterisation of the Glucocorticoid Receptor–14-3-3 Protein-Protein Interaction

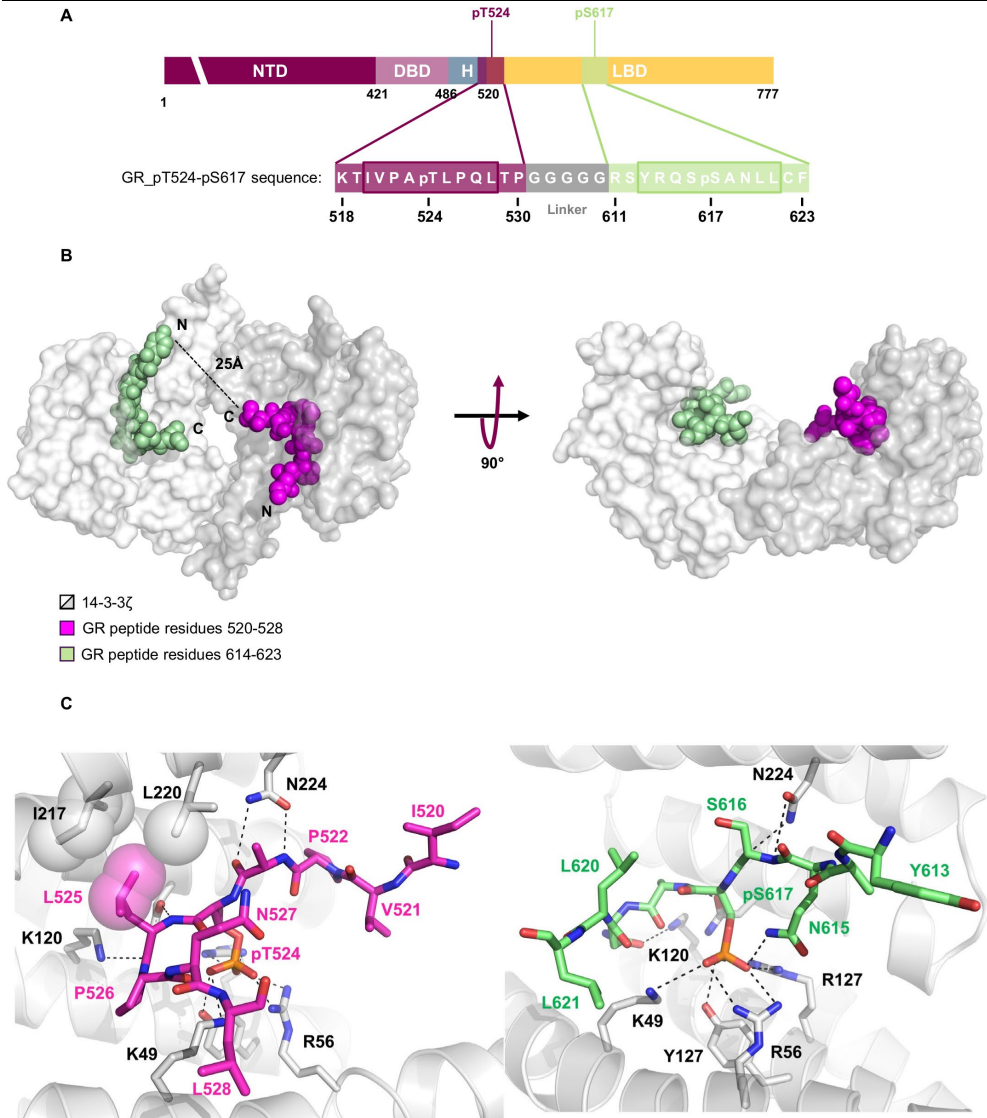


Figure 2.5. Crystal structure of GR_pT524-pS617 bound to 14-3-3ζ dimer. (A) Location within the GR sequence of the two 13-mer peptides centered on pT524 and pS617 respectively, and sequence of GR_pT524-pS617. The framed amino acids were assigned in the X-ray structure. (B) Surface representation of 14-3-3ζ dimer (white and grey solid surface) complexed with GR_pT524-pS617. Residues 520-528 are depicted in magenta and residues 614-623 in green. The black dashed line shows amino acid residues, not observed in the electron density, connecting the two binding sites. (C) Details of the interaction between GR_pT524-pS617 and 14-3-3ζ. Polar interactions are depicted as black dotted lines and hydrophobic contacts as magenta or white spheres with a semi-transparent surface.

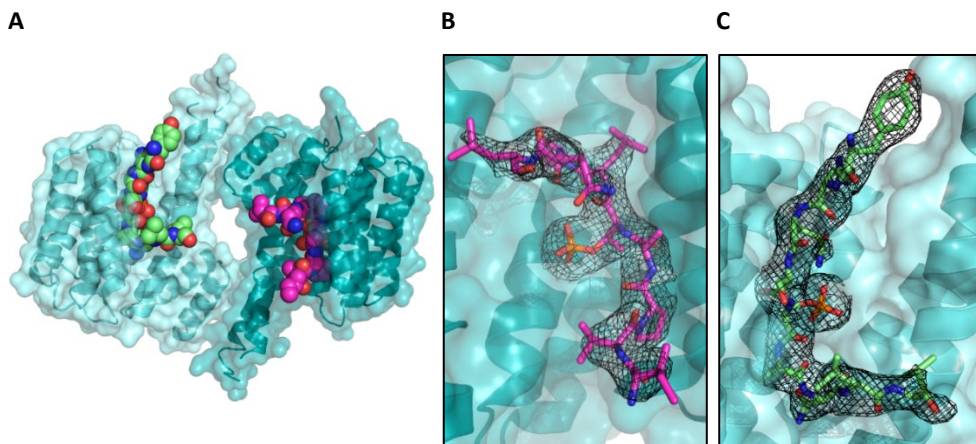


Figure 2.6. *GR_pT524-pS617 co-crystallized with 14-3-3 ζ .* (A) Surface representation of 14-3-3 ζ dimer (aquamarine solid surface and ribbons) complexed with GR_pT524-pS617, residues 520-528 are depicted in pink and residues 613-621 in green. (B) Electron density map of the residues 520-528 bound to 14-3-3 ζ ($2F_o-F_c$, contoured at 1σ). (C) Electron density map of the residues 613-621 bound to 14-3-3 ζ ($2F_o-F_c$, contoured at 1σ).

2.2.5. GR_pT524-pS617 orientation in the crystal structure with 14-3-3 ζ

I have refined GR_pT524-pS617 bound to 14-3-3 ζ in the pose corresponding to an inverted U (GR_U). However, because of the relative symmetry of this GR peptide and for comparison, another structure of GR_pT524-pS617 adopting an alternative N binding pose was also refined (GR_N) (Fig. 2.7 and 2.8). The orientation, GR_N, of GR_pT524-pS617 with respect to 14-3-3 differed from all the previous published crystal structures of a doubly phosphorylated peptide bound to 14-3-3 (PBD code 4IHL, 5D2D, 5D3E and 5D3F). To seek for evidence of a preferred orientation of the GR peptide in the X-ray structure and in particular the residues 611-623, several strategies were considered. Notably, insertion of heavy atoms in the GR sequence for crystallization purposes, paramagnetic NMR and modelling studies were envisioned. The peptide GR_pT524-pS617 bears a cysteine residue at the position 622 and in the crystal structure of GR_pT524-pS617 interacting with 14-3-3 ζ , C622 is bordering the electronic density where L621 was easily modelled. Alanine scan has previously confirmed that this residue is not crucial for the interaction with 14-3-3 since the binding affinity of GR_C622A was retained (Table 2.1). Hence, mutation of C622 into selenocysteine or selenomethionine, to introduce a selenium as heavy atom, could be a viable route to define the position of the residue 622 in the map thus the GR peptide orientation.

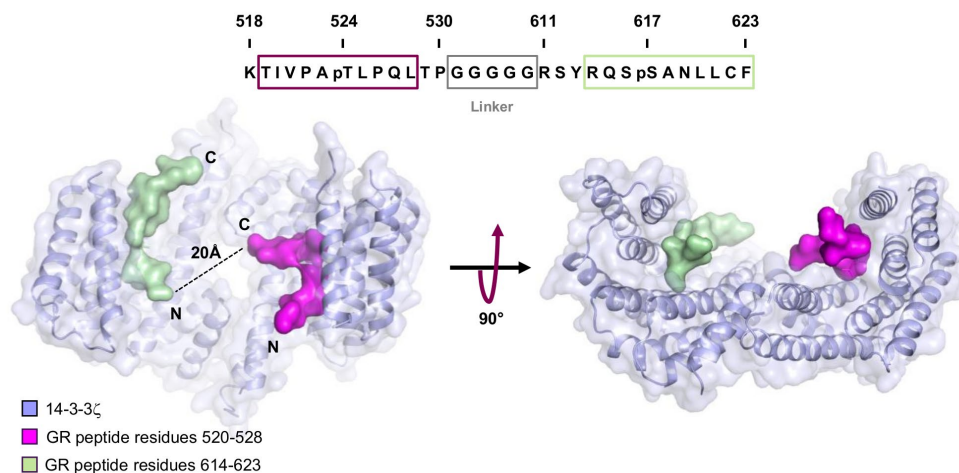


Figure 2.7. Schematic representation of the alternative GR peptide binding pose, GR_N.

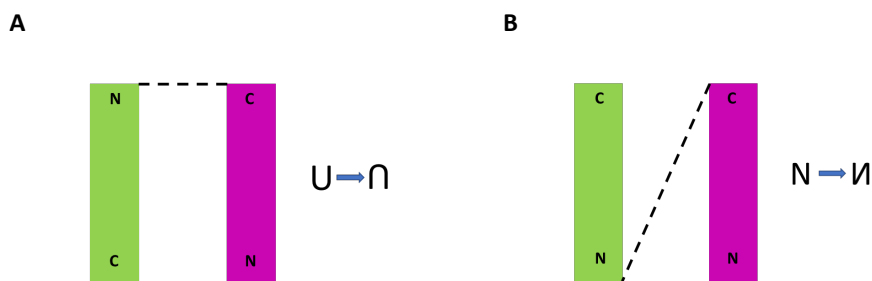
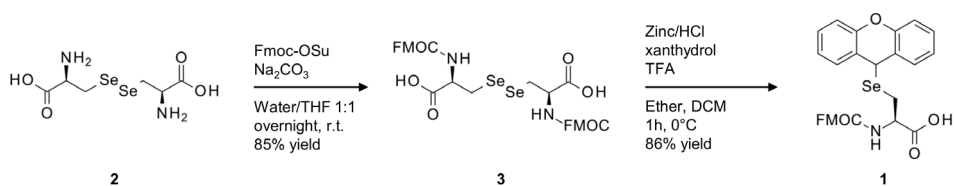


Figure 2.8. Binding pose nomenclature. (A) Inverted U. (B) Alternative N binding pose.

The commercially available selenocysteines for solid phase peptide synthesis (SPPS) cannot be deprotected using standard TFA conditions. Instead, they possess benzyl-type sidechain protecting groups which require harsh treatment or the use of toxic reagents for complete removal³¹. Such a treatment can potentially be detrimental and alter the peptide product. Selenocysteine protected with a xanthenyl group has been found to be TFA-labile and I synthesised Fmoc-Sec(Xan)-OH **1** as previously reported³¹. The two primary amines of the selenocysteine **2** were Fmoc protected using Fmoc N-hydroxysuccinimide ester and the corresponding bis Fmoc selenocysteine **3** was isolated in 85% yield. Reduction of the diselenide bond was performed in a biphasic reductive environment in the presence of Zinc/HCl followed by TFA catalysed nucleophilic substitution on xanthyrol to obtain **1** with 86% yield (Scheme 2.1). Despite a storage at -4 °C, product decomposition was observed which prevented its use for SPPS.

I considered the synthesis of a selenomethionine containing GR peptide with the advantage that selenomethionine does not require a side chain protecting group. The introduction of the selenomethionine dramatically modified the reactivity of the peptide and synthesis conditions had to be optimized. Indeed, the use of our standard conditions for SPPS, namely HATU/DIPEA, did not generate the expected product but rather elimination occurred to give the deselenated analogue. Switching to neutral coupling conditions with DIC/Oxyma solved the selenomethionine stability issue, but, because of these milder conditions, couplings of the phosphoserine and phosphothreonine were unsuccessful. That being the case, the phosphorylated residues and some other residues known to be challenging because of steric hindrance such as the amino acids S616-Y613 and V521-K518, were coupled using the original conditions. The standard Fmoc deprotection requires 20% piperidine in DMF. The formation of 3-(1-piperidinyl)alanyl via phosphoryl β -elimination of the phosphate group, however, has been observed. This side reaction has been reported to occur during the Fmoc deprotection step of the monobenzyl protected phosphoserine³². Oxidation of the carbon in the α position by piperidine generates the dehydroalanyl analogue. Subsequent nucleophilic attack by piperidine on the dehydroalanyl residue forms the 3-(1-piperidinyl)alanyl^{32,33}. To overcome this side reaction, the pKa of the base used for the Fmoc deprotection of the specific phosphorylated amino acid was lowered and two sets of conditions, 10% piperazine in DMF/EtOH 9:1, for solubility issues, and 50% morpholine in DMF were successful. A crystallization screening was initiated to co-crystallize the selenomethionine containing GR peptide with 14-3-3 ζ but the poorer resolution obtained from crystal diffraction, 3Å, was not, unfortunately, sufficient to map the position of the selenomethionine residue.



Scheme 2.1. Synthesis of Fmoc-Sec(Xan)-OH 1.

The next strategy, envisioned to identify the preferred orientation of the GR peptide, involved the use of paramagnetic NMR. GR_pT524-pS617 was spin labelled with the free radical 3-(2-Iodoacetamido)-PROXYL by nucleophilic substitution with the side chain SH of C622 in presence of ammonium bicarbonate as base and tris(hydroxypropyl)phosphine (THP) to reduce disulfide bonds. Monitoring the perturbations of the 2D ¹⁵N-¹H HSQC spectra of ¹⁵N-labelled 14-3-3 σ could reveal the

position of the free radical probe, but for reasons beyond my control I did not get access to the NMR spectrometer.

Modelling studies and scoring were performed. Both GR peptide orientations, GR_U and GR_N, are compatible with the unobserved pentaglycine section and the linker residues could be constructed using the ROSETTA remodel application (Fig. 2.9 and 2.10). The B-factors from the C α atoms of the bound peptides were calculated for both orientations and were found to be higher than the B-factors from previous published structures, in-line with the resolution. The average values of the corresponding GR peptides of the preferred (GR_U) and alternative (GR_N) structures were comparable (Fig 2.11 and Table 2.2). ROSETTA was used to score the structures of each GR monophosphorylated peptide–14-3-3 complex without structure refinement (score function ref2015, www.rosettacommons.org/docs/latest/rosetta_basics/scoring/score-types). The positive values denoted unfavourable scorings and the trend with respect to resolution was as expected. Using this scoring function, the average score for the GR monophosphorylated peptide section centred on pS617 was lower in the GR_N orientation structure than in the GR_U orientation. Nevertheless, the phosphorylated serine showed poorer internal conformation energy in the GR_N orientation compared to the GR_U orientation (Fig 2.11 and Table 2.3). Together, these data do not provide sufficient evidence to rule out the GR_N orientation in an unambiguous manner.

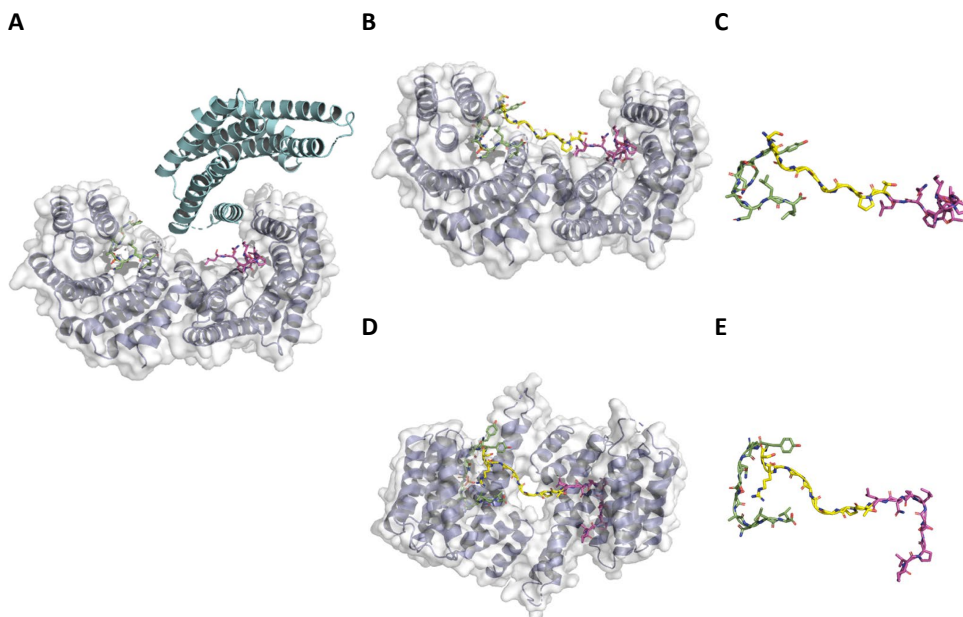


Figure 2.9. GR_U Missing loop modelling. (A) Crystal copy included in the modelling of the missing loop. (B) Side view of modelled missing loop depicted in yellow. (C) Peptide side-view. (D) Top view of modelled missing loop depicted in yellow. (E) Peptide top-view.

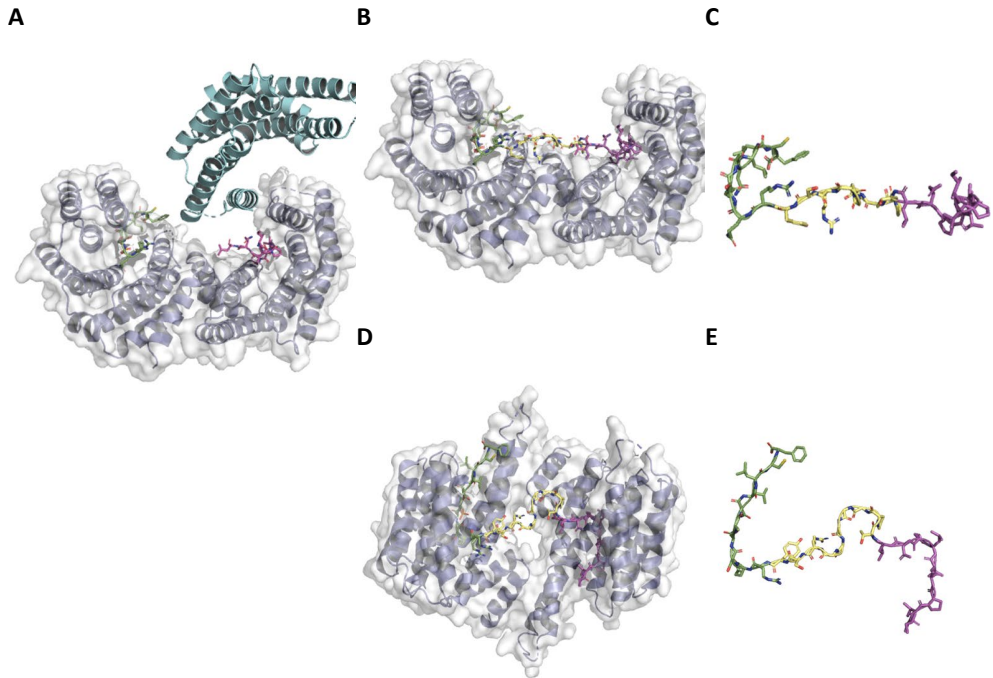


Figure 2.10. GR_N Missing loop modelling. (A) Crystal copy included in the modelling of the missing loop. (B) Side view of modelled missing loop depicted in yellow. (C) Peptide side-view. (D) Top view of modelled missing loop depicted in yellow. (E) Peptide top-view.

Phosphopeptide Investigation for the Characterisation of the Glucocorticoid Receptor–14-3-3 Protein-Protein Interaction

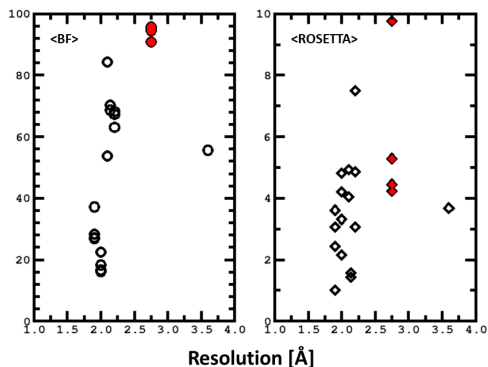


Figure 2.11. Average B-factors and average ROSETTA scores versus resolution. Graphical display of the data from Table 2.2 and Table 2.3.

Table 2.2. Peptide α B-factors

PDB	Resolution	Sequence in PDB	Protein Chain	Peptide Chain	-5	-4	-3	-2	-1	0	1	2	3	4	5	6	AV
1A37	3,6	--RST*TPN---	A	P	0,00	0,00	61,55	57,21	60,41	46,83	44,65	64,75	54,54	0,00	0,00	0,00	55,71
1A37	3,6	--RST*TPN---	B	Q	0,00	0,00	61,55	57,21	60,41	46,83	44,65	64,75	54,54	0,00	0,00	0,00	55,71
1Q1A	2	DRLYHLPA---	B	Q	0,00	0,00	30,22	20,15	14,60	12,07	4,73	18,00	14,56	23,65	0,00	0,00	16,25
1Q1A	2	RLYHLPA---	A	R	0,00	0,00	38,90	28,17	19,33	11,52	3,90	6,67	7,95	17,34	0,00	0,00	16,72
1Q1A	2	ARSHAYPA---	A	Q	0,00	0,00	41,32	31,76	21,76	16,80	12,02	13,62	15,46	27,00	0,00	0,00	22,47
1Q1B	2	ARSHAYPA---	B	S	0,00	0,00	35,62	20,29	10,48	7,35	10,23	16,50	28,19	0,00	0,00	0,00	18,38
4HKC	2,2	KRQYK*IL---	A	B	85,19	76,12	62,90	53,09	47,78	42,72	50,90	86,37	0,00	0,00	0,00	0,00	63,13
4IHL	2,2	QRST*TPNW---	A	P	102,98	93,79	67,13	52,12	40,22	43,12	48,62	67,50	89,54	0,00	0,00	0,00	67,22
4IHL	2,2	HR*Y*TPHA---	B	P	0,00	93,41	73,07	66,33	43,61	40,19	55,50	81,51	92,06	0,00	0,00	0,00	68,21
5D2D	2,1	--R*E*VISTG---	A	C	0,00	0,00	100,91	95,67	66,78	70,98	80,04	86,67	90,11	83,95	0,00	0,00	84,39
5D2D	2,1	RRRQ*V*LN*MT	B	C	0,00	80,54	64,37	50,07	45,47	37,60	33,65	35,55	45,30	44,03	68,95	84,77	53,65
SULO	2,14	---SP*FP---	A	C	0,00	0,00	0,00	84,82	73,17	62,72	62,82	68,36	0,00	0,00	0,00	0,00	70,38
SULO	2,14	--R*SP*FP---	B	D	0,00	0,00	83,38	77,20	66,02	58,70	58,52	68,48	0,00	0,00	0,00	0,00	68,80
6F08	1,9	RRPE*APAE---	A	Q	0,00	48,14	36,28	26,86	21,75	16,37	16,36	19,28	23,99	34,13	0,00	0,00	27,02
6F08	1,9	RRPE*APAE---	B	D	0,00	37,73	22,11	17,97	19,55	15,46	17,76	33,47	53,55	0,00	0,00	0,00	27,20
6F08	1,9	RRRPE*APAE---	I	K	83,36	61,46	38,81	29,13	24,19	20,76	18,51	24,88	34,48	0,00	0,00	0,00	37,29
6F08	1,9	RRRPE*APAE---	J	N	0,00	39,34	25,67	22,54	22,25	21,74	24,27	34,69	36,23	0,00	0,00	0,00	28,34
GR_U	2,75	IVPAL*PQL---	B	C	0,00	94,72	94,00	91,85	89,15	86,63	88,87	91,31	93,91	121,88	0,00	0,00	94,69
GR_U	2,75	YRQ*ANILLCF	A	D	0,00	97,79	94,84	89,93	84,69	81,32	84,24	87,49	88,48	109,49	0,00	0,00	90,06 (90,92)
GR_N	2,75	IVPAL*PQL---	B	C	0,00	95,51	94,25	92,05	89,52	87,52	89,74	91,90	94,57	119,97	0,00	0,00	95,00
GR_N	2,75	YRQ*ANILLCF	A	D	0,00	87,99	86,77	83,90	80,97	85,21	91,48	97,20	102,31	105,16	136,72	89,48 (95,77)	

Values from the PDB entries. Column 0 has the value of the phosphorylated residue in the binding pocket. The column AV has the average value. For GR_U and GR_N, this AV number is the average of the intervals in bold whereas the value in parenthesis corresponds to all values.

Table 2.3. ROSETTA residue score

PDB	Resolution	Sequence in PDB	Protein Chain	Peptide Chain	-5	-4	-3	-2	-1	0	1	2	3	4	5	6	AV
1A37	3,6	--RST*TPN---	A	P	0,00	0,00	2,51	3,63	1,20	12,51	3,10	-0,88	0,00	0,00	0,00	0,00	3,68
1A37	3,6	--RST*TPN---	B	Q	0,00	0,00	2,51	3,64	1,20	12,50	3,10	-0,87	0,00	0,00	0,00	0,00	3,68
1Q1A	2	DRLYHLPA---	B	Q	0,00	5,29	2,65	4,52	2,27	0,80	2,26	14,55	1,33	0,00	0,00	0,00	4,21
1Q1A	2	RLYHLPA---	A	R	0,00	5,06	6,15	5,73	2,53	1,47	3,41	10,83	0,00	0,00	0,00	0,00	3,21
1Q1A	2	ARSHAYPA---	A	Q	0,00	11,34	5,06	0,80	3,29	1,69	3,22	0,54	1,33	0,00	0,00	0,00	2,15
1Q1B	2	ARSHAYPA---	B	S	0,00	0,00	23,99	0,67	2,84	1,58	3,05	2,29	1,33	0,00	0,00	0,00	4,82
4HKC	2,2	KRQYK*IL---	A	B	4,55	8,99	6,71	5,39	4,91	0,87	4,68	2,78	0,00	0,00	0,00	0,00	4,86
4IHL	2,2	QRST*TPNW---	A	P	0,00	4,62	2,04	1,16	0,83	1,29	4,50	-1,44	0,87	5,80	0,00	0,00	3,87
4IHL	2,2	HR*Y*TPHA---	B	P	0,00	0,00	12,44	12,09	6,16	1,17	3,37	0,20	12,93	11,56	0,00	0,00	7,49
5D2D	2,1	--R*E*VISTG---	A	C	0,00	0,00	0,00	1,58	5,01	1,07	3,50	10,11	3,12	6,45	5,19	0,00	4,05
5D2D	2,1	RRRQ*V*LN*MT	B	C	0,00	8,82	5,19	11,20	5,62	2,77	4,78	2,19	3,11	2,04	3,63	4,87	4,93
SULO	2,14	---SP*FP---	A	C	0,00	0,00	0,00	1,95	-1,25	1,46	3,60	1,34	0,00	0,00	0,00	0,00	1,42
SULO	2,14	--R*SP*FP---	B	D	0,00	0,00	2,48	0,96	-1,91	1,54	3,49	2,84	0,00	0,00	0,00	0,00	1,56
6F08	1,9	RRPE*APAE---	A	Q	0,00	17,88	2,50	0,51	3,57	2,10	1,31	1,19	1,10	5,18	0,74	0,00	3,61
6F08	1,9	RRPE*APAE---	B	D	0,00	5,47	3,07	0,15	1,46	1,51	1,60	1,52	1,39	11,44	0,00	0,00	3,07
6F08	1,9	RRRPE*APAE---	I	K	4,55	2,40	4,03	0,72	0,96	2,64	1,46	4,80	1,64	1,06	0,00	0,00	2,43
6F08	1,9	RRRPE*APAE---	J	N	0,00	2,02	3,60	-2,06	0,79	1,99	1,39	-1,09	1,33	0,00	0,00	0,00	1,00
GR_U	2,75	IVPAL*PQL---	B	C	0,00	6,15	4,49	-0,39	1,43	7,44	7,24	-0,92	6,30	7,79	0,00	0,00	4,45
GR_U	2,75	YRQ*ANILLCF	A	D	0,00	10,80	15,12	22,46	6,04	2,41	-0,35	7,83	8,30	14,28	0,00	0,00	9,64 (9,77)
GR_N	2,75	IVPAL*PQL---	B	C	0,00	6,41	4,25	-0,61	1,49	7,57	6,20	-0,21	5,65	7,33	0,00	0,00	4,23
GR_N	2,75	YRQ*ANILLCF	A	D	0,00	0,00	5,88	4,39	0,95	16,63	1,67	1,71	5,82	6,04	6,13	3,67	5,39 (5,29)

Values obtained directly from the PDB coordinates without refining. Column 0 has the value of the phosphorylated

residue in the binding pocket. The column AV has the average value. For GR_U and GR_N, this AV number is the average of the intervals in bold whereas the value in parenthesis corresponds to all values.

2.3. Discussion

In this study, the GR–14-3-3 interaction has been systematically investigated at a GR peptide level, using biophysical assays, alanine scanning and X-ray crystallography. We particularly focused on 14-3-3 σ and 14-3-3 ζ , two very representative isoforms, since the seven 14-3-3 isoforms hold a high sequence similarity, notably in the amphipathic binding groove. Two GR phosphorylation sites within the GR LBD were identified as mediating the strongest binding to 14-3-3: T524 and S617. GR LBD has been previously reported to interact with 14-3-3, using yeast two hybrid assays, GST pull-down and Co-IP experiments, whilst GR β isoform, which shares the same N-terminal and DNA binding domain but contains a different LBD, did not^{14,19,20}. 14-3-3 binding sites are mostly located within intrinsically disordered (ID) regions or bordering the functional domains³⁴. Interestingly, GR residue T524 was anticipated to be within an ID region (globplot.embl.de) and crystal structure analysis of GR LBD placed this residue within a random coil³⁵. S617 was found in a relatively disordered area, *i.e.* the loop between helix 5 and β -sheet 1, but within an ordered domain, which to the best of our knowledge, might be one of the first examples of a 14-3-3 binding site located in ordered regions. Mechanistically, after phosphorylation, 14-3-3 partners bind in the amphipathic groove of 14-3-3, leading to a disorder-to-order transition, entropically disadvantageous, but enthalpically favourable, driven by the formation of charge-charge interactions with the phosphate group and hydrogen bonding to neighbouring residues³⁴.

One site, GR S134, previously reported to be a 14-3-3 recognition site and predicted by the algorithm used in this study, matches the mode 1 binding motif, RSX-pS/T-XP where X is any amino acid (cysteine excluded) and pS/T is a phosphorylated serine or threonine. Phosphorylation of GR S134, upon oxidative stimuli, was found to enhance GR interaction to 14-3-3 proteins¹⁸. Here, I report that GR_pS134 interacts with the ζ and σ isoforms of 14-3-3 but with a weaker binding affinity (90 μ M) than the two identified sites from GR LBD.

The dimeric GR_pT524-pS617 peptide revealed an impressive avidity gain over the monomeric components with a low nanomolar affinity toward 14-3-3. Examination of the crystal structure of GR LBD showed that T524 and S617 are both solvent exposed, and that the distance between these two residues in the crystal structure is 37Å, closely corresponding to the distance between the two phospho binding sites of 14-3-3. Other steroid hormone receptors, however, such as the androgen and the mineralocorticoid receptors, undergo a N/C interaction for complete transcriptional activity^{36,37}. Full length GR has not been crystallized yet and an interdomain interaction

through 14-3-3 binding, namely an interaction between NTD, such as S134, and LBD of GR, could be envisioned. Our biophysical assays showed that the affinity of GR_{pS134-pT524}, although 15-fold weaker than GR_{pT524-pS617}, is still in the sub-micromolar range ($K_d=0.55 \mu\text{M}$) which cannot exclude a potential interaction of GR_{pS134} with 14-3-3. Further experiments would be necessary to fully quantify the individual effect of the GR phosphosites in 14-3-3 binding and notably with full length GR.

14-3-3 has been shown to interact with various nuclear hormone receptors and modulate their activity, adding another layer of regulation beyond ligand-driven activation. 14-3-3 Interaction with ERR γ upon S179 phosphorylation, favours ERR γ cytoplasmic localization, alters its transcriptional activity and its ability to promote hepatic gluconeogenesis¹². 14-3-3 Interaction with ER α , upon T594 phosphorylation, inhibits ER α dimerization and transactivation¹¹. Interaction of 14-3-3 with PXR leads to the overexpression of P-glycoprotein (also known as multidrug resistance protein 1)¹³. Previous studies on GR–14-3-3 PPI have reported on the modulation of GR activity by 14-3-3 with different consequences assigned, including GR translocation and GR transcriptional activity^{14,16–20}. These studies focused on distinct 14-3-3 isoforms and different cellular contexts which could explain the seemingly conflicting results. The 14-3-3 isoforms have been shown to interact with different protein partners, to have different affinities, to give distinct *in vivo* effects on targets and to lead to specific tissue distribution^{38–40}.

2.4. Conclusion

In this chapter a complete and thorough characterisation of the GR–14-3-3 interaction at the peptide level has been presented by systematically and quantitatively investigating the role of GR phosphosites, both those reported in the literature and a further set identified by a bioinformatic approach, in interaction with 14-3-3. Biophysical experiments and alanine scanning clearly highlighted the potential for strong interactions with 14-3-3 by the phosphorylated GR residue T524, particularly in association with phosphorylated S617. Through an X-ray crystal analysis I was able to study the binding mode and pT524 was found, as expected, to bind with the phosphate in the positively charged site of 14-3-3 and to form hydrogen bonds and hydrophobic interactions with residues lining to the binding groove of one 14-3-3 monomer. The pS617 peptide showed similar interaction with the binding groove of the 14-3-3 monomer, combination into a dimeric peptide did not significantly alter the binding pattern. Drugs acting at the GR are a mainstay of much modern therapy and are very widely prescribed, despite multiple known side-effects, particularly when used systemically. It is therefore of great interest to understand the physiological regulation of GR. Collectively my results,

reported in this chapter, contribute to answering the long-standing question on the 14-3-3 regulation of GR signalling pathways, by a better apprehension of the 14-3-3 regulation of GR at a molecular level, and highlight the GR–14-3-3 axis as a potential target for therapeutic intervention in inflammatory disorders.

2.5. Acknowledgements

The author thanks Dr. Matthew W.D. Perry for conceiving and directing the project, Dr. Christian Ottmann for his strategic guidance and for the figures of the crystal structures, Dr. Anders Gunnarsson for his support with the biophysical experiments and analyses, Lisa Wisler for her help with co-crystallization, Dr. Leonardo De Maria, Dr. Karl Edman and for their support in the determination and analysis of the X-ray crystal structures and Dr. Arjan Snijder for his support with protein production and purification. The author thanks Dr. Anais Noisier for her help with peptide synthesis and Dr. Anna-Carin Carlsson, Dr. Linda Thunberg and Annika Langborg Weinmann MSc from the Separation Science Laboratory team for their support with peptides purification. The author acknowledges ESRF and DLS for providing access to their beamlines and Dr. Werngard Czechtizky for generous support of the project.

2.6. Materials and methods

Peptide synthesis

The peptides were synthesized via Fmoc/tBu solid-phase peptide synthesis using a Biotage® Initiator+ Alstra™ automated microwave peptide synthesizer or a Biotage® Syro II automated parallel peptide synthesizer. Peptide syntheses were monitored by reversed-phase (RP) UPLC-MS. Some peptides were bought from commercial custom peptide suppliers. Analytical RP-UPLC-MS was performed on a Waters Acquity UPLC system (PDA, sample manager, sample organizer, column oven modules) and Waters SQD2 mass spectrometer using the following column: Waters Acquity CSH C18 column, 130 Å, 1.7 µm, 50 × 2.1 mm at a flow rate of 0.5 mL/min at 45 °C. A linear gradient of mobile phase: A = H₂O + 10 mM formic acid, 1 mM ammonia and 0.03% TFA and B = acetonitrile/H₂O 95/5 v/v + 10 mM formic acid, 1 mM ammonia and 0.03% TFA was used with detection at 220 nm.

The peptides were purified by preparative RP HPLC-MS performed on Waters FractionLynx HPLC MS systems equipped with Waters 2545 pump module, Waters 2767 injector/fraction collector, and either Waters 2998 PDA detector and Waters 3100 mass spectrometer or Waters 2489 UV detector and Waters ZQ mass spectrometer, using the following columns: Waters Atlantis T3 OBD column, 100 Å, 5 µm, 150 × 19 mm; Waters XSelect CSH C18 OBD column, 130 Å, 5 µm, 150 × 19 mm or Waters XSelect CSH Fluoro-Phenyl OBD column, 130 Å, 5 µm, 150 × 19 mm. The mobile phases were: A = H₂O + 0.15% TFA and B = acetonitrile, with a flow of 30 mL/min

at room temperature. The fraction collection was triggered on mass. Gradient systems were adjusted according to the elution profiles and peak profiles obtained from the analytical RP-UPLC chromatograms.

Water was purified using a Millipore MilliQ water purification system. All solvents and reagents were purchased from commercial suppliers and used without further purification unless indicated otherwise. RP-HPLC solvents were purchased as LC/MS grade. Peptides were synthesized using standard Fmoc SPPS except for Fluoro(6FAM)_GR_pS113, Fluoro(6FAM)_GR_pS134-pT524, Fluoro(6FAM)_GR_pS83-pT524 and Fluoro(6FAM)_GR_pS83-pS134 which were purchased from ThermoFisher Scientific. Fmoc-amino acids were purchased from Chem-Impex International, Inc., with the following side-chain protection: Fmoc-Arg(Pbf)-OH, Fmoc-Asn(Trt)-OH, Fmoc-Asp(OtBu)-OH, Fmoc-Cys(Trt)-OH, Fmoc-Gln(Trt)-OH, Fmoc-Glu(OtBu)-OH, Fmoc-His(Trt)-OH, Fmoc-Lys(Boc)-OH, Fmoc-Ser(tBu)-OH, Fmoc-Thr(tBu)-OH, Fmoc-Trp(Boc)-OH, Fmoc-Tyr(tBu)-OH, Fmoc-Ser(PO(Obzl)OH)-OH, Fmoc-Thr(PO(Obzl)OH)-OH. Only L-Amino acids were used. 2-Chlorotrityl chloride resin (100-200 mesh), 1% DVB was purchased from Sigma-Aldrich. HATU was purchased from Chem-Impex International, Inc., DIPEA and FITC from Sigma-Aldrich. Acetic anhydride was purchased from Acros Organics.

General Protocol for SPPS. The peptides were synthesized via Fmoc/tBu solid-phase peptide. The first amino acid was attached to the 2-Chlorotrityl chloride resin following **method A** to reach a loading of 0,66 mmol/g. The peptide chains were then assembled according to **method B**. The peptides were then labelled by either addition of a fluorescein isothiocyanate (FITC) tag (**method C**) or N-terminal acetylation (**method D**) before being cleaved from the resin, deprotected according to **method E** and purified.

Method A: Attachment of the first amino acid on the 2-Chlorotrityl chloride resin. 2-Chlorotrityl chloride resin (0.3-0.8 meq/g, final loading 0,66 mmol/g) was swollen in DCM for 10 min and then the solvent was drained. The first amino acid (1 eq) was dissolved in DCM (1 mL) and DIPEA (3 eq) was added. The solution was added to the resin and stirred at room temperature under nitrogen bubbling. After 10 min DIPEA (7 eq) was added to the resin and the reaction mixture was stirred for 40 min. MeOH (0.8 μ L/mg of resin) was added to the resin and was stirred for 10 min. The mixture was drained, and the resin was washed with DMF (3 \times) and DCM (3 \times).

Method B1: Automated Fmoc SPPS, Biotage® Initiator+ Alstra™ automated microwave peptide synthesizer. The resin was swollen with DMF (2 \times) and the Fmoc N α -protecting group was removed with 20% piperidine in DMF (2 \times ; 3 min then 10 min) at room temperature. The amino acids dissolved in DMF (0.3 M) were repeatedly coupled with HATU (3 eq) in NMP (0.5 M) and DIPEA (6 eq) in NMP (2 M) at room temperature for 45 or 60 min. The resin was finally washed with DCM (6 \times).

Method B2: Automated Fmoc SPPS, Biotage® Syro II automated parallel peptide synthesizer. The resin was swollen with DMF (6 \times) and the Fmoc N α -protecting group was removed with 40% piperidine in DMF (3 min) followed by 20% piperidine in DMF (10 min) at room temperature. The amino acids (4 eq) dissolved in DMF (0.5 M) were repeatedly coupled with HATU (4 eq) in DMF (0.48 M) and DIPEA (8 eq) in NMP (2 M) at room temperature for 40 min. The resin was finally washed with DCM (3 \times), MeOH (3 \times) and Et₂O (3 \times).

Method C: Addition of a fluorescein isothiocyanate (FITC) tag at the N terminal position. After the final Fmoc deprotection, the resin was swollen with DCM (2 \times). In the dark, FITC (3 eq) was dissolved in DMF and HATU (3 eq) and DIPEA (4.5 eq) were added. The reaction mixture was added to the resin and stirred at room

temperature under nitrogen bubbling for 45 min. The mixture was drained, and the resin was washed with DMF (3 ×) and DCM (3 ×).

Method D: Acetylation of the N terminal position. After the final Fmoc deprotection, the resin was swollen with DCM (2 ×). A solution of acetic anhydride (10 eq) and DIPEA (10 eq) in DMF was added to the resin and stirred at room temperature under nitrogen bubbling for 15 min before the mixture was drained. This procedure was repeated twice, and the resin was washed with DMF (3 ×) and DCM (3 ×).

Method E: Cleavage from resin/side-chain deprotection. A solution of TFA/water/EDT/TIS 94:2.5:2.5:1 (5 mL) was added to the dry resin. The reaction mixture was shaken at room temperature for 3 h. TFA solution was then collected in cold diethyl ether. The resin was rinsed with TFA (1 mL, 3 ×) and the TFA solution collected. The precipitated peptide was centrifuged, and the crude peptide was lyophilized from acetonitrile-water.

14-3-3 full length expression and purification

The ζ and σ isoforms of human 14-3-3 were cloned in pProEx Htb vector as 6His-Linker (MSYYHHHHHDYDIPPTENLYFQGAMGS)-h14-3-3 and expressed in *E. coli* BL21 (DE3)STAR competent cells. Cultures were grown in Terrific Broth media supplemented by 3 mM MgCl₂, 0.02% glucose, 0.8% glycerol and 50 μ g/mL carbenicillin at 37 °C to an OD₆₀₀ of 0.4-0.6 and then induced overnight with 0.4 mM of IPTG at 18 °C to reach an OD₆₀₀ higher than 20. Cells were harvested by centrifugation (5 000g, 20 min) and lysed using a cell disruptor (Constant Systems LTD) at 25 KPSI in lysis buffer containing 50 mM Tris, 300 mM NaCl, 12.5 mM imidazole, 1 mM TCEP, 5 mM MgCl₂ and 1 tablet protease inhibitor Roche per 100 mL of lysis buffer. After centrifugation (35 000g, 45 min), the lysate was incubated with Ni-NTA derivatized Sepharose resin (Qiagen) overnight at 4 °C. The nickel-resin was washed with buffer containing 0.1% triton X-100 then with lysis buffer and the proteins were eluted with buffer containing 250 mM imidazole. 14-3-3 proteins were further purified by size exclusion chromatography on a Hiload 26/60 Superdex 75 per grade (Pharmacia Biotech) using HBS P+ buffer (10 mM HEPES pH 7.4, 150 mM NaCl, 0.005% v/v Tween-P20). The correct fractions were combined, concentrated, aliquoted, frozen in liquid nitrogen and stored at -80 °C.

14-3-3 Δ C expression and purification

Human 14-3-3 $\sigma\Delta$ C (C-terminally truncated, including residues 1-231, for crystallography purposes) was cloned in pProEx Htb vector and expressed in *E. coli* BL21 (DE3) competent cells. Cultures were grown in TB media at 37 °C to an OD₆₀₀ of 0.8-1 and then induced overnight with 0.4 mM of IPTG at 18 °C to reach an OD₆₀₀ higher than 20. Cells were harvested by centrifugation (10 000 g, 15 min) and lysed using a cell disruptor (Avestin EmulsiFlex C3 Homogenizer) at 20 KPSI in lysis buffer containing 50 mM Tris, 300 mM NaCl, 12.5 mM imidazole and 2 mM β -mercaptoethanol. After centrifugation (40 000 g, 30 min), the lysate was applied to a HisTrap HP column (GE), washed with lysis buffer and the 14-3-3 proteins were eluted with 50 mM Tris, 300 mM NaCl, 250 mM imidazole and 2 mM β -mercaptoethanol. The right fractions were combined, and the full-length proteins were dialyzed and rebuffed in 25 mM HEPES pH 7.5, 100 mM NaCl, 10 mM MgCl₂, 0.5 mM Tris(2-carboxyethyl)phosphine. The His Tag was removed via TEV cleavage. The cleavage solution was applied to the HisTrap HP column to remove the TEV protease. The protein was further purified via size exclusion chromatography on a Superdex75 (GE) using the following buffer: 20 mM Tris pH 7.4, 150 mM NaCl and 2 mM β -

mercaptoethanol. The correct fractions were combined, concentrated, aliquoted, frozen in liquid nitrogen and stored at -80°C.

FP assay with GR phosphorylated peptides and 14-3-3

The FITC labelled peptides were solubilized to a final concentration of 60 nM (for the mono phosphorylated peptides) or 10 nM (for the doubly phosphorylated peptides) and were titrated with 14-3-3 ζ or 14-3-3 σ in concentration dilution series from 300 μ M or 150 μ M, depending on the binding affinity of the peptide, in a 384-well flat bottom black polypropylene microplate (Greiner Bio-One). Following 30-minute incubation at room temperature, the plates were read on a plate reader PHERAstar (BMG LABTECH GmbH) for FP signal using white light and standard excitation (485 nm) and emission (520 nm). Measurements were performed as triplicates. Binding data were fit to a standard Hill equation using the software Genedata Screener[®]. The figures were made using the software GraphPad Prism 8. Fluorescence polarization data were expressed as millipolarization (mP) units and the dynamic range (Δ mP) was calculated according to equation (1):

$$\Delta\text{mP} = \text{mP of bound peptide} - \text{mP of free peptide}$$

Errors are standard error of the fit.

SPR assays with GR phosphorylated peptides and 14-3-3

SPR binding assays were performed using a Biacore 3000 (GE Healthcare). 6His tagged 14-3-3 proteins (3 μ M) were immobilized on a SPR sensorchip NTA derivatized carboxymethyl dextran hydrogel (Xantec Bioanalytics) at 4000 RU for 14-3-3 σ and 2000 RU for 14-3-3 ζ according to the manufacturer's instructions. A 96-well V-shaped polypropylene microtiter plate was prepared with different GR peptides concentrations in HBS P+ buffer and normalized to 1 or 3% v/v DMSO, depending on the maximum peptide concentration, using the HP D300 Digital Dispenser (Hewlett-Packard Company). In the dose response assay, ten dilutions of GR peptide from 300 μ M or 45 μ M, depending on the peptide binding affinity, were performed. The peptide samples were injected using the HBSP+ buffer with 1 or 3% v/v DMSO at a continuous flow rate of 20 μ L/min for 1 min on the immobilized 14-3-3 and before the next injection 2.5 min after. An extra waiting time of 12.5 min was set to allow complete dissociation of the doubly phosphorylated peptides. Measurements were performed as triplicates. When necessary data were corrected using a solvent correction curve. Binding data were fit to a standard Hill using the software Genedata Screener[®] and the figures were made using the software GraphPad Prism 8. Errors are standard error of the fit.

X-ray crystallography studies

Sitting drop co-crystallization of 14-3-3 ζ and GR peptides. Crystals were grown using the sitting drop vapor diffusion crystallization method by mixing 14-3-3 ζ AC with a mono-phosphorylated GR peptide in a 1:2 ratio or with a doubly phosphorylated peptide in a 1:1 ratio with a resulting protein concentration of 10 mg/mL in a crystallization buffer containing 20 mM HEPES pH 7.5, 2 mM MgCl₂ and 2 mM DTT. Sitting drops were formed by mixing equal volumes of protein/peptide solution and precipitant (2 \times 100 nL) on a 96-well Art Robbins Flat Ledge plate (Hampton Research) using a nanoliter liquid handler mosquito[®] (SPT Labtech) and equilibrated over a 80 μ L reservoir at 4 or 20 °C. Crystals were harvested after a few days, soaked in cryo-protectant containing the precipitant supplemented with 20% v/v glycerol and flash-cooled in liquid nitrogen before data collection.

GR_pT524 co-crystallized with 14-3-3ζ. The crystals were grown at 4 °C using a precipitant solution (1.29 M MgCl₂, 22.5% PEG 3350, 0.1 M Tris pH 8.3) supplemented with 10% of an additive containing 40% v/v of 2,5-Hexanediol. The crystals were harvested after 8 days.

GR_pS617 co-crystallized with 14-3-3ζ. The crystals were grown at 4 °C using a precipitant solution (2.04 M ammonium sulfate, 0.2 M sodium citrate) supplemented with 10% of an additive containing 0.33% w/v 3-aminobenzoic acid, 0.33% w/v 3-aminosalicylic acid, 0.33% w/v salicylic acid and 0.02 M HEPES sodium pH 6.8. The crystals were harvested after 5 days.

GR_pT524-pS617 co-crystallized with 14-3-3ζ. The crystals were grown at 20 °C using a precipitant solution (0.35 M MgCl₂, 24.4% PEG 3350, 0.1 M Bis Tris pH 5.5) supplemented with 10% of an additive containing 0.06 M CHAPS, 0.06 M HEPES, 0.06 M Tris, 0.25% w/v Hexamminecobalt(III) chloride and 0.02 M HEPES sodium pH 6.8. The crystals were harvested after 8 days.

Data collection and processing. Diffraction data were collected at the European Synchrotron Radiation Facility (ESRF) in Grenoble, France (0.976Å, 100 K, ESRF Beamline ID30B) and at Diamond Light Source (DLS) at the Harwell Science and Innovation Campus in Oxfordshire, UK (0.916Å, 100 K, DIAMOND Beamline I04-1). Molecular replacement was performed using Phaser from the ccp4i package and refinement and manual rebuilding was done using Buster and Coot software packages. The structures (PDB codes: 6Y08, 6YMO and 6YOS) were refined to a resolution of 2.09 Å, 2.01Å and 2.75Å with R_{work}/R_{free} factors of 0.224/0.235, 0.212/0.228 and 0.268/0.291, respectively. X-ray diffraction data collection and structure refinement statistics are summarized in Supplementary Table 2.S1. The figures were made using the software PyMol (DeLano Scientific LLC).

GR peptide analysis

Whenever possible, only a fraction of crude material was purified to isolate about 10 mg of pure peptide.

FITC labelled GR_pT8:

FITC labelled GR_pT8 peptide was prepared following General Protocol for SPPS. The crude peptide was purified by reverse-phase HPLC (gradient: 5% B for 1 min, 5-19% B in 3 min, 19-24% B in 15 min, Waters CSH C18 column) to afford the desired peptide as a white fluffy solid. Yield (28 mg) in > 95% purity according to analytical UPLC. Rt 4.32 min (3-60% B in 10 min).

$[M + 2H]^{2+}$ calculated for C₈₅H₁₁₉N₂₀O₃₅PS, 1022.5; found 1022.7.

FITC labelled GR_pS45:

FITC labelled GR_pS45 peptide was prepared following General Protocol for SPPS. The crude peptide was purified by reverse-phase HPLC (gradient: 5% B for 1 min, 5-25% B in 3 min, 25-30% B in 15 min, Waters CSH C18 column) to afford the desired peptide as a white fluffy solid. Yield (11 mg) in > 95% purity according to analytical UPLC. Rt 6.00 min (3-60% B in 10 min).

$[M + 2H]^{2+}$ calculated for C₈₀H₁₁₇N₁₆O₂₇PS, 899.5; found 899.7.

Acetylated GR_pS83:

Acetylated GR_pS83 peptide was prepared following General Protocol for SPPS. The crude peptide was purified by reverse-phase HPLC (gradient: 5% B for 1 min, 5-24% B in 3 min, 24-29% B in 15 min, Waters Xselect CSH

Phosphopeptide Investigation for the Characterisation of the Glucocorticoid Receptor–14-3-3 Protein-Protein Interaction

column) to afford the desired peptide as a white fluffy solid. Yield (12 mg) in > 95% purity according to analytical UPLC. Rt 5.69 min (3-60% B in 10 min).

[M + H]²⁺ calculated for C₆₃H₁₀₅N₁₄O₂₄PS, 1506.6; found 1506.4.

FITC labelled GR_pS83:

FITC labelled GR_pS83 peptide was prepared following General Protocol for SPPS. The crude peptide was purified by reverse-phase HPLC (gradient: 5% B for 1 min, 5-32%B in 3min, 32-37% in 15min, Waters Xselect CSH column) to afford the desired peptide as a white fluffy solid. Yield (12 mg) in > 95% purity according to analytical UPLC. Rt 7.13 min (3-60% B in 10 min).

[M + 2H]²⁺ calculated for C₈₈H₁₂₅N₁₆O₂₉PS₂, 983.6; found 984.0.

FAM labelled GR_pS113:

FAM labelled GR_pS113 peptide was purchased from Thermo Scientific with a purity over 95%.

Acetylated GR_pS134:

Acetylated GR_pS134 peptide was prepared following General Protocol for SPPS. The crude peptide was purified by reverse-phase HPLC (gradient: 5% B for 1 min, 5-25% B in 25 min, Kromasil C18 column) to afford the desired peptide as a white fluffy solid. Yield (15 mg) in > 95% purity according to analytical UPLC. Rt 2.40 min (3-60% B in 10 min).

[M + 2H]²⁺ calculated for C₆₂H₁₀₅N₂₀O₂₆P, 789.3; found 789.9.

FITC labelled GR_pS134:

FITC labelled GR_pS134 peptide was prepared following General Protocol for SPPS. The crude peptide was purified by reverse-phase HPLC (gradient: 5% B for 1 min, 20-35% B in 30 min, Kromasil C18 column) to afford the desired peptide as a white fluffy solid. Yield (42 mg) in > 95% purity according to analytical UPLC. Rt 4.50 min (3-60% B in 10 min).

[M + 2H]²⁺ calculated for C₈₇H₁₂₅N₂₂O₃₁PS, 1019.6; found 1020.2.

FITC labelled GR_pS203:

FITC labelled GR_pS203 peptide was prepared following General Protocol for SPPS. The crude peptide was purified by reverse-phase HPLC (gradient: 5% B for 1 min, 5-26% B in 3 min, 26-31% B in 15 min, Waters CSH C18 column) to afford the desired peptide as a white fluffy solid. Yield (26 mg) in > 95% purity according to analytical UPLC. Rt 6.10 min (3-60% B in 10 min).

[M + 2H]²⁺ calculated for C₈₄H₁₁₂N₁₇O₃₂PS, 968.0; found 968.2.

FITC labelled GR_pS211:

FITC labelled GR_pS211 peptide was prepared following General Protocol for SPPS. The crude peptide was purified by reverse-phase HPLC (gradient: 5% B for 1 min, 5-23% B in 3 min, 23-28% B in 15 min, Waters CSH C18 column) to afford the desired peptide as a white fluffy solid. Yield (13 mg) in > 95% purity according to analytical UPLC. Rt 5.13 min (3-60% B in 10 min).

[M + 2H]²⁺ calculated for C₈₄H₁₁₂N₁₇O₃₂PS, 1051.1; found 1051.1.

FITC labelled GR_pS226:

FITC labelled GR_pS226 peptide was prepared following General Protocol for SPPS. The crude peptide was purified by reverse-phase HPLC (gradient: 5% B for 1 min, 5-29% B in 3 min, 29-34% B in 15 min, Waters CSH

C18 column) to afford the desired peptide as a white fluffy solid. Yield (17 mg) in > 95% purity according to analytical UPLC. Rt 6.95 min (3-60% B in 10 min).

$[M + 2H]^{2+}$ calculated for $C_{83}H_{113}N_{16}O_{33}PS_2$, 979.5; found 979.6.

FITC labelled GR_pS234:

FITC labelled GR_pS234 peptide was prepared following General Protocol for SPPS. The crude peptide was purified by reverse-phase HPLC (gradient: 5% B for 1 min, 5-30% B in 3 min, 30-35% B in 15 min, Waters CSH C18 column) to afford the desired peptide as a white fluffy solid. Yield (27 mg) in > 95% purity according to analytical UPLC. Rt 7.28 min (3-60% B in 10 min).

$[M + 2H]^{2+}$ calculated for $C_{86}H_{113}N_{16}O_{33}PS$, 981.5; found 981.6.

FITC labelled GR_pS267:

FITC labelled GR_pS267 peptide was prepared following General Protocol for SPPS. The crude peptide was purified by reverse-phase HPLC (gradient: 5% B for 1 min, 5-29% B in 3 min, 29-34% B in 15 min, Waters CSH C18 column) to afford the desired peptide as a white fluffy solid. Yield (8 mg) in > 95% purity according to analytical UPLC. Rt 7.07 min (3-60% B in 10 min).

$[M + 2H]^{2+}$ calculated for $C_{83}H_{119}N_{16}O_{30}PS$, 942.5; found 942.7.

FITC labelled GR_pS404:

FITC labelled GR_pS404 peptide was prepared following General Protocol for SPPS. The crude peptide was purified by reverse-phase HPLC (gradient: 5% B for 1 min, 5-22% B in 3 min, 22-27% B in 15 min, Waters CSH C18 column) to afford the desired peptide as a white fluffy solid. Yield (16 mg) in > 95% purity according to analytical UPLC. Rt 5.33 min (3-60% B in 10 min).

$[M + 2H]^{2+}$ calculated for $C_{80}H_{111}N_{18}O_{31}PS_2$, 958.5; found 958.6.

Acetylated GR_pT493:

Acetylated GR_pT493 peptide was prepared following General Protocol for SPPS. The crude peptide was purified by reverse-phase HPLC (gradient: 0% B for 4min, 0-15% B in 15min, Waters Atlantis T3 column) to afford the desired peptide as a white fluffy solid. Yield (61 mg) in > 95% purity according to analytical UPLC. Rt 1.41 min (3-60% B in 10 min).

$[M + 2H]^{2+}$ calculated for $C_{68}H_{127}N_{22}O_{22}P$, 818.4; found 818.6.

FITC labelled GR_pT493:

FITC labelled GR_pT493 peptide was prepared following General Protocol for SPPS. The crude peptide was purified by reverse-phase HPLC (gradient: 5% B for 1 min, 5-18% B in 3 min, 18-23% B in 15 min, Waters Atlantis T3 column) to afford the desired peptide as a white fluffy solid. Yield (25 mg) in > 95% purity according to analytical UPLC. Rt 3.33 min (3-60% B in 10 min).

$[M + 2H]^{2+}$ calculated for $C_{93}H_{147}N_{24}O_{27}PS$, 1048.7; found 1049.3.

Acetylated GR_pT524:

Acetylated GR_pT524 peptide was prepared following General Protocol for SPPS. The crude peptide was purified by reverse-phase HPLC (gradient: 5% B for 1 min, 22-40% B in 25 min, Kromasil C18 column) to afford the desired peptide as a white fluffy solid. Yield (34 mg) in > 95% purity according to analytical UPLC. Rt 4.96 min (3-60% B in 10 min).

Phosphopeptide Investigation for the Characterisation of the Glucocorticoid Receptor–14-3-3 Protein-Protein Interaction

$[M + H]^+$ calculated for $C_{66}H_{114}N_{15}O_{22}P$, 1501.7; found 1501.7.

FITC labelled GR_pt524:

FITC labelled GR_pt524 peptide was prepared following General Protocol for SPPS. The crude peptide was purified by reverse-phase HPLC (gradient: 5% B for 1 min, 31-45% B in 30 min, Kromasil C18 column) to afford the desired peptide as a white fluffy solid. Yield (19 mg) in > 95% purity according to analytical UPLC. Rt 6.31 min (3-60% B in 10 min).

$[M + H]^+$ calculated for $C_{91}H_{134}N_{17}O_{27}PS$, 1962.2; found 1962.8.

Acetylated GR_pt561:

Acetylated GR_pt561 peptide was prepared following General Protocol for SPPS. The crude peptide was purified by reverse-phase HPLC (gradient: 5% B for 1 min, 10-50% B in 25 min, Kromasil C18 column) to afford the desired peptide as a white fluffy solid. Yield (18 mg) in 94% purity according to analytical UPLC. Rt 6.39 min (3-60% B in 10 min).

$[M + H]^+$ calculated for $C_{66}H_{114}N_{15}O_{22}P$, 1646.8; found 1646.7.

FITC labelled GR_pt561:

FITC labelled GR_pt561 peptide was prepared following General Protocol for SPPS. The crude peptide was purified by reverse-phase HPLC (gradient: 5% B for 1 min, 5-33% B in 3 min, 33-38% B in 15 min, Waters Xselect CSH C18 column) to afford the desired peptide as a white fluffy solid. Yield (4 mg) in > 95% purity according to analytical UPLC. Rt 7.55 min (3-60% B in 10 min).

$[M + 2H]^{2+}$ calculated for $C_{93}H_{133}N_{20}O_{28}PS_3$, 1053.7; found 1053.7.

Acetylated GR_ps617:

Acetylated GR_ps617 peptide was prepared following General Protocol for SPPS. The crude peptide was purified by reverse-phase HPLC (gradient: 5% B for 1 min, 20-28% B in 35 min, Kromasil C18 column) to afford the desired peptide as a white fluffy solid. Yield (10 mg) in > 95% purity according to analytical UPLC. Rt 4.46 min (3-60% B in 10 min).

$[M + H]^+$ calculated for $C_{68}H_{108}N_{21}O_{24}PS$, 1667.8; found 1667.3.

FITC labelled GR_ps617:

FITC labelled GR_ps617 peptide was prepared following General Protocol for SPPS. The crude peptide was purified by reverse-phase HPLC (gradient: 5% B for 1 min, 26-35% B in 25 min, Kromasil C18 column) to afford the desired peptide as a white fluffy solid. Yield (32 mg) in > 95% purity according to analytical UPLC. Rt 5.82 min (3-60% B in 10 min).

$[M + 2H]^{2+}$ calculated for $C_{93}H_{128}N_{23}O_{29}PS_2$, 1064.1; found 1064.7.

Acetylated GR_pt635:

Acetylated GR_pt635 peptide was prepared following General Protocol for SPPS. The crude peptide was purified by reverse-phase HPLC (gradient: 5% B for 1 min, 5-15% B in 3 min, 15-20% B in 15 min, Waters Xselect CSH C18 column) to afford the desired peptide as a white fluffy solid. Yield (17 mg) in > 95% purity according to analytical UPLC. Rt 4.89 min (3-60% B in 10 min).

$[M + H]^+$ calculated for $C_{69}H_{111}N_{18}O_{26}PS_3$, 1736.9; found 1735.6.

FITC labelled GR_pT635:

FITC labelled GR_pT635 peptide was prepared following General Protocol for SPPS. The crude peptide was purified by reverse-phase HPLC (gradient: 5% B for 1 min, 31-33 % B in 15 min, Kromasil C18 column) to afford the desired peptide as a white fluffy solid. Yield (10 mg) in 95% purity according to analytical UPLC. Rt 6.48 min (3-60% B in 10 min).

$[M + 2H]^{2+}$ calculated for $C_{94}H_{131}N_{20}O_{31}PS_4$, 1098.7; found 1099.2.

Acetylated GR_pT524-pS617:

Acetylated GR_pT524-pS617 peptide was prepared following General Protocol for SPPS. The crude peptide was purified by reverse-phase HPLC (gradient: 5% B for 1 min, 5-23% B in 3min, 23-28% B in 15min, Waters Xselect CSH C18 column) to afford the desired peptide as a white fluffy solid. Yield (38 mg) in > 95% purity according to analytical UPLC. Rt 5.40 min (3-60% B in 10 min).

$[M + 3H]^{3+}$ calculated for $C_{142}H_{233}N_{41}O_{49}P_2S$, 1131.6; found 1131.4.

FITC labelled GR_pT524-pS617:

FITC labelled GR_pT524-pS617 peptide was prepared following General Protocol for SPPS. The crude peptide was purified by reverse-phase HPLC (gradient: 5% B for 1 min, 5-29% B in 3min, 29-34% B in 15min, Waters Atlantis T3 column) to afford the desired peptide as a white fluffy solid. Yield (30 mg) in > 95% purity according to analytical UPLC. Rt 4.18 min (5-95% B in 10 min).

$[M + 3H]^{3+}$ calculated for $C_{167}H_{253}N_{43}O_{54}P_2S_2$, 1285.1; found 1285.3.

FITC labelled GR_pS83-pT524:

FITC labelled GR_pS83-pT524 peptide was prepared following General Protocol for SPPS. The crude peptide was purified by reverse-phase HPLC (gradient: 5% B for 1 min, 5-27% B in 3min, 27-32% B in 15min, Waters Xselect CSH C18 column) to afford the desired peptide as a white fluffy solid. Yield (7 mg) in > 95% purity according to analytical UPLC. Rt 7.28 min (10-50% B in 10 min).

$[M + 3H]^{3+}$ calculated for $C_{162}H_{250}N_{36}O_{54}P_2S_2$, 1231.3; found 1230.8.

FAM labelled GR_pS134-pT524:

FAM labelled GR_pS134-pT524 peptide was purchased from Thermo Scientific with a purity over 95%.

FAM labelled GR_pS83-pS134:

FAM labelled GR_pS83-pS134 peptide was purchased from Thermo Scientific with a purity over 95%.

FITC labelled GR_K518A:

FITC labelled GR_K518A peptide was prepared following General Protocol for SPPS. The crude peptide was purified by reverse-phase HPLC (gradient: 5% B for 1 min, 5-30% B in 3min, 30-35% B in 15min, Waters Xselect CSH C18 column) to afford the desired peptide as a white fluffy solid. Yield (11 mg) in > 95% purity according to analytical UPLC. Rt 7.09 min (3-60% B in 10 min).

$[M + 3H]^{3+}$ calculated for $C_{164}H_{246}N_{42}O_{54}P_2S_2$, 1266.0; found 1266.0.

FITC labelled GR_T519A:

FITC labelled GR_T519A peptide was prepared following General Protocol for SPPS. The crude peptide was purified by reverse-phase HPLC (gradient: 5% B for 1 min, 31-40% B in 30min, Kromasil C18 column) to afford the desired

peptide as a white fluffy solid. Yield (3 mg) in > 95% purity according to analytical UPLC. Rt 4.30 min (5-95% B in 10 min).

[M + 3H]³⁺ calculated for C₁₆₆H₂₅₁N₄₃O₅₃P₂S₂, 1275.0; found 1276.3.

FITC labelled GR_I520A:

FITC labelled GR_I520A peptide was prepared following General Protocol for SPPS. The crude peptide was purified by reverse-phase HPLC (gradient: 5% B for 1 min, 5-29% B in 3 min, 29-34% B in 15min, Waters Atlantis T3 column) to afford the desired peptide as a white fluffy solid. Yield (13 mg) in > 95% purity according to analytical UPLC. Rt 6.14 min (3-60% B in 10 min).

[M + 3H]³⁺ calculated for C₁₆₄H₂₄₇N₄₃O₅₄P₂S₂, 1271.0; found 1271.1.

FITC labelled GR_V521A:

FITC labelled GR_V521A peptide was prepared following General Protocol for SPPS. The crude peptide was purified by reverse-phase HPLC (gradient: 5% B for 1 min, 5-29% B in 3 min, 29-34% B in 15min, Waters Atlantis T3 column) to afford the desired peptide as a white fluffy solid. Yield (2 mg) in > 95% purity according to analytical UPLC. Rt 6.24 min (3-60% B in 10 min).

[M + 3H]³⁺ calculated for C₁₆₅H₂₄₉N₄₃O₅₄P₂S₂, 1275.7; found 1275.1.

FITC labelled GR_P522A:

FITC labelled GR_P522A peptide was prepared following General Protocol for SPPS. The crude peptide was purified by reverse-phase HPLC (gradient: 5% B for 1 min, 5-29% B in 3 min, 29-34% B in 15min, Waters Atlantis T3 column) to afford the desired peptide as a white fluffy solid. Yield (13 mg) in > 95% purity according to analytical UPLC. Rt 4.22 min (5-95% B in 10 min).

[M + 3H]³⁺ calculated for C₁₆₅H₂₅₁N₄₃O₅₄P₂S₂, 1276.4; found 1276.4.

FITC labelled GR_T524A-pS617:

FITC labelled GR_T524A-pS617 peptide was prepared following General Protocol for SPPS. The crude peptide was purified by reverse-phase HPLC (gradient: 5% B for 1 min, 34-37% B in 25 min, Kromasil C18 column) to afford the desired peptide as a white fluffy solid. Yield (8 mg) in > 95% purity according to analytical UPLC. Rt 6.11 min (3-60% B in 10 min).

[M + 3H]³⁺ calculated for C₁₆₆H₂₅₀N₄₃O₅₀PS₂, 1248.4; found 1249.2.

FITC labelled GR_L525A:

FITC labelled GR_L525A peptide was prepared following General Protocol for SPPS. The crude peptide was purified by reverse-phase HPLC (gradient: 5% B for 1 min, 5-28% B in 3 min, 28-33% B in 15min, Waters Atlantis T3 column) to afford the desired peptide as a white fluffy solid. Yield (20 mg) in > 95% purity according to analytical UPLC. Rt 4.05 min (5-95% B in 10 min).

[M + 3H]³⁺ calculated for C₁₆₄H₂₄₇N₄₃O₅₄P₂S₂, 1271.0; found 1271.1.

FITC labelled GR_P526A:

FITC labelled GR_P526A peptide was prepared following General Protocol for SPPS. The crude peptide was purified by reverse-phase HPLC (gradient: 5% B for 1 min, 5-30% B in 3 min, 30-35% B in 15min, Waters Atlantis T3 column) to afford the desired peptide as a white fluffy solid. Yield (3 mg) in > 95% purity according to analytical UPLC. Rt 6.49 min (3-60% B in 10 min).

$[M + 3H]^{3+}$ calculated for $C_{165}H_{251}N_{43}O_{54}P_2S_2$, 1276.4; found 1276.4.

FITC labelled GR_Q527A:

FITC labelled GR_Q527A peptide was prepared following General Protocol for SPPS. The crude peptide was purified by reverse-phase HPLC (gradient: 5% B for 1 min, 5-31% B in 3 min, 31-36% B in 15min, Waters Atlantis T3 column) to afford the desired peptide as a white fluffy solid. Yield (5 mg) in > 95% purity according to analytical UPLC. Rt 6.53 min (3-60% B in 10 min).

$[M + 3H]^{3+}$ calculated for $C_{165}H_{250}N_{42}O_{53}P_2S_2$, 1266.0; found 1266.1.

FITC labelled GR_L528A:

FITC labelled GR_L528A peptide was prepared following General Protocol for SPPS. The crude peptide was purified by reverse-phase HPLC (gradient: 5% B for 1 min, 5-27% B in 3 min, 27-32% B in 15min, Waters XSelect CSH C18 column) to afford the desired peptide as a white fluffy solid. Yield (18 mg) in > 95% purity according to analytical UPLC. Rt 6.16 min (3-60% B in 10 min).

$[M + 3H]^{3+}$ calculated for $C_{164}H_{247}N_{43}O_{54}P_2S_2$, 1271.0; found 1270.5.

FITC labelled GR_T529A:

FITC labelled GR_T529A peptide was prepared following General Protocol for SPPS. The crude peptide was purified by reverse-phase HPLC (gradient: 5% B for 1 min, 5-30% B in 3 min, 30-35% B in 15min, Waters Atlantis T3 column) to afford the desired peptide as a white fluffy solid. Yield (13 mg) in > 95% purity according to analytical UPLC. Rt 6.43 min (3-60% B in 10 min).

$[M + 3H]^{3+}$ calculated for $C_{166}H_{251}N_{43}O_{53}P_2S_2$, 1275.0; found 1275.6.

FITC labelled GR_P530A:

FITC labelled GR_P530A peptide was prepared following General Protocol for SPPS. The crude peptide was purified by reverse-phase HPLC (gradient: 5% B for 1 min, 5-30% B in 3 min, 30-35% B in 15min, Waters CSH C18 column) to afford the desired peptide as a white fluffy solid. Yield (8 mg) in 95% purity according to analytical UPLC. Rt 6.30 min (3-60% B in 10 min).

$[M + 3H]^{3+}$ calculated for $C_{165}H_{251}N_{43}O_{54}P_2S_2$, 1276.4; found 1275.9.

FITC labelled GR_R611A:

FITC labelled GR_R611A peptide was prepared following General Protocol for SPPS. The crude peptide was purified by reverse-phase HPLC (gradient: 5% B for 1 min, 5-29% B in 3 min, 29-34% B in 15min, Waters CSH C18 column) to afford the desired peptide as a white fluffy solid. Yield (2 mg) in > 95% purity according to analytical UPLC. Rt 6.74 min (3-60% B in 10 min).

$[M + 3H]^{3+}$ calculated for $C_{164}H_{246}N_{40}O_{54}P_2S_2$, 1256.7; found 1256.1.

FITC labelled GR_S612A:

FITC labelled GR_S612A peptide was prepared following General Protocol for SPPS. The crude peptide was purified by reverse-phase HPLC (gradient: 5% B for 1 min, 5-28% B in 3 min, 28-33% B in 15min, Waters CSH C18 column) to afford the desired peptide as a white fluffy solid. Yield (8 mg) in > 95% purity according to analytical UPLC. Rt 6.36 min (3-60% B in 10 min).

$[M + 3H]^{3+}$ calculated for $C_{167}H_{253}N_{43}O_{53}P_2S_2$, 1279.7; found 1279.2.

FITC labelled GR_Y613A:

FITC labelled GR_Y613A peptide was prepared following General Protocol for SPPS. The crude peptide was purified by reverse-phase HPLC (gradient: 5% B for 1 min, 5-27% B in 3 min, 27-32% B in 15min, Waters CSH C18 column) to afford the desired peptide as a white fluffy solid. Yield (6 mg) in > 95% purity according to analytical UPLC. Rt 6.30 min (3-60% B in 10 min).

[M + 3H]³⁺ calculated for C₁₆₁H₂₄₉N₄₃O₅₃P₂S₂, 1254.3; found 1253.7.

FITC labelled GR_R614A:

FITC labelled GR_R614A peptide was prepared following General Protocol for SPPS. The crude peptide was purified by reverse-phase HPLC (gradient: 5% B for 1 min, 5-31% B in 3 min, 31-36% B in 15min, Waters Atlantis T3 column) to afford the desired peptide as a white fluffy solid. Yield (1 mg) in > 95% purity according to analytical UPLC. Rt 6.83 min (3-60% B in 10 min).

[M + 3H]³⁺ calculated for C₁₆₄H₂₄₆N₄₀O₅₄P₂S₂, 1256.7; found 1256.9.

FITC labelled GR_Q615A:

FITC labelled GR_Q615A peptide was prepared following General Protocol for SPPS. The crude peptide was purified by reverse-phase HPLC (gradient: 5% B for 1 min, 25-35 % B in 35 min, Kromasil C18 column) to afford the desired peptide as a white fluffy solid. Yield (7 mg) in > 95% purity according to analytical UPLC. Rt 6.39 min (3-60% B in 10 min).

[M + 3H]³⁺ calculated for C₁₆₅H₂₅₀N₄₂O₅₃P₂S₂, 1266.0; found 1266.9.

FITC labelled GR_S616A:

FITC labelled GR_S616A peptide was prepared following General Protocol for SPPS. The crude peptide was purified by reverse-phase HPLC (gradient: 5% B for 1 min, 5-29% B in 3 min, 29-34% B in 15min, Waters Atlantis T3 column) to afford the desired peptide as a white fluffy solid. Yield (16 mg) in > 95% purity according to analytical UPLC. Rt 4.29 min (5-95% B in 10 min).

[M + 3H]³⁺ calculated for C₁₆₇H₂₅₃N₄₃O₅₃P₂S₂, 1279.7; found 1279.8.

FITC labelled GR_pT524-S617A:

FITC labelled GR_pT524-S617A peptide was prepared following General Protocol for SPPS. The crude peptide was purified by reverse-phase HPLC (gradient: 5% B for 1 min, 34-37% B in 25 min, Kromasil C18 column) to afford the desired peptide as a white fluffy solid. Yield (2 mg) in > 95% purity according to analytical UPLC. Rt 6.17 min (3-60% B in 10 min).

[M + 3H]³⁺ calculated for C₁₆₇H₂₅₂N₄₃O₅₀P₂S₂, 1253.1; found 1253.8.

FITC labelled GR_N619A:

FITC labelled GR_N619A peptide was prepared following General Protocol for SPPS. The crude peptide was purified by reverse-phase HPLC (gradient: 5% B for 1 min, 26-34% B in 35min, Kromasil C18 column) to afford the desired peptide as a white fluffy solid. Yield (9 mg) in > 95% purity according to analytical UPLC. Rt 6.41 min (3-60% B in 10 min).

[M + 3H]³⁺ calculated for C₁₆₆H₂₅₂N₄₂O₅₃P₂S₂, 1270.7; found 1271.4.

FITC labelled GR_L620A:

FITC labelled GR_L620A peptide was prepared following General Protocol for SPPS. The crude peptide was purified by reverse-phase HPLC (gradient: 5% B for 1 min, 5-29% B in 3 min, 29-34% B in 15min, Waters Atlantis T3 column) to afford the desired peptide as a white fluffy solid. Yield (1 mg) in > 95% purity according to analytical UPLC. Rt 6.16 min (3-60% B in 10 min).

$[M + 3H]^{3+}$ calculated for $C_{164}H_{247}N_{43}O_{54}P_2S_2$, 1271.0; found 1270.6.

FITC labelled GR_L621A:

FITC labelled GR_L621A peptide was prepared following General Protocol for SPPS. The crude peptide was purified by reverse-phase HPLC (gradient: 5% B for 1 min, 5-26% B in 3 min, 26-31% B in 15min, Waters CSH C18 column) to afford the desired peptide as a white fluffy solid. Yield (9 mg) in > 95% purity according to analytical UPLC. Rt 6.01 min (3-60% B in 10 min).

$[M + 3H]^{3+}$ calculated for $C_{164}H_{247}N_{43}O_{54}P_2S_2$, 1271.0; found 1271.0.

FITC labelled GR_C622A:

FITC labelled GR_C622A peptide was prepared following General Protocol for SPPS. The crude peptide was purified by reverse-phase HPLC (gradient: 5% B for 1 min, 5-27% B in 3 min, 27-32% B in 15min, Waters CSH C18 column) to afford the desired peptide as a white fluffy solid. Yield (5 mg) in > 95% purity according to analytical UPLC. Rt 6.24 min (3-60% B in 10 min).

$[M + 3H]^{3+}$ calculated for $C_{167}H_{253}N_{43}O_{54}P_2S$, 1274.4; found 1273.6.

FITC labelled GR_F623A:

FITC labelled GR_F623A peptide was prepared following General Protocol for SPPS. The crude peptide was purified by reverse-phase HPLC (gradient: 5% B for 1 min, 5-25% B in 3 min, 25-30% B in 15min, Waters CSH C18 column) to afford the desired peptide as a white fluffy solid. Yield (10 mg) in > 95% purity according to analytical UPLC. Rt 5.91 min (3-60% B in 10 min).

$[M + 3H]^{3+}$ calculated for $C_{161}H_{249}N_{43}O_{54}P_2S_2$, 1259.7; found 1259.1.

FITC labelled GR_pS524-pS617:

FITC labelled GR_pS524-pS617 peptide was prepared following General Protocol for SPPS. The crude peptide was purified by reverse-phase HPLC (gradient: 5% B for 1 min, 5-29% B in 3 min, 29-34% B in 15min, Waters Atlantis T3 column) to afford the desired peptide as a white fluffy solid. Yield (8 mg) in > 95% purity according to analytical UPLC. Rt 4.31 min (5-95% B in 10 min).

$[M + 3H]^{3+}$ calculated for $C_{166}H_{251}N_{43}O_{54}P_2S_2$, 1280.4; found 1280.7.

Acetylated selenomethionine containing GR peptide (GR_pT524-pS617_C622SeM):

Acetylated GR_pT524-pS617_C622SeM peptide was prepared following General Protocol for SPPS. The crude peptide was purified by reverse-phase HPLC to afford the desired peptide as a white fluffy solid. Yield (13 mg) in 93% purity according to analytical UPLC. Rt 3.42 min (3-93% B in 10 min).

$[M + 3H]^{3+}$ calculated for $C_{144}H_{237}N_{41}O_{49}P_2Se$, 1156.2; found 1157.1.

Phosphopeptide Investigation for the Characterisation of the Glucocorticoid Receptor–14-3-3 Protein-Protein Interaction

Table 2.S1. Data collection and refinement statistics (molecular replacement)

	GR_pT524–14-3-3 ζ ¹	GR_pS617–14-3-3 ζ ²	GR_pT524-pS617–14-3-3 ζ ³
Data collection			
Space group	C121	P2 ₁ 2 ₁ 2 ₁	P 4 ₃ 2 ₁ 2
Cell dimensions			
<i>a</i> , <i>b</i> , <i>c</i> (Å)	158.65, 99.88, 84.81	72.28, 104.35, 112.43	60.21, 60.21, 284.21
α , β , γ (°)	90.00, 93.73, 90.00	90.00, 90.00, 90.00	90.00, 90.00, 90.00
Resolution (Å)	84.47-2.09 (2.12-2.09)	47.33-2.02 (2.02-2.07)	58.90-2.75 (2.90-2.75)
<i>R</i> _{merge}	0.06	0.08	0.11
<i>I</i> / σ <i>I</i>	9.0 (0.6)	12.07 (0.53)	12.4 (1.3)
Completeness (%)	98.3 (97.8)	99.6 (95.8)	98.3 (94.0)
Redundancy	3.4 (3.4)	6.5 (6.3)	9.4 (6.9)
Refinement			
Resolution (Å)	60.85-2.09	47.33-2.02	58.90-2.75
No. reflections	76,616	56,503	14,250
<i>R</i> _{work} / <i>R</i> _{free}	0.224 / 0.235	0.212 / 0.228	0.268 / 0.291
No. atoms			
Protein	7,693	3,769	3,690
Ligand/ion	0	25	0
Water	240	236	0
<i>B</i> -factors			
Protein	76.7	78.2	92.8
Ligand/ion	-	59.5	-
Water	68.0	68.9	-
R.m.s. deviations			
Bond lengths (Å)	0.72	0.49	0.95
Bond angles (°)	0.69	0.60	0.88

*Values in parentheses are for highest-resolution shell

¹ One xtal for the GR_pT524–14-3-3 ζ structure

² One xtal for the GR_pS617–14-3-3 ζ structure

³ One xtal for the GR_pT524-pS617–14-3-3 ζ structure

2.7. References

1. Kino, T. GR-regulating Serine/Threonine Kinases: New Physiologic and Pathologic Implications. *Trends Endocrinol. Metab.* **29**, 260–270 (2018).
2. Cain, D. W. & Cidlowski, J. A. Immune regulation by glucocorticoids. *Nat. Rev. Immunol.* **17**, 233–247 (2017).
3. Souffriau, J. *et al.* A screening assay for Selective Dimerizing Glucocorticoid Receptor Agonists and Modulators (SEDIGRAM) that are effective against acute inflammation. *Sci. Rep.* **8**, 12894 (2018).
4. Kuna, P. *et al.* Efficacy and Tolerability of an Inhaled Selective Glucocorticoid Receptor Modulator – AZD5423 – in Chronic Obstructive Pulmonary Disease Patients: Phase II Study Results. *Basic Clin. Pharmacol. Toxicol.* **121**, 279–289 (2017).
5. Scheschowitsch, K., Leite, J. A. & Assreuy, J. New insights in glucocorticoid receptor signaling-more than just a ligand-binding receptor. *Frontiers in Endocrinology* **8**, 16 (2017).
6. Weikum, E. R., Knuesel, M. T., Ortlund, E. A. & Yamamoto, K. R. Glucocorticoid receptor control of transcription: Precision and plasticity via allosterity. *Nat. Rev. Mol. Cell Biol.* **18**, 159–174 (2017).
7. Deroo, B. J. *et al.* Proteasomal Inhibition Enhances Glucocorticoid Receptor Transactivation and Alters Its Subnuclear Trafficking. *Mol. Cell. Biol.* **22**, 4113–4123 (2002).
8. Pennington, K., Chan, T., Torres, M. & Andersen, J. The dynamic and stress-adaptive signaling hub of 14-3-3: emerging mechanisms of regulation and context-dependent protein–protein interactions. *Oncogene* **37**, 5587–5604 (2018).
9. Johnson, C. *et al.* Bioinformatic and experimental survey of 14-3-3-binding sites. *Biochem. J.* **427**, 69–78 (2010).
10. Rubio, M. P. *et al.* 14-3-3-affinity purification of over 200 human phosphoproteins reveals new links to regulation of cellular metabolism, proliferation and trafficking. *Biochem. J.* **379**, 395–408 (2004).
11. De Vries-van Leeuwen, I. J. *et al.* Interaction of 14-3-3 proteins with the Estrogen Receptor Alpha F domain provides a drug target interface. *Proc. Natl. Acad. Sci. U. S. A.* **110**, 8894–8899 (2013).
12. Kim, D. K. *et al.* PKB/Akt phosphorylation of ERR γ contributes to insulin-mediated inhibition of hepatic gluconeogenesis. *Diabetologia* **57**, 2576–2585 (2014).
13. Kim, S. W. *et al.* Role of 14-3-3 sigma in over-expression of P-gp by rifampin and paclitaxel stimulation through interaction with PXR. *Cell. Signal.* **31**, 124–134 (2017).

14. Wakui, H., Wright, A. P. H., Gustafsson, J. & Zilliacus, J. Interaction of the Ligand-activated Glucocorticoid Receptor with the 14-3-3 η Protein. *J. Biol. Chem.* **272**, 8153–8156 (1997).
15. Widén, C., Zilliacus, J., Gustafsson, J. Å. & Wikström, A. C. Glucocorticoid Receptor Interaction with 14-3-3 and Raf-1, a Proposed Mechanism for Cross-Talk of Two Signal Transduction Pathways. *J. Biol. Chem.* **275**, 39296–39301 (2000).
16. Kim, Y. S. *et al.* Role of 14-3-3 η as a Positive Regulator of the Glucocorticoid Receptor Transcriptional Activation. *Endocrinology* **146**, 3133–3140 (2005).
17. Hwang, Y., An, H. T., Kang, M. & Ko, J. Roles of 14-3-3 β and γ in regulation of the glucocorticoid receptor transcriptional activation and hepatic gluconeogenesis. *Biochem. Biophys. Res. Commun.* **501**, 800–806 (2018).
18. Gallihier-Beckley, A. J., Williams, J. G. & Cidlowski, J. A. Ligand-Independent Phosphorylation of the Glucocorticoid Receptor Integrates Cellular Stress Pathways with Nuclear Receptor Signaling. *Mol. Cell. Biol.* **31**, 4663–4675 (2011).
19. Kino, T. *et al.* Protein 14-3-3 σ Interacts With and Favors Cytoplasmic Subcellular Localization of the Glucocorticoid Receptor, Acting as a Negative Regulator of the Glucocorticoid Signaling Pathway. *J. Biol. Chem.* **278**, 25651–25656 (2003).
20. Habib, T. *et al.* AKT1 has dual actions on the glucocorticoid receptor by cooperating with 14-3-3. *Mol. Cell. Endocrinol.* **439**, 431–443 (2017).
21. Ge, Q. *et al.* Structural characterization of a unique interface between carbohydrate response element-binding protein (ChREBP) and 14-3-3 β protein. *J. Biol. Chem.* **287**, 41914–41921 (2012).
22. Henriksson, M. L. *et al.* A nonphosphorylated 14-3-3 binding motif on exoenzyme S that is functional in vivo. *Eur. J. Biochem.* **269**, 4921–4929 (2002).
23. Madeira, F. *et al.* 14-3-3-Pred: improved methods to predict 14-3-3-binding phosphopeptides. *Bioinformatics* **31**, 2276–2283 (2015).
24. Vandevyver, S., Dejager, L. & Libert, C. Comprehensive overview of the structure and regulation of the glucocorticoid receptor. *Endocr. Rev.* **35**, 671–693 (2014).
25. Stevers, L. M. *et al.* Characterization and small-molecule stabilization of the multisite tandem binding between 14-3-3 and the R domain of CFTR. *Proc. Natl. Acad. Sci. U. S. A.* **113**, E1152–E1161 (2016).
26. Bier, D. *et al.* Small-Molecule Stabilization of the 14-3-3/Gab2 Protein-Protein Interaction (PPI) Interface. *ChemMedChem* **11**, 911–918 (2016).
27. Molzan, M. & Ottmann, C. Synergistic binding of the phosphorylated S233- and S259-

- binding sites of C-RAF to One 14-3-3 ζ dimer. *J. Mol. Biol.* **423**, 486–495 (2012).
28. Kostecky, B., Saurin, A. T., Purkiss, A., Parker, P. J. & McDonald, N. Q. Recognition of an intra-chain tandem 14-3-3 binding site within PKC ϵ . *EMBO Rep.* **10**, 983–989 (2009).
 29. Obsil, T., Ghirlando, R., Klein, D. C., Ganguly, S. & Dyda, F. Crystal Structure of the 14-3-3 ζ :Serotonin N-Acetyltransferase Complex: A Role for Scaffolding in Enzyme Regulation. *Cell* **105**, 257–267 (2001).
 30. Stevers, L. M., de Vink, P. J., Ottmann, C., Huskens, J. & Brunsveld, L. A Thermodynamic Model for Multivalency in 14-3-3 Protein–Protein Interactions. *J. Am. Chem. Soc.* **140**, 14498–14510 (2018).
 31. Stevenson Flemer Jr. Fmoc-Sec(Xan)-OH: Synthesis and Utility of Fmoc Selenocysteine SPPS Derivatives with Acid-Labile Sidechain Protection. *J Pept Sci.* **21**, 53–59 (2015).
 32. Attard, T. J., O’Brien-Simpson, N. M. & Reynolds, E. C. Identification and suppression of β -elimination byproducts arising from the use of Fmoc-Ser(PO₃Bzl,H)-OH in peptide synthesis. *Int. J. Pept. Res. Ther.* **15**, 69–79 (2009).
 33. Lukszo, J., Patterson, D., Albericio, F. & Kates, S. A. 3-(1-Piperidinyl)alanine formation during the preparation of C-terminal cysteine peptides with the Fmoc/t-Bu strategy. *Lett. Pept. Sci.* **3**, 157–166 (1996).
 34. Sluchanko, N. N. & Bustos, D. M. Intrinsic disorder associated with 14-3-3 proteins and their partners. in *Progress in Molecular Biology and Translational Science* **166**, 19–61 (Elsevier Inc., Cambridge, 2019).
 35. Edman, K. *et al.* Ligand Binding Mechanism in Steroid Receptors: From Conserved Plasticity to Differential Evolutionary Constraints. *Structure* **23**, 2280–2290 (2015).
 36. Li, J., Fu, J., Toumazou, C., Yoon, H. G. & Wong, J. A Role of the Amino-Terminal (N) and Carboxyl-Terminal (C) Interaction in Binding of Androgen Receptor to Chromatin. *Mol. Endocrinol.* **20**, 776–785 (2006).
 37. Pippal, J. B., Yao, Y., Rogerson, F. M. & Fuller, P. J. Structural and Functional Characterization of the Interdomain interaction in the Mineralocorticoid Receptor. *Mol. Endocrinol.* **23**, 1360–1370 (2009).
 38. Aghazadeh, Y. & Papadopoulos, V. The role of the 14-3-3 protein family in health, disease, and drug development. *Drug Discov. Today* **21**, 278–287 (2016).
 39. Benzinger, A. *et al.* The crystal structure of the non-liganded 14-3-3 σ protein: Insights into determinants of isoform specific ligand binding and dimerization. *Cell Res.* **15**, 219–227 (2005).

40. Wilkert, E. W., Grant, R. A., Artim, S. C. & Yaffe, M. B. A structural basis for 14-3-3 σ functional specificity. *J. Biol. Chem.* **280**, 18891–18898 (2005).

Chapter 3

Activation of MINK1 Induces 14-3-3 Regulation of Glucocorticoid Receptor Through Protein-Protein Interaction

Abstract

Phosphorylation of the ligand-dependent transcription factor GR by serine/threonine kinases provides another level of GR regulation, beside direct ligand binding, by modulating GR signalling and transcriptional activity. The family of regulatory proteins, 14-3-3s, recognize and bind GR upon GR phosphorylation. Previous studies, however, have reported multiple potential phosphorylation sites and different kinases affecting the activity of GR. In chapter 2, GR phosphopeptides, biophysical experiments, X-ray crystallography and alanine scanning were used to identify two key residues, T534 and S617, located in the ligand binding domain of GR, whose phosphorylation triggers interaction with 14-3-3. Here, I sought to investigate longer GR constructs. Investigation of the kinases responsible for phosphorylation of these sites identified a key role for MINK1. Cell-based approaches confirmed the importance of these two GR phosphosites and MINK1 in GR–14-3-3 binding. Together our results provide a molecular-level insight into 14-3-3 regulation of GR and highlight both MINK1 and the GR–14-3-3 axis as potential targets for future therapeutic intervention.

3.1. Introduction

As mentioned in chapter 2 the ligand-dependent transcription factor GR mediates the actions of glucocorticoids, a class of steroid hormones (cortisol and close analogues) produced by the adrenal cortex, which influence a large array of fundamental processes including, notably, the inflammatory response^{1,2}. In addition to the modulation of GR by ligand binding, GR activity is further regulated by posttranslational modifications (PTMs) such as acetylation, nitrosylation, oxidation, SUMOylation, ubiquitination and phosphorylation. These PTMs add another layer of complexity in GR regulation, providing a tool to fine-tune GR activity and for a cell/tissue-specific GR signalling. About 20 sites, where PTMs occur, have been identified in the GR sequence^{3,4}. For example, GR transcriptional activity is regulated by histone acetyltransferases and histone deacetylases through acetylation/deacetylation of residues located in the hinge region, such as K494 and K495^{5,6}. SUMOylation, characterised by the addition of a small ubiquitin-related modifier-1 (SUMO-1) to a lysine residue, affects GR stability and GR transcriptional activity^{7,8}. Ubiquitination at L419 affects GR stability *via* the enzyme-mediated covalent attachment of ubiquitin residues and subsequent degradation of GR by the proteasome^{9,10}.

Serine/Threonine phosphorylation of GR is the PTM which has been the most extensively investigated¹¹. GR phosphorylation has been shown to be involved in corticosteroid binding, GR interaction with DNA, subcellular localization and cofactor recruitment⁴. The vast majority of the experimentally confirmed phosphorylated sites were found in the transactivation domain activation function 1 within the NTD. For example, phosphorylation at S203, S211 and S226 alter GR activity through modulation of GR binding affinity towards its coregulatory proteins^{12,13} and the specific phosphorylation of S203 was reported to play a role in GR subcellular trafficking¹⁴. GR NTD is an intrinsically disordered region and, upon phosphorylation, GR NTD has been shown to undergo a disorder to order conformational rearrangement that is involved in regulation of GR^{15,16}. Multiple serine/threonine kinases involved in the GR phosphorylation, and thus GR regulation, have been identified¹⁷. PKB phosphorylates S134, cyclin-dependent kinases (CDKs) 1 and 5 phosphorylate S203, S211 and S226. S211 is additionally phosphorylated by p38 MAPK, c-Jun N-terminal kinase (JNK) and indirectly phosphorylated by AMPK. Glycogen synthase kinase (GSK) 3 β phosphorylates S404¹⁷.

The interaction between 14-3-3 and GR is also mediated through GR phosphorylation and this PPI has been suspected to play a role in pathological inflammatory disorders¹⁸ and cancer¹⁹. Multiple phosphorylation sites and different kinases, however, have been reported and claimed to affect the activity of GR through induction of an interaction with 14-3-3¹⁸⁻²⁴. 14-3-3 has been shown to bind the ligand binding domain (LBD) of GR^{19,22,24} but also the phosphorylated residue S134¹⁸. Both

PKB¹⁹ and p38 MAPK¹⁸ were reported to phosphorylate GR and trigger the GR–14-3-3 PPI. Identification of the GR residues, whose phosphorylation is recognized by 14-3-3, and the kinases responsible for phosphorylation of these GR sites is crucial for a deeper understanding of the GR signalling network and the role of 14-3-3 in GR regulation. In the previous chapter, the GR–14-3-3 interaction has been thoroughly investigated using GR phosphorylated peptides centred on experimentally confirmed GR phosphosites and predicted 14-3-3 binding sites. Using biophysical assays, X-ray crystallography and alanine scanning, T524 of GR has been identified as the most important phosphosite in the binding with 14-3-3, particularly in association with S617. 14-3-3 typically binds phospho residues in disordered regions and both T524 and S617 are found in GR LBD and in a relatively disordered area which might also be prone to a disorder-to-order transition upon 14-3-3 binding. Herein, I describe further efforts in the quest to unravel the molecular mechanisms involved in the 14-3-3 regulation of GR. Using the bottom-up molecular approach, I sought to investigate the 14-3-3 interaction initially with GR LBD and finally full length GR. The role of the two GR phosphosites identified in chapter 2 was confirmed. The kinase MINK1, not previously associated with GR, was also found to phosphorylate the key T524 residue and, in a cellular system, this kinase was shown to be required for much of the binding of GR to 14-3-3. Hence, this work contributes to unravelling the long-standing question on the 14-3-3 regulation of GR signalling pathways, assessing the GR–14-3-3 PPI involvement in disease states and highlighting both MINK1 and the GR–14-3-3 axis as potential targets for future therapeutic intervention.

3.2. Results

The two potential 14-3-3-binding phosphosites identified, pT524 and pS617, are situated within the GR LBD. Hence, I aimed to test the binding affinity of a doubly phosphorylated full-length GR LBD with 14-3-3. The kinase(s) responsible for phosphorylation of GR LBD, however, have not yet been reported and various options were considered: (i) mutation of the amino acids T524 and S617 into the phosphomimetic glutamic acid, (ii) performing posttranslational phosphorylation of GR LBD by chemical synthesis²⁵ or (iii) identifying the relevant kinase(s) through screening. In chapter 2 GR_pT524-pS617, a doubly phosphorylated peptide consisted in two 13-mer GR monomers centred on pT524 and pS617 respectively and linked by a pentaglycine moiety, has been shown to bind to 14-3-3 ζ with a binding affinity in the low nanomolar range. The GR peptide GR_T524E-S617E, a 31-mer peptide analogue to GR_pT524-pS617 with the two phosphorylated sites mutated into glutamic acids, however, did not bind to 14-3-3 ζ as shown by SPR measurement (Fig. 3.1). Strategy (ii) was further investigated.

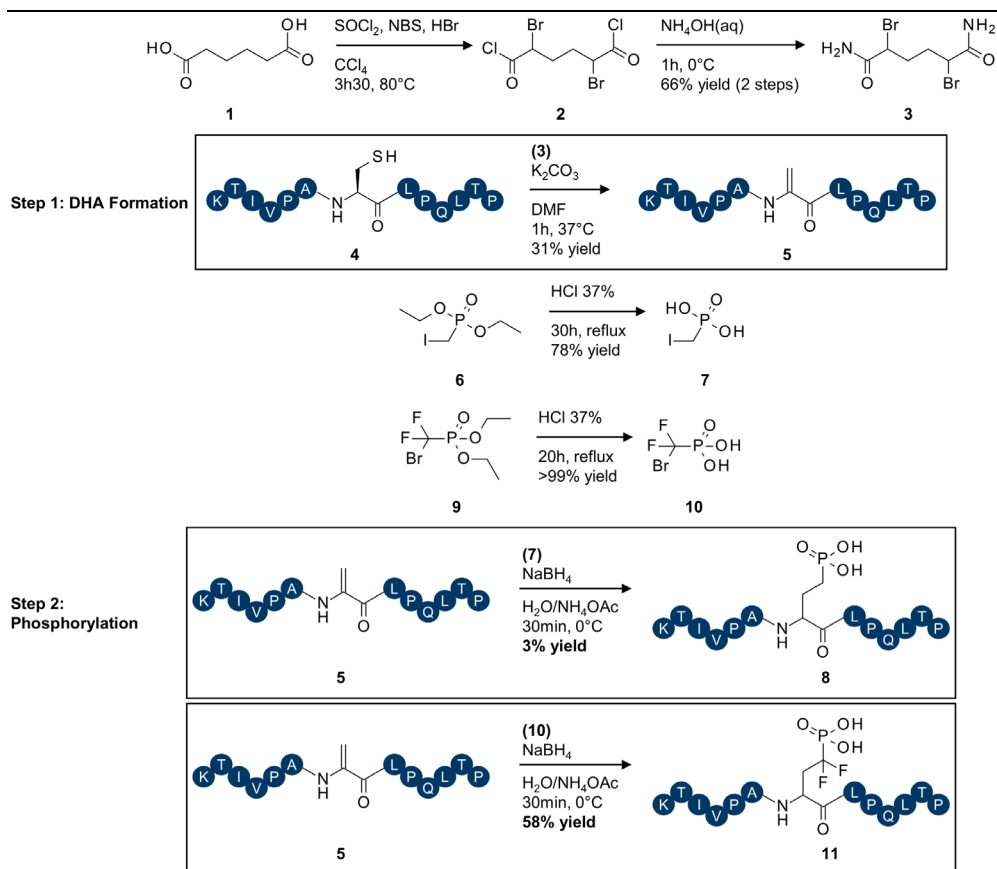
3.2.1. Posttranslational phosphorylation of GR LBD by chemical synthesis

I started to investigate the posttranslational modification of GR LBD by site selectively phosphorylate the two amino acids of interest, T524 and S617. Chemical posttranslational modification such as phosphorylation have been developed and exemplified notably with histone H3^{25,26}. The principle consists of a two-step synthesis, starting from the expressed and purified protein of interest with the targeted site mutated into cysteine; other cysteine residues are normally mutated to serine to avoid interference. Dialkylation of the aforementioned cysteine and elimination gives the corresponding dehydroalanine (DHA) containing protein and synthetic posttranslational phosphorylation is then performed on the intermediate DHA to obtain the phosphorylated product. This methodology was investigated using GR peptides for optimization.

The bis-alkylation–elimination of cysteine to DHA requires the synthesis of 2,5-dibromohexanediamide²⁶. Adipic acid (**1**) was treated with SOCl_2 followed by alpha bromination of the two newly formed acyl chloride moieties by use of NBS and hydrogen bromide (**2**). The corresponding bisamide (**3**) was obtained from **2** in the presence of ammonium hydroxide with a yield of 66% over the two steps. An analogue of the 13-mer GR peptide centred on T524 was synthesized, where the residue T524 was mutated into cysteine (GR_T524C, **4**). In the presence of **1** and potassium carbonate, complete bis alkylation of the cysteine occurred and subsequent elimination by elevation of the temperature to 37 °C afforded the corresponding DHA (**5**) with 31% yield after peptide purification.

Peptide phosphorylation was achieved through a radical reaction with NaBH_4 , which under these conditions acts as a hydrogen radical, between a phosphomethyl halide and DHA acting as a Michael acceptor. Oxygen was thoroughly removed from the buffer solutions by freeze-pump-thaw cycles to avoid competing oxidative cleavage of the peptide. The use of iodo-methyl phosphonic acid (**7**), obtained from the deprotection of dimethyl iodomethylphosphonate (**6**) by refluxing with HCl, generated side products such as peptide dimerization and reduction of DHA into alanine. The carba-phosphoserine product **8** was isolated and the two diastereoisomers were separated with a combined yield of only 3%. Neither the variation of the concentration, the number of equivalents nor the type of radical precursor, including samarium iodide, sodium cyanoborohydride, zinc or AIBN, improved the reaction outcome. The use of difluoromethyl-phosphonic acid as source of phosphonyl (**10**), however, dramatically optimized the reaction by eliminating any side reaction. Complete conversion of **5** into product **11** was observed and **11** was isolated as a racemate with 58% yield after peptide purification (Scheme 3.1).

Activation of MINK1 Induces 14-3-3 Regulation of Glucocorticoid Receptor Through Protein-Protein Interaction



Scheme 3.1. Posttranslational phosphorylation of a 13-mer GR peptide.

The binding affinity of the chemically phosphorylated GR peptides **8** and **11** was determined with 14-3-3 ζ . The two diastereoisomers of **8** and the diastereomeric mixture **11** retained most of the potency with binding affinities, by SPR measurement, of 71, 90 and 120 μM respectively. Comparison with the corresponding GR peptide centred on phosphorylated native residue T524 (GR_pT524) showed a 4- to 5-fold decrease in affinity (Table 3.1). This small drop in affinity could be rationalised because the chemical phosphorylation of GR peptides gives access to a (difluoro) carba-phosphoserine, thus lacking the methyl group at the beta position present in the native T524. In chapter 2 the respective binding affinities of the doubly phosphorylated peptide GR_pT524-pS617 and its diphosphoserine analogue, GR_pS524-pS617, with 14-3-3 ζ have been reported. An 8-fold drop in affinity, from 18 to 140 nM, was observed upon the mutation of pT524 into pS524 and demonstrated the importance of the methyl residue (Table 3.1).

Table 3.1. Binding affinity of GR peptides (GR_pT524, GR_pT524-pS617 and GR_pS524-pS617) and the chemically phosphorylated analogues (8 and 11)

Peptide name	Amino acid sequence	K _d with 14-3-3ζ (μM)
GR_pT524	KTIVPA pT LPQLTP	22 ± 8
8 (dia1)	KTIVPA CpS LPQLTP	71 ± 24
8 (dia2)	KTIVPA CpS LPQLTP	90 ± 15
11	KTIVPA diFCpS LPQLTP	122 ± 14
GR_pT524-pS617	KTIVPA pT LPQLTPGGGGGRSYRQS pS ANLLCF	0.018 ± 0.006
GR_pS524-pS617	KTIVPA pS LPQLTPGGGGGRSYRQS pS ANLLCF	0.136 ± 0.005

The phosphorylated amino acids are depicted in bold red. The GR peptides not chemically modified are highlighted in grey. Note the drop in affinity between **8** and **11** with GR_pT524 similarly to GR_pT524-pS617 with GR_pS524-pS617. Dia means diastereomers. All measurements were performed as triplicates.

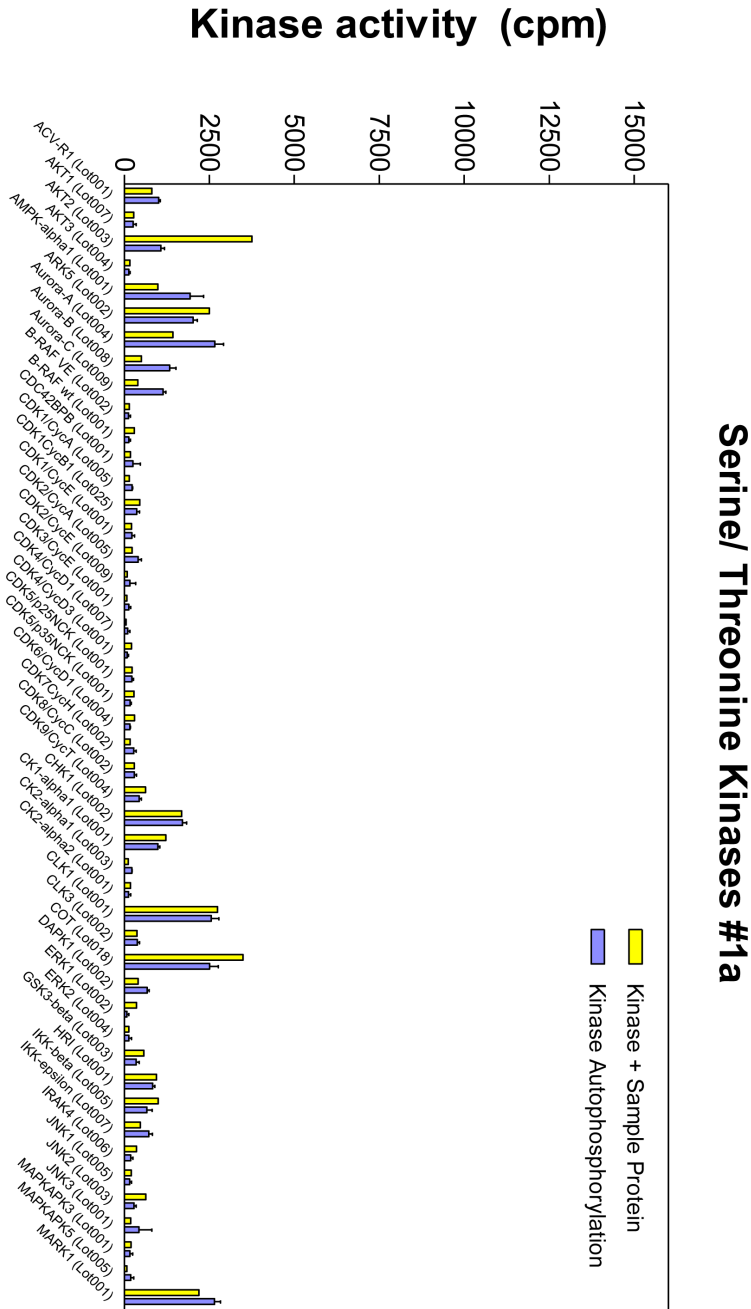
GR LBD was expressed with the mutations T524C, S617C, F602S²⁷ to increase protein solubility and the solvent exposed cysteines mutated as well to avoid side reactions (C622S and C638D). Unfortunately, the chemical phosphorylation was not applied on GR LBD for lack of time and the success of strategy iii.

3.2.2. Assessment of the GR LBD phosphorylation profile by kinase screening

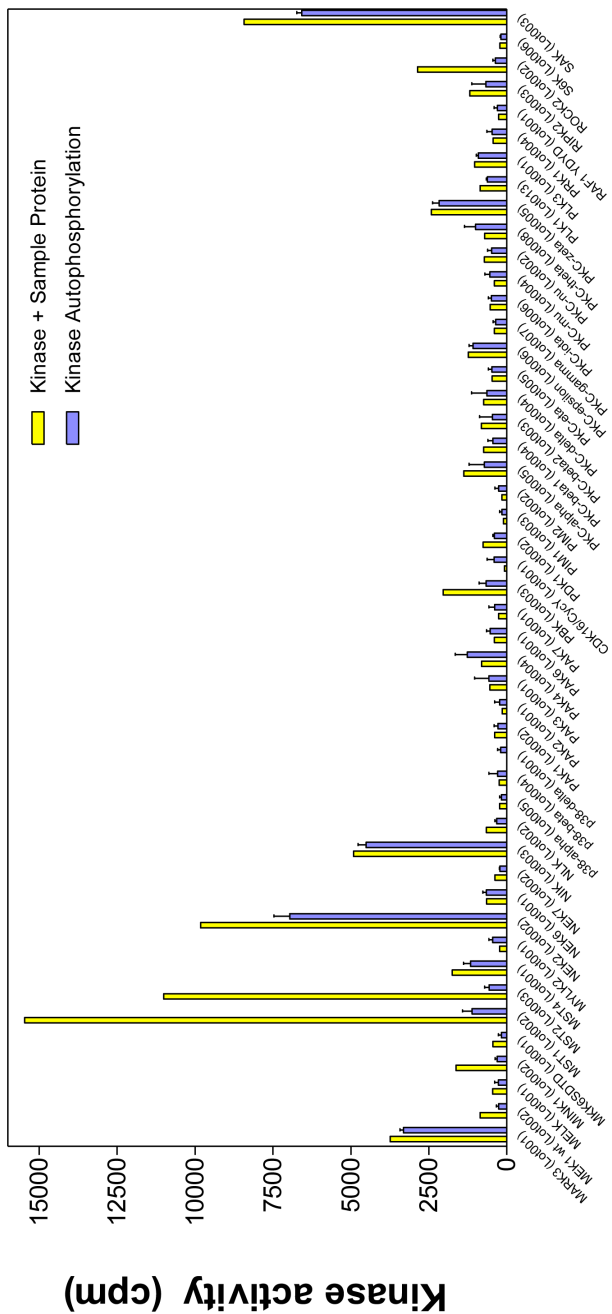
I aimed to identify the relevant kinase(s) using the strategy (iii). The expression of wildtype (wt) human GR LBD from *E. coli* was unsuccessful, owing to solubility problems. Switching to the GR LBD mutant F602S²⁷ and running the expression in the presence of dexamethasone, allowed us to express sufficient GR F602S N514-K777, to be purified and used as a substrate for candidate kinases. The phosphorylation profile of GR LBD was determined in a radiometric protein kinase filter-binding assay (performed by ProKinase GmbH, Germany) in which the activity of 245 serine/threonine kinases was measured (Fig. 3.1). The activity ratios, describing the ratio between the activity of a particular kinase with and without GR LBD, were calculated and I observed 38 kinases that displayed an activity ratio above 3, and 12 kinases above 5. MST2, MAP4K4, MST1 and TAOK2 were the kinases with the highest ratios, 19, 16, 14 and 13 respectively (Table 3.2). All of them belong to the STE20 kinase family, being upstream activators of the MAPK pathways. The 12 kinases with the highest activity ratios were selected for a follow-up assay where the phosphorylation profile of GR LBD was determined. MAP4K4, MINK1, MST1, MST2 and ROCK1 were observed to phosphorylate GR LBD (Table 3.3 and Fig. 3.2). The varying response may be due to the activity rate of the particular kinases having different kinetics

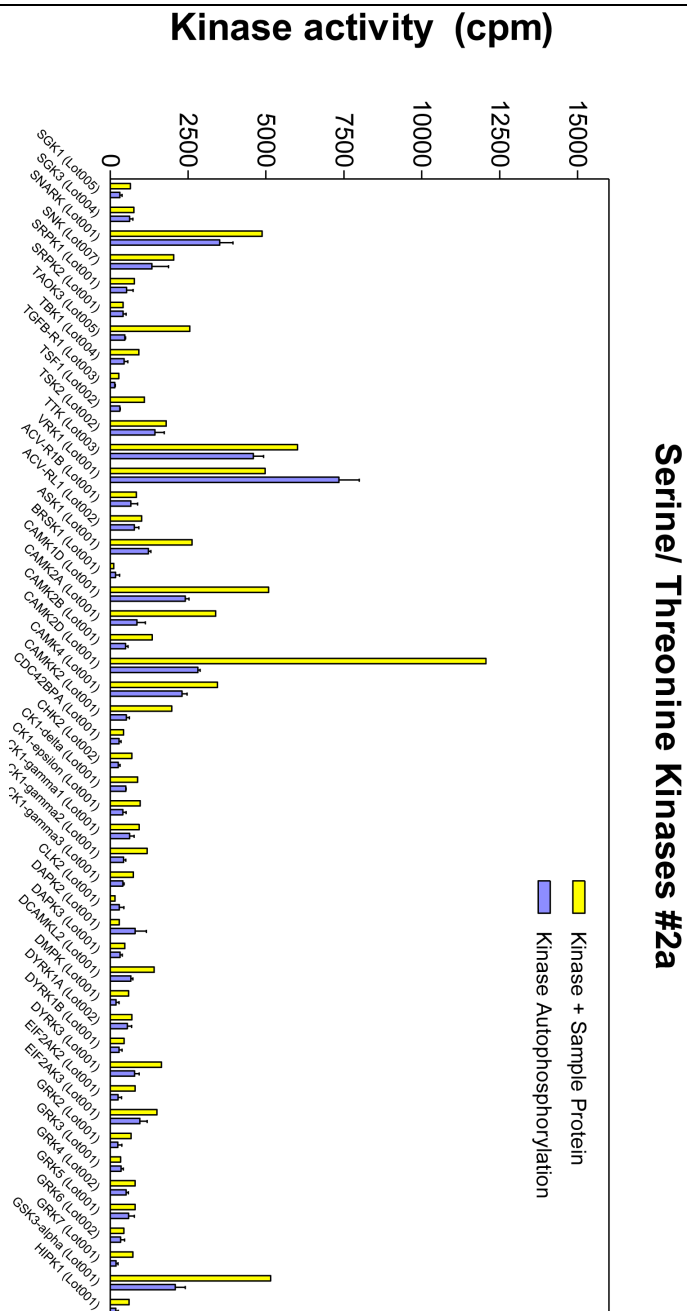
Activation of MINK1 Induces 14-3-3 Regulation of Glucocorticoid Receptor Through Protein-Protein Interaction

under the chosen conditions which were identical for all the assays and since the ATP concentration was fixed at 1 μ M, regardless of the ATP-Km of each kinase.

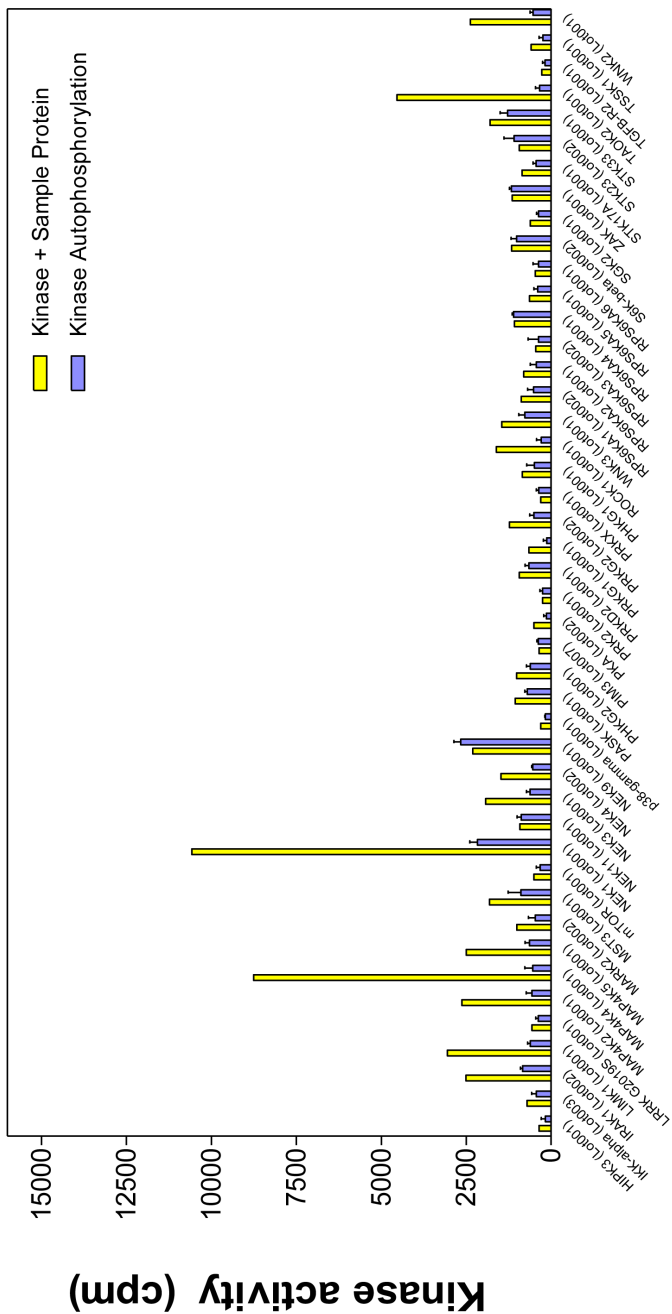


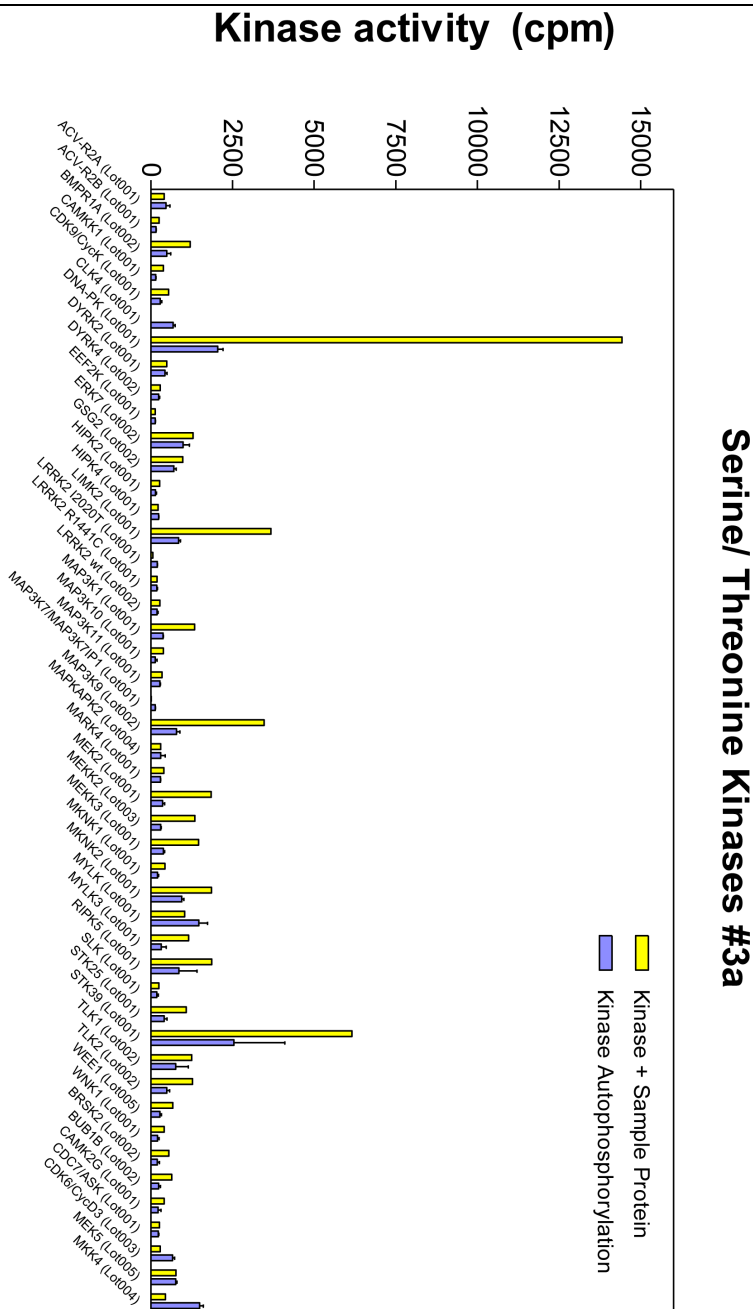
Serine/ Threonine Kinases #1b





Serine/ Threonine Kinases #2b





Serine/ Threonine Kinases #3b

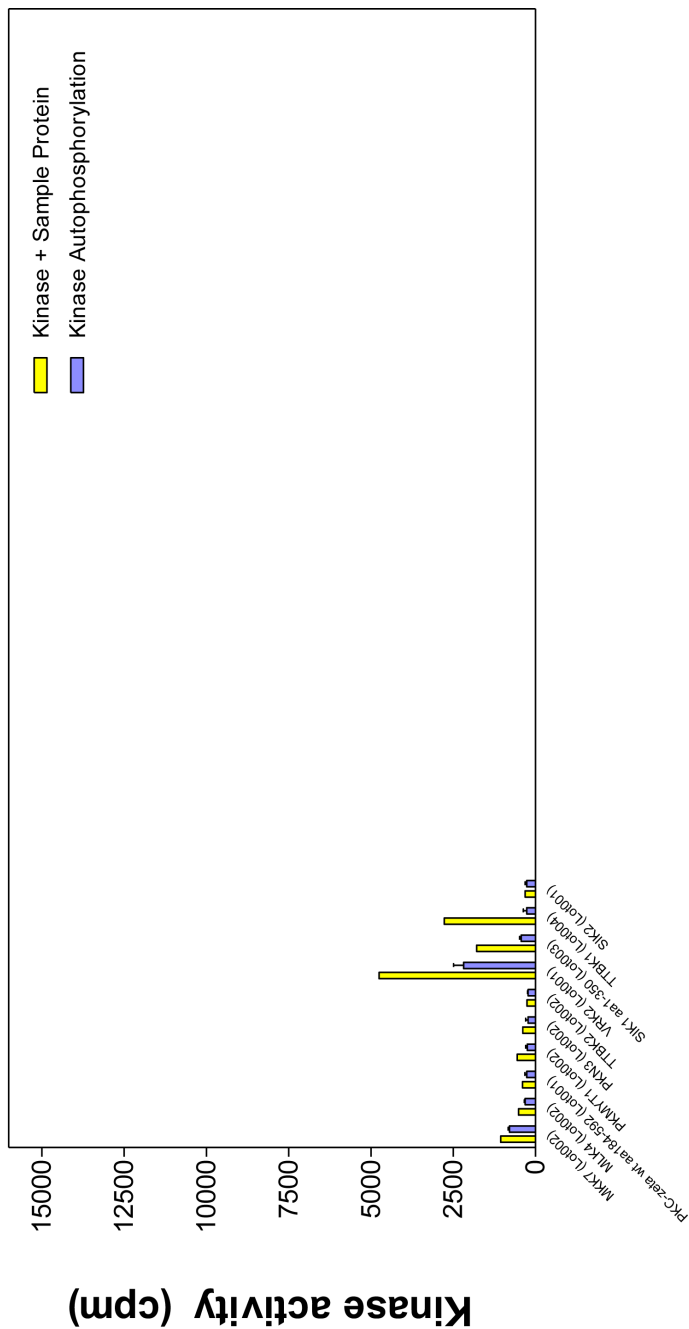


Figure 3.1. Results from the screening of 245 kinases with GR LBD.

Activation of MINK1 Induces 14-3-3 Regulation of Glucocorticoid Receptor Through Protein-Protein Interaction

Table 3.2. Results of phosphorylation for the kinases, with an activity ratio above 5, selected for hit confirmation

Kinase #	Kinase (ProKinase Lot #)	Enzyme, ng/well	Activity raw values	Kinase autophos., normalized mean n=3	Kinase autophos., SD	Substrate-BG, median n=3	Activity values, corrected (A-C)	Activity Ratio (A-C)/B
194	PRKG1 (Lot001)	12.5	801	130	103	145	656	5.04
125	MEK2 (Lot001)	100	1994	359	63	145	1849	5.14
130	MINK1 (Lot002)	10	1772	314	63	145	1627	5.18
227	TAOK3 (Lot005)	50	2698	469	27	145	2553	5.45
200	ROCK1 (Lot001)	4	1760	293	139	145	1615	5.51
69	DNA-PK (Lot001)	10	14574	2047	160	145	14429	7.05
201	ROCK2 (Lot002)	2.5	3007	370	80	145	2862	7.73
236	TTBK1 (Lot004)	10	2919	269	107	145	2774	10.30
226	TAOK2 (Lot001)	20	4685	342	123	145	4540	13.28
137	MST1 (Lot002)	5	15611	1117	304	145	15466	13.84
115	MAP4K4 (Lot001)	5	8905	546	232	145	8760	16.04
138	MST2 (Lot003)	10	11149	570	143	145	11004	19.31

All values in cpm.

Table 3.3. Results from the hit confirmation assay of the 12 selected kinases against GR LBD

	Enzyme	+		-		+		-		+		-					
		0.00		0.00		2.50		2.50		5.00		5.00		10.00		10.00	
		Sample (µg/50 µL)		Enzyme (ng/50 µL)		Mean	SD	Mean	SD	Mean	SD	Mean	SD	Mean	SD	Mean	SD
DNA-PK	20	1066	113	64	35	1292	77	122	15	1141	83	105	24	1125	231	228	242
MAP4K4	50	2172	184	64	35	11413	265	122	15	12338	407	105	24	9824	554	228	242
MEK2	50	114	19	64	35	907	188	122	15	1420	101	105	24	2084	266	228	242
MINK1	10	358	16	113	17	7669	326	69	28	9185	572	53	19	6685	1017	71	34
MST1	5	758	63	64	35	23494	744	122	15	26682	2122	105	24	18850	1042	228	242
MST2	10	773	99	64	35	67752	5956	122	15	73858	3161	105	24	56369	3882	228	242
PRKG1	12.5	87	33	177	70	1549	152	221	96	1364	236	176	39	991	87	145	27
ROCK1	4	415	142	177	70	18051	1164	221	96	21444	2560	176	39	16371	570	145	27
ROCK2	2.5	178	21	113	17	1774	269	69	28	1564	73	53	19	1180	112	71	34
TAOK2	10	132	23	177	70	603	49	221	96	591	17	176	39	559	191	145	27
TAOK3	50	363	81	177	70	2702	108	221	96	3154	368	176	39	2835	293	145	27
TTBK1	10	1144	42	177	70	3339	152	221	96	3555	67	176	39	2891	224	145	27

The phosphorylation profile of GR LBD by 12 selected kinases was determined in triplicate at three substrate concentrations (2.5, 5 and 10 µg/50 µL final assay concentration) in a radiometric filter assay. Kinase activity in cpm.

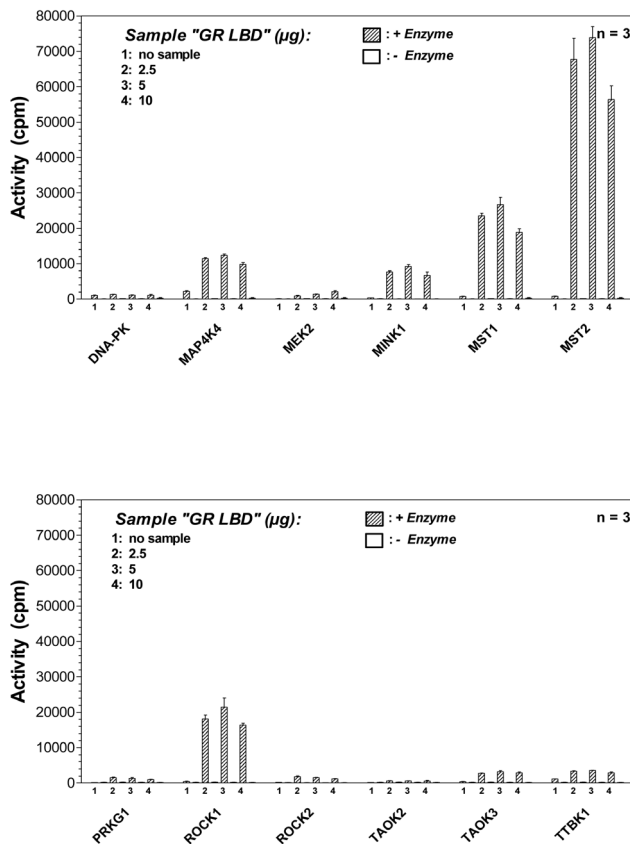


Figure 3.2. Results of the hit confirmation protein kinase assay displayed in bar diagram.

Phosphorylation of GR LBD by MAP4K4, MINK1, MST1, MST2 and ROCK1 followed by enzyme digestion and analysis by mass spectrometry revealed different phosphorylation patterns (Table 3.4). MAP4K4 showed mono- and diphosphorylation at T519 and T562. MST1 and MST2 both phosphorylated T562, T668, S682 and S746; each also phosphorylated additional sites, although these sites were markedly weaker in the LCMS analysis. MST2 showed a wider phosphorylation pattern than MST1 with up to seven phosphorylations observed. The two sites identified as most promising for 14-3-3 recognition (T524 and S617) were phosphorylated by ROCK1 and MINK1 respectively. In particular ROCK1 phosphorylated two different sites, T519 and S617, whilst MINK1 gave mainly mono and diphosphorylation of T524 and T562, with traces of phosphorylation at T635 (Table 3.4 and Fig. 3.3). Thus, the screening showed that MINK1 and ROCK1 can phosphorylate GR T524 and S617, respectively, *in vitro*.

Activation of MINK1 Induces 14-3-3 Regulation of Glucocorticoid Receptor Through Protein-Protein Interaction

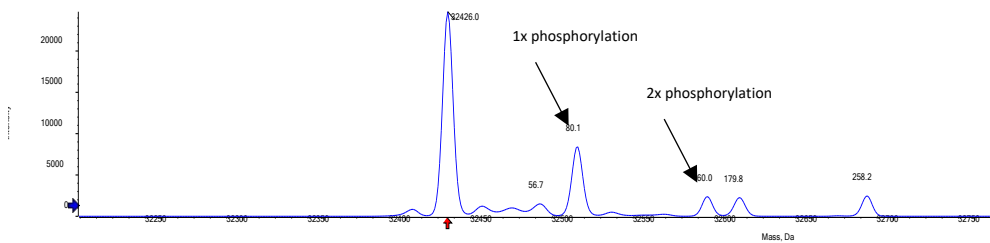
Table 3.4. Phosphorylation of GR LBD by five kinases identified from the kinase screen

Kinase name	Number of GR phosphorylation	GR phosphorylation sites with strong evidence	GR phosphorylation sites with weak evidence
MAP4K4	1 and 2	T519 and T562	
MINK1	1 and 2	T524 and T562	T635
MST1	Up to 5	T562, T668, S682 and S746	T524, T594 and T635
MST2	Up to 7	T562, T668, S682 and S746	T519, T556 and T635
ROCK1	1	T519 and S617	

For each kinase, intact mass and peptide mapping enable the identification of the phosphorylation state and phosphorylation sites. The kinases further investigated are highlighted in grey.

A

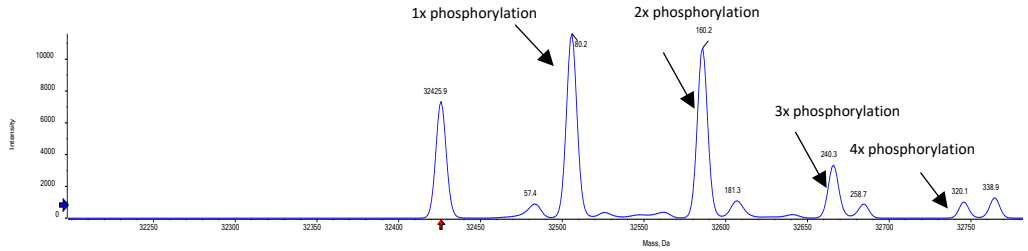
Spectrum from 290818 GR MAP4K4 .wiff2 (sample 1) – 290818 GR MAP4K4, +TOF MS (500 - 3000) from 3.111 to 3.586 min
Reconstruction, Input m/z: 656.8 to 2197.6 Da, Input spectrum isotope resolution: 2500



1	MHHHHHGGE	NLYFQGNPGN	KTIIVPATLPQ	LTPTLVSLLE	VIEPEVLYAG
51	YDSSVPDSTW	RIMTILNMLG	GRQVIAAVKW	AKAIPGFRNL	HLDDQMTLLQ
101	YSWMSLMAFA	LGWRSYRQSS	ANLLCFAPDL	IINEQRMTLP	CMYDQCKHML
151	YVSSSELHRLQ	VSYEEYLCMK	TLLLLSSVPK	DGLKSQELFD	EIRMTYIKEL
201	GKAIVKREGN	SSQNWQRFYQ	LTLLDSMHE	VVENLLNYCF	QTFLDKTMSI
251	EFPEMLAEII	TNQIPKYSNG	NIKLLFHQK		

B

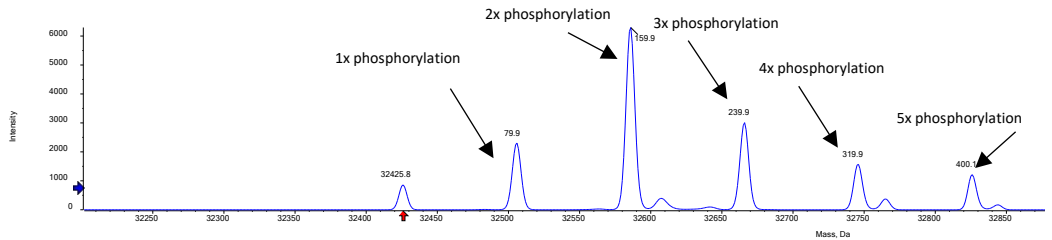
Spectrum from 290818 GR MINK1 .wiff2 (sample 1) – 290818 GR MINK1, +TOF MS (500 - 3000) from 3.120 to 3.595 min
 Reconstruction, Input m/z: 693.1 to 1665.8 Da, Input spectrum isotope resolution: 2500



1	MHHHHHHGGE	NLYFQGNPGN	KTIVPA ^T LPQ	LTPTLVSLLE	VIEPEVLYAG
51	YDSSVPDSTW	RIMT ^T LNMLG	GRQVIAAVKW	AKAIPGFRNL	HLDDQM ^T LLQ
101	YSWMSLMAFA	LGWRSYRQSS	ANLLCFAPDL	IINEQRMT ^T LP	CMYDQCKHML
151	YVSELHRLQ	VSYEELCMK	TLLLLSSVPK	DGLKSQELFD	EIRMTYIKEL
201	GKAIVKREGN	SSQNWQRFYQ	LTKLLDSMHE	VVENLLNYCF	QTFLDK ^T MSI
251	EFPEMLAEII	TNQIPKYSNG	NIKKLLFHQK		

C

Spectrum from 290818 GR MST1 .wiff2 (sample 1) – 290818 GR MST1, +TOF MS (500 - 3000) from 3.076 to 3.551 min
 Reconstruction, Input m/z: 681.6 to 1687.2 Da, Input spectrum isotope resolution: 2500

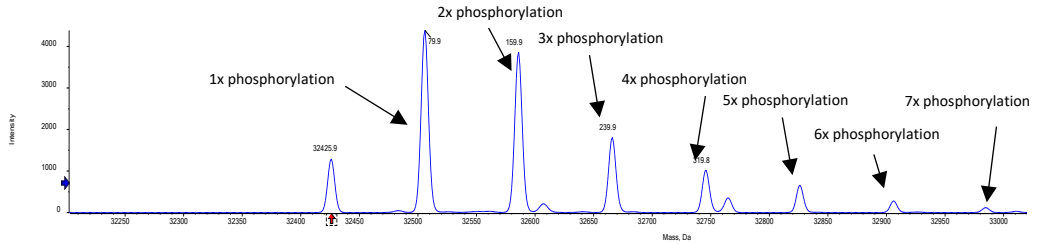


1	MHHHHHHGGE	NLYFQGNPGN	KTIVPA ^T LPQ	LTPTLVSLLE	VIEPEVLYAG
51	YDSSVPDSTW	RIMT ^T LNMLG	GRQVIAAVKW	AKAIPGFRNL	HLDDQM ^T LLQ
101	YSWMSLMAFA	LGWRSYRQSS	ANLLCFAPDL	IINEQRMT ^T LP	CMYDQCKHML
151	YVSELHRLQ	VSYEELCMK	TLLLLSSVPK	DGLKSQELFD	EIRMTYIKEL
201	GKAIVKREGN	SSQNWQRFYQ	LTKLLDSMHE	VVENLLNYCF	QTFLDK ^T MSI
251	EFPEMLAEII	TNQIPKYSNG	NIKKLLFHQK		

Activation of MINK1 Induces 14-3-3 Regulation of Glucocorticoid Receptor Through Protein-Protein Interaction

D

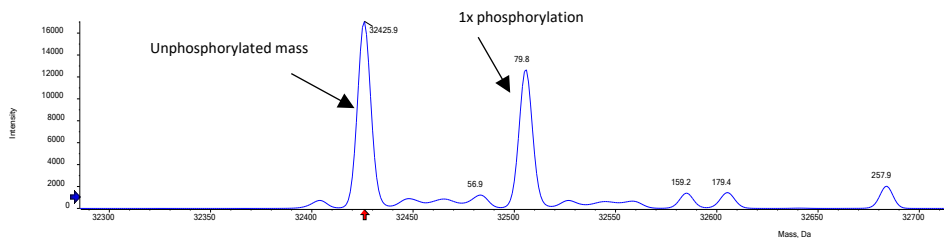
Spectrum from 290818 GR MST2 .wiff2 (sample 1) – 290818 GR MST2, +TOF MS (500 - 3000) from 3.120 to 3.595 min
Reconstruction, Input m/z: 708.0 to 1733.5 Da, Input spectrum isotope resolution: 2500



1	MHHHHHHGGE	NLYFQGNPGN	KTIVPATLPQ	LTPTLVSLLE	VIEPEVLYAG
51	YDSSVPDSTW	RIMTTLNMLG	GRQVIAAVKW	AKAIPGFRNL	HLDDQMTLLQ
101	YSWMSLMAFA	LGWRSYRQSS	ANLLCFAPDL	IINEQRM ⁵ TLP	CMYDQCKHML
151	YVSELHRLQ	VSYEELCMK	TLLLLSSVPK	DGLKSQELFD	EIRMTYIKEL
201	GKAIVKREGN	SSQNWRQRFYQ	LTKLLDSMHE	VVENLLNYCF	QTFLDKTM ⁵ S
251	EFPEMLAEII	TNQIPKYSNG	NIKKLLFHQK		

E

Spectrum from 290818 GR ROCK1 .wiff2 (sample 1) – 290818 GR ROCK1, +TOF MS (500 - 3000) from 3.085 to 3.595 min
Reconstruction, Input m/z: 691.5 to 1750.0 Da, Input spectrum isotope resolution: 2500



1	MHHHHHHGGE	NLYFQGNPGN	KTIVPATLPQ	LTPTLVSLLE	VIEPEVLYAG
51	YDSSVPDSTW	RIMTTLNMLG	GRQVIAAVKW	AKAIPGFRNL	HLDDQMTLLQ
101	YSWMSLMAFA	LGWRSYRQSS	ANLLCFAPDL	IINEQRM ⁵ TLP	CMYDQCKHML
151	YVSELHRLQ	VSYEELCMK	TLLLLSSVPK	DGLKSQELFD	EIRMTYIKEL
201	GKAIVKREGN	SSQNWRQRFYQ	LTKLLDSMHE	VVENLLNYCF	QTFLDKTM ⁵ S
251	EFPEMLAEII	TNQIPKYSNG	NIKKLLFHQK		

Figure 3.3. MS spectra and peptide mapping of GR LBD phosphorylated by 5 kinases. (A), MAP4K4. GR LBD was unphosphorylated (61%), monophosphorylated (27%) and diphosphorylated (12%). Phosphorylations detected at T519 and T562. **(B), MINK1.** 20% was unphosphorylated, 32% had one site, 35% two sites and 13% three sites

phosphorylated. Phosphorylation sites identified at T524, T562 and weakly at T635. (C), MST1. Only 5% of the protein was unphosphorylated, 14% had one phosphorylation, 33% 2, 15% 3, 11% 4, 9% 5, 7% 6 and 6% had 7. Phosphorylations found at: T562, T668, S682 and S746. Possible phosphorylations at T524, T594 and T635. (D), MST2. GR LBD showed 6 phosphorylation sites, possibly 7. 8% was unphosphorylated, 29% monophosphorylated, 25% twice, 12% 3 times, 9% 4 times, 7% 5 times, 6% 6 times and 4% 7 times. Phosphorylations detected at T562, T668, S682 and S746. Weaker indications of phosphorylations as T519, T556 and T635. (E), ROCK1. 54% of the protein was unphosphorylated and 46% had one phosphorylation. Phosphorylation sites detected at T519 and S617. The amount of each phosphorylation state was estimated using the areas under the trace. Sequence coverage is depicted in red and phosphorylation sites are highlighted in yellow.

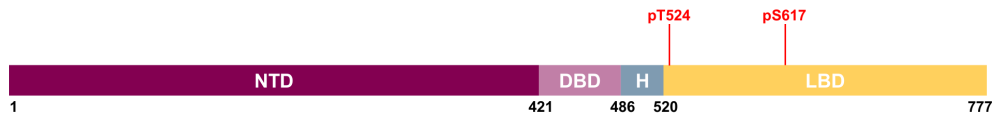
3.2.3. MINK1 phosphorylates GR LBD driving the interaction with 14-3-3

The ability of GR LBD, phosphorylated by either MINK1 or ROCK1, to interact with 14-3-3 was investigated. A far-Western blotting overlay assay was performed where I assessed the capacity of the different phosphorylated GR LBD, immobilized on a membrane, to bind the two recombinant yeast isoforms of 14-3-3 tagged with digoxigenin (BMH1-BMH2-digoxigenin). In this assay GR LBD phosphorylated by MINK1 showed direct interaction with 14-3-3 in a dose-dependent manner, whereas GR LBD phosphorylated by ROCK1 and the unphosphorylated GR LBD did not (Fig. 3.4b), highlighting the specificity and sensitivity of the assays towards phosphorylated substrates.

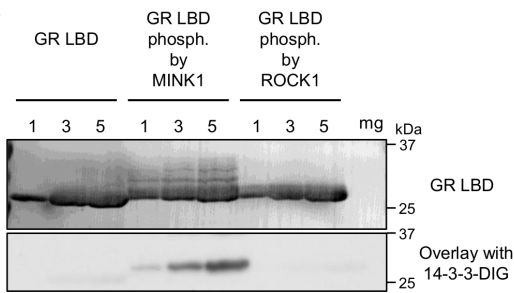
MINK1 phosphorylates GR LBD at residues T524, T562 and to a lesser extent T635. T524 and T635 have been identified by the 14-3-3-Pred webserver (www.compbio.dundee.ac.uk/1433pred)²⁸ as plausible 14-3-3 binding sites with T561 but not T562. The 13-mer peptide centred on pT562 showed a weak interaction with 14-3-3 ζ ($K_d=200 \mu\text{M}$). Interestingly, the 51-mer peptide GR_pT524-pT562, consisting of the two 13-mer peptides GR_pT524 and GR_pT562 with the native sequence as a linker, did not show a similar avidity effect as previously observed for GR_pT524-pS617. No significant trend has been reported between the effective molarity and the linker length^{29,30}. Instead, the effective molarity depends on the flexibility of the linker between the two different binding sites. Thus, the binding affinity of GR_pT524-pT562 with 14-3-3 ζ ($K_d=23$ and $15 \mu\text{M}$, measured by FP and SPR respectively) and its low effective molarity (0.2 mM) might suggest a more structured linker. Crystal structure analysis (PDB code 1M2Z) placed GR T562 in helix 3 which forms the spine of the protein. It is unlikely that this helix changes its structure, questioning the ability of GR T562 to interact with 14-3-3 proteins.

Activation of MINK1 Induces 14-3-3 Regulation of Glucocorticoid Receptor Through Protein-Protein Interaction

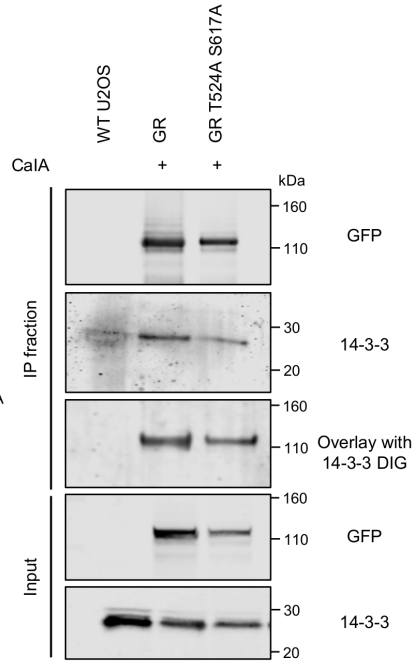
A



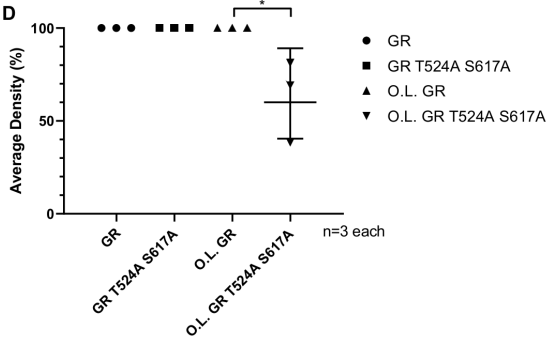
B



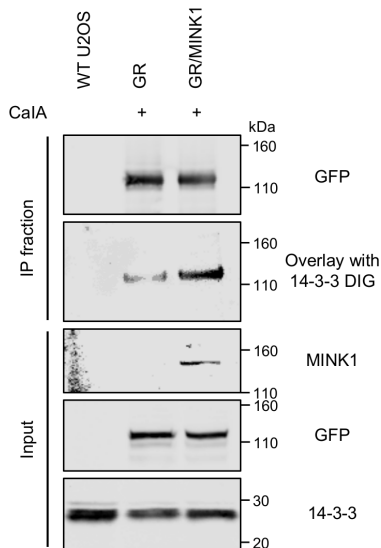
C



D



E



F

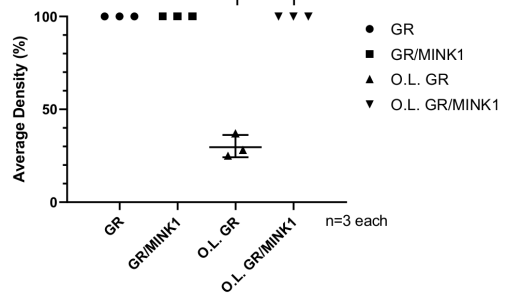


Figure 3.4. Interaction of GR LBD and full-length GR with pan 14-3-3. (A) Location within the GR sequence of pT524 and pS617. (B) Far-Western blotting overlay of GR LBD phosphorylated by MINK1 or ROCK1 with two recombinant yeast isoforms of 14-3-3 linked to digoxigenin (BMH1-BMH2-DIG). Unphosphorylated and in vitro phosphorylated GR LBD were detected using anti-6X His tag antibody. GR LBD-bound 14-3-3 proteins were detected using anti-DIG antibody. (C) U2OS cells were transiently transfected with GFP-GR or GFP-GR T524A S617A plasmids followed by stimulation with calyculin A. Cell lysates were immunoprecipitated with GFP-Trap beads. GFP-GR and GFP-GR mutant were detected using anti-GFP antibody, GR-associated 14-3-3 was detected using anti-pan 14-3-3 antibody. Far-Western blotting overlay was done by incubation of the GR-containing membrane with BMH1-BMH2-DIG and subsequent detection of GR-bound 14-3-3 protein using anti-DIG antibody. (D) Quantification of three independent experiments. Data is normalized to the amount of GFP-GR and GFP-GR mutant from the IP fraction. (E) U2OS cells were transiently transfected with GFP-GR or cotransfected with GFP-GR and FLAG-MINK1 plasmids followed by stimulation with calyculin A. Cell lysates were immunoprecipitated with GFP-Trap beads. FLAG-MINK1 was detected using anti-MINK1 antibody. Far-Western blotting overlay was done as previously mentioned. (F) Quantification of three independent experiments. Data is normalized to the amount of GFP-GR from the IP fraction. The error bars represent the standard deviation of the three independent assays. O.L.=overlay. All *p* values were obtained using *t*-test. **p* < 0.05, *****p* < 0.0001.

3.2.4. Interaction between full-length GR and 14-3-3

The interaction between full-length GR and 14-3-3 was investigated in a cellular system to validate the relevance of the peptide studies. In an initial experiment, HEK293 and U2OS cells were transiently transfected with wt GR and, after overnight starvation, the cells were treated with a panel of stimuli that have previously been shown to promote phosphorylation of 14-3-3-binding sites of other target proteins³¹. Results from co-immunoprecipitation (Co-IP) experiments and far-Western blotting overlay assay showed that GR interacted with 14-3-3 proteins upon stimulation with forskolin (a cell-permeable diterpenoid which activates adenylyl cyclase, increases intracellular cAMP concentration and thus activates PKA) and calyculin A (a cell-permeable potent and selective protein phosphatase inhibitor) (Fig. 3.5).

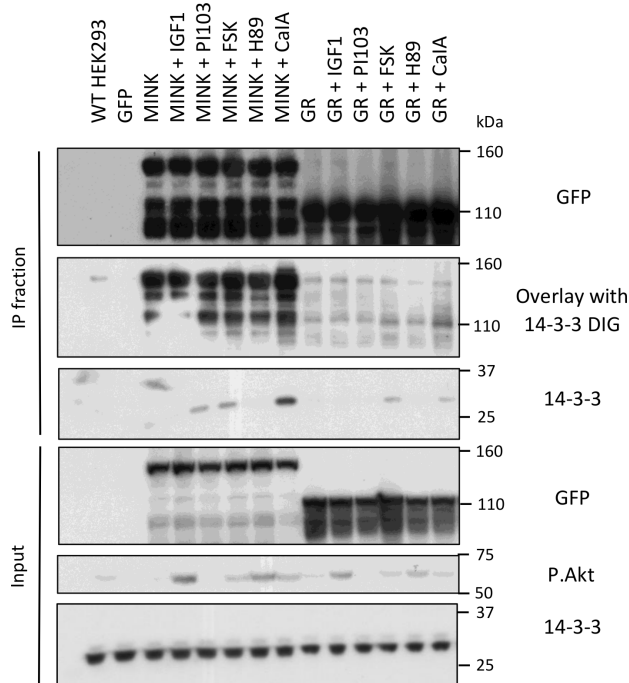


Figure 3.5. Initial Co-IP assay revealed the same stimuli trigger the GR–14-3-3 interaction as those that lead to phosphorylation of MINK1. HEK293 cells were transiently transfected with GFP-MINK1 or GFP-GR plasmids followed by overnight starvation and by a panel of stimulation. Cell lysates were immunoprecipitated with GFP-Trap beads. GFP-MINK1 and GFP-GR were detected using anti-GFP antibody, MINK1-associated 14-3-3 and GR-associated 14-3-3 were detected using anti-pan 14-3-3 antibody and far-western blotting overlay was done by incubation of the MINK1-containing membrane and GR-containing membrane with BMH1-BMH2-DIG and subsequent detection of MINK1 or GR-bound 14-3-3 proteins using anti-DIG antibody. FSK and CalA mean forskolin and calyculin A respectively.

The role of the previously identified GR phosphosites in the binding with 14-3-3 was investigated in cells. U2OS cells were transiently transfected with wt GR or the GR double mutant, T524A S617A, before treatment with calyculin A. Under our experimental conditions, Co-IP and far-Western blotting overlay experiments revealed a significant decrease, about 35%, of the interaction between 14-3-3 and GR double mutant as compared to wt GR (Fig. 3.4c and 3.4d). These results confirm the interaction between GR and 14-3-3 and highlight the importance of the phosphorylation of the two GR residues T524 and/or S614.

Upon stimulation with forskolin or calyculin A, MINK1 also interacts with 14-3-3 (Fig. 3.6) (consistent with unpublished data by Gavuthami Murugesan and CM, University of Dundee). Thus, the

GR–14-3-3 interaction and the MINK1–14-3-3 interaction are both promoted in parallel in cells stimulated with forskolin and calyculin A (Fig. 3.5). I established that U2OS cells have a very low endogenous expression of MINK1, as no signal from this kinase could be detected by Western blotting (Fig. 3.7). Therefore, U2OS cells were either transfected with wt GR or co-transfected with wt GR and MINK1. In the absence of further stimulation, no GR–14-3-3 interaction was observed in either cells. Stimulation with calyculin A increased the level of phosphorylated GR by preventing GR dephosphorylation, so that the protein was capable of binding to 14-3-3 in a far-Western overlay. This interaction increased, by about 70%, in the presence of overexpressed MINK1 (Fig 3.4e and 3.4f). Together these results suggest that activated MINK1 kinase phosphorylates GR and triggers the GR–14-3-3 PPI.

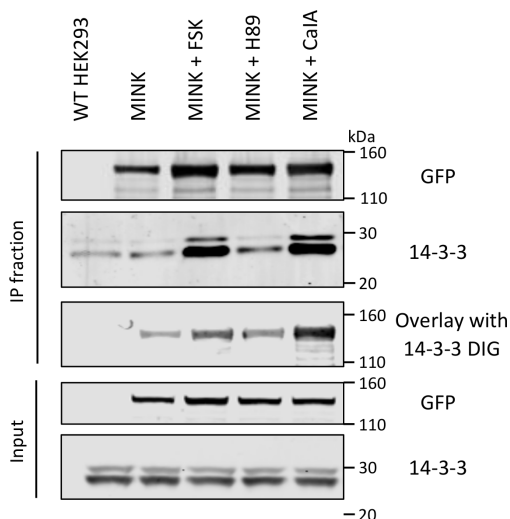


Figure 3.6. MINK1–14-3-3 PPI upon forskolin and calyculin A cell stimulation. HEK293 cells were transiently transfected with GFP-MINK1 plasmid followed by overnight starvation and by a panel of stimuli. Cell lysates were immunoprecipitated with GFP-Trap beads. GFP-MINK1 was detected using anti-GFP antibody, MINK1-associated 14-3-3 was detected using anti-pan 14-3-3 antibody and far-western blotting overlay was done by incubation of the MINK1-containing membrane with BMH1-BMH2-DIG and subsequent detection of MINK1-bound 14-3-3 proteins using anti-DIG antibody. CalA means calyculin A.

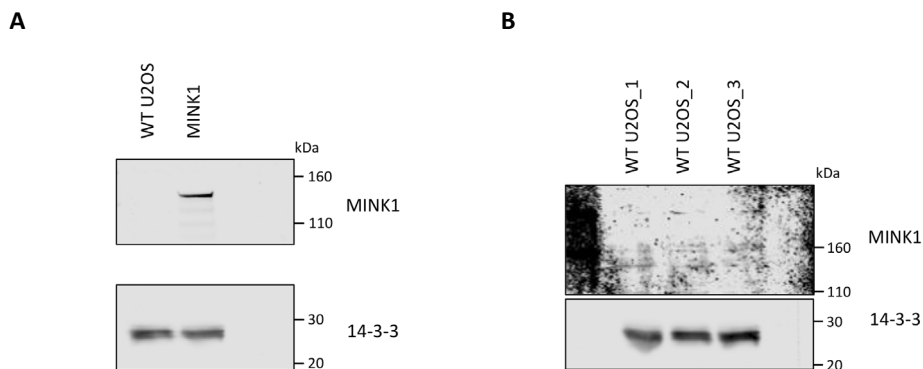


Figure 3.7. U2OS cells have a very low endogenous expression of MINK1. (A) Proteins from the cell lysates of U2OS cells and U2OS cells transiently transfected with GFP-MINK1 plasmid were resolved on a NuPAGE and transferred to a membrane. MINK1 was detected using anti-MINK1 antibody. (B) Proteins from three independent cell lysates of U2OS cells were resolved on a NuPAGE and transferred to a membrane. No endogenous MINK1 was detected using anti-MINK1 antibody even at the highest contrast offered by the Image Studio (LI-COR) software.

3.3. Discussion

In this study, the GR–14-3-3 interaction has been further investigated, from the previously synthesised GR peptides centred on the identified phosphosites to longer GR constructs. The two sites, T524 and S617, are located in the GR LBD, thus I sought to study the binding of the phosphorylated GR LBD to 14-3-3 using different strategies. The mutation of T524 and S617 to the phosphomimetic glutamic acid abolished the binding with 14-3-3, thus was not a viable route. Optimization of the synthetic route of the chemical posttranslational phosphorylation on peptides for an application on the GR LBD was found promising. Switching from the iodomethyl phosphonic acid (**7**) to the bromodifluoromethyl phosphonic acid (**10**) enabled the total conversion of the DHA containing peptide (**5**) to the phosphorylated analogue and suppressed the formation of side products. I speculate that the presence of the two fluorine atoms might stabilise the radical which can then react with DHA. Further experiments would be needed to confirm this hypothesis and to determine if the halogen of the radical precursor plays a role in the reaction. Optimization of the synthesis of the bisamide **3** could be considered as well, for example by replacing the highly toxic carbon tetrachloride used as solvent in the first step of the synthesis to one of its less harmful analogues such as chloroform or dichloromethane. GR LBD was expressed with the mutation of the solvent exposed cysteines, which are prone to react, to minimize protein destabilisation and in the presence of dexamethasone but the application of the posttranslational phosphorylation strategy to GR LBD was not performed. Other strategies were considered, including the mutation of the amino

acids surrounding T524 and S617 to enable these two sites to be recognized by a known kinase. This strategy was discarded due to the risk that the mutations disrupt the binding with 14-3-3. Recently, the biosynthesis of phosphorylated proteins by genetically encoding a phosphoserine and a phosphothreonine has been reported^{32,33} and could potentially be applied to the biosynthesis of the GR LBD phosphorylated at the positions 524 and 617. The technology, however, is not yet generally available.

Previous work has investigated the role of kinases in the 14-3-3 binding to GR. GR has been shown to interact with 14-3-3 ζ by phosphorylation of S134 in a p38 MAPK-dependent manner, repressing GR transcriptional activity¹⁸. 14-3-3 σ has been reported to bind two different portions of GR: GR S134 or GR LBD and to antagonize GR transcriptional activity through the role of PKB¹⁹. I identified MINK1 as an important kinase for phosphorylation of GR by screening and this kinase was found to phosphorylate GR residue T524 that our earlier work had identified as being potentially important for the GR–14-3-3 interaction. MINK1 (misshapen-like kinase 1) is a serine/threonine kinase part of the germinal centre kinase (GCK) family. MINK1 is ubiquitously expressed with a reported tissue-specific regulation^{34,35} and plays a role in various fundamental cellular processes. MINK1 has been shown to be involved in cell spreading and mobility, cell-matrix adhesion and cytoskeleton reorganisation³⁶. MINK1 promotes homeostasis and thrombosis via the regulation of platelet functions in mice³⁷. In addition, MINK1 activates both the JNK and p38 MAPK stress kinase pathways³⁸. Interestingly, MINK1 has not been previously associated with GR.

GR LBD, in vitro phosphorylated by MINK1, interacts with 14-3-3 as shown by the far-Western blotting overlay assay. Analysis of the phosphorylated sites identified T524 as well as T562 and some traces of phosphorylated T635 were observed. GR peptides centred on T562 and T635 displayed a weak binding affinity towards 14-3-3. Examination of the crystal structure of GR LBD showed that T635 is solvent accessible but placed both T562 and T635 in an ordered area which questioned their ability to interact with 14-3-3. To determine the role of T524, T562 and T635 in the binding with 14-3-3, GR LBD could be expressed with two of these amino acids simultaneously mutated into alanine. In vitro phosphorylation of these mutated GR LBD by MINK1 and determination of their binding affinity, using the far-Western blotting overlay assay or SPR to measure a K_d , would provide a clear picture of their individual contribution.

The role of the two GR phosphosites identified in chapter 2 were here confirmed using cell-based assays. This cell-based approaches revealed that the affinity between GR double mutant, T524A S617A, and 14-3-3 decreased by 35% as compared to wt GR but was not abolished. These results suggest that 14-3-3 interacts with GR through multiple sites. Further experiments would be necessary

to fully quantify the individual effect of the GR phosphosites in 14-3-3 binding with full length GR as well as their biological role by monitoring GR translocation, GR transcriptional activity or GR protein level.

3.4. Conclusion

This chapter 3 complements the characterisation of the GR–14-3-3 interaction in a bottom-up manner. Using expressed GR LBD and then full-length GR, I have confirmed that the GR residues identified in chapter 2, can be phosphorylated. A kinase (MINK1), not previously associated with GR, has been found to phosphorylate T517 and action of this kinase has been shown to lead to recognition of GR by 14-3-3. These findings were validated in cellular systems. Fully unravelling the underlying signalling network of GR is of a great interest, due to the enormous importance of GR drugs and their widespread use, despite their many side-effects. Together our data contribute to answering the long-standing question on the 14-3-3 regulation of GR signalling pathways and highlight both MINK1 and the GR–14-3-3 axis as potential targets for future therapeutic intervention in inflammation related disorders.

3.5. Acknowledgements

The author thanks Dr. Matthew W.D. Perry for conceiving and directing the project, Dr. Christian Ottmann for his strategic guidance, Dr. Anders Gunnarsson for his support with the biophysical experiments and analyses, Dr. Arjan Snijder for his support with protein production and purification, Marianna Longo, Prof. Carol Mackintosh, Dr. Ian Ganley, Dr. Stefan Vollmer and Dr. Sofia Winslow for their assistance in cell-based assays. The author thanks ProQinase GmbH for the kinase screen and Dr. Anna Hoyle for her help with peptide mapping. The author acknowledges Dr. Werngard Czechtizky for generous support of the project.

3.6. Materials and methods

Peptide synthesis

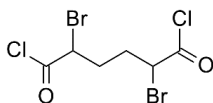
Peptides were synthesized according to the method reported in chapter 2. Fluoro(6FAM)_GR_pT524-pT562 and acetylated_GR_pT524-pT562 were purchased from ThermoFisher Scientific.

Chemical phosphorylation of GR peptides

All solvents and reagents were purchased from commercial suppliers and were used without purification or were prepared according to published procedures. Analytical RP-UPLC-MS and preparative RP HPLC-MS were performed according to the materials and methods reported in chapter 2.6 unless otherwise stated. Nuclear magnetic resonance (NMR) spectra were acquired at 25 °C on a Bruker Avance II, III or AVIII500

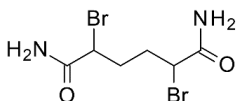
spectrometer at 500 MHz ^1H -frequency and 126 MHz ^{13}C -frequency. Chemical shifts (δ) are reported in parts per million (ppm) relative to residual DMSO signal (δ 2.50 ppm in ^1H NMR and 39.5 ppm in ^{13}C NMR). Coupling constants (J) are reported as Hz. NMR abbreviations are used as follows: br = broad, s = singlet, d = doublet, t = triplet, q = quartet, m = multiplet. Protons on heteroatoms such as COOH protons are only reported when detected in NMR and can therefore be missing.

2,5-dibromohexanedioyl dichloride (**2**)²⁶



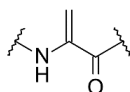
Adipic acid (5.00 g, 34.21 mmol) was suspended in thionyl chloride (14.9 mL, 205.3 mmol) to give a colourless suspension. The reaction mixture was heated to reflux and stirred for 1.5 h. The reaction mixture was allowed to cool to ambient temperature. CCl_4 (20 mL) and NBS (14.6 g, 82.11 mmol) were added. The reaction was stirred vigorously and 2 drops of HBr (48% aq) was added. The reaction mixture was heated to reflux and stirred for 2 h. The reaction mixture was allowed to cool to ambient temperature and then cooled in ice-water to 0 °C. The succinimide was filtered out and the filtrate was concentrated under vacuum to give the title compound as a black oil. The crude product was used for the next reaction.

2,5-dibromohexanediamide (**3**)



Ammonium hydroxide (26% aq) (40 mL, 672.0 mmol) was charged to a round-bottomed flask and cooled to 0 °C. **2** (11.7 g, 34.21 mmol) was added in portions over 20 min. After the addition was complete the reaction mixture was stirred vigorously at 0 °C for 1 h. The resultant precipitate was collected and purified by recrystallisation from MeOH/H₂O 1:1, washed with a little MeOH and dried under high vacuum to give the title compound (mixture of diastereomers) as a white solid (6.83 g, 66% yield). ^1H NMR (500 MHz, DMSO) δ 1.78–2.08 (m, 4H), 4.26–4.4 (m, 2H), 7.30 (s, 2H), 7.68 (s, 2H). ^{13}C NMR (126 MHz, DMSO) δ 32.5, 32.6, 48.2, 48.5, 169.8, 169.9. Purity > 95% according to analytical UPLC., Rt 1.47 and 1.54 min (3-60% B in 10 min). MS (ESI) m/z [$\text{M} + \text{H}$]⁺ calculated for $\text{C}_6\text{H}_{10}\text{Br}_2\text{N}_2\text{O}_2$: 303.0, found: 303.0.

Ac-KTIVPA(DHA)LPQLTP-COOH (**5**)



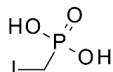
DHA:

Ac-KTIVPA(LPQLTP-COOH (1.07 g, 0.580 mmol) was dissolved in DMF (5 mL) to give a colourless solution. K_2CO_3 (0.400 g, 2.90 mmol) and **3** (0.874 g, 2.90 mmol) were added. The reaction mixture was stirred at ambient temperature for 40 min then at 37 °C for 1.25 h. The reaction mixture was poured in a falcon tube filled with cold ether, centrifuged and the supernatant was removed. The compound was purified by preparative HPLC on a Kromasil C8 column (10 μm 250x50 ID mm) using a gradient of 24-26% acetonitrile in H₂O/ACN/TFA 95/5/0.1

Activation of MINK1 Induces 14-3-3 Regulation of Glucocorticoid Receptor Through Protein-Protein Interaction

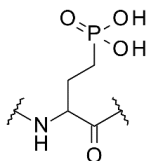
buffer over 25 min with a flow of 100 mL/min and compound detection by UV at 220 nm. Fractions containing product were combined to give the title compound as a white solid (252 mg, 31% yield). Purity > 95% according to analytical UPLC. Rt 5.08 min (3-60% B in 10 min). MS (ESI) m/z $[M + H]^+$ calculated for $C_{65}H_{109}N_{15}O_{18}$: 1389.7, found: 1389.3.

Iodomethylphosphonic acid (**7**)³⁹



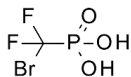
Diethyl(iodomethyl)phosphonate (0.5 mL, 3.06 mmol) was dissolved in concentrated HCl 37% (4 mL) and water (2 mL) to give a light-yellow solution. The reaction mixture was heated to reflux and stirred for 30 h. The reaction mixture was allowed to cool to ambient temperature. Charcoal was added and the mixture was filtered, evaporated and dried under high vacuum. The crude material was recrystallized from 1,2 dichloroethane and dried under high vacuum to give the title compound as a white solid (531 mg, 78% yield). 1H NMR (500 MHz, DMSO) δ 2.97 (d, J = 9.9 Hz, 2H). ^{13}C NMR (126 MHz, DMSO) δ -7.8 (d, J = 146.0 Hz).

Ac-KTIVPA(CpS)LPQLTP-COOH (**8**)

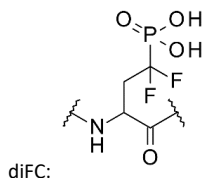


CpS:

Oxygen was thoroughly removed from the buffer solutions by freeze-pump-thaw cycles to avoid competing oxidative cleavage and the whole procedure was performed under a flow of nitrogen. Peptide **5** (100 mg, 0.07 mmol) was dissolved in a mixture of water (13 mL) and ammonium acetate (5 M, 2.88 mL, 14.40 mmol). Compound **7** (1.60 g, 7.20 mmol) was added to give a light pink suspension. The mixture was poured onto $NaBH_4$ (817 mg, 21.60 mmol), cooled to 0 °C. Strong bubbling and foam were observed. The reaction mixture was stirred at 0 °C for 1 h. Additional $NaBH_4$ (272 mg) was added and the reaction mixture was stirred for additional 30 min. HCl 1M was added until pH 7 and the reaction mixture was freeze dried. The two diastereomers were separated by preparative HPLC on a Waters Atlantis T3 ODB column (5 μ m 19x150 mm) using a gradient of 5%B for 1 min, 5-21% B over 3 min, 21-26% B over 15 min (A: water/TFA 100/0.15, B: acetonitrile) with a flow of 30 mL/min. The compounds were detected by mass. Product containing fractions were combined and freeze dried to give the title compounds as white solids (diastereomer 1: 2.0 mg, 1.9% yield; diastereomer 2: 1.5 mg, 1.4% yield). Diastereomer 1: purity > 95% according to analytical UPLC. Rt 4.89 min (5-60% B in 9.3 min). Diastereomer 2: purity > 85% according to analytical UPLC. Rt 5.01 min (5-60% B in 9.3 min). MS (ESI) m/z $[M + H]^+$ calculated for $C_{66}H_{114}N_{15}O_{21}P$: 1485.7, found: 1485.9.

Bromo(difluoro)methylphosphonic acid (10)³⁹

Diethyl (bromodifluoromethyl)phosphonate (2 mL, 10.81 mmol) was treated with concentrated HCl (30 mL, 987.44 mmol) to give a colourless solution. The reaction mixture was heated to reflux and stirred for 20 h. The reaction mixture was allowed to cool to ambient temperature and the solvent was evaporated under reduced pressure. The residue was dried azeotropically with toluene (3 x 15 mL) and then under high vacuum to give the title compound as a light red oil (2.54 g, > 99% yield). ¹³C NMR (126 MHz, DMSO) δ 121.0 (td, J = 329.8, 210.7 Hz).

Ac-KTIVPA(diFCpS)LPQLTP-COOH (11)

Oxygen was thoroughly removed from the buffer solutions by freeze-pump-thaw cycles to avoid competing oxidative cleavage and the whole procedure was performed under a flow of nitrogen. Peptide **5** (72 mg, 0.05 mmol) was dissolved in water (72 mL) and ammonium acetate (5 M, 8 mL, 40.00 mmol). Compound **10** (854 mg, 3.89 mmol) was dissolved in water (4.3 mL) and degassed by freeze-thaw cycles (3 x). The phosphonic acid solution was added to the peptide solution and the whole reaction mixture was poured onto NaBH₄ (392 mg, 10.37 mmol) cooled to 0 °C. Vigorous bubbling and foam were observed. The reaction mixture was stirred at 0 °C for 1 h. Further NaBH₄ (150 mg) was added and the reaction mixture was stirred for additional 30 min (2 x). The crude mixture was concentrated and dried under high vacuum to afford a white oil. The oil was desalted with a PD-10 desalting column filled with Sephadex G-25 resin. The appropriate fractions were combined and freeze dried. An attempt to separate the two diastereomers was performed by preparative HPLC on a Waters XSelect CSH C18 ODB column (5 μ m 19x150 mm) using a gradient of 5% B for 1 min, 5-21% B in 3 min, 21-26% B in 15 min (A: water/TFA 100/0.15, B: acetonitrile) with a flow of 30 mL/min. The compounds were detected by mass. The fractions were enriched but final analysis showed a mixture 50/50 again. The fractions were combined and freeze dried to give the title compound as a white solid (46 mg, 58% yield). Purity > 95% according to analytical UPLC. Mixture of diastereomers, Rt 5.08 and 5.15 min (3-60% B in 10 min). MS (ESI) *m/z* [M + H]²⁺ calculated for C₆₆H₁₁₂F₂N₁₅O₂₁P: 760.9, found: 761.2.

14-3-3 expression and purification

14-3-3s were expressed and purified according to the method reported in chapter 2

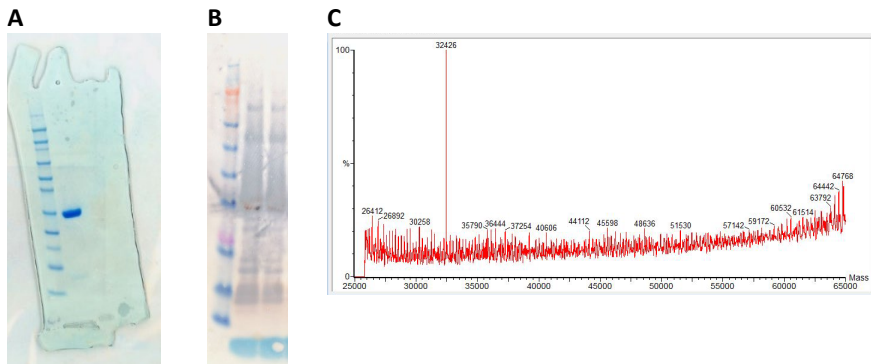
GR LBD expression and purification

GR N514-K777 and GR F602S N514-K777 were cloned in pET24a base vector as N-terminal 6His tag with adjacent TEV cleavage site (ENLYFQG) and expressed in *E. coli* BL21 (DE3)STAR competent cells. Cultures were grown in TB media 5052 auto induction: TB media supplemented by 3 mM MgCl₂, 0.05% glucose, 0.5% glycerol,

Activation of MINK1 Induces 14-3-3 Regulation of Glucocorticoid Receptor Through Protein-Protein Interaction

0.2% lactose, 100 µg/mL kanamycin and 100 µM dexamethasone at 37 °C to an OD₆₀₀ of 1 and then induced for 48 h at 16 °C. The culture was centrifuged (5 000 g, 20 min) and the pellet was lysed using a cell disruptor (Constant Systems LTD) at 25 KPSI in lysis buffer containing 50 mM Tris pH 8, 1% CHAPS, 10% glycerol, 1 mM TCEP, 50 µM dexamethasone and 1 tablet protease inhibitor Roche per 100 mL of lysis buffer. The lysate was incubated with Ni-NTA derivatized Sepharose resin (Qiagen) overnight at 4 °C washed with buffer containing 60 mM NaCl, 30 mM imidazole and eluted with buffer containing 30 mM NaCl, 300 mM imidazole. GR LBD proteins were further purified by size exclusion chromatography on a HiLoad 16/60 Superdex 75 per grade (Pharmacia Biotech) using the following buffer: 50 mM Tris pH 9, 1 mM TCEP and 25 µM dexamethasone. The correct fractions were combined, concentrated, aliquoted, frozen in liquid nitrogen and stored at -80 °C.

a, Purity of GR_F602S_LBD_N514_K777 proteins: 95% according to SDS-PAGE. **b**, Western blot of the GR_F602S_LBD_N514_K777 proteins at two concentrations. Monomeric, dimeric and oligomeric forms were observed. **c**, Mass calculated for GR_F602S_LBD_N514_K777, 32.43 kDa; found 32.43 kDa.



FP assay with GR phosphorylated peptides and 14-3-3

FP assays were conducted according to the method reported in chapter 2

SPR assays with GR phosphorylated peptides and 14-3-3

SPR assays were conducted according to the method reported in chapter 2

Radiometric protein kinase filter-binding assay

The kinase screen was performed by ProQinase GmbH, Freiburg im Breisgau, Germany. A radiometric protein kinase filter-binding assay was used for measuring the kinase activity of the 245 serine/threonine kinases. All protein kinases provided by ProQinase were expressed in Sf9 insect cells or in E.coli as recombinant GST-fusion proteins or His-tagged proteins. All kinases were produced from human cDNAs. Kinases were purified by either GSH-affinity chromatography or immobilized-metal affinity chromatography. Affinity tags were removed from a number of kinases during purification. The purity of the protein kinases was examined by SDS-PAGE/Coomassie staining, the identity was checked by mass spectroscopy. Kinases from external vendors (Carna Biosciences Inc.; Life Technologies (Invitrogen Corporation); Merck-Millipore (Millipore Corporation)) were expressed, purified and quality-controlled by virtue of the vendors readings. The reaction cocktails were pipetted into 96-well V-shaped polypropylene microtiter plates in the following order: kinase solution (10 µL) and buffer/ATP/test sample mixture

(40 μL). The reaction cocktails contained 60 mM HEPES-NaOH pH 7.5, 3 mM MgCl_2 , 3 mM MnCl_2 , 3 μM Na-orthovanadate, 1.2 mM DTT, 1 μM ATP/[γ - ^{33}P]-ATP (8.68 \times 1005 cpm per well), protein kinase (1-400 ng/50 μL) and sample protein (5 μg /50 μL) with minor modifications as stated in the Supporting Information. Each assay plate comprised one well for a buffer/substrate control containing no enzyme. The assay plates were incubated at 30 $^\circ\text{C}$ for 60 min and the reaction cocktails were stopped with 20 μL of 10% v/v H_3PO_4 . The reaction cocktails were transferred into 96-well glass-fibre filter plates (MultiScreen MSFC, Millipore), pre-wetted with 150 mM H_3PO_4 , followed by 10 min incubation at room temperature. After washing with 250 μL of 150 mM H_3PO_4 (3 \times) and with 20 μL of 100% ethanol and drying for 30 min at 40 $^\circ\text{C}$, 50 μL of scintillator (Rotiszint Eco plus, Roth) were added to each well and incorporation of $^{33}\text{P}_i$ ("counting of cpm") was determined with a microplate scintillation counter (Microbeta, Perkin Elmer). Modification to the reaction cocktails are the following. All PKC assays (except the PKC- μ and the PKC- ν assay) additionally contained 1 mM CaCl_2 , 4 mM EDTA, 5 $\mu\text{g}/\text{mL}$ phosphatidylserine and 1 $\mu\text{g}/\text{mL}$ 1,2-dioleoyl-glycerol. The MYLK2, CAMK1D, CAMK2A, CAMK2B, CAMK2D, CAMK4, CAMKK2 and DAPK2 assays additionally contained 1 $\mu\text{g}/\text{mL}$ calmodulin and 0.5 mM CaCl_2 . The PRKG1 and PRKG2 assays additionally contained 1 μM cGMP. The DNA-PK assay additionally contained 2.5 $\mu\text{g}/\text{mL}$ DNA.

Peptide mapping

The protein samples were phosphorylated as described above with non-radioactive ATP. 10, 5, 3, 1 μg of protein sample, supplemented with 25% NuPAGE™ LDS Sample Buffer (4 \times) and 10% NuPAGE™ Sample Reducing Agent (10 \times), was run on a NuPAGE™ 4-12% Bis-Tris Protein Gels, 1.0 mm with MOPS buffer and the bands were revealed using Coomassie Brilliant Blue. Bands of interest were cut from the gel to be washed with water, 1:1 acetonitrile/water, 100 mM ammonium bicarbonate, 1:1 acetonitrile/100 mM ammonium bicarbonate successively for 10 min. The bands were reduced and alkylated with a solution of 10 mM DTT in 100 mM ammonium bicarbonate for 45 min at 65 $^\circ\text{C}$ followed by a solution of 50 mM iodoacetamide in ammonium bicarbonate for 20 min in the dark. The samples were washed with 50 mM ammonium bicarbonate, 1:1 100 mM ammonium bicarbonate/acetonitrile and 100% acetonitrile successively for 10 min each and dried. The bands were digested with 10 ng/ μL trypsin and 12.5 ng/ μL chymotrypsin in 50 mM ammonium bicarbonate at room temperature overnight. The material was extracted twice with 0.1% TFA/60% acetonitrile and was analysed by mass spectrometry. The data files generated were searched against the in-house or Swissprot database using the software Mascot Daemon (Matrix Science). The searches were then manually verified. Material obtained from the trypsin and the chymotrypsin digestion was analysed onto ESI MSMS using X500B mass spectrometer (Sciex) using the Exion chromatography system (Sciex): 20 minute reversed phase gradient with 2.1 \times 100 mm Waters Acquity UPLC CSH C18 analytical column and the X500B for analysis at a flow rate of 300 $\mu\text{L}/\text{min}$. Data were collected in positive ion mode and an autoswitching setup was initiated with automatic precursor selection based on peak intensity and charge state. The collision energies were automatically adjusted based on the precursor and nitrogen was used as the collision gas. Electrospray parameters were as follows: curtain gas, 30 psi; ion source gas 1, 30 psi; ion source gas 2, 40 psi; and temperature, 400 $^\circ\text{C}$. TOF MS mass range was set for 300-1800 Da and TOF MSMS mass range was 100-1500 Da.

Intact mass

The protein samples were phosphorylated as described above with non-radioactive ATP. The samples were diluted to 0.01 mg/mL in 0.1% formic acid and 5% acetonitrile and were analysed by mass spectrometry. The TIC peak data was used to generate the m/z spectrum and the data were deconvoluted to give final mass. The protein samples were analysed on Exion chromatography system (Sciex) with 3.5 μ m, 2.1x50 mm, 300 Å Waters XBridge Protein BEH C4 as column and a reversed phase gradient for 5 min. Acquisition was performed on X500B QTOF flow rate of 500 μ l/min with a Turbo V™ ion source using protein mode acquisition and detector voltage selected over a range of 500–3000 Da. Electrospray parameters were as follows: curtain gas, 50 psi; ion source gas 1, 50 psi; ion source gas 2, 50 psi; and temperature, 400 °C. The X500B collected data in positive ion mode over a mass range of 500–3000 Da. Standard mobile phases were used (Mobile Phase A: 0.1% formic acid in water, Mobile Phase B: 0.1% formic acid in acetonitrile).

Cell culture, transfection and stimulation

15 cm Nunc™ cell culture dishes, DMEM Gibco®, trypsin-EDTA (0.05%) phenol red Gibco®, DPBS without Calcium and Magnesium Gibco®, Opti-MEM Gibco®, penicillin-streptomycin (10,000 U/mL) Gibco® and Fetal Bovine Serum (origin New Zealand) Gibco® were purchased from ThermoFisher Scientific. The transfection reagent Lipofectamine™ 2000 was purchased from ThermoFisher Scientific and X-tremeGENE™ 9 DNA, Roche from Sigma-Aldrich. The compounds forskolin, H89 and calyculin A were purchased from Sigma-Aldrich, IGF-1 was purchased from Cell Signaling Technology whilst the pyridinylfuranopyrimidine inhibitor PI103 was a kind gift of Professor Carol Mackintosh (Division of Cell and Developmental Biology, School of Life Sciences, University of Dundee, Scotland). Reagents required for western-blotting, namely NuPAGE™ 4-12% Bis-Tris Protein Gels, 1.0 mm, NuPAGE™ LDS Sample Buffer (4X), NuPAGE™ Sample Reducing Agent (10X) and Coomassie Brilliant Blue were purchased from ThermoFisher Scientific. The primary antibodies used in the Co-IP experiments were: D8H2 (Cell Signaling Technology), GFP (Sigma-Aldrich), Anti-MAP4K6 antibody–C-terminal (abcam), pan 14-3-3 (Cell Signaling Technology), Phospho-VASP Ser239 (Cell Signaling Technology) and Phospho-Akt (Ser473) (Cell Signaling Technology). The BMH1-BMH2-digoxigenin probe was a kind gift of Professor Carol Mackintosh (Division of Cell and Developmental Biology, School of Life Sciences, University of Dundee, Scotland).

The HEK293 and U2OS cell lines (ATCC) were cultured in DMEM medium, supplemented with 10% foetal bovine serum and 1% penicillin-streptomycin (10,000 U/mL) at 37 °C in a 5% CO₂ environment. For Co-IP assay, 3 × 10⁶ cells were seeded in a 15 cm cell culture dish. At 60–70% confluence, the HEK293 cells were transiently transfected with a mixture of 6 μ g GFP- MINK1 or GFP-GR DNA and 24 μ l lipofectamine 2000 in 2 mL Opti-MEM for 24 h. At 60–70% confluence, the U2OS cells were transiently transfected with a mixture of 8 μ g GFP-MINK1 or GFP-GR and/or FLAG-MINK1 DNA and 32 μ l X-tremeGENE™ 9 DNA in 2 mL Opti-MEM for 24 h. Stimulation with forskolin, H89, IGF-1 and PI303 was preceded by a cell starvation step where the cells were incubated with DMEM medium without supplement overnight. The cells were treated with the right compound at the concentration and during the time stated in the table below.

Cells were treated as followed:

COMPOUND	STOCK CONCENTRATION	CONDITIONS
IGF1	100 µg/mL	100 ng/mL for 20 min
PI103	10 mM	1 µM 30 min
Forskolin	20 mM	20 µM for 30 min
H89	20 mM	30 µM for 30 min
Calyculin A	10µM	50 nM for 10 min

TREATMENT NAME	PROCEDURE
IGF1	Treatment with IGF1
PI103	Pre-treatment with PI103 then treatment with IGF1
Forskolin	Treatment with forskolin
H89	Pre-treatment with H89 then treatment with forskolin
Calyculin A	Treatment with calyculin A

Co-immunoprecipitation assay

Cells were collected and lysed in radioimmunoprecipitation assay (RIPA) buffer containing 50 mM Tris-HCl pH8, 150 mM NaCl, 1 mM EDTA, 0.1% SDS, 1% Na deoxycholate, 1% NP-40 supplemented with protease inhibitor cocktail. After lysis, the concentration of protein was quantified by Bradford test. Dilution/washing buffer containing 50 mM Tris-HCl pH8, 150 mM NaCl and 1 mM EDTA was added to reach equal concentration and 50 µL were saved as input fraction for future analysis. Equal volumes of protein solution were incubated with 10 µL GFP-Trap Agarose beads® (ChromoTek) at 4 °C for 2 h. 50 µL were saved as flowthrough fraction for future analysis and the beads were washed with dilution/washing buffer (2 ×). 30 µL NuPAGE™ LDS Sample Buffer (4 ×) were added to the beads and proteins from the input, flowthrough and IP fractions were denatured at 95 °C for 5 min.

Eluted proteins were resolved on a NuPAGE™ 4-12% Bis-Tris Protein Gels, 1.0 mm. The gels were transferred to polyvinylidene difluoride (PVDF) membranes (previously activated in methanol) which were then blocked with Intercept® (TBS) blocking buffer (LI-COR). After washing with TBST, the membranes were probed at 4 °C overnight with the primary antibodies listed in the Supporting Information. After washing with TBST, the membranes were incubated with the specific rabbit IRDye 800CW secondary antibody (LI-COR) for 1 h at room temperature. After washing with TBST, the blots were detected using an Odyssey CLx Imaging system (LI-COR). Data analysis was performed using Image Studio (LI-COR).

Far-Western blot assay

Samples containing proteins from Co-IP assay or GR LBD *in vitro* phosphorylated were loaded on a NuPAGE™ 4-12% Bis-Tris Protein Gels, 1.0 mm and separated. The gels were transferred to polyvinylidene difluoride membranes which were blocked with Intercept® (TBS) blocking buffer (LI-COR). After washing with TBST, the membranes were probed at 4 °C overnight with BMH1-BMH2-digoxigenin probe diluted in 5% bovine serum albumin (BSA) TBST. After washing with TBST, the membranes were incubated with anti-digoxigenin antibody (R&D Systems) at 4 °C overnight. After washing with TBST, the membranes were incubated with the specific mouse IRDye 800CW or IRDye 680LT secondary antibody (LI-COR) for 1 h at room temperature. After washing with TBST, the blots were detected using an Odyssey CLx Imaging system (LI-COR). Data analysis was performed using Image

Activation of MINK1 Induces 14-3-3 Regulation of Glucocorticoid Receptor Through Protein-Protein Interaction

Studio (LI-COR). Measurements were performed as triplicates. The figures were made using the software GraphPad Prism 8 and significance (two-tailed p value) was assessed by t-test. Asterisks were attributed for the following significance values: *p < 0.05, **p < 0.01, ***p < 0.001, ****p < 0.0001.

GR peptide analysis

FITC labelled GR_pT562:

FITC labelled GR_pT562 peptide was prepared following General Protocol for SPPS. The crude peptide was purified by reverse-phase HPLC (gradient: 5% B for 1 min, 5–33% B in 3 min, 33–38% B in 15 min, Waters Xselect CSH C18 column) to afford the desired peptide as a white fluffy solid. Yield (5 mg) in 83% purity according to analytical UPLC. Rt 4.14 min (3–93% B in 9 min).

[M + 2H]²⁺ calculated for C₉₂H₁₃₀N₁₉O₂₈PS₃, 1039.2; found 1039.4.

Acetylated GR_pT524-pT562:

Acetylated GR_pT524-pT562 peptide was purchased from Thermo Scientific with a purity over 95%.

FITC labelled GR_pT524-pT562:

FITC labelled GR_pT524-pT562 peptide was purchased from Thermo Scientific with a purity over 95%.

3.7. References

1. Ronchetti, S., Migliorati, G., Bruscoli, S. & Riccardi, C. Defining the role of glucocorticoids in inflammation. *Clin. Sci.* **132**, 1529–1543 (2018).
2. Scheschowitsch, K., Leite, J. A. & Assreuy, J. New insights in glucocorticoid receptor signaling—more than just a ligand-binding receptor. *Frontiers in Endocrinology* **8**, 16 (2017).
3. Chanpimol, S., Seamon, B., Hernandez, H., Harris-love, M. & Blackman, M. R. Glucocorticoid receptor control of transcription: precision and plasticity via allostery. *Nat. Rev. Mol. Cell Biol.* **18**, 159–174 (2017).
4. Vandevyver, S., Dejager, L. & Libert, C. Comprehensive overview of the structure and regulation of the glucocorticoid receptor. *Endocr. Rev.* **35**, 671–693 (2014).
5. Kino, T. & Chrousos, G. P. Acetylation-mediated epigenetic regulation of glucocorticoid receptor activity: Circadian rhythm-associated alterations of glucocorticoid actions in target tissues. *Mol. Cell. Endocrinol.* **336**, 23–30 (2011).
6. Nader, N., Chrousos, G. P. & Kino, T. Circadian rhythm transcription factor CLOCK regulates the transcriptional activity of the glucocorticoid receptor by acetylating its hinge region lysine cluster: potential physiological implications. *FASEB J.* **23**, 1572–1583 (2009).
7. Le Drean, Y., Mincheneau, N., Le Goff, P. & Michel, D. Potentiation of glucocorticoid receptor transcriptional activity by sumoylation. *Endocrinology* **143**, 3482–3489 (2002).
8. Tian, S., Poukka, H., Palvimo, J. J. & Jänne, O. A. Small ubiquitin-related modifier-1 (SUMO-1) modification of the glucocorticoid receptor. *Biochem. J.* **367**, 907–911 (2002).
9. Deroo, B. J. *et al.* Proteasomal Inhibition Enhances Glucocorticoid Receptor Transactivation

- and Alters Its Subnuclear Trafficking. *Mol. Cell. Biol.* **22**, 4113–4123 (2002).
10. Kino, T., Liou, S. H., Charmandari, E. & Chrousos, G. P. Glucocorticoid receptor mutants demonstrate increased motility inside the nucleus of living cells: Time of fluorescence recovery after photobleaching (FRAP) is an integrated measure of receptor function. *Mol. Med.* **10**, 80–88 (2004).
 11. Gallihier-Beckley, A. J. & Cidlowski, J. A. Emerging Roles of Glucocorticoid Receptor Phosphorylation in Modulating Glucocorticoid Hormone Action in Health and Disease. *IUBMB Life* **61**, 979–986 (2009).
 12. Chen, W. *et al.* Glucocorticoid receptor phosphorylation differentially affects target gene expression. *Mol. Endocrinol.* **22**, 1754–1766 (2008).
 13. Garza, A. M. S., Khan, S. H. & Kumar, R. Site-Specific Phosphorylation Induces Functionally Active Conformation in the Intrinsically Disordered N-Terminal Activation Function (AF1) Domain of the Glucocorticoid Receptor. *Mol. Cell. Biol.* **30**, 220–230 (2010).
 14. Wang, Z., Frederick, J. & Garabedian, M. J. Deciphering the phosphorylation ‘code’ of the glucocorticoid receptor in vivo. *J. Biol. Chem.* **277**, 26573–26580 (2002).
 15. Kumar, R. & Thompson, E. B. Role of phosphorylation in the modulation of the glucocorticoid receptor’s intrinsically disordered domain. *Biomolecules* **9**, 1–10 (2019).
 16. Khan, S. H., McLaughlin, W. A. & Kumar, R. Site-specific phosphorylation regulates the structure and function of an intrinsically disordered domain of the glucocorticoid receptor. *Sci. Rep.* **7**, 15440 (2017).
 17. Kino, T. GR-regulating Serine/Threonine Kinases: New Physiologic and Pathologic Implications. *Trends Endocrinol. Metab.* **29**, 260–270 (2018).
 18. Gallihier-Beckley, A. J., Williams, J. G. & Cidlowski, J. A. Ligand-Independent Phosphorylation of the Glucocorticoid Receptor Integrates Cellular Stress Pathways with Nuclear Receptor Signaling. *Mol. Cell. Biol.* **31**, 4663–4675 (2011).
 19. Habib, T. *et al.* AKT1 has dual actions on the glucocorticoid receptor by cooperating with 14-3-3. *Mol. Cell. Endocrinol.* **439**, 431–443 (2017).
 20. Hwang, Y., An, H. T., Kang, M. & Ko, J. Roles of 14-3-3 β and γ in regulation of the glucocorticoid receptor transcriptional activation and hepatic gluconeogenesis. *Biochem. Biophys. Res. Commun.* **501**, 800–806 (2018).
 21. Kim, Y. S. *et al.* Role of 14-3-3 η as a Positive Regulator of the Glucocorticoid Receptor Transcriptional Activation. *Endocrinology* **146**, 3133–3140 (2005).
 22. Kino, T. *et al.* Protein 14-3-3 σ Interacts With and Favors Cytoplasmic Subcellular

- Localization of the Glucocorticoid Receptor, Acting as a Negative Regulator of the Glucocorticoid Signaling Pathway. *J. Biol. Chem.* **278**, 25651–25656 (2003).
23. Widén, C., Zilliacus, J., Gustafsson, J. Å. & Wikström, A. C. Glucocorticoid Receptor Interaction with 14-3-3 and Raf-1, a Proposed Mechanism for Cross-Talk of Two Signal Transduction Pathways. *J. Biol. Chem.* **275**, 39296–39301 (2000).
 24. Wakui, H., Wright, A. P. H., Gustafsson, J. & Zilliacus, J. Interaction of the Ligand-activated Glucocorticoid Receptor with the 14-3-3 η Protein. *J. Biol. Chem.* **272**, 8153–8156 (1997).
 25. Wright, T. H. *et al.* Posttranslational mutagenesis: A chemical strategy for exploring protein side-chain diversity. *Science* **354**, aag1465 (2016).
 26. Chalker, J. M. *et al.* Methods for converting cysteine to dehydroalanine on peptides and proteins. *Chem. Sci.* **2**, 1666–1676 (2011).
 27. Bledsoe, R. K. *et al.* Crystal Structure of the Glucocorticoid Receptor Ligand Binding Domain Reveals a Novel Mode of Receptor Dimerization and Coactivator Recognition. *Cell* **110**, 93–105 (2002).
 28. Madeira, F. *et al.* 14-3-3-Pred: improved methods to predict 14-3-3-binding phosphopeptides. *Bioinformatics* **31**, 2276–2283 (2015).
 29. Krishnamurthy, V. M., Semetey, V., Bracher, P. J., Shen, N. & Whitesides, G. M. Dependence of effective molarity on linker length for an intramolecular protein-ligand system. *J. Am. Chem. Soc.* **129**, 1312–1320 (2007).
 30. Stevers, L. M., de Vink, P. J., Ottmann, C., Huskens, J. & Brunsveld, L. A Thermodynamic Model for Multivalency in 14-3-3 Protein-Protein Interactions. *J. Am. Chem. Soc.* **140**, 14498–14510 (2018).
 31. Chen, S. *et al.* Complementary regulation of TBC1D1 and AS160 by growth factors, insulin and AMPK activators. *Biochem. J.* **409**, 449–459 (2008).
 32. Zhang, M. S. *et al.* Biosynthesis and genetic encoding of phosphothreonine through parallel selection and deep sequencing. *Nat. Methods* **14**, 729–736 (2017).
 33. Rogerson, D. T. *et al.* Efficient genetic encoding of phosphoserine and its nonhydrolyzable analog. *Nat. Chem. Biol.* **11**, 496–503 (2015).
 34. Nicke, B. *et al.* Involvement of MINK, a ste20 family kinase, in ras oncogene-induced growth arrest in human ovarian surface epithelial cells. *Mol. Cell* **20**, 673–685 (2005).
 35. McCarty, N. *et al.* Signaling by the kinase MINK is essential in the negative selection of autoreactive thymocytes. *Nat. Immunol.* **6**, 65–72 (2005).
 36. Hu, Y. *et al.* Identification and functional characterization of a novel human Misshapen/Nck

- interacting kinase-related kinase, hMINK β . *J. Biol. Chem.* **279**, 54387–54397 (2004).
37. Yue, M. *et al.* Misshapen/NIK-related kinase (mink1) is involved in platelet function, hemostasis, and thrombus formation. *Blood* **127**, 927–937 (2016).
38. Dan, I. *et al.* Molecular cloning of MINK, a novel member of mammalian GCK family kinases, which is up-regulated during postnatal mouse cerebral development. *FEBS Lett.* **469**, 19–23 (2000).
39. Crofts, P. C. & Kosolapoff, G. M. The Preparation and the Determination of Apparent Dissociation Constants of Some Substituted Aliphatic Phosphonic Acids. *J. Am. Chem. Soc.* **75**, 5738–5740 (1953).

Chapter 4

Identification of Small Molecule Stabilisers of the Glucocorticoid Receptor 14-3-3 Protein-Protein Interaction

Abstract

Given the importance of GR agonists in medicine, despite their numerous adverse side effects, it is of great interest to fully delineate the regulatory network of GR. Post-translational modifications form part of this regulatory network including phosphorylation. After phosphorylation GR interacts with 14-3-3, adding another layer of regulation beyond the ligand-driven activation. Here, I identified the first stabilisers of GR–14-3-3 PPI. Screening 8,000 compounds led to the discovery of hits. To foster confidence in their stabilisation activity, these hits were further investigated in an array of experiments using biophysical assays, 1D and 2D NMR spectroscopy, and analysis of near neighbours enabled us to outline initial structure activity relationships. At least two compounds were found to have promise for further development. These hits provide starting points for future development into potent tool compounds which could contribute to answering the long-standing question of the physiological role of the GR–14-3-3 PPI and leverage novel opportunities for future therapeutic interventions.

4.1. Introduction

The human genome project defined the total number of potential protein targets for pharmacological intervention. Within cells, however, most proteins are part of networks that involve multiple partners and the number of interactions that are involved has been estimated to be of the order of 650 000¹. Modulation of such interactions offers the potential to affect signalling and regulatory networks and thus have effects on the behaviour of cells. In order to address conditions that are not adequately treated by current therapeutics it is necessary to go beyond single targets and seek to manipulate PPIs, thus expanding the number of potentially druggable targets significantly. Modulation of PPIs can be either through inhibition or stabilisation of the interaction, depending on the desired outcome.

Inhibition of PPIs has become a well-established, if still challenging, therapeutic strategy. Marketed PPI inhibitors include Tirofiban, Daclatasvir and Venetoclax, with further compounds in development^{2,3}. In contrast stabilisation of PPIs has been less explored, although natural products that use this mechanism have been identified and developed into drugs. For example, the immunosuppressants cyclosporin A and FK506 (tacrolimus) induce the binding of cyclophilin A and FK506 binding protein respectively, to the phosphatase calcineurin. The complex of protein and drug inhibits the phosphatase activity by blocking the access to the active site³. Thalidomide, and related immunomodulatory imide drugs (IMiDs) have been identified in the past decade to exert some of their effects through stabilisation of PPIs between the CRL4^{CRBN} E3 ubiquitin ligase and neosubstrates, such as the B cell transcription factors, Ikaros, Aiolos, the kinase casein kinase 1A1 and, particularly relevant to the notorious teratogenic effects of thalidomide, the transcription factor SALL4⁴. IMiDs promote the proteasomal degradation of these targets and are used therapeutically in multiple myeloma and the del(5q) myelodysplastic syndrome (MDS)^{5,6,7}. The stabilisation of non-natural PPIs has been exploited in the design of bifunctional molecules (PROTACs) hijacking cereblon and other E3 ligases to induce proteasomal degradation of selected proteins⁸.

GR is a ligand dependent transcription factor which belongs to the superfamily of nuclear hormone receptors, a highly conserved protein family. GR controls fundamental processes including immunoregulatory and anti-inflammatory responses. Within cells, the location and activation state of GR is regulated by a complex and dynamic PPI network, with transcription factors, coactivators, corepressors and enzymes, including both kinases and phosphatases^{9,10}. The full implications of these PPIs in GR regulatory pathways remain, however, unclear. Given the importance of GR agonists in the treatment of inflammation, immunological conditions and some cancers, despite their many side-effects¹¹, it is of great importance to understand the regulatory network controlling GR. In this regard,

we and others have turned our attention towards the hub-protein 14-3-3¹². 14-3-3 proteins are involved in the regulation of a wide range of cellular processes, including cell cycle progression, apoptosis, intracellular protein trafficking and signal transduction. 14-3-3 proteins act as dimers which contain two amphipathic binding grooves and interact with their protein partners *via* recognition of phosphorylated serine/threonine residues. After phosphorylation, GR has been shown to interact with 14-3-3, and this interaction has been hypothesised to play a part in the localisation and activity of GR in pathological inflammatory disorders and cancer^{13,14}.

In the quest to understand the physiological role of the GR–14-3-3 PPI, phosphosites on GR that are recognised by 14-3-3 and the kinases responsible for the phosphorylation of these residues have been previously identified (Munier *et al*, submitted). The most high-affinity GR peptides have been co-crystallised with 14-3-3 ζ and two binding pockets created at the interface of the GR peptide and 14-3-3 protein have been observed. In this chapter, I describe how I use this information, together with high-throughput screening (HTS), to identify, for the first time, stabilisers of the GR–14-3-3 PPI. Such tool compounds could contribute to answering the long-standing question of the physiological role of the GR–14-3-3 PPI.

4.2. Results

4.2.1. Ligandability of the GR–14-3-3 PPI interface

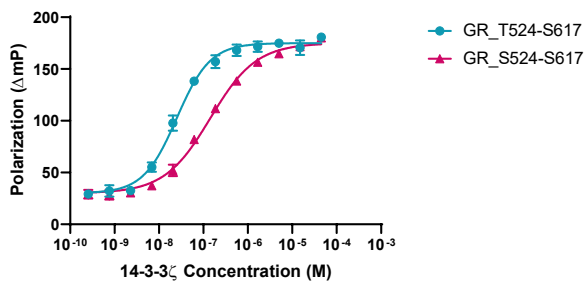
In the previous chapters, GR–14-3-3 PPI has been investigated at a GR peptide level using biophysical assays, and X-ray crystallography. pT524 of GR has been found to be the most important phosphosite, particularly in association with pS617 in GR recognition by 14-3-3. Kinase screening revealed MINK1 as a key player in GR T524 phosphorylation and cell experiments confirmed the importance of the two GR phosphosites and the role of MINK1 in the binding of GR with 14-3-3 (Munier *et al*, submitted). I have co-crystallized the GR peptide, GR_pT524-pS617 (Fig. 2.5 and Fig. 2.6), with 14-3-3 ζ (PDB code 6YOS) to build a model for studying the interaction between GR and 14-3-3. The crystal structure of GR_pT524-pS617 bound to 14-3-3 ζ elucidated the mechanistic details of the interaction. GR_pT524-pS617 was found to interact with the two central binding channels of a 14-3-3 ζ dimer mainly through electrostatic interactions between pT524 and pS617 and the basic pockets of the 14-3-3 dimer, consisting of K49, R56 and R127. Proline at the GR position 526 produced a sharp change in the chain direction, exiting the C-terminus of the GR peptide from the binding groove and creating a new pocket at the interface of the GR peptide and 14-3-3. Similarly, a second pocket was formed between GR residues 618-621 and the second 14-3-3 unit. Small molecules have been shown

to bind in similar pockets for other 14-3-3–ligand combinations⁴⁵. I was interested to see if I could identify novel ligands that could bind in the pocket and stabilise the PPI between 14-3-3 and GR.

4.2.2. Screening of 8K compounds to identify plausible stabilisers of GR–14-3-3 PPI

I tested 7,000 small molecules and 700 fragments from the AstraZeneca collection to identify stabilisers of the interaction between a GR phosphopeptide, as a surrogate for GR, and 14-3-3. These compounds were chosen to provide chemical diversity to maximize the chemical space coverage. FP was used as a primary assay for its rapidity, its sensitivity and the small amount of material required. GR_pT524-pS617 was not suitable for use in screening, due to its potent binding affinity with 14-3-3 ζ ($K_d=18$ nM) resulting in a narrow assay window. Instead, a less potent analogue GR peptide was identified. Mutation of the GR pT524 into pS reduced the affinity of the peptide toward 14-3-3 ζ by 8-fold ($K_d=140$ nM) (Fig. 4.1). With a ligand of this potency I was able to optimize the assay for maximal robustness (z prime factor=0.9). Concentrations of 14-3-3 ζ and GR_pS524-pS617 were set to obtain 20% occupancy and compounds were tested at a single concentration (small molecules, 100 μ M; fragments, 1 mM). As I hoped, the compounds showed differential abilities to modulate the GR peptide–14-3-3 interaction and a relatively low threshold was set to determine the compounds for further investigation. From 7,000 small molecules, 482 were found above this threshold at least twice in the three different replicates; similarly, from 700 fragments, 110 were selected (Fig. 4.2).

A



B

Peptide name	Sequence	K_d with 14-3-3 ζ by FP (nM)
GR_pT524-pS617	KTIVPA pTLPQLTPGGGGGRSYRQS pS ANLLCF	18 \pm 6
GR_pS524-pS617	KTIVPA pSLPQLTPGGGGGRSYRQS pS ANLLCF	136 \pm 5

Figure 4.1. Comparison between the binding affinity of GR_pT524-pS617 and the mutated GR peptide, GR_pS524-pS617. (A) Dose-response curves of FP assays GR_pT524-pS617 and GR_pS524-pS617 with 14-3-3 ζ . (B)

Identification of Small Molecule Stabilisers of the Glucocorticoid Receptor 14-3-3 Protein-Protein Interaction

Amino acid sequence of GR_pT524-pS617 and GR_pS524-pS617 and their binding affinity (K_d) with 14-3-3 ζ measured by FP. Phosphorylated sites are depicted in bold black.

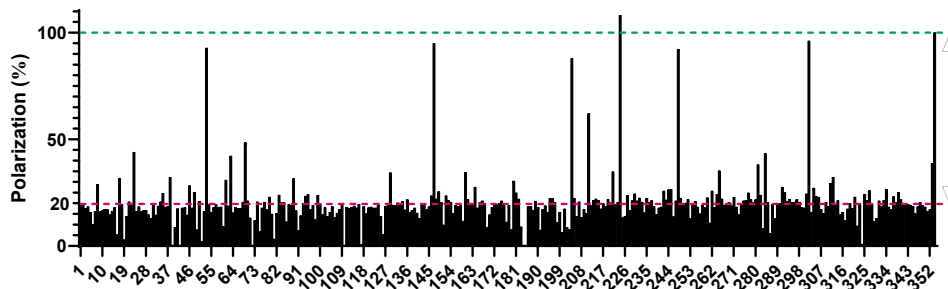


Figure 4.2. Example of the results obtained from the primary screen: FP assay single concentration. The 384-well plate consisted of one column without compound (average value reported as number 1 on the bar graph), 352 small molecules at a concentration of 100 μ M (number 2-353 on the bar graph), and one column with a concentration of GR_pS524-pS617 to reach steady state (average value reported as number 354 on the bar type graph). The polarization value between GR_pS524-pS617 and 14-3-3 ζ in the absence of any compound, with a concentration of GR_pS524-pS617 to reach 20% occupancy, is depicted in pink dashed line. The maximum polarization value is depicted in green dashed line. The double arrow represents the assay window. Compounds with a value above this maximum polarization value were disregarded.

The identified compounds were counter-screened using SPR as an orthogonal assay to exclude false positives resulting from interference with the FP assay. Using similar assay conditions to the primary screen, 47 small molecules and 7 fragments were selected to go forward within the screening workflow (Fig. 4.3). To control for the most probable artefact in the FP assay, namely aggregation, which also occurs in the SPR assay, the selected compounds were titrated in an FP concentration-dependent assay, either in the presence of GR peptides and 14-3-3 proteins or only with labelled GR peptides. Thus, any signal observed in the absence of 14-3-3 ζ was assigned as an artefact and the compounds were disregarded. I identified 4 small molecules and 2 fragments which exhibited a concentration-dependent response but did not give a signal in the absence of 14-3-3 protein (Fig. 4.5 and Fig. 4.6). These hits showed a similar stabilisation activity, about 2-fold, at 200 μ M and 2 mM for the small molecules and the fragments respectively, except for compound 3 which stabilised the GR-derived phosphopeptide-14-3-3 by 4-fold (Fig. 4.7).

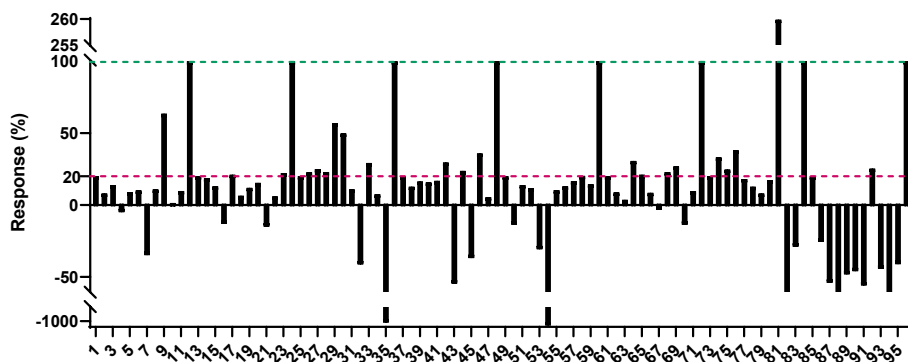


Figure 4.3. Example of the results obtained from the counter screen: SPR assay single concentration. The 96-well plate consisted in the first column without compound (number 1, 13, 25, 37, 49, 61, 73 and 85 on the bar graph), 72 small molecules at a concentration of 100 μM , and the last column with a concentration of GR_pS524-pS617 to reach steady state (number 12, 24, 36, 48, 60, 72, 84 and 96 on the bar type graph). The SPR signal between GR_pS524-pS617 and 14-3-3 ζ in the absence of any compound, with a concentration of GR_pS524-pS617 to reach 20% occupancy, is depicted in pink dashed lines. The maximum polarization value is depicted in green dashed lines.

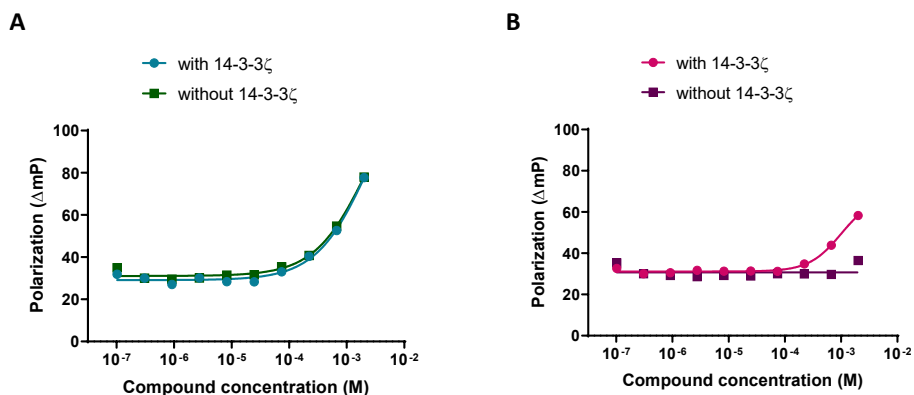


Figure 4.5. Example of the results obtained from the final screen: FP assay concentration response. (A) Dose-response curves of a false positive compound with GR_pS524-pS617 and with or without 14-3-3 ζ . Concentration-dependent polarization values were observed in the absence of 14-3-3 ζ . (B) Dose-response curves of a true positive compound with GR_pS524-pS617 and with or without 14-3-3 ζ . No concentration-dependent polarization value was observed in the absence of 14-3-3 ζ .

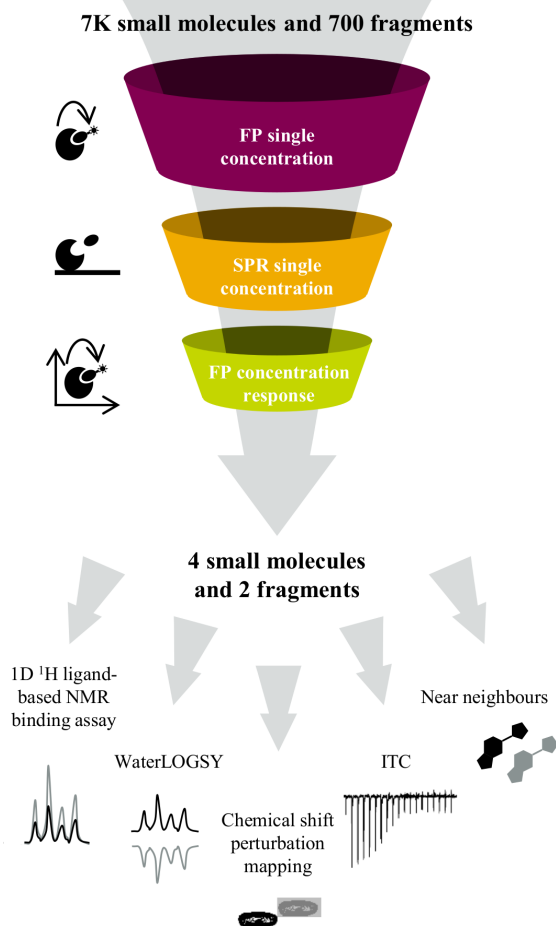


Figure 4.6. Screening workflow to identify 6 plausible stabilisers and the subsequent confirmation strategy.

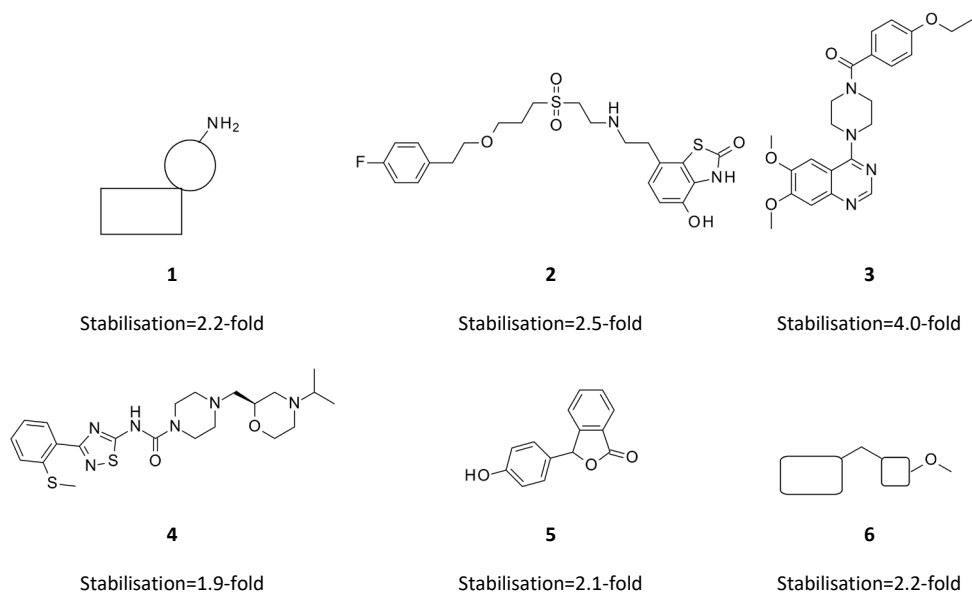


Figure 4.7. Identification of 6 plausible stabilisers of the GR–14-3-3 PPI by screening. Chemical structure of hits 1–6 and their stabilisation activity calculated by FP at 200 μ M for compound 1–4 and 2 mM for the fragments 5 and 6.

4.2.3. Confirmation of the identified hits

The 6 hits were further investigated in an array of experiments. 1D ^1H ligand-based NMR binding assays were performed in the absence and presence of the GR peptide–14-3-3 ζ complex. Hits 1–5 showed broadening of their signal on addition of peptide and 14-3-3 ζ , indicating an interaction of these compounds with the GR peptide–14-3-3 complex. The signal of fragment 6, however, did not broaden (Fig. 4.8).

Identification of Small Molecule Stabilisers of the Glucocorticoid Receptor 14-3-3 Protein-Protein Interaction

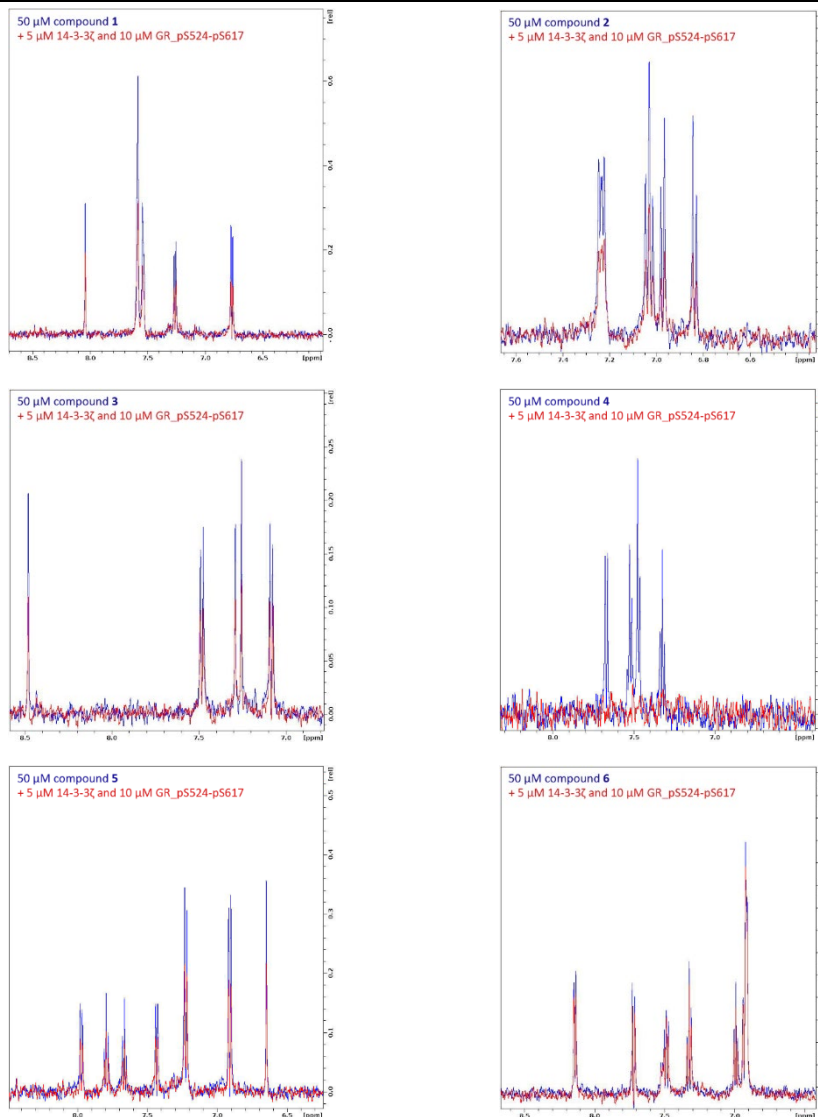


Figure 4.8. $1D\ ^1H$ NMR spectra of compound 1-6 respectively (50 μM), depicted in red, overlapped with those recorded after addition of 14-3-3 ζ (5 μM) and GR peptide (10 μM), depicted in blue.

WaterLOGSY was used to further assess the binding of the hit molecules to both 14-3-3 ζ , 14-3-3 σ and their respective complexes with the GR peptide. All six compounds showed an interaction with 14-3-3 ζ in the presence and absence of GR_pS524-pS617. Hits **1**, **2**, **3** and **5** were also detected to bind 14-3-3 σ with and without GR_pS524-pS617. **4.1**, a structurally related compound to **4**,

interacted with 14-3-3 σ only in the presence of the GR peptide. Fragment **6** did not show any binding to 14-3-3 σ (Fig. 4.9-4.14 and Table 4.1), raising the question of selectivity for **6** towards 14-3-3 ζ .

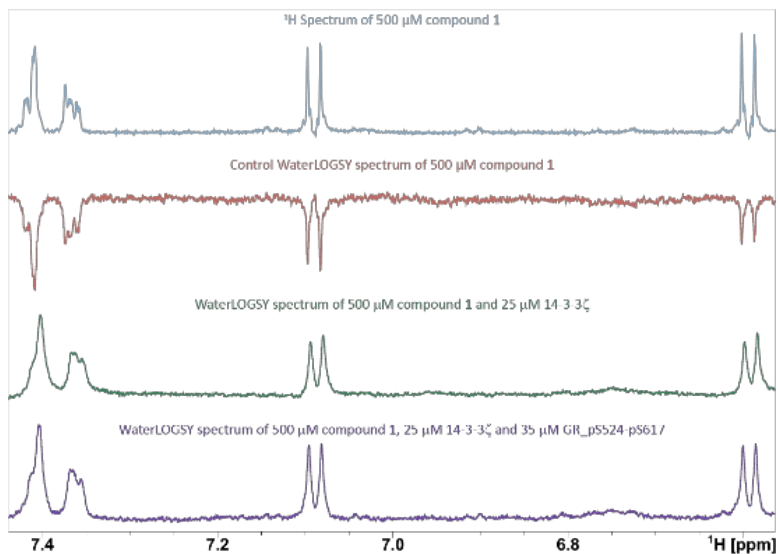
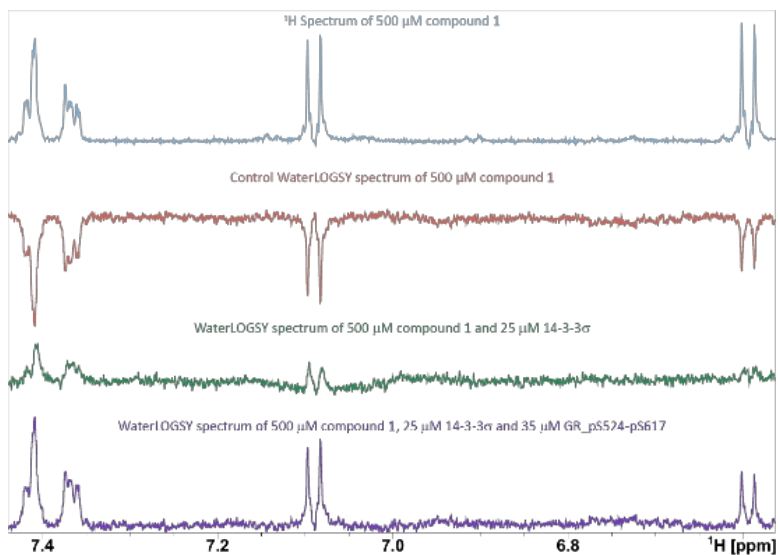
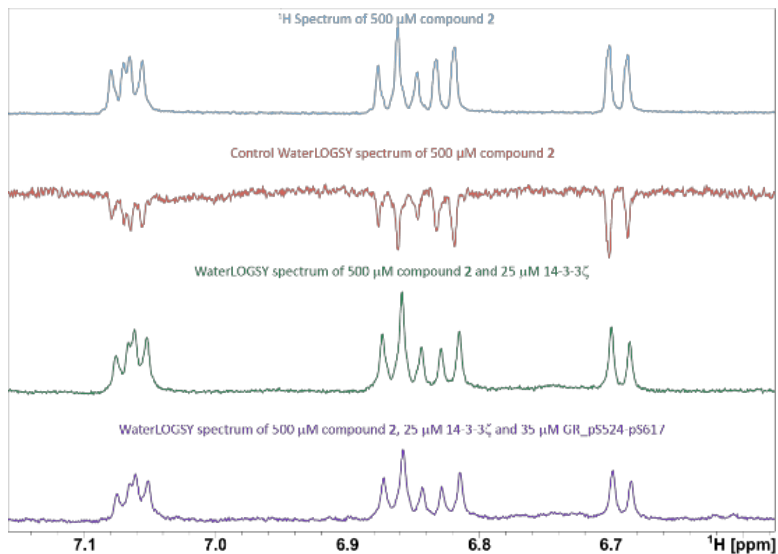
A**B**

Figure 4.9. Compound **1** binds to (A) 14-3-3 ζ and (B) 14-3-3 σ in the presence and absence of GR_p5524-p5617. ^1H spectrum of 500 μM compound **1** (blue spectrum) and WaterLOGSY spectra of 500 μM compound **1** (red spectrum), with 25 μM 14-3-3 (green spectrum) or with 25 μM 14-3-3 and 35 μM GR_p5524-p561 (purple spectrum). NMR

signals are negatively phased in the WaterLOGSY spectrum of compound **1** but inverted in the presence of the GR peptide–14-3-3 complex, indicating binding.

A



B

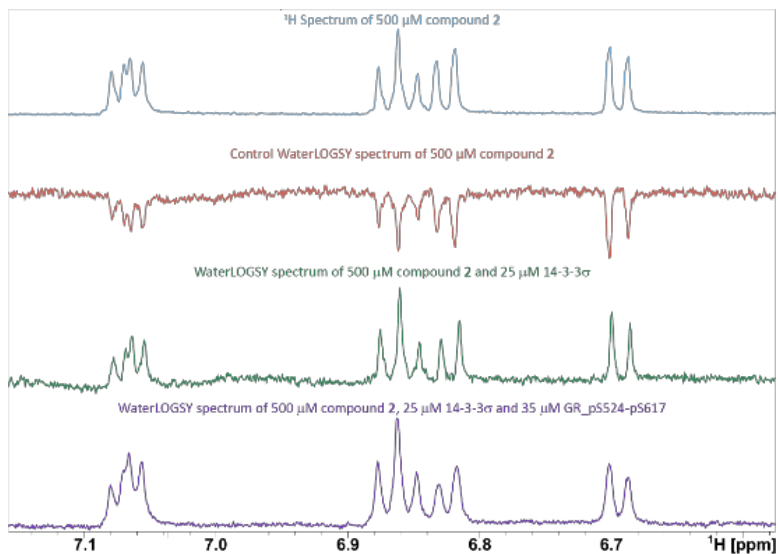


Figure 4.10. Compound 2 binds to (A) 14-3-3 ζ and (B) 14-3-3 σ in the presence and absence of GR_pS524-pS617. ^1H spectrum of 500 μM compound **2** (blue spectrum) and WaterLOGSY spectra of 500 μM compound **2** (red spectrum), with 25 μM 14-3-3 (green spectrum) or with 25 μM 14-3-3 and 35 μM GR_pS524-pS617 (purple

spectrum). NMR signals are negatively phased in the WaterLOGSY spectrum of compound **2** but inverted in the presence of the GR peptide–14-3-3 complex, indicating binding.

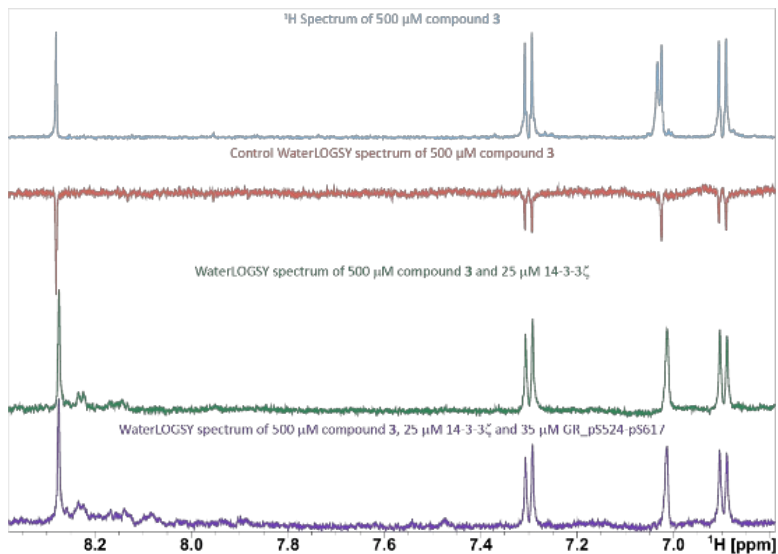
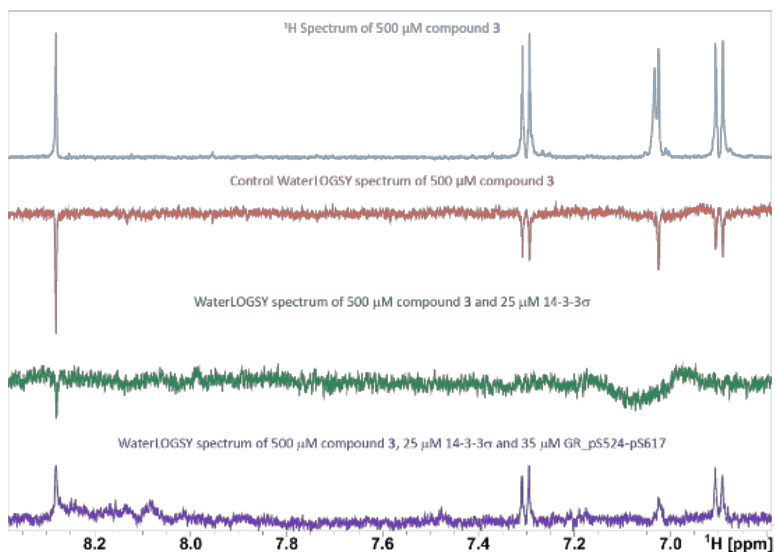
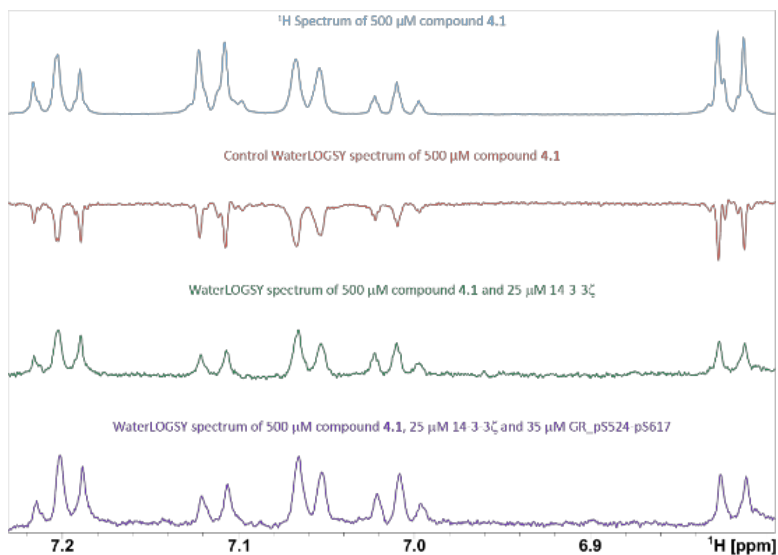
A**B**

Figure 4.11. Compound **3 binds to (A) 14-3-3 ζ and (B) 14-3-3 σ in the presence and absence of GR_pS524-pS617.** ^1H spectrum of 500 μM compound **3** (blue spectrum) and WaterLOGSY spectra of 500 μM compound **3** (red spectrum), with 25 μM 14-3-3 (green spectrum) or with 25 μM 14-3-3 and 35 μM GR_pS524-pS617 (purple

Identification of Small Molecule Stabilisers of the Glucocorticoid Receptor 14-3-3 Protein-Protein Interaction

spectrum). NMR signals are negatively phased in the WaterLOGSY spectrum of compound **3** but disappear or are inverted in the presence of the GR peptide–14-3-3 complex, indicating binding.

A



B

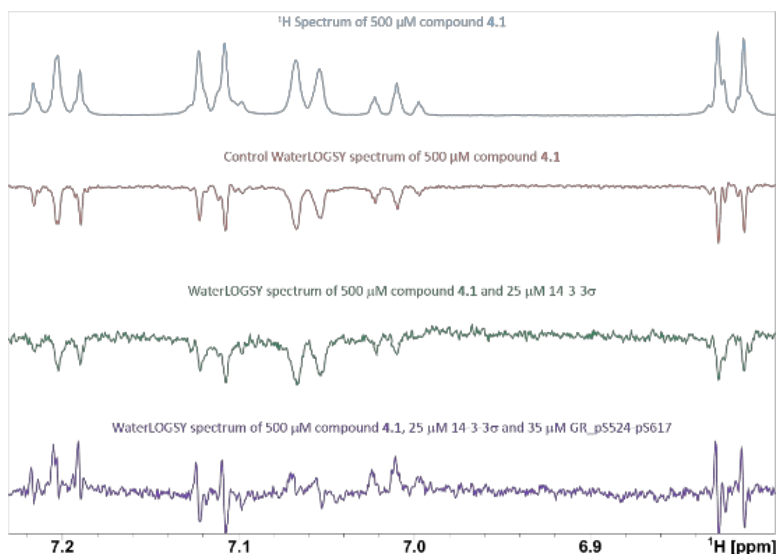


Figure 4.12. Compound 4.1 binds to (A) 14-3-3 ζ in the presence and absence of GR_pS524-pS617 but to (B) 14-3-3 σ only in the presence of GR_pS524-pS617. ^1H spectrum of 500 μM compound 4.1 (blue spectrum) and WaterLOGSY spectra of 500 μM compound 4.1 (red spectrum), with 25 μM 14-3-3 (green spectrum) or with 25 μM 14-3-3 and 35 μM GR_pS524-pS61 (purple spectrum). NMR signals are negatively phased in the WaterLOGSY

spectrum of compound 4.1, inverted in the presence of the GR peptide–14-3-3 complex, indicating binding but negatively phased with 14-3-3 σ only, suggesting no interaction.

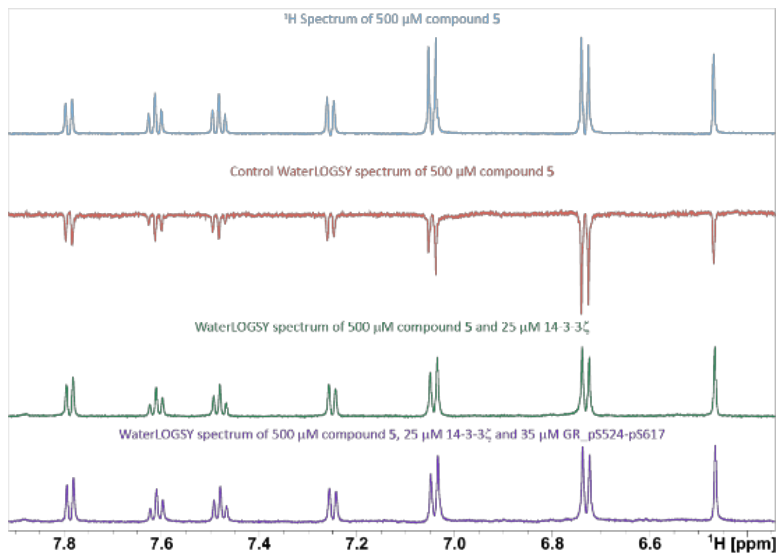
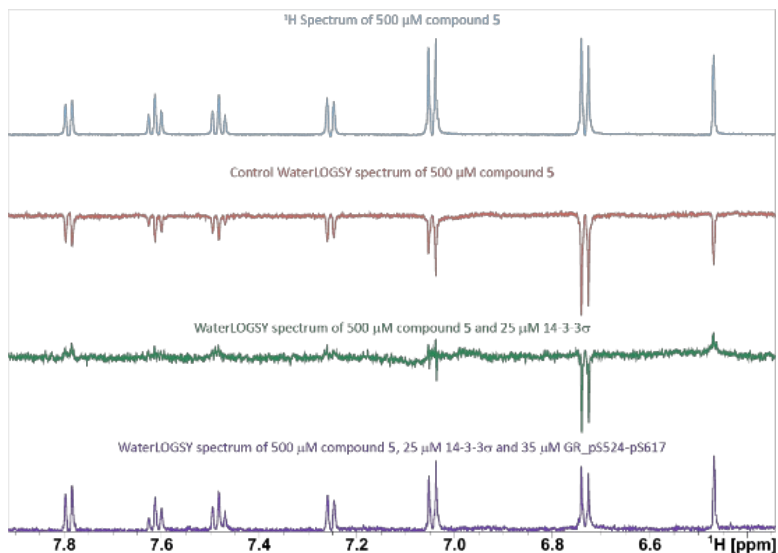
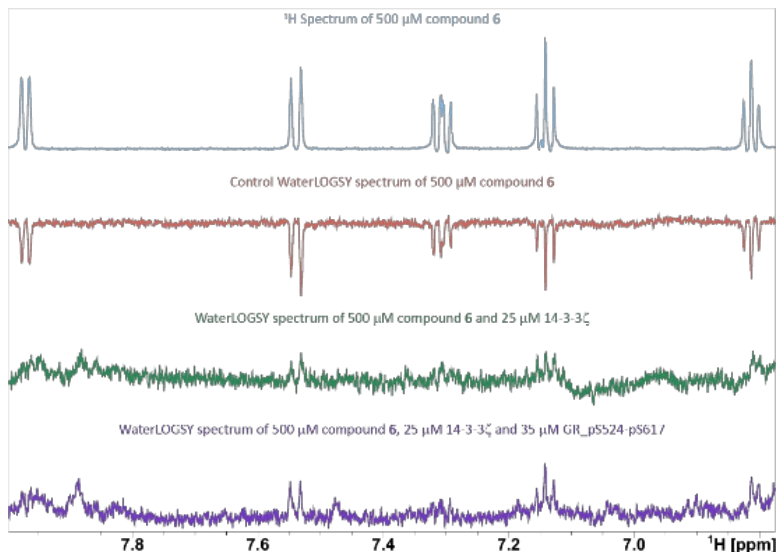
A**B**

Figure 4.13. Compound 5 binds to (A) 14-3-3 ζ and (B) 14-3-3 σ in the presence and absence of GR_pS524-pS617. ^1H spectrum of 500 μM compound 5 (blue spectrum) and WaterLOGSY spectra of 500 μM compound 5 (red spectrum), with 25 μM 14-3-3 (green spectrum) or with 25 μM 14-3-3 and 35 μM GR_pS524-pS617 (purple

Identification of Small Molecule Stabilisers of the Glucocorticoid Receptor 14-3-3 Protein-Protein Interaction

spectrum). NMR signals are negatively phased in the WaterLOGSY spectrum of compound 5 and at least some signals disappear or are inverted in the presence of the GR peptide-14-3-3 complex, indicating binding.

A



B

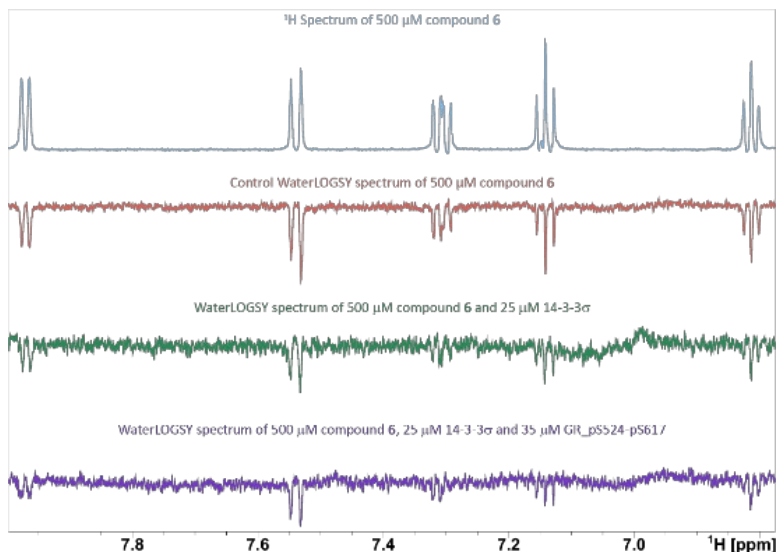


Figure 4.14. Compound 6 binds to (A) 14-3-3 ζ but not to (B) 14-3-3 σ in the presence and absence of GR_p5524-p5617. ^1H spectrum of 500 μM compound 6 (blue spectrum) and WaterLOGSY spectra of 500 μM compound 6 (red spectrum), with 25 μM 14-3-3 (green spectrum) or with 25 μM 14-3-3 and 35 μM GR_p5524-p5617 (purple spectrum). NMR signals are negatively phased in the WaterLOGSY spectrum of compound 6. They disappear or are

inverted in the presence of the GR peptide–14-3-3 ζ complex, indicating binding but are still negatively phased with GR peptide–14-3-3 σ , suggesting no interaction.

Table 4.1. Binding assessment of the hits 1, 2, 3, 4.1, 5 and 6 to 14-3-3 ζ , 14-3-3 σ , GR_pS524-pS617–14-3-3 ζ and GR_pS524-pS617–14-3-3 σ complexes by WaterLOGSY

Compound number	14-3-3 ζ	GR_pS524-pS617–14-3-3 ζ	14-3-3 σ	GR_pS524-pS617–14-3-3 σ
1	Binding	Binding	Binding	Binding
2	Binding	Binding	Binding	Binding
3	Binding	Binding	Binding	Binding
4.1	Binding	Binding	No binding	Binding
5	Binding	Binding	Binding	Binding
6	Binding	Binding	No binding	No binding

The ability of these compounds to bind to the GR-derived phosphopeptide–14-3-3 complex has also been investigated using protein-based NMR spectroscopy. Chemical shift perturbation mapping was performed based on the assigned resonances of the 14-3-3 σ ^1H - ^{15}N 2D spectrum¹⁶. The 2D ^{15}N - ^1H HSQC spectra of ^{15}N -labelled 14-3-3 σ in the absence and the presence of GR_pS524-pS617 were acquired with or without the potential stabilisers. The intensities of the correlation peaks corresponding to specific amino acid residues along the 14-3-3 σ sequence (I) were monitored in each experiment and compared to the intensities of the corresponding correlation peaks in the spectrum of 14-3-3 σ alone (I0). Upon addition of **1** to 14-3-3 σ , a weak, but significant, peak broadening, namely the decrease of the (I/I0) ratio, was observed for resonances corresponding to a pocket above the amphipathic binding groove formed at the interface of the GR peptide and the 14-3-3 protein, at the top of helices αH and αI of 14-3-3 (Fig. 4.15). This pocket has already been shown to accommodate low molecular weight molecules^{17,18}. The peak broadening induced by **1** was also observed in the presence of GR_pS524-pS617 suggesting that at least one of the phosphoepitopes leaves space for the binding of compound **1**. However, no perturbations of the 2D ^{15}N - ^1H HSQC spectra of ^{15}N -labelled 14-3-3 σ were visible for the other five hits.

Identification of Small Molecule Stabilisers of the Glucocorticoid Receptor 14-3-3 Protein-Protein Interaction

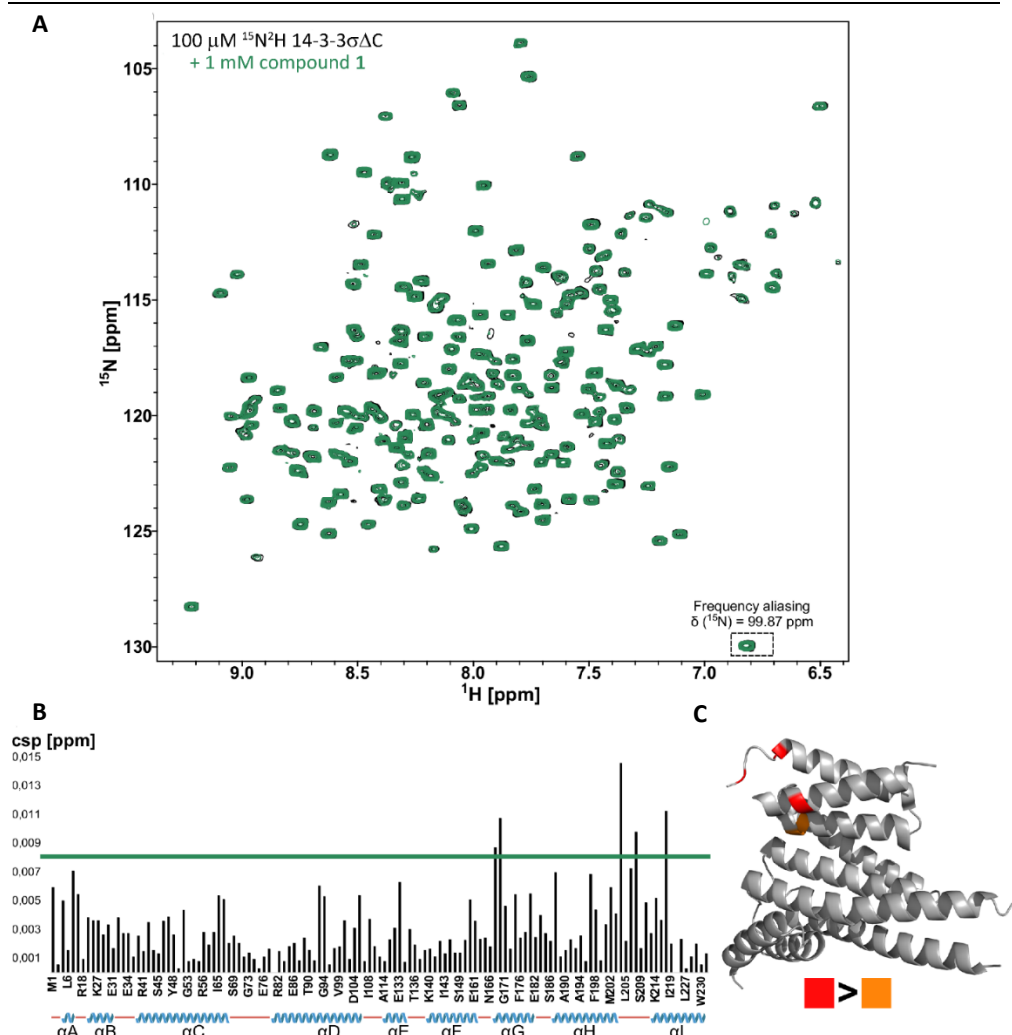
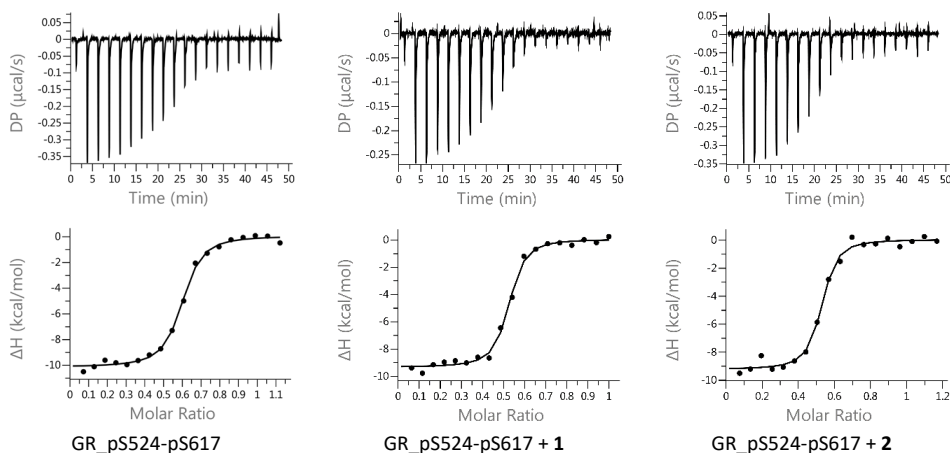


Figure 4.15. **1** binds to the upper part of the amphipathic groove formed at the interface of GR and 14-3-3. (A) ^1H - ^{15}N TROSY-HSQC spectra of $^{15}\text{N}^2\text{H}$ labelled 14-3-3 $\sigma\Delta\text{C}$ (100 μM , black) and with **1** (1 mM, green). (B) Plot of the I/O values of ^1H - ^{15}N correlation peak intensities in the spectrum of $^{15}\text{N}^2\text{H}$ labelled 14-3-3 $\sigma\Delta\text{C}$ (100 μM) with **1** (1 mM) compared to the corresponding correlation peak intensities in the 14-3-3 $\sigma\Delta\text{C}$ reference spectrum versus the amino acid sequence. A total of 131 correlation peak intensity ratios are shown. The x axis is not proportional to the sequence length. The helices of 14-3-3 $\sigma\Delta\text{C}$ are identified below the x axis as blue cartoons and disordered regions are depicted in red lines. The line on the plot represents a I/O ratio of 0.008 ppm, considered significant. (C) Mapping on the 14-3-3 $\sigma\Delta\text{C}$ crystal structure (PDB code 1YZ5) of the amino acid residues corresponding to the 5 most affected resonances by **1** (red and orange).

To evaluate the thermodynamics of the stabilising effect of the six identified hits, isothermal titration calorimetry (ITC) was used. With this technique, GR_pS524-pS617 was shown to bind 14-3-3 ζ with a binding affinity of 104 nM. The same titrations were then performed with the compounds (small molecules, 200 μ M; fragments, 2 mM). The small molecule **1** was seen to stabilise the GR-14-3-3 interaction by 1.7-fold with a K_d between GR_pS524-pS617 and 14-3-3 of 63 nM. This stabilisation of **1** measured by ITC was in line with the stabilisation activity measured by FP during the screening. Compound **3** displayed a 1.6-fold stabilisation of GR-14-3-3 PPI with a K_d of 65 nM, the fragment **5** stabilised the GR-14-3-3 complex by less than 1.5-fold with a K_d of 86 nM whilst none of **2**, **4** or **6** showed any stabilisation by ITC (Fig. 4.16 and Table 4.2). Of note, the unfavourable entropy of the binding of GR_pS524-pS617 to 14-3-3 proteins might be due to the loss of the GR peptide degrees of freedom. The interaction is, however, driven by the enthalpically favourable recognition of the phosphates. The addition of any of the binding ligands actually reduces the enthalpy of the interaction but increases the entropy, presumably by displacement of water. Indeed, the less favourable enthalpy may reflect that the ligand displaces water that binds to 14-3-3 more enthalpically favourably than it does itself, but that the entropy of the released water makes the process favourable from a free-energy perspective (Table 4.2).



Identification of Small Molecule Stabilisers of the Glucocorticoid Receptor 14-3-3 Protein-Protein Interaction

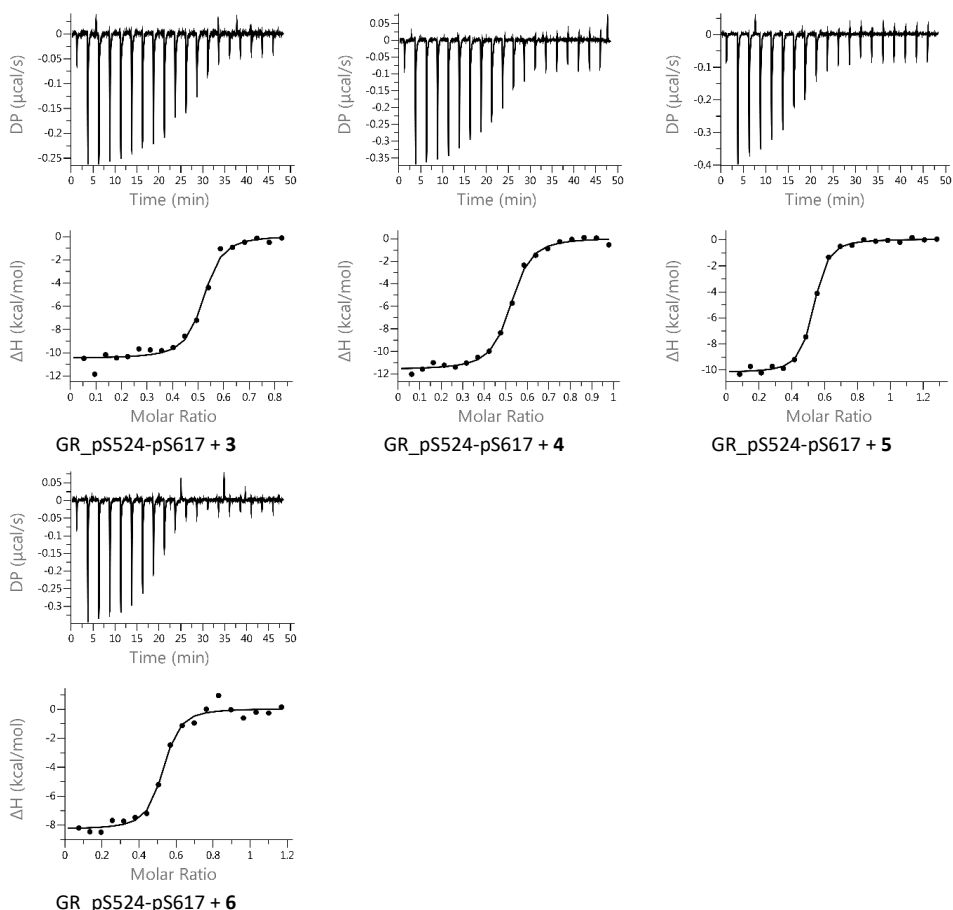


Figure 4.16. Representative example of one ITC binding curve of GR_pS524-pS617 with 14-3-3 ζ in the absence or in the presence of the six hits identified by screening (1, 2, 3, 4, 5 and 6).

Table 4.2. Binding affinity of GR_pS524-pS617 and 14-3-3 ζ in the absence or in the presence of the hits 1 - 6

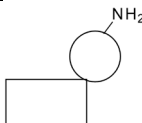
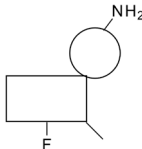
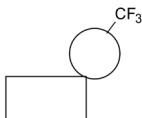
	GR_pS524-pS617	GR_pS524-pS617 + 1	GR_pS524-pS617 + 2	GR_pS524-pS617 + 3	GR_pS524-pS617 + 4	GR_pS524-pS617 + 5	GR_pS524-pS617 + 6
Temp. (°C)	25.1	25.1	25.1	25.1	25.1	25.1	25.1
GR peptide (μ M)	127 \pm 13	150 \pm 19	138 \pm 9	127 \pm 23	130 \pm 14	152 \pm 26	143 \pm 25
14-3-3 ζ (μ M)	25	25	25	25	25	25	25
Hit (mM)		0.2	0.2	0.2	0.2	2	2
N (sites)	0.5	0.5	0.5	0.5	0.5	0.5	0.5
K _d (nM)	104 \pm 9	63 \pm 29	97 \pm 15	65 \pm 16	104 \pm 39	86 \pm 13	99 \pm 28
Δ H (kcal/mol)	-11.2 \pm 0.5	-9.2 \pm 0.7	-9.9 \pm 0.8	-10.4 \pm 1.0	-10.5 \pm 1.7	-10.5 \pm 0.7	-8.5 \pm 0.8
Δ G (kcal/mol)	-9.53 \pm 0.06	-9.90 \pm 0.35	-9.58 \pm 0.10	-9.82 \pm 0.15	-9.56 \pm 0.24	-9.65 \pm 0.10	-9.57 \pm 0.17
- Δ S (kcal/mol)	1.68 \pm 0.50	-0.69 \pm 0.42	0.27 \pm 0.83	-0.56 \pm 1.07	-0.90 \pm 1.82	0.84 \pm 0.67	-1.07 \pm 0.97

4.2.4. Assessment of the structure activity relationship of the identified hits

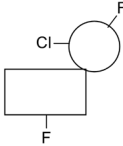
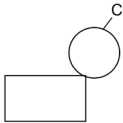
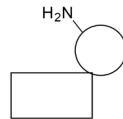
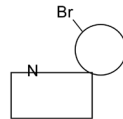

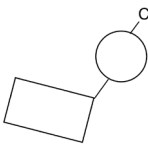
The SAR of the identified hits and their near neighbours (NN) was investigated. NN of each individual hit were selected from the AstraZeneca collection and clustered by structural fingerprints to give 700 small molecules and 350 fragments. None of these NN had previously been tested in the HTS. I saved 10% of the compounds found in each cluster to build a representative subset of NN and the stabilisation activity for these was determined in an FP assay with the GR-derived phosphopeptide–14-3-3ζ complex. For five of the six original hits (**1**, **2**, **4**, **5** and **6**) the beginning of SAR was observed from these near neighbours.

Methyl substitution was tolerated (**1.1**). Replacement of the amino group in **1** with a CF₃ was favourable (**1.2**). Substitution on the same position with a fluorine (in conjunction with a Cl group; **1.3**) reduced the stabilisation activity and the chlorine (**1.4**) gave an almost inactive compound. Introduction of substituents on the heterocycle depicted as a cycle such as an amino group (**1.5**) and a bromine (in conjunction with a nitrogen-containing heterocyclic group, **1.6**) largely decreased the activity of these compounds. More drastic changes were also tolerated, thus **1.7** retained some activity. The most significant change was **1.8** where a linker was introduced within the core of the compound (Table 4.3), **1.8** was the most effective stabiliser identified and offers potential for further exploration.

Table 4.3. Stabilisation activity of 1 and 8 NN determined at 100 μM by FP assay

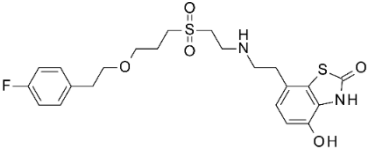
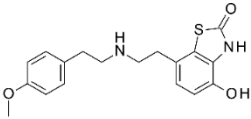
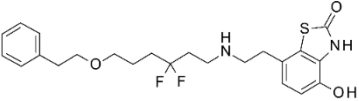
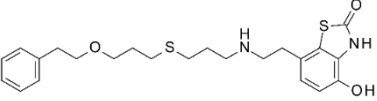
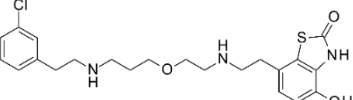
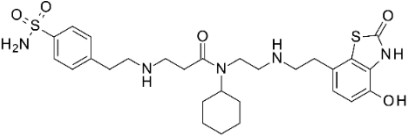
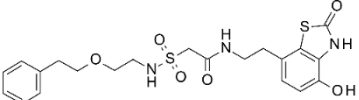
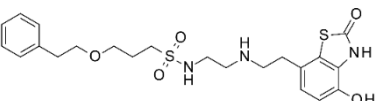
Compound number	Compound structure	Stabilisation at 100 μM by FP
1		1.8 ± 0.1
1.1		1.7 ± 0.1
1.2		2.1 ± 0.3

Identification of Small Molecule Stabilisers of the Glucocorticoid Receptor 14-3-3 Protein-Protein Interaction

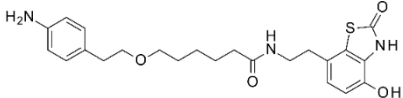
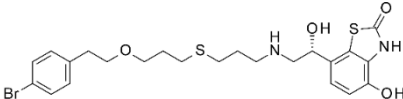
1.3		1.3 ± 0.1
1.4		1.1 ± 0.1
1.5		1.2 ± 0.1
1.6		1.1 ± 0.1
1.7		1.5 ± 0.1
1.8		2.3 ± 0.1

For compound **2**, consisting of two aromatic moieties joined by a linker, I found that all of the NN which showed stabilisation had a linker length between 12 and 13 atoms. A shorter linker (**2.1** and **2.2**) was detrimental in terms of stabilisation activity. The composition of the linker did not seem to be critical as considerable variation was tolerated. The central sulfone of **2** could be replaced by a difluoromethyl (**2.3**), a thioether (**2.4**), an ether (**2.5**) and an amide (**2.6**). Sulfonamide containing linkers showed the highest activity, either with a 12-atom (**2.7**) or 13-atom linker length (**2.8**). Replacement of this central sulfone of **2** with a methylene group (**2.9**), however, abolished the stabilisation. Small substituents in the phenyl ring made little difference with similar activities, including a bromide (**2.10**) or a sulfonamide (**2.6**) in the para position and a chlorine in meta (**2.5**) (Table 4.4).

Table 4.4. Stabilisation activity of 2 and 10 NN determined at 100 μM by FP assay

Compound number	Compound structure	Stabilisation at 100 μM by FP
2		2.0 \pm 0.5
2.1	Fragment of 2	1.3 \pm 0.1
2.2		1.4 \pm 0.1
2.3		2.8 \pm 0.1
2.4		2.7 \pm 0.1
2.5		2.6 \pm 0.1
2.6		2.5 \pm 0.1
2.7		2.9 \pm 0.5
2.8		3.4 \pm 0.1

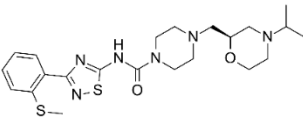
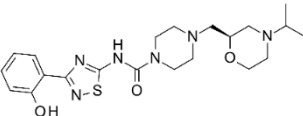
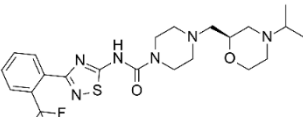
Identification of Small Molecule Stabilisers of the Glucocorticoid Receptor 14-3-3 Protein-Protein Interaction

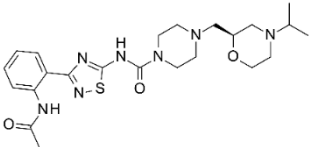
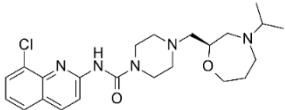
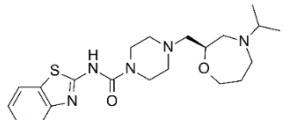
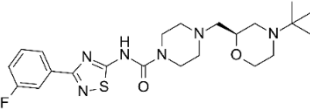
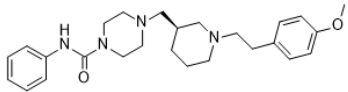
2.9		0.8 ± 0.1
2.10		2.8 ± 0.3

Moving to hit **4**, I started by looking at simple analogues with changes to the substitution of the phenyl thiadiazole. Replacement of the thiomethyl in **4** with an alcohol (**4.1**) was roughly equipotent given the errors, however, a CF₃ (**4.2**) or an acetamide group (**4.3**) reduced stabilisation. Looking at replacements for the thiadiazole, significant variation was found to be tolerated, thus fused ring systems (**4.4**, **4.5**) could replace the phenyl thiadiazole, though note the homomorpholine replacement for morpholine with these two examples. Compound **4.6** has two, apparently trivial modifications, a 3-fluoro substituent on the phenyl and a *t*-butyl for an isopropyl on the morpholine, however these abolished the stabilisation.

Surprisingly, the more extensively modified compound **4.7**, has the best stabilisation of anything in this series and represents the best starting point for further optimisation.

Table 4.5. Stabilisation of 4 and 7 NN determined at 100 μM by FP assay

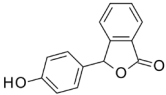
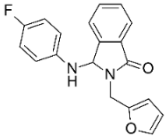
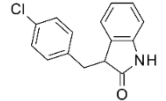
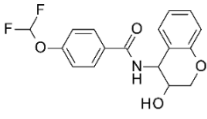
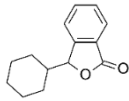
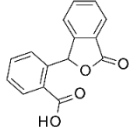
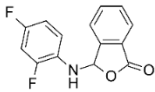
Compound number	Compound structure	Stabilisation at 100 μM by FP
4		1.5 ± 0.1
4.1		1.6 ± 0.1
4.2		1.2 ± 0.1

4.3		1.3 ± 0.1
4.4		1.6 ± 0.1
4.5		1.5 ± 0.1
4.6		1.0 ± 0.1
4.7		2.2 ± 0.1

Many analogues of fragments **5** and **6** were disregarded as an FP signal was observed even in the absence of 14-3-3ζ. The higher false positive rate might be due to the fragment concentration (10 times higher than the small molecule concentration). The remaining compounds, however, suggested a beginning of SAR. For example, **5.1** retained activity whilst an increased stabilisation was observed for fragments **5.2** and **5.3**. A 2-carboxylic acid substituent on the phenyl ring was not tolerated (**5.5**). Replacement of the phenol ring in **5** with a simple cyclohexane (**5.4**) or a 2,4-difluorophenylamino group (**5.6**) gave inactive compounds (Table **4.6**).

Identification of Small Molecule Stabilisers of the Glucocorticoid Receptor 14-3-3 Protein-Protein Interaction

Table 4.6. Stabilisation of 5 and 6 NN determined at 1 mM by FP assay

Compound number	Compound structure	Stabilisation at 1 mM by FP
5		1.6 ± 0.1
5.1		1.6 ± 0.1
5.2		2.0 ± 0.1
5.3		2.4 ± 0.1
5.4		0.9 ± 0.1
5.5		1.0 ± 0.1
5.6		1.0 ± 0.1

Turning to compound 6, quite modest changes resulted in significantly reduced stabilisation, thus, **6.1** with addition of a CF₃ to the heterobicyclic group depicted as a rectangle and a para-methoxy for the meta of **6** drops in stabilisation quite markedly whilst the chlorine substituted compound (**6.2**) is weaker still. Introduction of an amide into the linker (**6.3**) results in no stabilisation at all. In contrast to the loss of stabilisation seen for substitution on the heterobicyclic group depicted as a rectangle with **6.1**, **6.2**, and **6.3**, a much larger 4-benzamide substituent was tolerated for **6.4** and **6.5**, though

in these cases in conjunction with a different substituent depicted as a square and a narrow rectangle respectively (Table 4.7).

Table 4.7. Stabilisation of 6 and 5 NN determined at 1 mM by FP assay

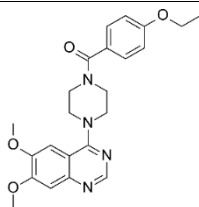
Compound number	Compound structure	Stabilisation at 1 mM by FP
6		2.3 ± 0.2
6.1		1.6 ± 0.1
6.2		1.3 ± 0.1
6.3		1.0 ± 0.1
6.4		1.8 ± 0.6
6.5		2.4 ± 0.3

The stabilisation activity of **3** was the highest one among the identified hits. All the derivatives of **3** from the representative subset, however, showed a major drop in the activity, with a value close to 1. The closest NN of **3** that I tested, bearing an OCF₃ (**3.1**) in place of the OCH₂CH₃ group, for example, was inactive (Table 4.8). The absence of SAR for **3** and its NN suggested an unspecific binding of this compound.

Table 4.8. Stabilisation activity of 3 and its closest NN determined at 100 μM by FP assay

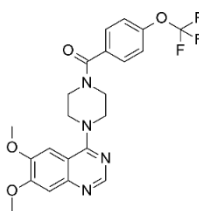
Compound number	Compound structure	Stabilisation at 100 μM by FP
-----------------	--------------------	-------------------------------

3



3.7 ± 0.3

3.1



1.1 ± 0.1

4.3. Discussion and conclusion

In this chapter 4 I report for the first time on the identification of small molecules and fragments binding to a GR peptide, as a surrogate for GR, and 14-3-3 protein to stabilise this PPI. Hits were discovered from screening about 8,000 chemically diverse molecules and they were further tested to foster confidence in their stabilising effect. Accumulated evidence highlighted **1** as a promising compound. This compound **1** was shown to bind the GR peptide–14-3-3 complex by FP, SPR and NMR and to stabilise the interaction by almost 2-fold at 200 μM by ITC. The ability of **1** to bind GR peptide–14-3-3 was further assessed by chemical shift perturbation mapping and the residues of 14-3-3 that could be seen to exhibit shifts upon binding with **1** were located in the upper part of the amphipathic groove formed at the interface of GR and 14-3-3. Extension of **1** to a series enables the observation of a beginning of SAR. My results also identified fragment **5** as encouraging. Its ability to bind and stabilise the GR–14-3-3 complex was supported by biophysical experiments such as FP, SPR, ITC, ¹H NMR and WaterLOGSY. Additionally, NN of **5** showed a differential capacity to stabilise GR peptide–14-3-3. The small molecules **2** and **4** did not induce chemical shift perturbation in the 2D ¹⁵N-¹H HSQC spectra of ¹⁵N-labelled 14-3-3σ and no stabilisation was observed by ITC. Nevertheless, data suggested an interaction and a stabilisation of the GR peptide–14-3-3 protein complex with **2**, **4** and their close analogues, respectively. Further experiments such as co-crystallisation of these hits would be a great interest to rationalise the binding mode and for a hit to lead optimization supported by structure-based drug design.

Fully delineating the underlying signalling network of GR is of a particular relevance due to the enormous importance of GR drugs and their widespread use despite their many side-effects. The

stabilisers identified in this study provide starting points for future development into tool compounds. The non-competitive nature of these molecules offers a potential advantage over conventional inhibitors and could make a significant contribution in the quest to understand the physiological role of the GR-14-3-3 PPI as well as provide novel opportunities for future therapeutic interventions.

4.4. Acknowledgements

The author thanks Dr. Matthew W.D. Perry for conceiving and directing the project, Dr. Christian Ottmann for his strategic guidance, Dr. Fredrik Wågberg for his assistance with the optimisation of the screening conditions, Dr. Anders Gunnarsson for his support with the biophysical experiments, Dr. Fredrik Edfeldt for his assistance with the ^1H NMR experiments, Dr. Isabelle Landrieu and Dr. Joao Neves for performing the WaterLOGSY and 2D NMR experiments. The author thanks Dr. Werngard Czechtizky for generous support of the project.

4.5. Materials and methods

Peptide synthesis

Peptides were synthesized according to the method reported in chapter 2.

14-3-3 expression and purification

The σ and ζ isoforms of human 14-3-3 and 14-3-3 ΔC (C-terminally truncated, including residues 1-231, for crystallography purposes) were expressed and purified according the method reported in chapter 2.

Production of $^{15}\text{N}^2\text{H}$ labelled 14-3-3 $\sigma\Delta\text{C}$ for NMR spectroscopy

The $^{15}\text{N}^2\text{H}$ labelled 14-3-3 $\sigma\Delta\text{C}$ (cleaved after T231) for NMR studies was expressed and purified as described by João Filipe Neves *et al*¹⁶.

FP assays

The FITC labelled peptide and 14-3-3 ζ were diluted with HBS P+ buffer (10 mM HEPES pH 7.4, 150 mM NaCl, 0.005% v/v Tween-P20) to a concentration of 10 nM and 40 nM respectively either with a fixed compound concentration (small molecule, 100 μM ; fragment, 1 mM), or in concentration dilution series from 200 μM (small molecule) or 2 mM (fragment), dilution factor 3, in a 384-well flat bottom black polypropylene microplate (Greiner Bio-One). Following 30-minute incubation at room temperature, the plates were read on a plate reader PHERAstar (BMG LABTECH GmbH) for FP signal using white light and standard excitation (485 nm) and emission (520 nm). Measurements were performed as triplicates. Binding data were fit to a standard Hill equation using the software Genedata Screener[®]. The figures were made using the software GraphPad Prism 8. Fluorescence polarization data were expressed as millipolarization (mP) units and the dynamic range (ΔmP) was calculated according to equation (1):

$$\Delta\text{mP} = \text{mP of bound peptide} - \text{mP of free peptide}$$

Errors are standard error of the fit.

SPR experiments

SPR binding assays were performed using a Biacore 3000 (GE Healthcare). His6 tagged 14-3-3 ζ proteins (3 μ M) were immobilized on a SPR sensorchip NTA derivatized carboxymethyl dextran hydrogel (Xantec Bioanalytics) at 2000 RU according to the manufacturer's instructions. A 96-well V-shaped polypropylene microtiter plate was prepared with GR peptide (18 nM) and compound concentrations (small molecule, 100 μ M; fragment, 1 mM) in HBS P+ buffer and normalized to 1% v/v DMSO, using the HP D300 Digital Dispenser (Hewlett-Packard Company). The samples were injected using the HBS P+ buffer with 1% v/v DMSO at a continuous flow rate of 20 μ L/min for 1 min on the immobilized 14-3-3 and before the next injection 2.5 min after. An extra waiting time of 12.5 min was set to allow complete dissociation of the phosphorylated peptide. Measurements were performed as triplicates. Binding data were fit to a standard Hill equation using the software Genedata Screener® and the figures were made using the software GraphPad Prism 8. Errors are standard error of the fit.

ITC

ITC experiments were performed using a Malvern MicroCal iTC200 (Malvern Instruments Ltd.) at 25 °C in ITC buffer containing 25 mM HEPES pH 7.5, 100 mM NaCl, 10 mM MgCl₂ and 0.5 mM TCEP. A solution of 25 μ M 14-3-3 ζ was introduced in the cell and titrated by a series of 19 2- μ L injections of 140 μ M GR peptide together with 200 μ M small molecule or 2 mM fragment. The final concentration of DMSO was 1.5% v/v. Measurements were performed at least as triplicates. Data were analysed with MicroCal PEAQ IT software using a single binding site model with a molar binding stoichiometry (N) fixed to 0.5 and varying association constant, molar binding enthalpy (Δ H) and concentration in the syringe to minimize the pipetting errors.

1D Binding NMR experiments

1D ¹H NMR experiments. Spectra were recorded at 25 °C on a 800 MHz Bruker spectrometer in 5 mm tubes (final volume 0.45 mL). Spectra were, first, recorded on the compound (50 μ M) dissolved in 50 mM dTris pH 7.4, 10% D₂O, 11 μ M trimethylsilyl propanoic acid. Then 14-3-3 ζ (5 μ M) and GR peptide (10 μ M) were added, and the spectra were acquired.

WaterLOGSY NMR experiments

WaterLOGSY spectra were recorded at 16 °C on a 600 MHz Bruker Avance III HD spectrometer equipped with a CPQCI cryogenic probe in 5 mm tubes (final volume 530 μ L). The spectra were acquired with 32768 complex data points, 1024 scans per increment and a mixing time of 1.7 s (acquisition time of 93 min). Samples were prepared in a buffer containing 100 mM sodium phosphate pH 6.8, 50 mM NaCl, and 10% v/v D₂O. A final concentration of 2% v/v DMSO-d₆ was kept constant for all experiments. WaterLOGSY spectra were acquired on samples containing compound (500 μ M) with 14-3-3 σ or 14-3-3 ζ (25 μ M). After addition of GR peptide (35 μ M), WaterLOGSY spectra were acquired again. A 1H spectrum with water-suppression was additionally recorded for each sample. Spectra were collected, processed and analysed with Topspin 3.6 (Bruker Biospin).

15N-1H TROSY-HSQC NMR spectroscopy

Transverse Relaxation Optimized Spectroscopy- Heteronuclear Single Quantum Coherence Spectroscopy (¹H-¹⁵N TROSY-HSQC¹⁶) spectra were recorded at 32 °C on a 900 MHz Bruker Avance Neo spectrometer equipped with a cryoprobe in 3 mm tubes (final volume 200 μ L). The spectra were acquired with

3072 and 128 complex data points in the direct and indirect dimension respectively, with 184 scans per increment in a buffer containing 100 mM sodium phosphate, 50 mM NaCl, pH 6.8, 4% v/v DMSO-d₆, 1 mM DTT, protease inhibitor cocktail (Roche) and 10% v/v D₂O. Spectra were recorded with ¹⁵N²H labelled 14-3-3σΔC (100 μM) in the presence and absence of compound (1 mM) and GR peptide (300 μM). Assignments of the backbone resonances of ¹⁵N²H labelled 14-3-3σ have been previously reported¹⁶. The reference for the ¹H chemical shift was relative to 4,4-dimethyl-4-silapentane-1-sulfonic acid (DSS) while ¹⁵N chemical shift values were referenced indirectly. Spectra were collected and processed with Topspin 4.0 (Bruker Biospin) and analysed with Sparky 3.12 (T. D. Goddard and D. G. Kneller, SPARKY 3). CSPs verified as chemical shift positions (in ppm) on the 1H-15N TROSY-HSQC were calculated using the following equation:

$$\Delta\delta = \sqrt{\Delta\delta(^1H)^2 + [0.14 * \Delta\delta(^{15}N)^2]}$$

Acetylated GR_pS524-pS617:

Acetylated GR_pS524-pS617 peptide was prepared following General Protocol for SPPS. The crude peptide was purified by reverse-phase HPLC (gradient: 22-32% B in 20min, Kromasil C18 column) to afford the desired peptide as a white fluffy solid. Yield (60 mg) in > 95% purity according to analytical UPLC. Rt 5.51 min (3-60% B in 10 min).

[M + 3H]³⁺ calculated for C₁₄₁H₂₃₁N₄₁O₄₉P₂S, 1126.9; found 1126.8.

FITC labelled GR_pS524-pS617:

FITC labelled GR_pS524-pS617 peptide was prepared following General Protocol for SPPS. The crude peptide was purified by reverse-phase HPLC (gradient: 5% B for 1 min, 5-29% B in 3 min, 29-34% B in 15min, Waters Atlantis T3 column) to afford the desired peptide as a white fluffy solid. Yield (8 mg) in > 95% purity according to analytical UPLC. Rt 4.31 min (5-95% B in 10 min).

[M + 3H]³⁺ calculated for C₁₆₆H₂₅₁N₄₃O₅₄P₂S₂, 1280.4; found 1280.7.

Key compound synthesis and characterisation

General details: All solvents and reagents were purchased from commercial suppliers and were used without purification or were prepared according to published procedures. Nuclear magnetic resonance (NMR) spectra were acquired at 25 °C (except for **3** and **4** whose spectra were acquired at 55 °C) on a Bruker Avance II, III, AV300, AV400 or AVIII500 spectrometer at 600 MHz ¹H-frequency and 151 MHz ¹³C-frequency. Chemical shifts (δ) are reported in parts per million (ppm) relative to residual DMSO signal (δ 2.50 ppm in ¹H NMR and 39.5 ppm in ¹³C NMR) or CDCl₃ signal at (7.26 ppm for ¹H NMR and 77.2 ppm for ¹³C NMR). Coupling constants (J) are reported as Hz. NMR abbreviations are used as follows: br = broad, s = singlet, d = doublet, t = triplet, q = quartet, m = multiplet. Protons on heteroatoms such as COOH protons are only reported when detected in NMR and can therefore be missing. Analytical RP-UPLC-MS was performed on a Waters Acquity UPLC system (PDA, sample manager, sample organiser, column oven modules) and Waters SQD2 mass spectrometer using the following column: Waters Acquity HSS C8 column, 1.8 μm, 2.1 x 50 mm at a flow rate of 1 mL/min at 40 °C or Waters Acquity CSH C8 column, 1.7 μm, 2.1 x 50 mm at a flow rate of 1 mL/min at 60 °C. A linear gradient of mobile phase: A=H₂O + 10 mM formic acid, 1 mM ammonium formate buffer at pH 3 and B=CH₃CN + 10 mM formic acid, 1 mM ammonium formate buffer was used.

(1) (Purity > 95% HRMS (ESI) m/z [M + H]⁺ calculated: XXX.0861, found: XXX.0866)

(1.1) (Purity=85%, HRMS (ESI) m/z [M + H]⁺ calculated: XXX.0923, found: XXX.0923)

(1.2) (Purity > 95%, HRMS (ESI) m/z [M + H]⁺ calculated: XXX.0735, found: XXX.0745)

(1.3) (Purity > 95%, HRMS (ESI) m/z [M + H]⁺ calculated: XXX.0174, found: XXX.0177)

(1.4) (Purity > 95%, HRMS (ESI) m/z [M + H]⁺ calculated: XXX.0362, found: XXX.0364)

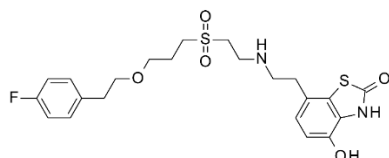
(1.5) (Purity=57%, HRMS (ESI) m/z [M + H]⁺ calculated: XXX.0966, found: XXX.0968)

(1.6) (Purity=95%, HRMS (ESI) m/z [M + H]⁺ calculated: XXX.9810, found: XXX.9810)

(1.7) (Purity=91%, HRMS (ESI) m/z [M + H]⁺ calculated: XXX.0639, found: XXX.0644). The following compound is commercially available: (1.8) (purity > 95%).

7-[2-[2-[3-[2-(4-fluorophenyl)ethoxy]propylsulfonyl]ethylamino]ethyl]-4-hydroxy-3H-1,3-benzothiazol-2-one

(2)



Compound 2 is commercially available, CAS Registry Number: 154189-44-3. ¹H NMR (600 MHz, DMSO) δ 1.85 – 1.96 (m, 2H), 2.80 (q, J = 8.3, 6.9 Hz, 4H), 3.14 (s, 2H), 3.18 – 3.23 (m, 2H), 3.49 (t, J = 6.2 Hz, 4H), 3.57 (t, J = 6.9 Hz, 2H), 6.75 (d, J = 8.2 Hz, 1H), 6.86 (d, J = 8.3 Hz, 1H), 7.09 (t, J = 8.8 Hz, 2H), 7.26 (dd, J = 8.4, 5.8 Hz, 2H), 8.80 (br s, 1H), 10.12 (s, 1H), 11.74 (s, 1H). 2 protons are obscured. ¹³C NMR (151 MHz, DMSO) δ 169.2, 160.8 (d, J = 241.2 Hz), 141.8, 135.2 (d, J = 3.0 Hz), 130.6 (d, J = 7.9 Hz), 124.9, 123.8, 123.0, 114.9 (d, J = 20.9 Hz), 112.6, 70.9, 67.7, 49.6, 48.1, 46.5, 34.6, 21.7. 3 carbons are obscured. Purity > 95% according to analytical UPLC. Rt 1.17 min (10-99% B in 4 min). HRMS (ESI) m/z [M + H]⁺ calculated for C₂₂H₂₇FN₂O₅S₂: 483.1424, found: 483.1421.

(2.1) (Purity > 95%, HRMS (ESI) m/z [M + H]⁺ calculated: XXX.1167, found: XXX.1164)

7-[2-[2-[3-[2-(3-chlorophenyl)ethylamino]propoxy]ethylamino]ethyl]-4-hydroxy-3H-1,3-benzothiazol-2-one

(2.5) (Purity=70%, HRMS (ESI) m/z [M + H]⁺ calculated for C₂₂H₂₈ClN₃O₃S: 450.1618, found: 450.1630)

N-[2-(4-hydroxy-2-oxo-3H-1,3-benzothiazol-7-yl)ethyl]-2-[2-(2-phenylethoxy)ethylsulfamoyl]acetamide (2.7)

(Purity=69%, HRMS (ESI) m/z [M + H]⁺ calculated for C₂₁H₂₅N₃O₆S₂: 480.1263, found: 480.1271).

The following compounds are commercially available:

4-hydroxy-7-[2-[2-(4-methoxyphenyl)ethylamino]ethyl]-3H-1,3-benzothiazol-2-one (2.2) (CAS Registry Number: 774508-73-5, purity > 95%)

7-[2-[[3,3-difluoro-6-(2-phenylethoxy)hexyl]amino]ethyl]-4-hydroxy-3H-1,3-benzothiazol-2-one (2.3) (CAS Registry Number: 579480-16-3, purity > 95%)

4-hydroxy-7-[2-[3-[2-(2-phenylethoxy)propylsulfanyl]propylamino]ethyl]-3H-1,3-benzothiazol-2-one (2.4) (CAS Registry Number: 579480-48-1, purity > 95%)

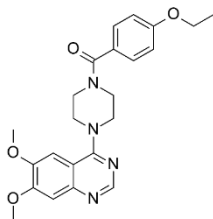
N-cyclohexyl-N-[2-[2-(4-hydroxy-2-oxo-3H-1,3-benzothiazol-7-yl)ethylamino]ethyl]-3-[2-(4-sulfamoylphenyl)ethylamino]propanamide (2.6) (CAS Registry Number: 1034763-02-4, purity=72%)

N-[2-[2-(4-hydroxy-2-oxo-3H-1,3-benzothiazol-7-yl)ethylamino]ethyl]-3-(2-phenylethoxy)propane-1-sulfonamide (2.8) (CAS Registry Number: 579480-92-5, purity > 95%)

6-[2-(4-aminophenyl)ethoxy]-N-[2-(4-hydroxy-2-oxo-3H-1,3-benzothiazol-7-yl)ethyl]hexanamide (2.9) (CAS Registry Number: 143454-93-7, purity=88%)

7-[(1R)-2-[3-[2-(4-bromophenyl)ethoxy]propylsulfanyl]propylamino]-1-hydroxy-ethyl]-4-hydroxy-3H-1,3-benzothiazol-2-one (2.10) (CAS Registry Number: 928629-24-7, purity > 95%).

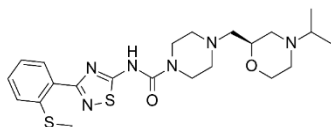
[4-(6,7-dimethoxyquinazolin-4-yl)piperazin-1-yl]-(4-ethoxyphenyl)methanone (3)



Compound **3** was synthesized by amide coupling between 4-ethoxybenzoic acid (CAS Registry Number: 619-86-3) and 6,7-dimethoxy-4-piperazin-1-yl-quinazoline (CAS Registry Number: 21584-72-5). ^1H NMR (600 MHz, DMSO) δ 1.34 (t, $J = 7.0$ Hz, 3H), 3.66 – 3.7 (m, 4H), 3.73 (s, 4H), 3.92 (s, 3H), 3.94 (s, 3H), 4.09 (q, $J = 7.0$ Hz, 2H), 6.96 – 7.01 (m, 2H), 7.18 (s, 1H), 7.23 (s, 1H), 7.39 – 7.44 (m, 2H), 8.55 (s, 1H). ^{13}C NMR (151 MHz, DMSO, 55°C) δ 169.2, 162.6, 159.4, 154.3, 152.2, 148.5, 148.2, 128.9, 127.5, 114.0, 110.4, 107.1, 103.3, 63.1, 55.7, 55.6, 48.9, 14.4. Purity = 95% according to analytical UPLC. Rt 1.24 min (10-99% B in 4 min). HRMS (ESI) m/z [M + H] $^+$ calculated for $\text{C}_{23}\text{H}_{26}\text{N}_4\text{O}_4$: 423.2032, found: 423.2033.

[4-(6,7-dimethoxyquinazolin-4-yl)piperazin-1-yl]-[4-(trifluoromethoxy)phenyl]methanone (3.1) is commercially available (CAS Registry Number: 2306303-64-8) (Purity > 95%).

4-[[[(2S)-4-isopropylmorpholin-2-yl]methyl]-N-[3-(2-methylsulfanylphenyl)-1,2,4-thiadiazol-5-yl]piperazine-1-carboxamide (4)



Compound **4** was synthesized by amide coupling using standard reaction conditions. ^1H NMR (600 MHz, DMSO) δ 0.97 (t, $J = 6.1$ Hz, 6H), 1.88 – 1.96 (m, 1H), 2.16 (td, $J = 11.2, 3.1$ Hz, 1H), 2.34 – 2.48 (m, 9H), 2.56 – 2.63 (m, 2H), 2.71 (d, $J = 11.2$ Hz, 1H), 3.46 (td, $J = 11.1, 2.4$ Hz, 2H), 3.55 (t, $J = 4.9$ Hz, 5H), 3.76 (d, $J = 11.1$ Hz, 1H), 7.23 (t, $J = 7.4$ Hz, 1H), 7.39 (d, $J = 7.9$ Hz, 1H), 7.41 – 7.46 (m, 1H), 7.92 (dd, $J = 7.7, 1.2$ Hz, 1H). ^{13}C NMR (151 MHz, DMSO, 55°C) δ 166.1, 138.9, 131.2, 130.0, 129.5, 125.0, 123.7, 73.5, 66.0, 60.49, 53.7, 52.9, 52.5, 47.9, 43.7, 18.1, 17.7, 15.3. 2 carbons are obscured. Purity > 95% according to analytical UPLC. Rt 0.94 min (10-99% B in 4 min). LCMS (ESI) m/z [M + H] $^+$ calculated for $\text{C}_{22}\text{H}_{32}\text{N}_6\text{O}_2\text{S}_2$: 477.2106, found: 477.2109.

N-[3-(2-hydroxyphenyl)-1,2,4-thiadiazol-5-yl]-4-[[[(2S)-4-isopropylmorpholin-2-yl]methyl]piperazine-1-carboxamide (4.1) (Purity=84%, HRMS (ESI) m/z [M + H] $^+$ calculated for $\text{C}_{21}\text{H}_{30}\text{N}_6\text{O}_3\text{S}$: 447.2178, found: 447.2186)

4-[[[(2S)-4-isopropylmorpholin-2-yl]methyl]-N-[3-[2-(trifluoromethyl)phenyl]-1,2,4-thiadiazol-5-yl]piperazine-1-carboxamide (4.2) (Purity=87%, HRMS (ESI) m/z [M + H]⁺ calculated for C₂₂H₂₉F₃N₆O₂S: 499.2103, found: 499.2112)

N-[3-(2-acetamidophenyl)-1,2,4-thiadiazol-5-yl]-4-[[[(2S)-4-isopropylmorpholin-2-yl]methyl]piperazine-1-carboxamide (4.3) (Purity=81%, HRMS (ESI) m/z [M + H]⁺ calculated for C₂₃H₃₃N₇O₃S: 488.2444, found: 488.2452)

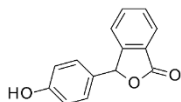
N-(8-chloro-2-quinolyl)-4-[[[(2S)-4-isopropyl-1,4-oxazepan-2-yl]methyl]piperazine-1-carboxamide (4.4) (Purity=93%)

N-(1,3-benzothiazol-2-yl)-4-[[[(2S)-4-isopropyl-1,4-oxazepan-2-yl]methyl]piperazine-1-carboxamide (4.5) (Purity=71%, HRMS (ESI) m/z [M + H]⁺ calculated for C₂₁H₃₁N₅O₂S: 418.2277, found: 418.2286)

4-[[[(2S)-4-tert-butylmorpholin-2-yl]methyl]-N-[3-(3-fluorophenyl)-1,2,4-thiadiazol-5-yl]piperazine-1-carboxamide (4.6) (Purity=96%, HRMS (ESI) m/z [M + H]⁺ calculated for C₂₂H₃₁FN₆O₂S: 463.2291, found: 463.2296).

The following compound is commercially available: **4-[[[(3R)-1-[2-(4-methoxyphenyl)ethyl]-3-piperidyl]methyl]-N-phenyl-piperazine-1-carboxamide (4.7)** (CAS Registry Number: 894800-51-2, purity > 95%).

rac-(3R)-3-(4-hydroxyphenyl)-3H-isobenzofuran-1-one (5)



Compound 4 is commercially available, CAS Registry Number: 7468-76-0. ¹H NMR (600 MHz, CDCl₃) δ 4.86 (s, 1H), 6.36 (s, 1H), 6.8 – 6.85 (m, 2H), 7.11 – 7.16 (m, 2H), 7.29 – 7.34 (m, 1H), 7.56 (t, J = 7.5 Hz, 1H), 7.66 (td, J = 7.5, 1.0 Hz, 1H), 7.96 (d, J = 7.7 Hz, 1H). ¹³C NMR (151 MHz, CDCl₃) δ 170.7, 156.6, 149.9, 134.5, 129.5, 129.3, 128.8, 126.1, 125.8, 123.1, 116.0, 82.9. Purity > 95% according to analytical UPLC. Rt 1.42 min (5-95% B in 3 min). HRMS (ESI) m/z [M + H]⁺ calculated for C₁₄H₁₀O₃: 227.0630, found: 227.0702.

The following compounds are commercially available: **rac-(3S)-3-(4-fluoroanilino)-2-(2-furylmethyl)isoindolin-1-one (5.1)** (CAS Registry Number: 901715-09-1, purity > 95%), **rac-(3R)-3-[(4-chlorophenyl)methyl]indolin-2-one (5.2)** (CAS Registry Number: 131609-35-3, purity > 95%), **rac-(3R)-3-cyclohexyl-3H-isobenzofuran-1-one (5.4)** (CAS Registry Number: 92251-57-5, purity > 95%), **2-[rac-(1S)-3-oxo-1H-isobenzofuran-1-yl]benzoic acid (5.5)** (CAS Registry Number: 109407-76-3, purity > 95%), **rac-(3S)-3-(2,4-difluoroanilino)-3H-isobenzofuran-1-one (5.6)** (CAS Registry Number: 663884-80-8, purity=84%). **4-(difluoromethoxy)-N-[rac-(3R,4S)-3-hydroxychroman-4-yl]benzamide (5.3)** (Purity > 95%, HRMS (ESI) m/z [M + H]⁺ calculated for C₁₇H₁₅F₂NO₄: 336.1047, found: 336.1052).

(6) (Purity > 95, HRMS (ESI) m/z [M + H]⁺ calculated: XXX.1059, found: XXX.1131)

(6.1) (Purity > 95%, HRMS (ESI) m/z [M + H]⁺ calculated: XXX.1011, found: XXX.1015)

(6.3) (Purity > 95%, HRMS (ESI) m/z [M + H]⁺ calculated: XXX.1246, found: XXX.1248)

(6.4) (Purity > 95%, HRMS (ESI) m/z [M + H]⁺ calculated: XXX.1457, found: XXX.1460)

(6.5) (Purity > 95%, HRMS (ESI) m/z [M + H]⁺ calculated: XXX.1715, found: XXX.1726)

The following compound is commercially available: **(6.2)** (purity > 95%).

4.6. References

1. Stumpf, M. P. H. *et al.* Estimating the size of the human interactome. *Proc. Natl. Acad. Sci. U. S. A.* **105**, 6959–6964 (2008).
2. Scott, D. E., Bayly, A. R., Abell, C. & Skidmore, J. Small molecules, big targets: Drug discovery faces the protein-protein interaction challenge. *Nat. Rev. Drug Discov.* **15**, 533–550 (2016).
3. Bosch, J. PPI inhibitor and stabilizer development in human diseases. *Drug Discov. Today Technol.* **24**, 3–9 (2017).
4. Matyskiela, M. E. *et al.* SALL4 mediates teratogenicity as a thalidomide-dependent cereblon substrate. *Nat. Chem. Biol.* **14**, 981–987 (2018).
5. Andrei, S. A. *et al.* Stabilization of protein-protein interactions in drug discovery. *Expert Opin. Drug Discov.* **12**, 925–940 (2017).
6. Hughes, S. J. & Ciulli, A. Molecular recognition of ternary complexes: A new dimension in the structure-guided design of chemical degraders. *Essays Biochem.* **61**, 505–516 (2017).
7. Petzold, G., Fischer, E. S. & Thomä, N. H. Structural basis of lenalidomide-induced CK1 α degradation by the CRL4 CRBN ubiquitin ligase. *Nature* **532**, 127–130 (2016).
8. Schapira, M., Calabrese, M. F., Bullock, A. N. & Crews, C. M. Targeted protein degradation: expanding the toolbox. *Nat. Rev. Drug Discov.* **18**, 949–963 (2019).
9. Kino, T. GR-regulating Serine/Threonine Kinases: New Physiologic and Pathologic Implications. *Trends Endocrinol. Metab.* **29**, 260–270 (2018).
10. Weikum, E. R., Knuesel, M. T., Ortlund, E. A. & Yamamoto, K. R. Glucocorticoid receptor control of transcription: Precision and plasticity via allostery. *Nat. Rev. Mol. Cell Biol.* **18**, 159–174 (2017).
11. Cain, D. W. & Cidlowski, J. A. Immune regulation by glucocorticoids. *Nat. Rev. Immunol.* **17**, 233–247 (2017).
12. Pennington, K., Chan, T., Torres, M. & Andersen, J. The dynamic and stress-adaptive signaling hub of 14-3-3: emerging mechanisms of regulation and context-dependent protein–protein interactions. *Oncogene* **37**, 5587–5604 (2018).
13. Galliher-Beckley, A. J., Williams, J. G. & Cidlowski, J. A. Ligand-Independent Phosphorylation of the Glucocorticoid Receptor Integrates Cellular Stress Pathways with Nuclear Receptor Signaling. *Mol. Cell. Biol.* **31**, 4663–4675 (2011).
14. Habib, T. *et al.* AKT1 has dual actions on the glucocorticoid receptor by cooperating with 14-3-3. *Mol. Cell. Endocrinol.* **439**, 431–443 (2017).
15. Ballone, A., Centorrino, F. & Ottmann, C. 14-3-3: A Case Study in PPI Modulation. *Molecules*

- 23**, 1–14 (2018).
16. Neves, J. F. *et al.* Backbone chemical shift assignments of human 14-3-3 σ . *Biomol. NMR Assign.* **13**, 103–107 (2019).
 17. Valenti, D. *et al.* Set-up and screening of a fragment library targeting the 14-3-3 protein interface. *Medchemcomm* **10**, 1796–1802 (2019).
 18. Sijbesma, E. *et al.* Identification of Two Secondary Ligand Binding Sites in 14-3-3 Proteins Using Fragment Screening. *Biochemistry* **56**, 3972–3982 (2017).

Chapter 5

Early Exploration of the Structure Activity Relationship of Small Molecule Stabilisers of the Glucocorticoid Receptor 14-3-3 Protein-Protein Interaction

Abstract

GR is part of a complex interactome which further refines GR activity through PPI. 14-3-3 proteins belong to this network and modulate the GR transcriptional activity by binding to this transcription factor. 14-3-3 could, therefore, provide an opportunity for GR modulation beyond direct ligand-driven activation, which is associated with many undesired side-effects when used therapeutically in a systemic application. Here, the role of known 14-3-3 PPI stabilisers on the GR–14-3-3 interaction was investigated. Fusicoccin A was found to destabilise the GR–14-3-3 PPI whilst mizoribine acted as a non-specific binder. Pyrrolidone1, in contrast, was shown to stabilise this interaction. A focussed compound library of pyrrolidone1 analogues were investigated and preliminary SAR was identified. Co-crystallization of the most promising molecule with 14-3-3 ζ and a 13-mer peptide corresponding to GR_pT524 further characterised the binding mode. Comparison with previously determined structures identified some starting points that could provide greater selectivity between 14-3-3 PPIs. A selective stabiliser could contribute to a better understanding of the physiological role of 14-3-3 in the modulation of GR activity and provide a novel therapeutic strategy for the regulation of inflammation.

5.1. Introduction

14-3-3s are ubiquitous adapter proteins, acting as dimers, that recognise and bind, through their highly conserved amphipathic groove, phosphorylated serines and threonines¹. Upon binding, 14-3-3s mediate the physiological effect of their protein partners by regulating their activity, their cellular localization or their ability to further interact with other proteins². 14-3-3s have been shown to bind to several hundred client partners, many of which are implicated in disease-relevant processes, thus making them attractive targets for potential therapeutic intervention³. Notably, 14-3-3s interact with GR⁴⁻¹⁰ which mediates the cellular signalling of glucocorticosteroid hormones by acting as ligand-dependent transcription factors. Upon binding of GCs, GR translocates to the nucleus and binds to DNA sequences to regulate gene expression. GR plays a crucial role in a wide range of fundamental processes as well as conditions including inflammatory conditions^{11,12}. GR agonists are widely prescribed as anti-inflammatory agents, though systemic administration is associated with multiple undesired effects. Hence it is of a great interest to better understand the regulatory role of the GR interactome to identify novel therapeutic strategies with the potential for reduced detrimental side-effects. 14-3-3 potentially provides an opportunity for a subtle additional modulation by adding another layer of GR regulation beyond direct ligand-driven activation. Indeed, 14-3-3 has been shown to modulate GR transcriptional activity⁴⁻¹⁰.

In chapter 2 and 3, the GR–14-3-3 interaction has been thoroughly studied to investigate the 14-3-3 binding sites of GR. Based on these findings, a screening of 8,000 compounds was performed, in chapter 4, and novel plausible stabilisers of the GR–14-3-3 interaction were identified. In this chapter, the search of GR–14-3-3 PPI stabilisers has been extended by focusing on natural and synthetic compounds which have already been reported to stabilise one or more 14-3-3 PPI(s). The GR–14-3-3 interaction was, however, not stabilised by Fusicoccin A nor by mizoribine. Pyrrolidone1, a readily accessible synthetic molecule that has been shown to stabilise the PMA2–¹³, ER α – and CaMKK2–14-3-3 PPIs¹⁴, on the other hand, was found to act as a stabiliser of this interaction. A focused compound library of analogues of pyrrolidone1 was investigated to initiate the exploration of SAR around the pyrrolidone scaffold. Through systematic investigation of the stabilisation activity of these structurally related compounds in the GR–14-3-3 systems, some preliminary structural features were identified. One compound showed an increased stabilisation activity in comparison to pyrrolidone1 and co-crystallization of this promising hit with the GR peptide, GR_pT524, and 14-3-3 ζ enabled us to understand the binding mode. The observed gain in stabilisation and the understanding that has been made provides a starting point towards the achievement of greater 14-3-3–client partner selectivity.

This unique mode of GR antagonism through PPI stabilisation may provide a viable strategy to overcome the inherent challenges linked to the drug discovery for GR.

5.2. Results

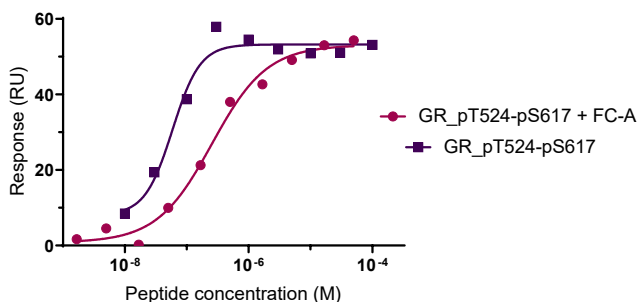
5.2.1. Destabilisation of the GR–14-3-3 PPI by Fusicoccin A

FC-A is produced by the fungus *Phomopsis amygdali* and belongs to the class of diterpene glycosides. FC-A has been originally found to stabilise the complex between the plasma membrane H⁺-ATPase and 14-3-3 leading to a widening of the stomatal pore and wilting of the leaf¹⁵. Biophysical experiments showed that FC-A stabilises the 14-3-3–PMA2 peptide interaction by 90-fold. X-ray crystallography revealed that the fused carbon rings of FC-A filled a hydrophobic cavity created at the interface of the 14-3-3 protein and the PMA2 peptide (called FC pocket) while the sugar moiety is solvent exposed¹⁶. This natural product has been found to stabilise other 14-3-3 PPIs such as CFTR, C-Raf and ER α ¹⁷. Co-crystallization of GR peptides with 14-3-3 enabled the observation of a similar FC pocket (pocket size estimation of 390Å³) and raised the question of whether FC-A could also stabilise the GR–14-3-3 interaction. GR peptides (GR_pT524, GR_pS617 and GR_pT524-pS617) were respectively titrated with 14-3-3 ζ and 14-3-3 σ in the absence and in the presence of FC-A (1 mM) in an SPR experiment. FC-A did not stabilise any of these interactions, instead they were all destabilised. The binding affinity of GR_pT524 with 14-3-3 ζ dropped by 4-fold (from K_d=22 to 90 μM), the affinity of GR_pS617 with 14-3-3 ζ dropped by 11-fold (from K_d=27 to 300 μM) whilst the affinity of GR_pT524-pS617 with 14-3-3 ζ dropped by 8-fold (from K_d=34 to 260 nM) (Fig. 5.1). Similar results were observed with 14-3-3 σ .

A

Peptide Name	K_d with 14-3-3 ζ by SPR (nM)	
	- FC-A	+ FC-A (1 mM)
GR_pT524-pS617	34 \pm 24	260

B



C

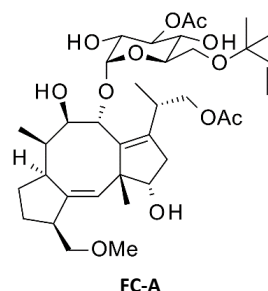
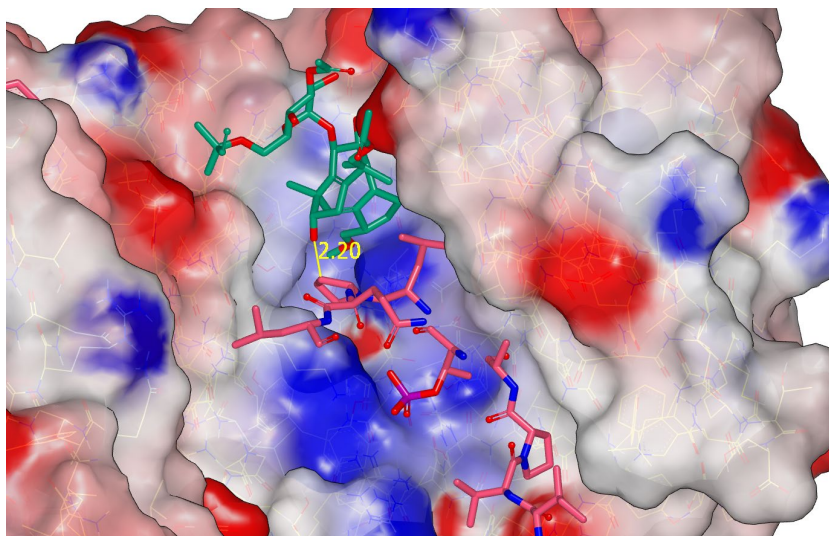


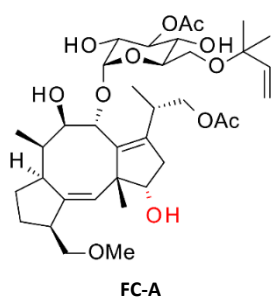
Figure 5.1. FC-A destabilises the interaction between GR_pT524-pS617 and 14-3-3 ζ by 8-fold. (A) Binding affinity of GR_pT524-pS617 with 14-3-3 ζ in the absence and in the presence of FC-A (1 mM). (B) Concentration-response curves of SPR assays of GR_pT524-pS617 with 14-3-3 ζ in the absence and in the presence of FC-A (1 mM). (C) Structure of FC-A.

Analysis of the crystal structure of GR_pT524-pS617 bound to 14-3-3 ζ (PDB code 6YOS) and superimposition with the crystal structure of 14-3-3 ζ in complex with CFTR R-domain peptide and FC-A (PDB code 5D3F) provided a molecular explanation for the decreased activity. Notably, a clash could be observed between of the hydroxy group from the cyclopentene of FC-A and P526 from GR_pT524-pS617. Superimposition with the crystal structure of 14-3-3 ζ in complex with Gab2 peptide and the FC-A analogue ISIR-005, missing the hydroxy group (PDB code 5EXA) suggested that the lack of a C12 hydroxylation would eliminate the clash and enable the stabilisation of the GR–14-3-3 interaction (Fig. 5.2). This hypothesis remains to be tested.

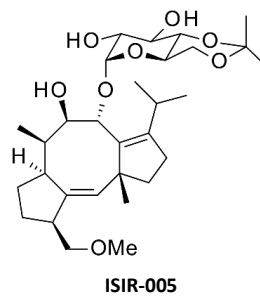
A



B



C



D

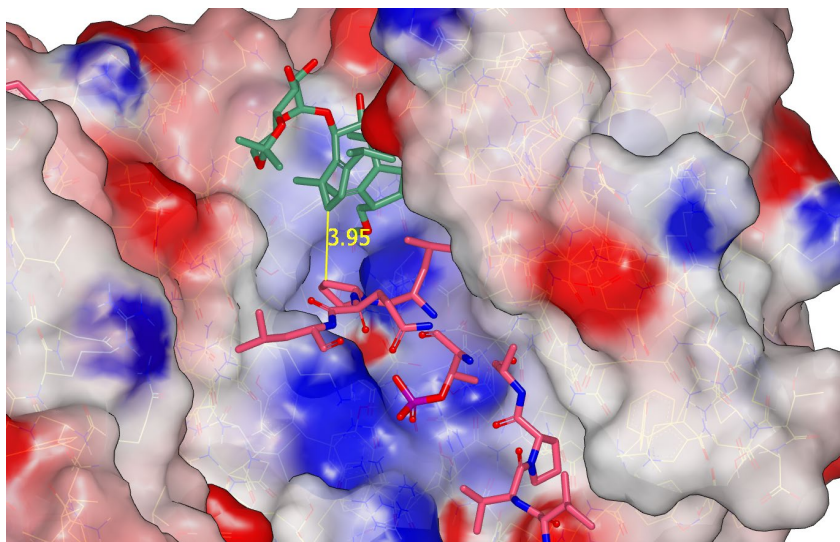


Figure 5.2. Crystal structure analysis revealed that C12 hydroxylation clashes with P526 from GR_pT524-pS617. (A) Superimposition of GR_pT524-pS617 bound to 14-3-3 ζ (PDB code 6YOS) and CFTR R-domain peptide bound to 14-3-3 ζ and stabilised by FC-A (PDB code 5D3F). GR_pT524-pS617 is depicted in magenta sticks and FC-A in green sticks. 14-3-3 is depicted in solid surface coloured according to electrostatics and CFTR R-domain peptide is not shown. (B) Structure of FC-A, with the hydroxy moiety clashing with P526 depicted in red. (C) Structure of ISIR-005. (D) Superimposition of GR_pT524-pS617 bound to 14-3-3 ζ (PDB code 6YOS) and Gab2 peptide bound to 14-3-3 ζ and stabilised by ISIR-005 (PDB code 5EXA). GR_pT524-pS617 is depicted in magenta sticks and ISIR-005 in green sticks. 14-3-3 is depicted in solid surface coloured according to electrostatics and Gab2 peptide is not shown.

5.2.2. Mizoribine: a non-specific binder

The imidazole nucleoside mizoribine is a natural product isolated from *Eupenicillium brefaldianum* with reported immunosuppressive activity^{18,19}. Further investigations identified mizoribine as a stabiliser of the interaction between GR and 14-3-3. 14-3-3 were found to interact with mizoribine using mizoribine-affinity column chromatography and this small molecule was shown to increase the transcriptional activity of GR by 2-fold at 5 mM and by about 2.5-fold at 20 mM²⁰. To determine the effect of mizoribine on the interaction between GR_pT524-pS617 and 14-3-3 ζ , mizoribine was titrated with GR_pT524-pS617 in the presence of various concentrations of 14-3-3 ζ by FP assay. The concentrations of 14-3-3 protein (5 and 20 nM) and peptide (5 nM) were chosen to reach around 20% of binding affinity and an extra measurement without 14-3-3 was performed as control. Stabilisation of the GR peptide–14-3-3 interaction by mizoribine would be translated by an increase of the polarization values correlating with the increase of mizoribine concentration. Indeed,

the polarization values increased, mainly for the three highest concentrations (2.2, 6.7 and 20 mM). Nevertheless, the polarization values also increased in the absence of 14-3-3 suggesting a non-specific binding of mizoribine and not a stabilisation (Fig. 5.3).

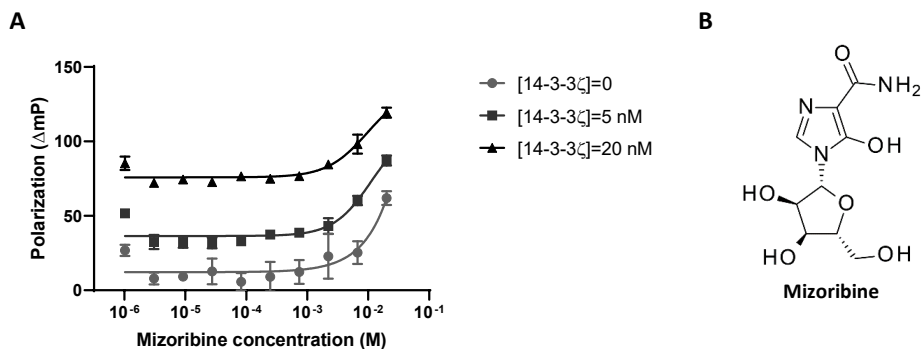


Figure 5.3. Mizoribine interacts non-specifically with the complex GR–14-3-3. (A) Concentration-response curves of FP assays of mizoribine with GR_pT524-pS617 (5 nM) and different concentrations of 14-3-3ζ (0, 5 and 20 nM). (B) Structure of mizoribine.

5.2.3. Stabilisation of GR–14-3-3 PPI by pyrrolidone1

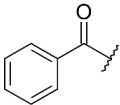
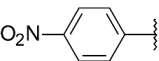
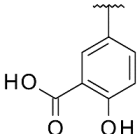
Pyrrolidone1 (**7**) has been identified as a stabiliser of the interaction between the plant proton pump PMA2 and 14-3-3 and co-crystallization of **7** with the PMA2 peptide and 14-3-3 showed that the stabiliser partially filled the FC binding pocket created at the interface of the two partners²¹. Compound **7** has been reported to stabilise other 14-3-3–ligand systems, such as ERα and CaMKK2¹⁴. I therefore tested **7** in the GR–14-3-3 system and observed interaction with the GR_pS524-pS617–14-3-3 complex by both FP and SPR experiments. Using resolved enantiomers ((R)-**7** and (S)-**7**) the R enantiomer ((R)-**7**) was found to be the stabiliser of the GR peptide–14-3-3 interaction with a stabilising activity at 200 μM of 1.8 versus 1.3 for (S)-**7** (Table 5.1), in line with previous reported results on the ERα– and CaMKK2–14-3-3 PPIs¹⁴. The stabilisation activity of (R)-**7** was supported by ITC measurements. Indeed, in the presence of 100 μM (R)-**7**, the binding affinity of the GR-derived phosphorylated peptide with 14-3-3ζ went from 104 nM to 76 nM (Fig. 5.4).

5.2.4. Contribution of the nitro benzyl and the salicylic acid moiety in the stabilisation of the GR–14-3-3 PPI

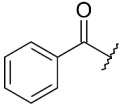
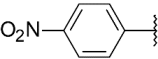
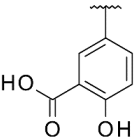
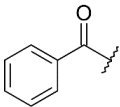
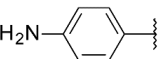
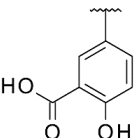
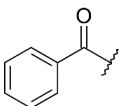
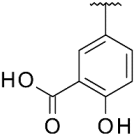
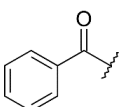
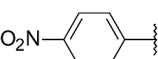
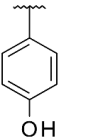
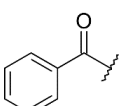
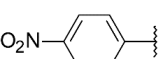
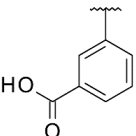
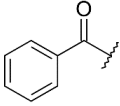
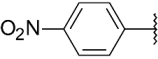
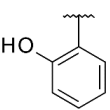
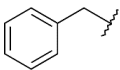
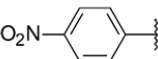
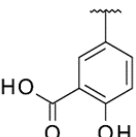
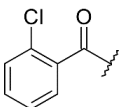
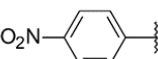
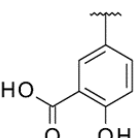
A focused set of analogues of **7** was designed and synthesized by Francesco Bosica using a one-pot multi-component condensation²². I investigated the stabilisation effect of 38 of these structurally related compounds on the GR–14-3-3 PPI for an initial exploration of SAR around the

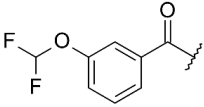
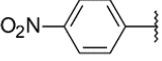
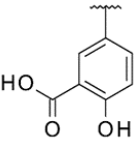
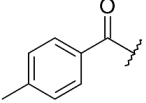
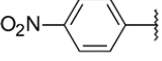
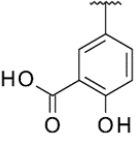
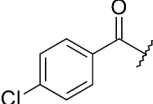
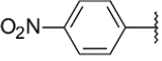
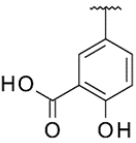
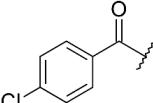
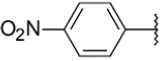
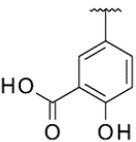
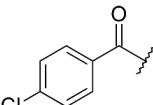
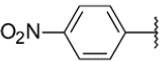
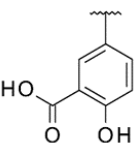
pyrrolidone scaffold. Only some specific compounds, however, will be discussed in this chapter (Table 5.1). I sought to explore the contribution of the nitro benzyl ring. The nitro functionality has been previously reported to accept a hydrogen bond from the 14-3-3 σ residue K122 (PDB code 6TJM). As expected, reduction to the corresponding aniline (**7.1**) as well as the complete removal of the nitrophenyl group (**7.2**) caused a total loss of activity in the GR peptide–14-3-3 ζ system (Table 1). I next focused my attention on the salicylate moiety. The carboxylate group of (R)-**7** forms a bidentate interaction with the 14-3-3 σ residue R41 and makes contact with N42 through a hydrogen bond (PDB code 6TJM). Interestingly, removal of the carboxylate (**7.3**) did not impair the stabilising activity of **7.3** on the GR–14-3-3 PPI which was comparable to the stabilising activity of (R)-**7** measured by FP and SPR. Similarly, compound **7.3** has been reported with a moderate reduction of its activity for the 14-3-3–ER α and CaMKK2 complexes. This moderate loss of activity, despite the loss of the bidentate charge-charge interaction formed by the carboxylate group, one of the strongest non-covalent interaction types, was rationalised by, first, the enthalpic penalty due to desolvation of the carboxylate and second, the enthalpic penalty for this carboxylate group to fit into the negatively charged FC pocket. The hydroxy group of the salicylate moiety has been found to interact with the 14-3-3 σ residue E115 through a hydrogen bond. As expected, removal of the hydroxy group (**7.4**) was unfavourable and greatly decreased the ability of **7.4** to stabilise the GR–14-3-3 ζ interaction. Although the 2-OH analogue (**7.5**) showed a reduced activity as compared to (R)-**7**, it was still found to stabilise the GR–14-3-3 interaction to a certain extent (Table 5.1).

Table 5.1. Stabilisation of pyrrolidone1 and close analogues on the GR peptide–14-3-3 interaction

Compound number	R1	R2	R3	Stabilising activity at 200 μ M by FP	Stabilising activity at 100 μ M by SPR
(R)- 7				1.8 \pm 0.1	2.8 \pm 0.3

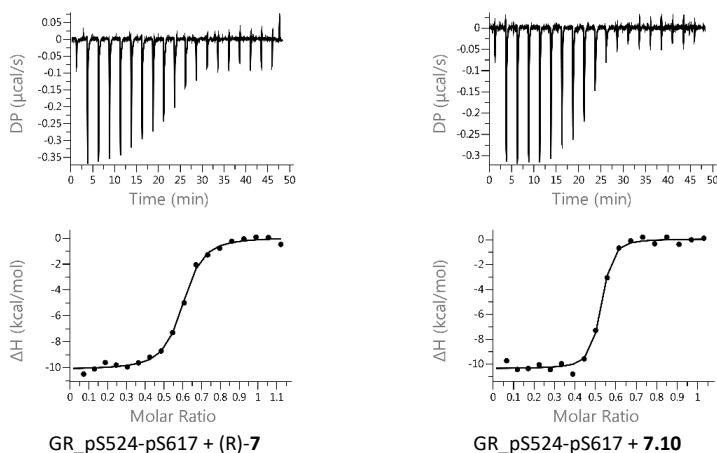
Early Exploration of the Structure Activity Relationship of Small Molecule Stabilisers of the Glucocorticoid Receptor 14-3-3 Protein-Protein Interaction

(S)-7				1.3 ± 0.1	ND
7.1				1.0	ND
7.2		H		1.0	ND
7.3				1.7 ± 0.1	2.9 ± 0.3
7.4				1.2 ± 0.1	ND
7.5				1.4 ± 0.1	ND
7.6				1.8 ± 0.1	2.9 ± 0.8
7.7				1.3 ± 0.1	ND

7.8				1.1 ± 0.1	ND
7.9				1.7 ± 0.1	4.4 ± 0.8
7.10				2.6 ± 0.1	5.0 ± 0.6
(R)- 7.10				2.0 ± 0.2	ND
(S)- 7.10				1.3 ± 0.1	ND

The stabilising activity was determined at 200 μM by FP and 100 μM by SPR. All the experiments were performed in triplicate. When the stabilising activity was found to be greatly impaired, the compound was not further tested by SPR. ND means not determined.

A



B

	GR_pS524-pS617	GR_pS524-pS617 + (R)-7	GR_pS524-pS617 + 7.10
Temp. (°C)	25.1	25.1	25.1
GR peptide (µM)	127 ± 13	133 ± 18	144 ± 13
14-3-3ζ (µM)	25	25	25
Hit (mM)		0.1	0.1
N (sites)	0.5	0.5	0.5
K _d (nM)	104 ± 9	76 ± 24	28 ± 13
ΔH (kcal/mol)	-11.2 ± 0.5	-12.0 ± 1.0	-11.3 ± 0.9
ΔG (kcal/mol)	-9.53 ± 0.06	-9.74 ± 0.21	-9.65 ± 0.15
-TΔS (kcal/mol)	1.68 ± 0.50	2.26 ± 1.03	1.61 ± 0.50

Figure 5.4. Binding affinity of GR_pS524-pS617 and 14-3-3ζ in the absence or in the presence of the (R)-7 and 7.10. (A) Representative example of one ITC binding curve of GR_pS524-pS617 with 14-3-3ζ in the absence or in the presence of (R)-7 and 7.10. (B) Binding affinity of GR_pS524-pS617 and 14-3-3ζ in the absence or in the presence of (R)-7 and 7.10. All experiments were performed in triplicate.

5.2.5. Increased stabilisation with para substitution of the benzo ketone

I investigated the contribution of the benzo ketone (Table 5.1). Interestingly, the benzyl analogue (7.6) did not affect the stabilisation activity towards GR peptide. Analysis of the crystal structure of ERα peptide bound to 14-3-3σ and stabilised by 7 (PDB code 6TJM) showed that the benzo ketone ring points towards a narrow sub-pocket formed by both ERα peptide and 14-3-3 which

drastically restricts substitution on this ring. As suspected, introduction of substituents on the 2- and 3-position of the benzo ketone such as a chlorine substituent on the 2-position (**7.7**) and an OCHF₂ on the 3-position (**7.8**), was unfavourable and greatly decreased the activity of these compounds. The substituents on these positions probably clash with the residues from both 14-3-3 and GR. Introduction of a methyl group on the 4-position (**7.9**), however, led to a higher stabilising activity of this compound in comparison to **7**. Interestingly, a larger gain in stabilisation was observed upon chlorine substitution on the same position (**7.10**) (Table 5.1). These results were in line with ITC measurement since **7.10** showed an 4-fold stabilisation of the GR_pS524-pS617–14-3-3 interaction (from a K_d of 104 nM to 24 nM) (Fig. 5.4).

The ability of **7.10** to bind and stabilise the GR_pS524-pS617–14-3-3 interaction was further assessed by chemical shift perturbation mapping. Observation of the changes in the intensity ratio (I/I₀) of resonances in the fully-assigned ¹H-¹⁵N TROSY-HSQC spectrum of 14-3-3σΔC in the presence (I) or absence (I₀) of **7.10**, enabled us to identify the residues which exhibit a shift upon binding with **7.10**. These residues were located in the FC binding pocket, indicating that the compound binds in this pocket, as expected (Fig. 5.5). In addition, compound **7.10** could be seen to bind to the GR_pS524-pS617–14-3-3 complex, not only to 14-3-3σ (Fig. 5.6 and 5.7).

Compound **7.10** was evaluated as a racemate. Therefore, a chiral separation was performed and the absolute configuration was determined by vibrational circular dichroism (VCD) (Fig. 5.S1). The stabilisation activity of the two enantiomers was measured and similar to **7**, the R enantiomer ((R)-**7.10**) was found to be the active configuration (Table 5.1).

Early Exploration of the Structure Activity Relationship of Small Molecule Stabilisers of the
Glucocorticoid Receptor 14-3-3 Protein-Protein Interaction

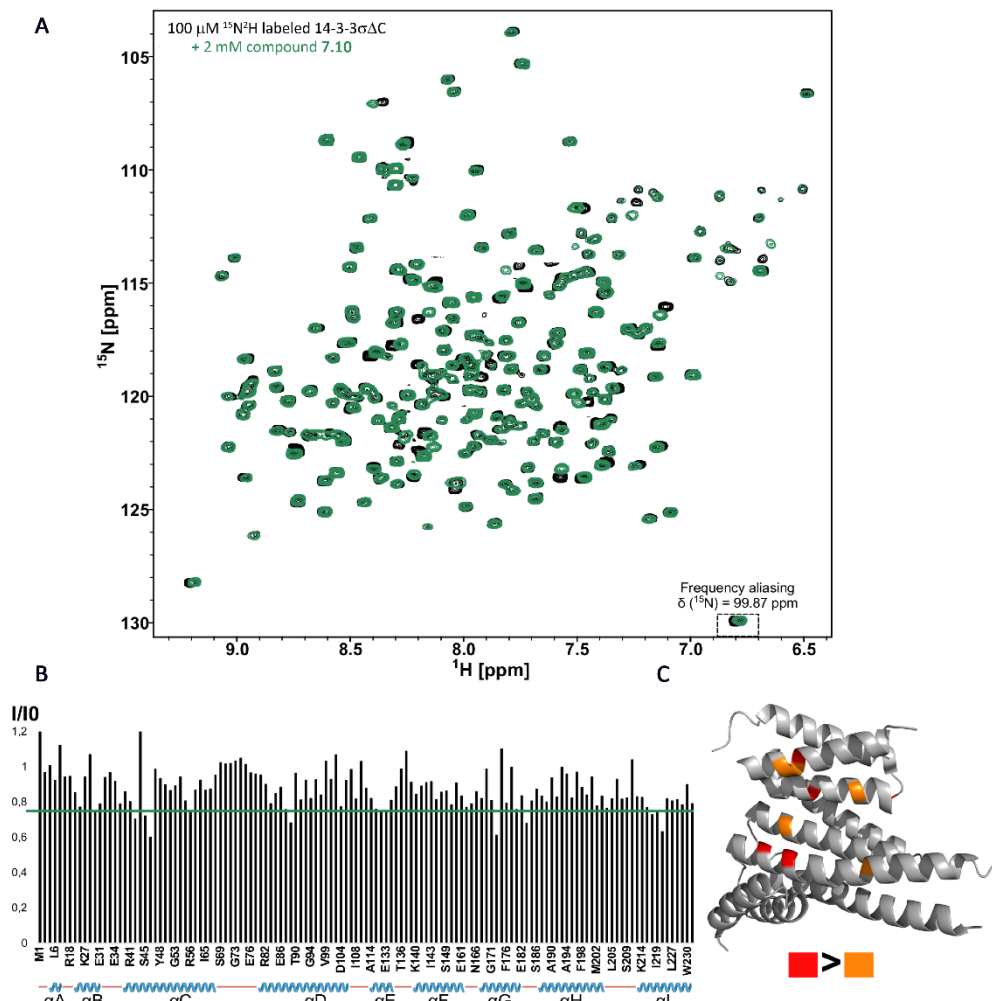


Figure 5.5. Compound 7.10 binds in the amphipathic groove formed at the interface of GR and 14-3-3. (A) ^1H - ^{15}N TROSY-HSQC spectra of ^{15}N labeled 14-3-3 ΔC (100 mM, black) and with **7.10** (2 mM, green). (B) Plot of the I/I_0 values of ^1H - ^{15}N correlation peak intensities in the spectrum of ^{15}N labeled 14-3-3 ΔC (100 mM) with **7.10** (2 mM) compared to the corresponding correlation peak intensities in the reference spectrum (14-3-3 ΔC , 100 mM) versus the amino acid sequence. A total of 131 correlation peak intensity ratios are shown. The x axis is not proportional to the sequence length. The helices of 14-3-3 ΔC are identified below the x axis as blue cartoons and disordered regions as red lines. The line on the plot represents a I/I_0 ratio of 0.75, considered significant. (C) Mapping on the crystal structure of 14-3-3 ΔC (PDB ID: 1YZ5) of the amino acid residues corresponding to the 10 most affected resonances (red and orange) by **7.10**.

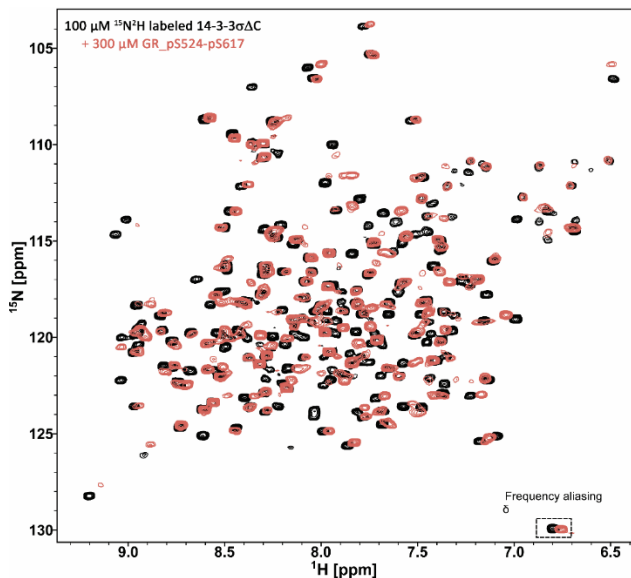


Figure 5.6. ^1H - ^{15}N TROSY-HSQC spectra of $^{15}\text{N}^2\text{H}$ labelled 14-3-3 $\sigma\Delta\text{C}$ (100 μM , black) and with GR_pS524-pS617 (300 μM , red)

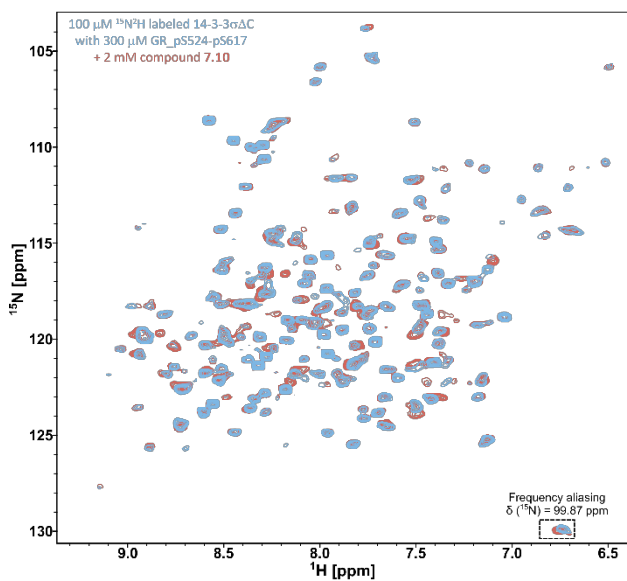


Figure 5.7. ^1H - ^{15}N TROSY-HSQC spectra of $^{15}\text{N}^2\text{H}$ labelled 14-3-3 $\sigma\Delta\text{C}$ (100 μM) with GR_pS524-pS617 (300 μM , blue) and 7.10 (2 mM, red). Addition of 7.10 induced chemical shift perturbation in the GR peptide–14-3-3 spectra.

5.2.6. Co-crystallization of **7.10** with GR peptide and 14-3-3 ζ

Compound **7.10** was co-crystallized with the 13-mer GR peptide centred on the phosphorylated residue T524 and 14-3-3 ζ (PDB code 6ZFI) to get a deeper understanding of the molecular details of the interaction and further characterize the binding mode (Fig. **5.8**). The structure was solved to a resolution of 1.96Å and the electron density allowed the assignment of 11 amino acids of GR_pT524. The crystal structure of this ternary complex was consistent with the previously reported apo crystal structure of GR_pT524 bound to 14-3-3 ζ (PDB code 6YO8), with the GR peptide making similar interactions with 14-3-3. Each of the two FC binding pockets created when the GR_pT524 peptides bind to the 14-3-3 dimer could be seen to contain a molecule of **7.10**. Only the R configuration of **7.10** could be modelled into the observed electronic density, which is consistent with previous observations with (R)-**7** and the FP data from (R)-**7.10** and (S)-**7.10**. Compound **7.10** shared most of its protein contact surface with 14-3-3, making electronic interactions. Notably, the carboxylate group of **7.10** formed a bidentate interaction with the 14-3-3 ζ residue R41 and an additional hydrogen bond interaction with N42. A polar interaction was also observed between the salicylate hydroxyl group and H164 making another hydrogen bond. The carbonyl of the pyrrolidone ring formed an antiparallel interaction with the carbonyl moiety of the sidechain of N42. The 14-3-3 residue K120 was involved in a hydrogen bond with the carbonyl of GR P526 on one side and the nitro group of **7.10** on the other side. Together these results were consistent with the previously published crystal structure of ER α , 14-3-3 σ and **7**, and the SAR observed in this chapter. In addition, the residues L220, L216 and I217 from the 14-3-3 protein and L525 from GR_T524 formed a well-defined hydrophobic pocket which nicely accommodated the extra chlorine (Fig. **5.8**). The additional hydrophobic contacts and the increased occupancy of the FC binding pocket of **7.10** provided a defined molecular explanation for the increased activity of **7.10** in stabilising the GR peptide–14-3-3 interaction and rationalised the stabilising activity of **7.9** bearing a methyl on the 4-position which most probably fits nicely in this hydrophobic sub-pocket.

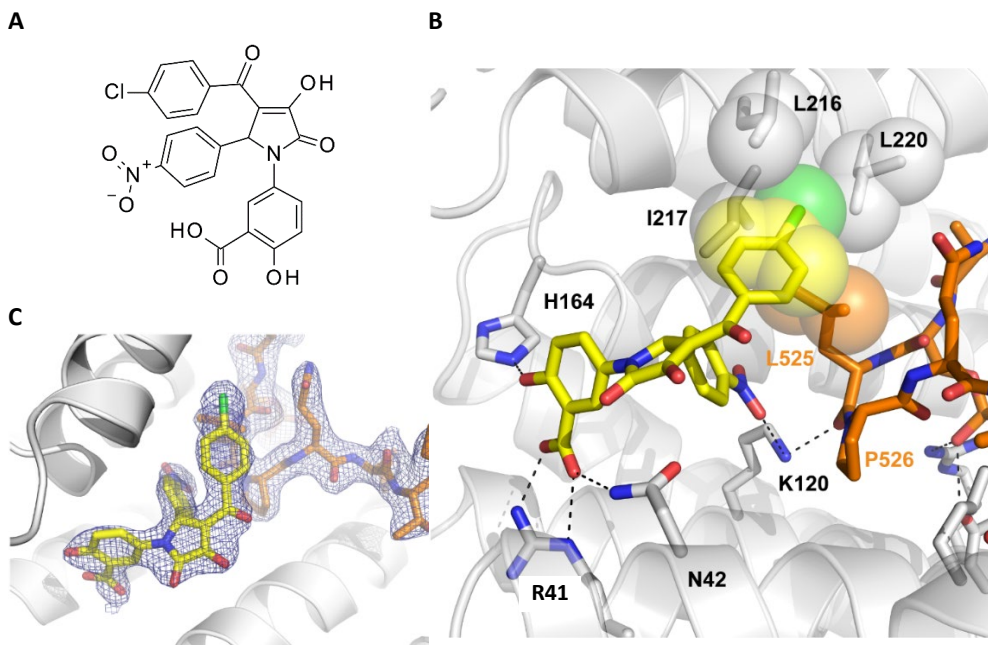


Figure 5.8. Compound 7.10 stabilise the GR peptide–14-3-3 interaction by binding at the interface of the two partners acting as a molecular glue. (A) Structure of 7.10. (B) Electron density map of 7.10 (yellow, red, blue and green sticks) bound to GR_pT524 (orange, red and blue sticks) and 14-3-3 ζ (white ribbons ($2F_o - F_c$, contoured at 1 σ)). (C) Details of the interaction of 7.10 with GR_pT524 and 14-3-3 ζ . Polar interactions are depicted as black dotted lines and hydrophobic contacts as yellow, green or orange sticks with a semi-transparent surface.

5.3. Discussion

Natural products and synthetic compounds have been previously identified as stabilisers of 14-3-3 PPIs^{17,23}. In this chapter, I investigated the role of three known 14-3-3 PPI stabilisers on the interaction between GR and 14-3-3, FC-A, mizoribine and pyrrolidone1. FC-A has been shown to stabilise many 14-3-3–client protein interactions but did not stabilise the GR-derived phosphorylated peptide–14-3-3 interaction. Instead SPR assays showed that FC-A destabilised this PPI by 8-fold. Crystal structure comparison of GR_pT524–pS617 bound to 14-3-3 with the CFTR–14-3-3 complex stabilised by FC-A revealed a potential clash of the hydroxy group on the C12-position of FC with the GR peptide; an FC-A analogue, ISIR-005, that lacks this substituent would be a promising candidate to test. Further biophysical experiments could be envisioned to confirm the crystal structure analysis and determine if ISIR-005 stabilises the GR–14-3-3 PPI. The semi-synthetic tool compound ISIR-005 has been found to stabilise the interaction between peptides derived from Gab2 and 14-3-3 which could provide a new therapeutic approach in cancer²⁴. ISIR-005, however, has a highly complex structure

because of its 5-8-5 fused ring scaffold and its 11 stereocentres. This chemical complexity means that ISIR-005 is extremely challenging for medicinal chemistry optimisation, owing to the synthetic challenges. This prompted us to investigate more drug-like compounds.

Mizoribine, which has been proposed to stabilise the GR–14-3-3 PPI, acted in my hands as a non-specific binder for the GR peptide–14-3-3 interaction, since an increased signal was observed even in the absence of 14-3-3 in the FP assay. The drug-like small-molecule, pyrrolidone1, showed a stabilisation activity but lacks specificity. Pyrrolidone1 was initially identified by screening a 37,000-member compound library and has previously been shown to stabilise the PMA2–¹³, ER α – and CaMKK2–14-3-3 PPI¹⁴. A focused compound library of analogues of pyrrolidone1 has been designed and synthesized to investigate the stabilisation of the ER α – and CaMKK2–14-3-3 PPIs. Here 38 of these analogues were tested with the GR–14-3-3 PPI and the most relevant compounds were discussed to shape a preliminary SAR. Common observations with these three systems were found such as a loss of stabilising activity upon removal of the nitro functionality thus the hydrogen bond with the 14-3-3 σ residue K122 and removal of the hydroxy group of the salicylate moiety thus the polar interaction with the 14-3-3 σ residue E115 (Bosica*, Munier* *et al*). X-ray analysis of the ternary complex PMA2 peptide–14-3-3–pyrrolidone1, have shown that pyrrolidone1 mostly binds to 14-3-3 with a reported protein contact surface with 14-3-3 of 83%¹³. A strategy to gain specificity would be to increase the contact surface with the 14-3-3 protein partner by designing compounds with more intimate contacts and productive interactions with this 14-3-3 protein partner. Co-crystallization of 14-3-3 PPIs generally involve 14-3-3 proteins and a short peptide, modelling the client protein. This limited knowledge on the protein partner and its 3D structure can be challenging for a rational design of specific stabilisers. Despite these limitations, **7.10** exemplifies this strategy. Compound **7.10** bears a chlorine on the 4-position of the benzo ketone ring which led to a gain of stabilisation for the GR peptide–14-3-3 ζ system. Interestingly, the additional chlorine of **7.10** made little difference in the binding with either CaMKK2 or ER α , where similar activity was observed to pyrrolidone1 (Bosica*, Munier* *et al*). Co-crystallization of **7.10** with GR peptide and 14-3-3 ζ enabled further insights into the molecular details of the interaction and showed that the chlorine substituent extended the benzo ketone ring deeper in the hydrophobic sub-pocket formed by both protein partners. The extra contact surface and hydrophobic contact of **7.10** with 14-3-3 and GR peptide might be a starting point towards achieving target specificity.

5.4. Conclusion

This chapter 5 focuses on the stabilisation of the GR–14-3-3 PPI by known 14-3-3 stabilisers. FC-A was found to destabilise the GR–14-3-3 interaction and mizoribine to act as a non-specific binder. Pyrrolidone1, however, showed a stabilisation effect. Investigation of analogues and measurement of their stabilisation activity by biophysical assays such as FP and ITC, enable to identify some SAR principles and a new compound with a higher activity and specificity towards the GR–14-3-3 system than pyrrolidone1. Such a compound could be used as a tool compound to further understand the role of 14-3-3 in the GR transcriptional activity and potentially provide a new and viable strategy to further regulate GR beyond direct ligand-driven activation, thus overcoming some of the inherent challenges linked to the drug discovery for GR.

5.5. Acknowledgements

The author thanks Dr. Matthew W.D. Perry for conceiving and directing the project, Dr. Christian Ottmann for his strategic guidance, Francesco Bosica and Dr. Gavin O'Mahony for providing the analogues of pyrrolidone1, Dr. Isabelle Landrieu and Dr. Joao Neves for performing the 2D NMR experiments, Lisa Wisler for her support in the co-crystallization of **7.10** with GR and 14-3-3, Dr. Karl Edman for his help with the determination and analysis of the X-ray crystal structure, Dr. Linda Thunberg for the chiral separation of **7.10** and Dr. Richard Lewis for the VCD analysis. The author acknowledges SLS for providing access to their beamlines and Dr. Werngard Czechtizky for generous support of the project.

5.6. Materials and methods

Peptide synthesis

Peptides were synthesized according to the method reported in chapter 2.

14-3-3 expression and purification

The σ and ζ isoforms of human 14-3-3 and 14-3-3 Δ C (C-terminally truncated, including residues 1-231, for crystallography purposes) were expressed and purified according to the method reported in chapter 2.

Production of $^{15}\text{N}^2\text{H}$ labelled 14-3-3 $\sigma\Delta$ C for NMR spectroscopy

The $^{15}\text{N}^2\text{H}$ labelled 14-3-3 $\sigma\Delta$ C proteins were expressed and purified according to the method reported in chapter 4.

FP, SPR and ITC assays

FP, SPR and ITC were performed according to the method reported in chapter 4.

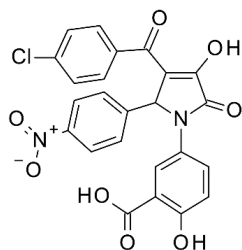
^{15}N -1H TROSY-HSQC NMR spectroscopy

^1H - ^{15}N TROSY-HSQC was recorded and analysed according to the method reported in chapter 4.

Small molecule synthesis

FC-A was a kind gift of Professor Christian Ottmann (Department of Biomedical Engineering, Eindhoven University of Technology, Netherlands). Mizoribine was purchased from Sigma-Aldrich. Pyrrolidone1 and its analogues were a kind gift of by Francesco Bosica (Research and Early Development, CVRM, BioPharmaceuticals R&D, AstraZeneca, Gothenburg, Sweden) and the author only synthesized the following compound.

General details: All solvents and reagents were purchased from commercial suppliers and were used without purification or were prepared according to published procedures. Nuclear magnetic resonance (NMR) spectra were acquired according to the method reported in chapter 3. Chemical shifts (δ) are reported in parts per million (ppm) relative to residual DMSO signal (δ 2.50 ppm in ^1H NMR and 39.5 ppm in ^{13}C NMR). Coupling constants (J) are reported as Hz. NMR abbreviations are used as follows: br = broad, s = singlet, d = doublet, t = triplet, q = quartet, m = multiplet. Protons on heteroatoms such as COOH protons are only reported when detected in NMR and can therefore be missing. Analytical RP-UPLC-MS was performed on a Waters Acquity UPLC system (PDA, sample manager, sample organiser, column oven modules) and Waters SQD2 mass spectrometer using the following column: Waters Acquity HSS C18 column, 1.8 μm , 2.1 x 50 mm at a flow rate of 1 mL/min at 40 °C. A linear gradient of mobile phase: A=H₂O + 10 mM formic acid, 1 mM ammonium formate buffer at pH 3 and B=CH₃CN + 10 mM formic acid, 1 mM ammonium formate buffer was used.



5-(3-(4-chlorobenzoyl)-4-hydroxy-2-(4-nitrophenyl)-5-oxo-2,5-dihydro-1H-pyrrol-1-yl)-2-hydroxybenzoic acid (7.10). 4-nitrobenzaldehyde (95 mg, 0.62 mmol) and 5-amino-2-hydroxybenzoic acid (97 mg, 0.62 mmol) were added to a solution of methyl 4-(4-chlorophenyl)-2,4-dioxobutanoate (150 mg, 0.62 mmol) in AcOH (5 mL) in a microwave vial. The reaction mixture was heated at 120 °C for 180 min in a single mode microwave reactor for 60 min. The solid was collected, washed with diethyl ether and dried under reduced pressure to give the title compound **11** (74 mg, 24%) as a yellow solid. ^1H NMR (500 MHz, DMSO) δ 6.43 (s, 1H), 6.90 (d, J = 8.8 Hz, 1H), 7.53 (d, J = 8.4 Hz, 2H), 7.67 – 7.75 (m, 5H), 8.02 (d, J = 2.6 Hz, 1H), 8.06 (d, J = 8.5 Hz, 2H). ^{13}C NMR (126 MHz, DMSO) δ 187.8, 171.1, 164.4, 158.8, 152.4, 147.2, 144.4, 137.4, 136.6, 130.5, 129.3, 128.3, 127.4, 124.9, 123.5, 118.6, 117.6, 113.0, 60.7. Purity > 99% according to analytical UPLC. Rt 1.69 min (10-99% B in 4 min). HRMS (ESI) m/z [$M + \text{H}$]⁺ calculated for C₂₄H₁₅ClN₂O₈: 495.0595, found: 495.0583.

Chiral separation of (R)- 7.10 and (S)-7.10. The racemic **7.10** was dissolved to a concentration of 20 mg/mL in MeOH:IPA 2:1 supplemented with TEA, separated by supercritical fluid chromatography using the column Chiralpak IC, 250 x 50 mm particle size 5 μm , at a flow rate of 13 mL/min at 40 °C. The buffer MeOH:IPA:TEA 25:75:0.1 in CO₂ was used with detection at 270 nm. The appropriate fractions were combined and freeze-dried.

Analytical RP-UPLC-MS was performed using the column Reprosil NR, 250 × 4.6 mm particle size 8 μm, at a flow rate of 0.8 mL/min at 25 °C. The buffer MeOH:IPA:TEA 50:50:0.1 in CO₂ was used with detection at 357 nm. (R)-**7.10**: purity > 99% according to analytical UPLC, Rt 3.20 min. (S)-**7.10**: purity > 99% according to analytical UPLC, Rt 4.86 min.

Vibrational circular dichroism

Experimental protocol: (R)-**7.10** (5.0 mg) and (S)-**7.10** (5.4 mg) were dissolved in 150 μl DMSO-d₆ respectively. Approximately 90 μl of each solution was transferred to a 0.100 mm BaF₂ cell and VCD spectra acquired for 12 hours in a Biotools ChiralIR2X instrument. The resolution was 4 cm⁻¹. The same cell was used for measurement of both samples.

Computational Spectral Simulations: A Monte Carlo molecular mechanics search for low energy geometries was conducted for the S enantiomer of an analogue of this compound with Cl replaced by H. *MacroModel* within the *Maestro* graphical interface (Schrödinger Inc.) was used to generate 123 starting coordinates for conformers. All conformers within 5 kcal/mole of the lowest energy conformer were used as starting point for density functional theory (DFT) minimizations within *Gaussian09*.

Optimized structures, harmonic vibrational frequencies/intensities, VCD rotational strengths, and free energies at STP (including zero-point energies) were determined at B3LYP/6-31G* level of theory. Three conformations were found that contributed over 10% to the Boltzmann distribution. An in-house program was used to fit Lorentzian line shapes (12 cm⁻¹ line width) to the computed spectrum of a Boltzmann distributed average thereby allowing direct comparisons between simulated and experimental spectra (Fig. 5.S1).

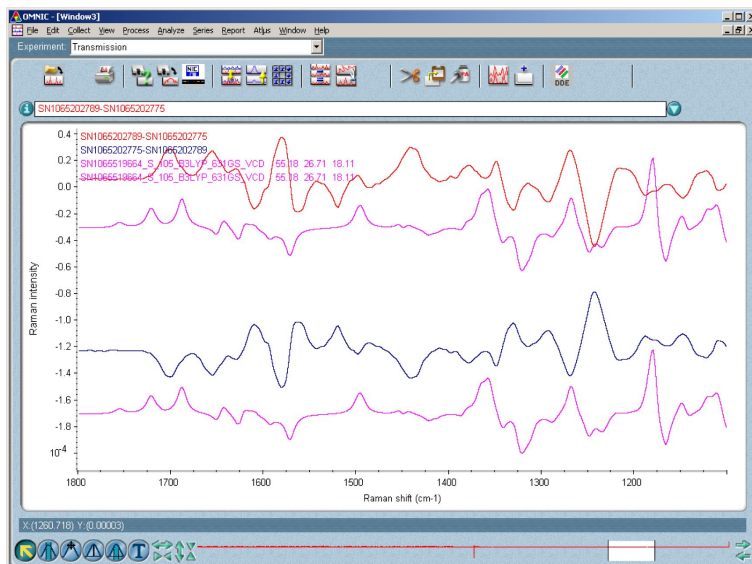


Figure 5.S1. Comparison of calculated and experimental spectra of (S)-7.10. The calculated spectrum for the (S) enantiomer is shown in pink. The experimental spectra are shown in red and green (subtracted from each other so the two experimental spectra are inversions of each other). There is a reasonable match between the experimental

Early Exploration of the Structure Activity Relationship of Small Molecule Stabilisers of the Glucocorticoid Receptor 14-3-3 Protein-Protein Interaction spectrum ((*S*)-**7.10**, red) and the calculated spectrum for the (*S*) enantiomer, particularly in the region 1200-1300 cm^{-1} .

X-ray crystallography studies

Hanging co-crystallization of 14-3-3 ζ , GR_pT524 and 7.10. Crystals were grown using the hanging drop vapor diffusion crystallization method by mixing 14-3-3 ζ ΔC with GR_pT524 in a 1:2 ratio with a resulting protein concentration of 10 mg/mL in a crystallization buffer containing 20 mM HEPES pH 7.5, 2 mM MgCl_2 and 2 mM DTT. Compound **7.10** (2 mM) was added to the mixture and after overnight incubation at 4 °C, hanging drops were formed by mixing equal volumes of protein/peptide/ligand solution and precipitant (0.4 M MgCl_2 , 27% PEG 3350, 0.1 M Bis Tris pH 6.5) (2 × 1 mL) on a 15-well EasyXtal (Qiagen) and equilibrated over a 500 μL reservoir at 4 °C. Crystals were harvested after 13 days, soaked in cryo-protectant containing the precipitant supplemented with 20% v/v glycerol and flash-cooled in liquid nitrogen before data collection.

Data collection and processing. Diffraction data were collected at the Swiss Light Source (SLS) in Switzerland (1.00003Å, 100 K, SLS Beamline X06SA). Molecular replacement was performed using Phaser from the ccp4i package and refinement and manual rebuilding was done using Buster and Coot software packages. The structure (PDB code: 6ZFI) was refined to a resolution of 1.96 Å with $R_{\text{work}}/R_{\text{free}}$ factors of 0.223/0.242. X-ray diffraction data collection and structure refinement statistics are summarized in Supplementary Table 5.S2. The figures were made using the software PyMol (DeLano Scientific LLC).

Table 5.S2. Data collection and refinement statistics (molecular replacement)

GR_pT524-14-3-3ζ-7.10 ⁴	
Data collection	
Space group	P22 ₁ 2 ₁
Cell dimensions	
<i>a</i> , <i>b</i> , <i>c</i> (Å)	122.57, 78.07, 57.35
α , β , γ (°)	90.00, 90.00, 90.00
Resolution (Å)	65.85-1.96 (2.13-1.96)
<i>R</i> _{merge}	0.09
<i>I</i> / σ <i>I</i>	12.7 (1.5)
Completeness (%)	94.1 (55.3)
Redundancy	7.4 (6.9)
Refinement	
Resolution (Å)	65.85-1.96
No. reflections	31,952
<i>R</i> _{work} / <i>R</i> _{free}	0.223 / 0.242
No. atoms	
Protein	3,887
Ligand/ion	99
Water	283
<i>B</i> -factors	
Protein	44.4
Ligand/ion	81.6
Water	46.5
R.m.s. deviations	
Bond lengths (Å)	1.38
Bond angles (°)	0.80

*Values in parentheses are for highest-resolution shell.

⁴ One xtal

5.7. References

1. Pennington, K., Chan, T., Torres, M. & Andersen, J. The dynamic and stress-adaptive signaling hub of 14-3-3: emerging mechanisms of regulation and context-dependent protein–protein interactions. *Oncogene* **37**, 5587–5604 (2018).
2. Johnson, C. *et al.* Visualization and Biochemical Analyses of the Emerging Mammalian 14-3-3-Phosphoproteome. *Mol. Cell. Proteomics* **10**, M110.005751 (2011).
3. Aghazadeh, Y. & Papadopoulos, V. The role of the 14-3-3 protein family in health, disease, and drug development. *Drug Discov. Today* **21**, 278–287 (2016).
4. Hwang, Y., An, H. T., Kang, M. & Ko, J. Roles of 14-3-3 β and γ in regulation of the glucocorticoid receptor transcriptional activation and hepatic gluconeogenesis. *Biochem. Biophys. Res. Commun.* **501**, 800–806 (2018).
5. Habib, T. *et al.* AKT1 has dual actions on the glucocorticoid receptor by cooperating with 14-3-3. *Mol. Cell. Endocrinol.* **439**, 431–443 (2017).
6. Galliher-Beckley, A. J., Williams, J. G. & Cidlowski, J. A. Ligand-Independent Phosphorylation of the Glucocorticoid Receptor Integrates Cellular Stress Pathways with Nuclear Receptor Signaling. *Mol. Cell. Biol.* **31**, 4663–4675 (2011).
7. Kim, Y. S. *et al.* Role of 14-3-3 η as a Positive Regulator of the Glucocorticoid Receptor Transcriptional Activation. *Endocrinology* **146**, 3133–3140 (2005).
8. Kino, T. *et al.* Protein 14-3-3 σ Interacts With and Favors Cytoplasmic Subcellular Localization of the Glucocorticoid Receptor, Acting as a Negative Regulator of the Glucocorticoid Signaling Pathway. *J. Biol. Chem.* **278**, 25651–25656 (2003).
9. Widén, C., Zilliacus, J., Gustafsson, J. Å. & Wikström, A. C. Glucocorticoid Receptor Interaction with 14-3-3 and Raf-1, a Proposed Mechanism for Cross-Talk of Two Signal Transduction Pathways. *J. Biol. Chem.* **275**, 39296–39301 (2000).
10. Wakui, H., Wright, A. P. H., Gustafsson, J. & Zilliacus, J. Interaction of the Ligand-activated Glucocorticoid Receptor with the 14-3-3 η Protein. *J. Biol. Chem.* **272**, 8153–8156 (1997).
11. Kino, T. GR-regulating Serine/Threonine Kinases: New Physiologic and Pathologic Implications. *Trends Endocrinol. Metab.* **29**, 260–270 (2018).
12. Scheschowitsch, K., Leite, J. A. & Assreuy, J. New insights in glucocorticoid receptor signaling-more than just a ligand-binding receptor. *Frontiers in Endocrinology* **8**, 16 (2017).
13. Rose, R. *et al.* Identification and structure of small-molecule stabilizers of 14-3-3 protein-protein interactions. *Angew. Chemie - Int. Ed.* **49**, 4129–4132 (2010).
14. Bosica, A. F. *et al.* Design Of Drug-Like Protein-Protein Interaction Stabilizers Guided By

- Chelation-Controlled Bioactive Conformation Stabilization. *Chem. - A Eur. J.* (2020).
doi:10.1002/chem.202001608
15. De Boer, B. Fusicocin - A key to multiple 14-3-3 locks? *Trends Plant Sci.* **2**, 60–66 (1997).
 16. Würtele, M., Jelich-Ottmann, C., Wittinghofer, A. & Oecking, C. Structural view of a fungal toxin acting on a 14-3-3 regulatory complex. *EMBO J.* **22**, 987–994 (2003).
 17. Ballone, A., Centorrino, F. & Ottmann, C. 14-3-3: A Case Study in PPI Modulation. *Molecules* **23**, 1–14 (2018).
 18. Mizuno, K. *et al.* Studies on bredinin. I. Isolation, characterization and biological properties. *J. Antibiot. (Tokyo)*. **27**, 775–782 (1974).
 19. Yoshioka, H., Nakatsu, K., Hayashi, M. & Mizuno, K. Studies on bredinin. II The molecular structure of bredinin. *Tetrahedron Lett.* **16**, 4031–4034 (1975).
 20. Takahashi, S., Wakui, H., Gustafsson, J. A., Zilliacus, J. & Itoh, H. Functional interaction of the immunosuppressant mizoribine with the 14-3-3 protein. *Biochem. Biophys. Res. Commun.* **274**, 87–92 (2000).
 21. Richter, A., Rose, R., Hedberg, C., Waldmann, H. & Ottmann, C. An optimised small-molecule stabiliser of the 14-3-3-PMA2 protein-protein interaction. *Chem. - A Eur. J.* **18**, 6520–6527 (2012).
 22. Ma, K. *et al.* Rational design of 2-pyrrolinones as inhibitors of HIV-1 integrase. *Bioorganic Med. Chem. Lett.* **21**, 6724–6727 (2011).
 23. Stevers, L. M. *et al.* Modulators of 14-3-3 Protein-Protein Interactions. *J. Med. Chem.* **61**, 3755–3778 (2017).
 24. Bier, D. *et al.* Small-Molecule Stabilization of the 14-3-3/Gab2 Protein-Protein Interaction (PPI) Interface. *ChemMedChem* **11**, 911–918 (2016).

Chapter 6

Epilogue: Towards the Modulation of GR Activity

Beyond Ligand Binding

6.1. Introduction

The epilogue summarizes the main findings to identify small molecules which stabilise the GR–14-3-3 PPI and reports on the future experiments which could be performed to expand beyond the work reported in this thesis. In particular, this chapter develops on the possibilities to quantitatively characterise the GR–14-3-3 PPI and investigate the biological relevance of this interaction. It describes the opportunities to use the small molecule stabilisers, identified in chapters 4 and 5, for a more comprehensive insight into 14-3-3 regulation of GR. Finally, it highlights the potential of the GR–14-3-3 PPI stabilisation for the development of a novel class of therapeutics as a new strategy to overcome the side effects inherent to GR agonist in the treatment of inflammation.

6.2. Quantitative characterisation of the GR–14-3-3 PPI

I have identified, through studies with GR constructs and in cells, that the kinase MINK1 is an important enzyme in phosphorylation of T524 and is required for GR binding to 14-3-3. The kinase profiling identified that MINK1 was capable of phosphorylating GR and the far Western blot demonstrated that this actually happened in cells upon stimulation. In this assay, GR LBD *in vitro* phosphorylated by MINK1 was shown to interact with the two recombinant yeast isoforms of 14-3-3, as reported in chapter 3. For quantitative determination of the role of MINK1, measurement of the binding affinity of phosphorylated GR LBD or full-length GR with 14-3-3 could be envisioned using SPR. I have started to explore this option without going to the end of the process. 6His tagged 14-3-3 could not be immobilized following the optimized protocol on the NTA derivatized SPR sensorchip because GR LBD was expressed with the same tag and could potentially bind to the surface and generate a false signal. Instead, an SPR sensorchip coated with biotin was selected. This chip enables a reversible immobilization of biotinylated bait molecules, using the avidin mutant switchavidin, as a robust but switchable bridge between the chip and the biotinylated bait. Complete chip regeneration can be obtained in acidic conditions using citric acid and SDS (Fig. 6.1)¹. 14-3-3 ζ proteins were biotinylated with EZ-Link-NHS-PEG₁₂-Biotin in a 1:1 ratio and purified by size exclusion chromatography. The immobilization of biotinylated 14-3-3 and switchavidin on the chip surface was then optimized by assessing the best 14-3-3: switchavidin ratio to get the maximum response with the shortest injection time (Fig. 6.2). To confirm the method, GR_T524-S617 was titrated and its measured binding affinity with 14-3-3 ζ was found to be in line with the one determined with the method using the NTA derivatized SPR sensorchip ($K_d=43$ and 30 nM, respectively). Single point measurement of MINK1 phosphorylated GR LBD–14-3-3 ζ affinity, however, did not show any interaction. The functionality of the phosphorylated GR LBD proteins was verified by testing their ability to bind GR cofactors which

revealed that the protein had been denatured. The most likely explanation for this is a consequence of sub-optimal storage conditions. In brief, I showed this by using the peptide derived peroxisome proliferator-activated receptor gamma coactivator 1 (PRGC1) immobilized on a biotinylated chip. Non-phosphorylated GR LBD was found to interact with PRGC1 in the presence of dexamethasone, as expected², whereas MINK1 phosphorylated GR LBD did not, even when the buffer was supplemented with the steroid ligand (Fig. 6.3). Moving forward, this biophysical assay could be utilized to determine the K_d of newly *in vitro* phosphorylated GR constructs and provide quantitative information on the GR–14-3-3 interaction.

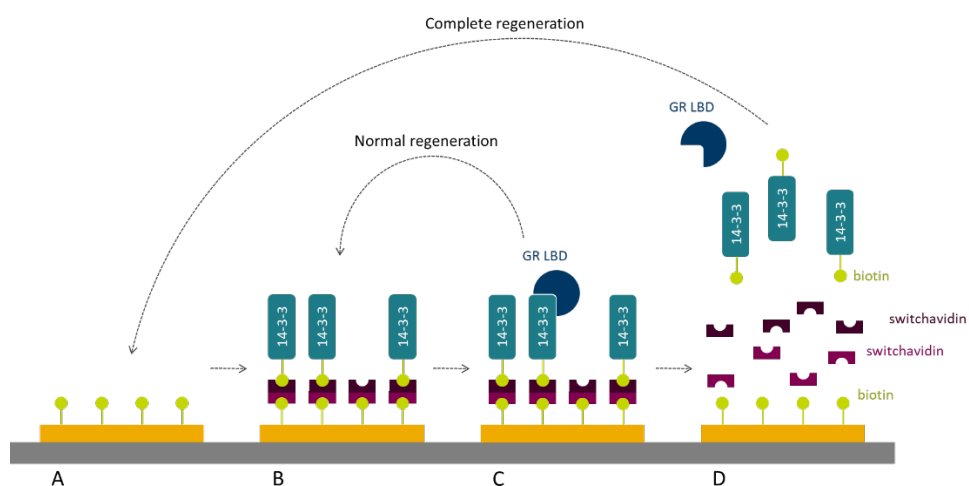
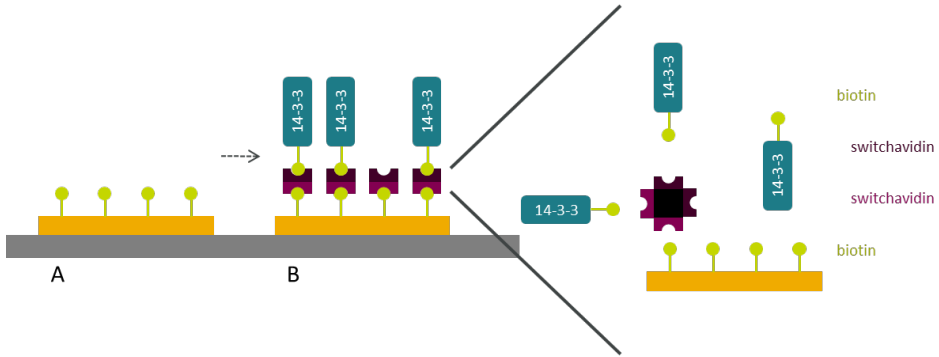


Figure 6.1. Reversible functionalization of the SPR sensorchip coated with biotin with biotinylated 14-3-3 and switchavidin. Immobilization on the SPR sensorchip coated with biotin (A) of the biotinylated 14-3-3 and switchavidin (B). SPR direct binding assay for determination of GR affinity (C). Normal regeneration can be performed with HBSP+ buffer (C to B) or complete regeneration of the chip surface can be done using a solution 5% citric acid, 0.5% SDS pH 1.8 (D to A).

A



B

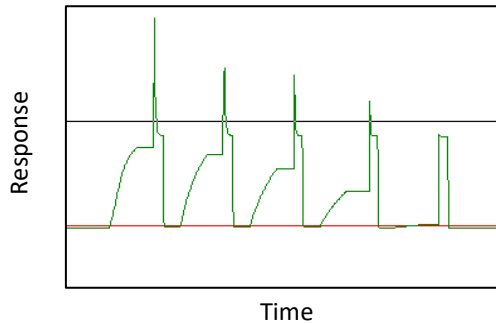


Figure 6.2. Determination of the best ratio biotinylated 14-3-3 ζ :switchavidin. (A) Avidin and the mutant switchavidin form a tetramer which can bind up to 4 biotins. If switchavidin binds 4 biotinylated 14-3-3 ζ , no binding with the biotin from the chip will be possible. If the amount of biotinylated 14-3-3 ζ is too low, not enough biotinylated 14-3-3 ζ will be bound to the chip to get a decent signal. Ideally, we would like to reach 3 biotinylated 14-3-3 ζ bound to switchavidin which can then bind to the biotin of the chip. (B) Injection of different ratios biotinylated 14-3-3 ζ :switchavidin (0:1, 1:1, 2:1, 3:1, 4:1, from left to right) with the same injection time followed by complete regeneration of the surface between each cycle. The black line is the maximum response which can be obtained (also called the capacity of the chip). The higher the ratio 14-3-3 ζ :switchavidin, the stronger the signal but this is not clearly visible on this graph because a much longer injection time than the one set in this assay is also required to reach steady state. The ratio 4:1 killed the immobilization of the complex because all the monomers of switchavidin are already bound to 14-3-3.

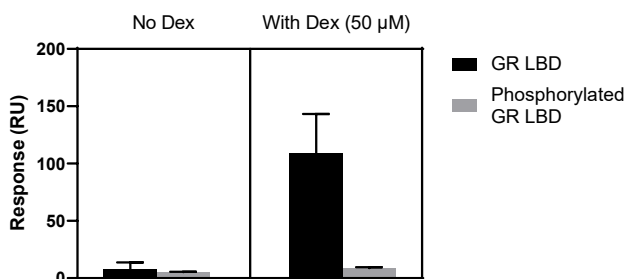


Figure 6.3. Assessment of the functionality of the GR LBD proteins. In the presence of dexamethasone (50 μM), a massive response of non-phosphorylated GR LBD (500 nM) indicates a binding with the immobilized peptide derived PRGC1 whereas no interaction between MINK1 phosphorylated GR LBD (500 nM) was detected with PRGC1 showing a denaturation of these proteins. Dex means dexamethasone. Measurements were performed as duplicate and the error bars represent the standard deviation of these two independent experiments.

6.3. Biological relevance of the GR–14-3-3 PPI

Previous studies have reported differential 14-3-3 regulatory activities on the biological role of GR, which might be explained by different experimental conditions, such as the 14-3-3 isoforms and the cell lines. 14-3-3 isoforms β, γ, ε, ζ, η and θ have been reported to positively regulate GR transcriptional activity to various extents in HepG2 cells³. 14-3-3η has been reported to up regulate GR activity in COS-7 cells⁴ which was further rationalized by a 14-3-3-mediated inhibition of GR proteolytic degradation⁵. 14-3-3ζ has been reported, however, to have a negative effect on GR transcriptional activity in U2OS cells, since GR activity was repressed by cellular stress and this was assigned to be through the p38 MAPK-mediated phosphorylation of S134, driving GR interaction with 14-3-3ζ⁶. 14-3-3σ has been reported to exhibit ambivalent effects on GR⁷. On one side, 14-3-3σ repress GR transcriptional activity by shifting GR localization to the cytoplasm and reducing the probability of GR to bind to GREs in HCT116 cells⁸. On the other side, 14-3-3σ increases GR transcriptional activity in HepG2 hepatocarcinoma cells³.

Determination of the biological relevance of the two 14-3-3 binding sites of GR identified in this work would be of great interest and would potentially enable a deeper understanding of the 14-3-3 regulation of GR. Further experiments could be envisioned. The stability of wt GR and the GR double mutant T524A S617A could be easily assessed by the quantification of GR proteins using Western blotting. The transcriptional activity of the two same GR constructs could be monitored by real-time reverse transcription polymerase chain reaction (RT-PCR) experiments. 14-3-3 has been

shown to up regulate glucose production by increasing GR mediated PEPCK and G6Pase expression³. Thus, the role of T524 and S617 in glucose production could be investigated, using the GR double mutant. I have developed an immunofluorescence assay to monitor GR translocation by microscopy. U2OS cells were transiently transfected with GR fused with the green fluorescent protein (GFP) and, in a first attempt, GR translocation was observed from the cytoplasm to the nucleus after a 4-hour treatment with dexamethasone, despite a poor transfection efficiency of GFP-GR using polyethylenimine (PEI) (Fig. 6.4). To increase the transfection efficiency in this cell line, different conditions were screened. The transfection reagent was either changed for lipofectamine 2,000 or X-tremeGENE, variation of the amount of GFP-GR DNA was investigated as well as the presence or the absence of antibiotics in the DMEM media (Fig. 6.5a). Optimization of the conditions increased the transfection efficiently from less than 5% to more than 60% using X-tremeGENE, 1 µg of GR DNA and media completed with 10% FBS, 1% glutamine and 1% Penicillin-Streptomycin (PS) (Fig. 6.5). U2OS cells transiently transfected with GFP-GR, using these conditions, were treated with dexamethasone for different times and after 30 min, GR could already be observed exclusively in the nucleus (Fig. 6.6). This assay which has been developed could be utilized to determine the role of T524 and S617 in the GR sub-cellular localization.

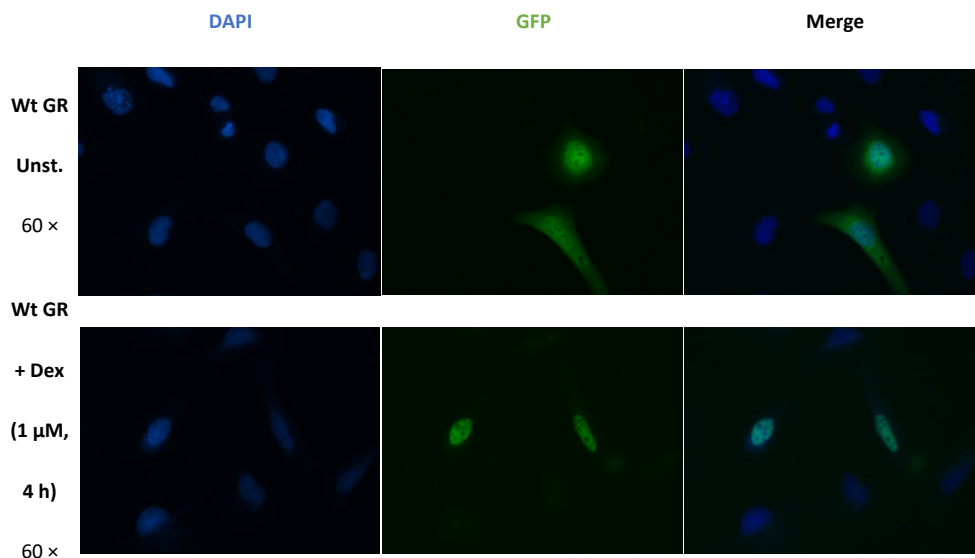


Figure 6.4. Immunofluorescence microscopy of U2OS cells transfected with wt GFP-GR. U2OS cells were transiently transfected with a solution of wt GR DNA (0.2 µg) and PEI (1 µL) in Opti-MEM (100 µL) per well in a 6-well cell culture plate. Cells were treated for 4 h then fixed without further staining. All images were captured on a Nikon Eclipse Ti widefield microscope using NIS-Elements (Nikon) software and analysed with ImageJ software. Unst means unstimulated and Dex dexamethasone.

A

Conditions #	1	2	3	4	5	6	7	8	9	10	11	12
Transfection Reagent	Lipo-fect.	Lipo-fect.	Lipo-fect.	Lipo-fect.	Lipo-fect.	Lipo-fect.	X-treme GENE	X-treme GENE	X-treme GENE	X-treme GENE	X-treme GENE	X-treme GENE
GR DNA (μ g)	0.5	0.5	1	1	2	2	0.5	0.5	1	1	2	2
Media	All	No PS	All	No PS	All	No PS	All	No PS	All	No PS	All	No PS
Transfection efficiency (%)	10	13	11	22	7	18	35	39	62	57	50	43

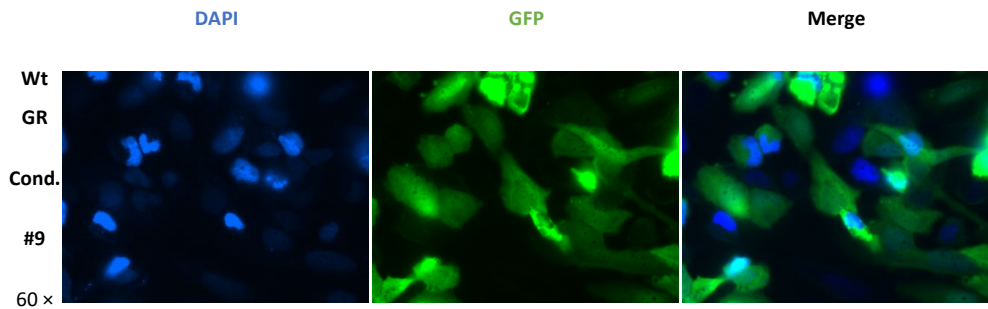
B


Figure 6.5. Optimization of the transfection efficiency of GFP-GR in U2OS cells. (A) U2OS cells were transiently transfected with GFP-GR DNA according to the conditions 1 to 12 per well in a 6-well cell culture plate. Cells were fixed without further staining. All images were captured on a Nikon Eclipse Ti widefield microscope using NIS-Elements (Nikon) software and analysed with ImageJ software. The transfection efficiency was calculated from the number of transfected cells and the total number of cells in 8 different images. The conditions, which gave the highest percentage of transfection, are highlighted in black. (B) Example of U2OS cells transfected according to conditions 9. Lipofect means lipofectamine 2,000 and all means complete media.

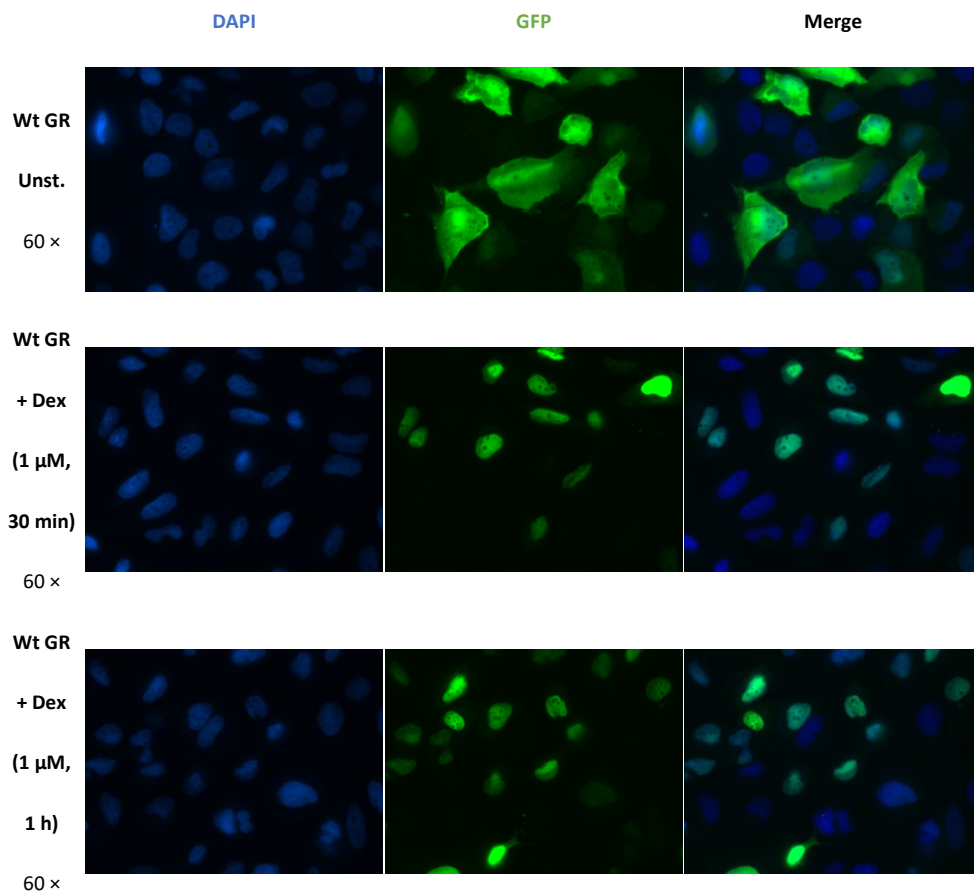


Figure 6.6. Translocation of GFP-GR to the nucleus upon dexamethasone treatment. A, U2OS cells were transiently transfected following conditions 9 in a 6-well cell culture plate. Cells were treated for different times (30 min, 1 h, 2 h and 4 h) then fixed without further staining. All images were captured on a Nikon Eclipse Ti widefield microscope using NIS-Elements (Nikon) software and analysed with ImageJ software. Only the results from 30 min and 1 h treatment are shown since similar observations were obtained at the longer time points. Unst means unstimulated and Dex dexamethasone.

6.4. Insight into 14-3-3 regulation of GR through the use of small molecule stabilisers

I have identified, through screening of AstraZeneca compounds and analogues of a known 14-3-3 PPI stabiliser, described in chapter 4 and 5, hit compounds which stabilise the interaction between a GR-derived phosphopeptide and 14-3-3 ζ . Through a hit to lead optimization, aided by the ability to obtain high-resolution X-ray crystal structures of the complexes, these compounds could be

developed into tool compounds and could then be used to further delineate the role of 14-3-3 in GR regulation. PPI modulation can be either through inhibition or stabilisation. Total inhibition of 14-3-3 proteins, however, is unlikely to be a viable therapeutic option because of the numerous 14-3-3 client proteins and would be expected to result in many unwanted effects. Selective inhibition of a 14-3-3 PPI also is expected to be challenging, because the 14-3-3 binding sites are often located within intrinsically disordered regions, thus lacking secondary structure⁹. Greater selectivity could potentially be achieved *via* identification of allosteric inhibitors of 14-3-3 complex formation. The discovery of 14-3-3 secondary pockets might indicate a possible means to achieve 14-3-3 PPI modulation beyond the 14-3-3 binding channel¹⁰. Allosteric drug discovery, however, has mostly been serendipitous and remains challenging despite the development of tools for more rational design¹¹. Stabilisation potentially offers a greater opportunity for selectivity. The FC binding pocket created at the interface of the 14-3-3–client protein upon interaction is made, by definition, partly by the 14-3-3 protein surface and partly by the surface of 14-3-3 binding partner. Hence optimization of the stabiliser with 14-3-3 will increase its potency whereas the optimization with the client protein will potentially increase its selectivity, similarly to FC-A which stabilises many 14-3-3 PPIs¹² but destabilises the GR–14-3-3 interaction due to a steric clash with P526. Chapter 5 reports on the identification of a pyrrolidone-based compound (**7.10**) which showed a gain in stabilisation of the GR–14-3-3 interaction in comparison to pyrrolidone1 (**7**). Comparison with other 14-3-3 PPIs, such as ER α and CaMKK2, highlighted the selectivity of **7.10** for GR. Co-crystallization of the ternary complex, including 14-3-3, GR peptide and **7.10**, gave structural insights explaining the molecular basis for the increased potency. Introduction of a chlorine substituent on the 2-position of the benzo ketone provided extra contact surface of **7.10** with 14-3-3 and GR by filling the empty cavity at the GR–14-3-3 interface and making hydrophobic contacts. Additionally, to a potentially greater selectivity, PPI stabilisation might be an opportunity to develop compounds with a lower binding affinity than for PPI inhibition. By the non-competitive nature of the stabilisers, its affinity is, theoretically, not required to be in the low nanomolar range. The small molecule **1**, identified in chapter 4, and the compound **7.10**, reported in chapter 5, stabilised the GR–14-3-3 interaction by 2- and 4-fold at 200 μ M and 100 μ M respectively. These compounds could already give an insight into 14-3-3 regulation of GR such as 14-3-3 mediated GR stability, GR transcriptional activity and GR translocation using the optimized immunofluorescent assay described previously in this chapter. Caco-2 assay showed that **1** is cell permeable (with an apparent intrinsic permeability from A to B of 30.8×10^{-6} cm/s), however **7.10** was poorly cell permeable ($P_{app}(A \text{ to } B)=0.103 \times 10^{-6}$ cm/s). The difference between the apparent intrinsic

permeability and efflux values probably represents both poorer intrinsic permeability of **7.10** and that **7.10** is a substrate for efflux transporters ($P_{app}(B \text{ to } A)=10.5$ and 2.95×10^{-6} cm/s for **1** and **7** respectively). This could affect the uptake of **7.10** in cells, but this is unlikely to be an issue for in vitro assays.

6.5. Modulation of GR activity in drug discovery for the regulation of inflammation

Glucocorticoids (GCs) are widely used in the clinic for their anti-inflammatory and immunosuppressive effects. Their actions are mediated by GR which, upon binding with GCs, dissociates from its inhibitory complex, changes its conformation resulting in the exposure of nuclear localization signals leading to translocation to the nucleus where GR binds DNA and regulates the expression of target genes¹³. Cortisone and hydrocortisone are endogenous GCs that are also made synthetically and used as medicines other synthetic GCs include, for example, dexamethasone and prednisolone. They differ in pharmacokinetics and pharmacodynamics. GCs are indicated for short- and long-term treatment including inflammatory skin diseases such as atopic dermatitis, and seasonal allergic rhinitis as well asthma and rheumatoid arthritis¹⁴. GR affects the transcription of numerous genes and because GCs activate all GR activities, they are associated with a large range of effects both desirable and undesirable. GCs side effects range from glaucoma, infection, cardiovascular conditions, diabetes, osteoporosis, oedema to psychiatric and neurologic diseases¹⁵. Wherever possible, GCs are, therefore, applied topically to minimize the undesirable systemic effects, for example through inhalation to the lung and the use of creams and sprays to the skin. A second drawback of the use of GCs in clinic is the GCs resistance which can be genetic though mutation of the GR encoding gene or acquired due to long-term GC treatment. Notably, GCs have been shown to downregulate the level of GR proteins through proteasomal degradation, impairing GR activity¹⁶.

To overcome these limitations, the dual role of GR in immune gene regulation has been under investigation and it is becoming evident that GR, though the activity of GCs, possesses an anti- and pro-inflammatory role by transactivation and transrepression of specific genes^{14,17}. The use of transgenic mice, with a mutation in the DNA binding domain of GR preventing the receptor dimerization, showed reduced GR transactivation while retaining transrepression activities, in other words the down-regulation of other transcription factors. The transrepression of gene expression was thought to be sufficient to reduce inflammation while preventing side effects and a novel class of therapeutic agents known as selective glucocorticoid receptor agonists and modulators (SEGRAMs) was developed^{15,18}. Further research, however, has proposed that not all the therapeutic effects were a result of GR transrepression whilst not all the side effects were consequences of GR transactivation,

refining this pharmacological concept^{18,19}. GR dimerization was found to be required in the treatment of acute inflammatory disorders and life-threatening inflammatory conditions whilst GR monomers, which have been reported to be more suitable for long-term GC therapy including the treatment of chronic inflammatory conditions reducing important side effects, notably hyperglycemia^{14,15,19}. As a consequence, selective dimer GR agonists and modulators (SEDIGRAMs)^{19,20} and selective monomer GR agonists and modulators (SEMOGRAMs) have been designed¹⁹.

Other avenues of research have emerged. For example, cell-specific drug delivery uses antibody-GC conjugates²¹, peptide-GC conjugates²² and GCs encapsulated in liposomes²³ to reduce systemic adverse effects. Combination therapies such as the simultaneous activation of GR and PPAR γ using appropriate agonists, have been shown to counteract known CG side effects in mice^{24,25}. GR is part of a large network and interacts with many other protein partners which refine GR activity²⁶. Targeting these PPIs would provide a strategy for a GR regulation beyond direct ligand binding and would potentially overcome the inherent challenges linked to the drug discovery for GR. GR cofactors have been investigated as a plausible therapeutic target such as FKBP5, part of the inhibitory complex bound to GR in the cytoplasm, for the prevention and treatment of stress-related psychiatric disorders²⁷. Stabilisation of the GR–14-3-3 PPI could play an important role in this approach. Further experiments are necessary to fully understand the role of the 14-3-3 binding sites of GR, identified in this work, and the action of MINK1 of GR regulation, using for example, MINK1 inhibitors. In addition, co-crystallization of the hits found by screening will rationalize their stabilising activity and will provide a starting point for structure-based design.

6.6. Conclusion

GR is a ligand dependant transcription factor and plays a crucial role in inflammation. As part of a large interactome, GR interacts with many protein partners which further regulate its transcriptional activity. 14-3-3 has been shown to interact with GR and, through a comprehensive study of the role of GR phosphosites and using a bottom-up approach from GR 13-mer peptides to confirmation in a cell system, two 14-3-3 binding sites of GR were identified as well as their associated kinases. Screening of AstraZeneca compounds and analogues of a known 14-3-3 PPI stabiliser led to the identification of hits which stabilised of the GR–14-3-3 interaction. Extensive biophysical studies, including X-ray co-crystallography and protein NMR spectroscopy, provided an insight into the molecular details of the interaction. Analysis of structurally related compounds enabled us to identify principles for SAR and selectivity. Further experiments would be of a great interest moving forwards, such as the quantitative characterisation of the GR–14-3-3 PPI using the already developed SPR assay

and the investigation of the biological relevance of this interaction. In particular, the study of the role of 14-3-3 on GR translocation by immunofluorescence microscopy. Stabilisation of 14-3-3 PPIs provides a considerable opportunity in drug discovery through a potentially greater selectivity. In addition, the stabiliser needs to be present at a concentration sufficient to be bound to the target and at such a concentration an effective amount of the target is engaged, but, by its nature, it does not have to compete with other endogenous ligands. Modulation of GR activity in drug discovery principally relies on GR agonists which are associated with many side effects. The development of the identified hits into tool compounds would contribute to unravelling some long-standing questions on the 14-3-3 regulation of GR and potentially pave the way for a new therapeutic approach in the treatment of inflammation.

6.7. Acknowledgements

The author thanks Dr. Matthew W.D. Perry for conceiving and directing the project, Dr. Christian Ottmann for his strategic guidance, Dr. Anders Gunnarsson for his support with the biophysical experiments and Marianna Longo and Dr. Carol Mackintosh for their assistance in cell-based assays and with immunofluorescence microscopy. The author thanks Dr. Werngard Czechtizky for generous support of the project.

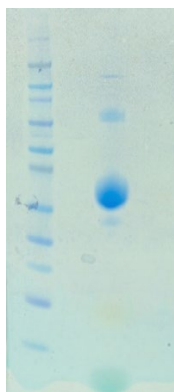
6.8. Materials and methods

Biotinylation of 14-3-3ζ

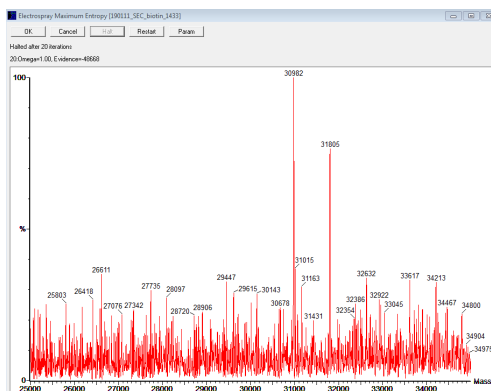
14-3-3ζ (0.14 μmol, 50 μL) was diluted in HBS P+ (350 μL) and NHS-PEG12 biotin (0.14 μmol, 6 μL) was added. The reaction mixture was gently shaken at room temperature for 2 h. Biotinylated 14-3-3ζ proteins were purified by size exclusion chromatography.

A, Purity of Biotinylated 14-3-3ζ proteins: 90% according to SDS-PAGE. **B**, Mass calculated for 14-3-3ζ, 30.99 kDa; found 30.98 kDa and for biotinylated 14-3-3ζ, 31.81 kDa; found 31.81 kDa.

A



B



Surface plasmon resonance (SPR) assays with GR LBD

SPR binding assays were performed using a Biacore 3000 (GE Healthcare) instrument. Biotinylated 14-3-3 proteins or biotinylated PRGC1 peptides (300 nM) (peptide sequence: Biotin-GSGSGSPQEAEEPSLLKLLAPANT) with switchavidin (100 nM) were immobilized on an SPR sensorchip BD500M (coating 500nm biotin, immobilized in a carboxymethyl dextran hydrogel, medium density, use: immobilization of streptavidin conjugates, Xantec Bioanalytics) at 2000 RU, flow 10 μ /min, injection volume 10 μ L according to the manufacturer's instructions. A 96-well V-shaped polypropylene microtiter plate was prepared with (un)phosphorylated GR LBD diluted to 500 nM either in HBS P+ buffer supplemented with dexamethasone (50 μ M) or HBS P+ buffer. The protein samples were injected using the HBSP+ buffer at a continuous flow rate of 20 μ L/min for 1 min onto the immobilized 14-3-3 chip followed by a wash for 2.5 min prior to the next injection. The regeneration of the surface was performed with a solution of 5% citric acid and 0.5% SDS pH 1.8 (10 μ L). The figures were made using the software GraphPad Prism 8. Errors are standard error of the fit.

Immunofluorescence microscopy

U2OS cell lines (ATCC) were cultured in DMEM medium, supplemented with 10% foetal bovine serum and 1% penicillin-streptomycin (10,000 U/mL) at 37 $^{\circ}$ C in a 5% CO₂ environment. Cells were seeded in a 10 cm cell culture dish. At 60–70% confluence, the U2OS cells were transiently transfected with a mixture GFP-GR DNA (4 μ g) and X-tremeGENE (16 μ L) in Opti-MEM (1 mL) for 24 h. Cells were dissociated using trypsin (2 mL) completed with supplemented DMEM (8 mL). In a 6-well cell culture plate, 1 mL of the solution was added per well containing a cover slip and completed with supplemented DMEM (1 mL). The plate was incubated for 24 h.

Cells were treated with dexamethasone (1 μ M) or EtOH as control for 30 min, 1 h, 2 h or 4 h. Cells were washed with PBS (2 \times), fixed with 3.7% formaldehyde for 20 min and the reaction was quenched with DMEM for 10 min. Cells were washed with PBS then distilled water and placed on a glass slide with a drop of mounting solution (Pro long gold anti fade reagent with DAPI). Glass slides were dried in the dark overnight. All images were captured

on a Nikon Eclipse Ti widefield microscope with the lens 60 × using NIS-Elements (Nikon) software and analysed with ImageJ software.

6.9. References

1. Fu, Y., Ji, J. & Bi, Q. Regenerative biosensor chips based on switchable mutants of avidin—A systematic study. *J. Tribol.* **134**, 011701 (2012).
2. Liu, X., Wang, Y. & Ortlund, E. A. First high-resolution crystal structures of the glucocorticoid receptor ligand-binding domain–peroxisome proliferator-activated γ coactivator 1- α complex with endogenous and synthetic glucocorticoids. *Mol. Pharmacol.* **96**, 408–417 (2019).
3. Hwang, Y., An, H. T., Kang, M. & Ko, J. Roles of 14-3-3 β and γ in regulation of the glucocorticoid receptor transcriptional activation and hepatic gluconeogenesis. *Biochem. Biophys. Res. Commun.* **501**, 800–806 (2018).
4. Wakui, H., Wright, A. P. H., Gustafsson, J. & Zilliacus, J. Interaction of the Ligand-activated Glucocorticoid Receptor with the 14-3-3 η Protein. *J. Biol. Chem.* **272**, 8153–8156 (1997).
5. Kim, Y. S. *et al.* Role of 14-3-3 η as a Positive Regulator of the Glucocorticoid Receptor Transcriptional Activation. *Endocrinology* **146**, 3133–3140 (2005).
6. Galliher-Beckley, A. J., Williams, J. G. & Cidlowski, J. A. Ligand-Independent Phosphorylation of the Glucocorticoid Receptor Integrates Cellular Stress Pathways with Nuclear Receptor Signaling. *Mol. Cell. Biol.* **31**, 4663–4675 (2011).
7. Habib, T. *et al.* AKT1 has dual actions on the glucocorticoid receptor by cooperating with 14-3-3. *Mol. Cell. Endocrinol.* **439**, 431–443 (2017).
8. Kino, T. *et al.* Protein 14-3-3 σ Interacts With and Favors Cytoplasmic Subcellular Localization of the Glucocorticoid Receptor, Acting as a Negative Regulator of the Glucocorticoid Signaling Pathway. *J. Biol. Chem.* **278**, 25651–25656 (2003).
9. Sluchanko, N. N. & Bustos, D. M. Intrinsic disorder associated with 14-3-3 proteins and their partners. in *Progress in Molecular Biology and Translational Science* **166**, 19–61 (Elsevier Inc., Cambridge, 2019).
10. Sijbesma, E. *et al.* Identification of Two Secondary Ligand Binding Sites in 14-3-3 Proteins Using Fragment Screening. *Biochemistry* **56**, 3972–3982 (2017).
11. Lu, S., He, X., Ni, D. & Zhang, J. Allosteric Modulator Discovery: From Serendipity to Structure-Based Design. *J. Med. Chem.* **62**, 6405–6421 (2019).
12. Ballone, A., Centorrino, F. & Ottmann, C. 14-3-3: A Case Study in PPI Modulation. *Molecules* **23**, 1–14 (2018).

13. Kino, T. GR-regulating Serine/Threonine Kinases: New Physiologic and Pathologic Implications. *Trends Endocrinol. Metab.* **29**, 260–270 (2018).
14. Desmet, S. J. & De Bosscher, K. Glucocorticoid receptors: Finding the middle ground. *J. Clin. Invest.* **127**, 1136–1145 (2017).
15. Timmermans, S., Souffriau, J. & Libert, C. A general introduction to glucocorticoid biology. *Front. Immunol.* **10**, (2019).
16. Wallace, A. D., Cao, Y., Chandramouleeswaran, S. & Cidlowski, J. A. Lysine 419 Targets Human Glucocorticoid Receptor for Proteasomal Degradation. *Steroids* **75**, 1016–1023 (2010).
17. Scheschowitsch, K., Leite, J. A. & Assreuy, J. New insights in glucocorticoid receptor signaling-more than just a ligand-binding receptor. *Frontiers in Endocrinology* **8**, 16 (2017).
18. Sundahl, N., Bridelance, J., Libert, C., De Bosscher, K. & Beck, I. M. Selective glucocorticoid receptor modulation: New directions with non-steroidal scaffolds. *Pharmacol. Ther.* **152**, 28–41 (2015).
19. De Bosscher, K., Beck, I. M., Ratman, D., Berghe, W. Vanden & Libert, C. Activation of the Glucocorticoid Receptor in Acute Inflammation: The SEDIGRAM Concept. *Trends Pharmacol. Sci.* **37**, 4–16 (2016).
20. Souffriau, J. *et al.* A screening assay for Selective Dimerizing Glucocorticoid Receptor Agonists and Modulators (SEDIGRAM) that are effective against acute inflammation. *Sci. Rep.* **8**, 12894 (2018).
21. Thomsen, K. L. *et al.* Anti-CD163-dexamethasone conjugate inhibits the acute phase response to lipopolysaccharide in rats. *World J. Hepatol.* **8**, 726–730 (2016).
22. Sangar, M. L. C. *et al.* A potent peptide-steroid conjugate accumulates in cartilage and reverses arthritis without evidence of systemic corticosteroid exposure. *Sci. Transl. Med.* **12**, (2020).
23. Metselaar, J. M., Wauben, M. H. M., Wagenaar-Hilbers, J. P. A., Boerman, O. C. & Storm, G. Complete remission of experimental arthritis by joint targeting of glucocorticoids with long-circulating liposomes. *Arthritis Rheum.* **48**, 2059–2066 (2003).
24. Deckers, J. *et al.* Co-Activation of Glucocorticoid Receptor and Peroxisome Proliferator-Activated Receptor- γ in Murine Skin Prevents Worsening of Atopic March. *J. Invest. Dermatol.* **138**, 1360–1370 (2018).
25. Bougarne, N. *et al.* PPAR α blocks glucocorticoid receptor α -mediated transactivation but cooperates with the activated glucocorticoid receptor α for transrepression on NF- κ B. *Proc.*

- Natl. Acad. Sci. U. S. A.* **106**, 7397–7402 (2009).
26. Petta, I. *et al.* The Interactome of the Glucocorticoid Receptor and Its Influence on the Actions of Glucocorticoids in Combatting Inflammatory and Infectious Diseases. *Microbiol. Mol. Biol. Rev.* **80**, 495–522 (2016).
27. Binder, E. B. The role of FKBP5, a co-chaperone of the glucocorticoid receptor in the pathogenesis and therapy of affective and anxiety disorders. *Psychoneuroendocrinology* **34**, 186–195 (2009).

Summary

Small Molecule Stabilisation of the Glucocorticoid Receptor and 14-3-3 Protein-Protein Interaction

Classically drug targets have been single proteins, e.g. enzymes or GPCRs. In the search for new targets, however, it is necessary to go beyond these established groups and look into other opportunities. With an estimated 650,000 protein-protein interactions (PPI) in human cells, the ability to modulate these interactions potentially significantly enlarges the “drugable genome”. 14-3-3 proteins are a family of seven highly conserved regulatory proteins and have been reported to interact with the glucocorticoid receptor (GR), a nuclear receptor which functions as a ligand dependent transcription factor, and modulate its activity. Different reports, however, have ascribed both positive and negative regulatory roles to GR/14-3-3 interactions. Given the importance of GR agonists in medicine it is of great interest to understand the role(s) of these interactions and to study their modulation.

Chapter 1 describes the role of 14-3-3 in the inflammatory response. 14-3-3 proteins are placed at the centre of a signalling hub, interacting with many protein partners involved in the regulation of inflammation and playing a role at all levels of the immune response. 14-3-3s modulate the transcriptional activity by binding to transcription factors such as NF- κ B, JAK-STAT, PPAR and GR. 14-3-3s modulate the signal transduction through the recognition of receptors such as TLRs, RLRs and pyrin, and PARs. 14-3-3s were found to be part of the regulation of immune cells such as T cell, B cell, macrophages and neutrophils. Most importantly, aberrant 14-3-3 protein expression has been associated with chronic inflammatory disorders including autoimmune and respiratory diseases, highlighting 14-3-3 as a potential, yet not realized, opportunity to identify possible targets for future therapeutic intervention in inflammatory related disorders.

In chapter 2, the interaction between GR and 14-3-3 has been investigated. 14-3-3 proteins recognise phosphorylated serine and threonine residues. A prediction web server was used to identify potential 14-3-3 binding sites of GR. 13-mer phosphopeptides centred on the identified residues were synthesized both with N-terminal acetylation and with an FITC label. The binding affinity of these peptides with 14-3-3 was measured by surface plasmon resonance (SPR) and fluorescence

polarization (FP) respectively. Two peptides with K_d in the low μM range were identified; both belong to the GR ligand binding domain (LBD); these were centred on T524 and S617. Other GR phosphosites have been reported in the literature. 13-mer peptides centred on these experimentally identified phosphosites were synthesized, however, only one of them exhibited measurable interaction with 14-3-3. This reinforces the value of the prediction method used to identify potential 14-3-3 binding sites. 14-3-3 acts as a dimer and can potentially bind two phosphorylated residues. A dimeric peptide consisting of the two previously identified 13-mers linked by a pentaglycine moiety was synthesized. This peptide exhibited greatly enhanced binding affinity to 14-3-3 with K_d 18 – 30 nM (assay dependent). Both 13-mer peptides and the 31mer dimeric peptide were co-crystallized with 14-3-3 and their structures were determined by X-ray analysis. Additionally, an alanine scan of the 31-mer peptide was performed to identify the most significant residues for the interaction with 14-3-3.

Chapter 3 described the study of the interaction between 14-3-3 and longer GR constructs. Two different options were investigated. First, a chemical posttranslational modification of GR LBD was envisioned by site selectively synthesising a chemical analogue of phosphorylated T524 and S617. The two-step reaction was optimized on a 13-mer GR peptide. This peptide showed similar binding with 14-3-3 as the corresponding phosphopeptide. Looking forward, this approach could be applied to GR LBD. The second strategy relied on a kinase screen on GR LBD; MINK1 and ROCK1 were shown to phosphorylate the two residues identified previously. GR LBD phosphorylated by MINK1 was shown to interact with 14-3-3 by far-Western blotting overlay assay. The significance of T524, S617 and the role of MINK1 were investigated further in cellular systems. Comparison of wild-type GR and a double mutant T524A S617A showed that the mutant exhibits a weaker interaction between 14-3-3 and GR after stimulation of the cells by calyculin A than is seen with wild-type. In addition, wild-type GR exhibits a stronger interaction with 14-3-3 when cells are co-transfected with MINK1 and upon stimulation by calyculin A. This work highlights both MINK1 and the GR–14-3-3 axis as potential targets for future therapeutic intervention.

Stabilisation of the GR–14-3-3 interaction, using the previously identified phosphopeptide as a surrogate for GR, was investigated in chapter 4. About 8,000 AstraZeneca compounds were screened by FP followed by a counter screen using SPR. Hits that showed stabilisation were further investigated by 1D and 2D nuclear magnetic resonance spectroscopy and thermal shift assay. In addition, near neighbours of each hit were identified and the binding affinity of a representative subset was tested with 14-3-3 with the aim to observe a structure-activity relationship. Finally, six compounds were confirmed as stabilisers. These hits could be used as starting points to discover tool

compounds for use in future cell assays to investigate the opportunity to modulate biological processes through stabilisation of a PPI.

In chapter 5, the stabilisation of the GR–14-3-3 interaction, using the previously identified phosphopeptide, was further investigated through screening of analogues of known 14-3-3 PPI stabilisers such as pyrrolidone1. One analogue of pyrrolidone1, with a chlorine substituent on the 2-position of the benzo ketone, showed 4-fold stabilisation of the GR peptide–14-3-3 interaction at 100 μ M and its binding mode has been rationalized by co-crystallization with 14-3-3 and the 13-mer GR peptide centred on T524. Together this data highlights preliminary structural principles towards the achievement of target selectivity and provides a novel strategy to modulate GR activity beyond ligand binding and to overcome the inherent challenges linked to the drug discovery for GR.

Chapter 6 further expands on the concept of modulation of GR activity beyond ligand binding. First, this chapter focusses on the future experiments which could be performed to broaden the work reported in this thesis. An SPR assay was developed to quantitatively characterise the GR–14-3-3 PPI as well as an immunofluorescence assay using microscopy to investigate the biological relevance of the 14-3-3 binding sites of GR, the kinase MINK1 and the stabilisers identified in the previous chapter. Briefly reviewing the PPI stabilisation approach and the therapeutic strategies developed to target GR highlighted an opportunity for modulation of GR activity through PPI stabilisation which potentially provide a new therapeutic approach in the treatment of inflammation.

List of publications

C.C. Munier, L. De Maria, K. Edman, A. Gunnarsson, M. Longo, C. Mackintosh, A. Snijder, L. Wissler, L. Brunsveld, C. Ottmann and M.W.D. Perry. 14-3-3 Regulation of Glucocorticoid Receptor via Protein-Protein Interaction Induced by MINK1 Phosphorylation, manuscript submitted to the Journal of Biological Chemistry.

C.C. Munier, C. Ottmann and M. Perry. 14-3-3 Modulation of the Inflammatory Response, review submitted to Pharmacological Research.

C.C. Munier*, F. Bosica*, S. Andrei, K. Edman, A. Gunnarsson, L. Wissler, C. Ottmann, M.W.D. Perry and G. O'Mahony. Small molecule stabilisation of 14-3-3 protein-protein interactions: a prospective insight in structure activity relationship and selectivity, *manuscript in preparation*, aiming at Communications Chemistry.

* Contributed equally to this work

C.C. Munier, F. Edfeldt, A. Gunnarsson, I. Landrieu, J. Neves, C. Ottmann and M.W.D. Perry. Identification of Small Molecule Stabilisers of the Glucocorticoid Receptor 14-3-3 Protein-Protein Interaction, *manuscript in preparation*, aiming at ACS Medicinal Chemistry Letters.

L. Iralde-Lorente, G. Tassone, L. Clementi, L. Franci, C.C. Munier, Y. Cau, M. Mori, M. Chiariello, A. Angelucci, M.W.D. Perry, C. Pozzi, S. Mangani and M. Botta. Identification of Phosphate-Containing Compounds as New Inhibitors of 14-3-3/c-Abl Protein-Protein Interaction. *ACS Chem Biol.* **15**, 1026–1035 (2020). <https://doi.org/10.1021/acscchembio.0c00039>.

Curriculum Vitae



Claire Munier was born on June 14th, 1991, in Mont Saint Aignan, France. In 2010 she enrolled to « Classes Préparatoires », a 2-year full time higher education in mathematics, physics and chemistry, at Lycée Descartes, Tours, France. In 2012 she successfully passed the competitive exams to enter at CPE, an engineer school in Chemistry, Physics and Electronic, Lyon, France. At CPE, she studied organic chemistry, analytical chemistry, biochemistry, process engineering and she specialized in organic chemistry by simultaneously following the master program “Organic Synthesis and Chemistry of Biologically Active Molecules” at the University of Lyon, France. In 2014 she performed a 12-month industrial placement at Boehringer Ingelheim, Biberach, Germany, where she synthesized small molecules in a parallel fashion within a CombiChem group, working on two LO projects targeting COPD and liver fibrosis. Notably, she synthesized two compounds which were selected for in-depth preclinical profiling. In 2016 she performed a 6-month industrial placement at Roche, Basel, Switzerland, where she designed and synthesized small molecules with antimicrobial activity, working on a LI project with a special focus on phys-chem property optimization and in particular on solubility enhancement. In 2016 she obtained her master’s degree in chemistry and a double degree in organic chemistry, both first class honours. She started her PhD project in the MedChem department of Early Respiratory & Immunology (R&I) at AstraZeneca, Gothenburg, Sweden, and within the Marie Curie Network TASPPI (TARgeted Small-molecule Stabilisation of Protein-Protein Interaction). She was under the supervision of Dr. Matthew Perry (AstraZeneca, Sweden) and Dr. Christian Ottmann (Eindhoven University of Technology, Netherlands). Her research focused on the small molecule stabilisation of the Glucocorticoid Receptor (GR) 14-3-3 Protein-Protein Interaction. During her PhD, she notably performed a 3-month secondment in the academic group of Prof. Ian Ganley at School of Life Sciences, University of Dundee, UK where she developed cell-based experiments to investigate the biological relevance of potential 14-3-3 binding sites of GR and newly identified stabilisers. In 2020 she finished her doctorate studies of which the most important results are presented in this thesis.

Acknowledgement

My PhD project has given me the fantastic opportunity to work across multiple disciplines and to collaborate extensively with scientists from AstraZeneca, Eindhoven University of Technology, the School of Life Sciences at the University of Dundee and within the TASPPI consortium. I feel honoured and proud to have been surrounded by many great colleagues but also friends and family over the last four years and I would like to deeply thank them for their help and their support.

First, I would like to thank my industrial supervisor Dr. Matthew Perry for offering me a PhD position within the R&I MedChem Department at AstraZeneca, Sweden. Thank you Matthew for your efficient supervision and support, helping me to succeed in my PhD project. I have been particularly impressed by your passion, your dedication and your strong desire to pass on your expertise covering the entire early drug discovery process. Thank you for your trust, your encouragement and your optimism at all-time. Working alongside you enabled me to grow as a scientist and as an individual.

I would like to deeply thank my academic supervisor Dr. Christian Ottmann for the continuous support and stimulating guidance. Your vibrant passion for 14-3-3 PPI modulators and your energy have inspired me throughout my entire PhD project. Thank you Christian for offering me the chance to spend the last 6 months of my PhD in your excellent research group at Eindhoven University of Technology. I truly admire the fantastic environment for young researchers you have created around you.

To Prof. Luc Brunsveld, thank you for welcoming me in your Chemical Biology group at Eindhoven University of Technology and for your fruitful discussions and suggestions concerning my project.

I would like to thank Dr. Kurt Amrein, Prof. Patricia Dankers, Prof. Onno Meijer and Prof. Wilbert Zwart, for critically reading my thesis and being part of my defence committee.

During my PhD, I got the chance to work alongside amazing and genuinely talented AstraZeneca scientists from multiple departments who greatly help me to drive this project to a successful conclusion. I would like to thank you all for taking the time to share your knowledge and to answer all the questions I could have. It has been an immense pleasure to collaborate with all of you and you are part of the reason why I was so exciting going to work every morning. In particular, I would like to say a big thank you to the New Modality team from CVRM for training me on the state-of-the-art peptide chemistry: Dr. Johan Broddefalk, Dr. Ahlke Hayen, Dr. Maria Ölwegård-Halvarsson

and most importantly Dr. Anais Noisier. It was always with the same excitement that I came to KK2 to talk about projects or life. Many thanks to the Separation Science Laboratory team from Pharmaceutical Sciences for training me on peptide purification: Dr. Anna-Carin Carlsson, Dr. Linda Thunberg and Ms. Annika Langborg Weinmann. I feel lucky to have worked in such a friendly atmosphere. Many thanks to Dr. Euan Gordon for your assistance in ordering the right plasmids and a special thank you to Dr. Arjan Snijder for your great support in protein expression and purification, your never-ending patience and your continuously good humour. I would like to thank the Structure & Biophysics team from Discovery Sciences and particularly Dr. Anders Gunnarsson for sharing with me your impressive expertise on SPR. Working with you in the lab has always been so much fun! Many thanks to Dr. Stefan Geschwindner and Rosy Har for your help with TSA and to Dr. Fredrik Edfeldt for your support with the NMR binding assays. Big thank you to Lisa Wissler who has been a fantastic teacher in protein crystallization! I also would like to thank the crystallographers Dr. Patrik Johansson, Dr. Jens Petersen, Dr. Jenny Sandmark, and especially Dr. Karl Edman. Thank you Karl for teaching everything related to molecular replacement, refinement and manual rebuilding and using a Linux interface! I have struggled many times with the Linux commands, but you have always been here to help despite your fully booked outlook calendar. I would like to say a big thank you to Dr. Leonardo De Maria for your modelling and scoring studies on GR peptides, Dr. Anna Hoyle for your help with peptide mapping, Dr. Fredrik Wågberg for your valuable advice about HTS, Silvio Di Castro and Tommy Thorsell for your help with ordering compounds from the AstraZeneca library and Dr. Richard Lewis for the VCD experiments on the para-chloro compound. To Dr. Stefan Vollmer and Dr. Sofia Winslow, I would like to deeply thank you for your assistance in cell-based assays and to Josefina Edsbagge, thank you for writing the MTAs for the external collaborations.

I would like to thank Prof. Carol MacKintosh and Prof. Ian Ganley for welcoming me in their lab at the School of Life Sciences at the University of Dundee. A big thank you to Marianna for being such a great buddy and teaching me everything I know about cell culture, Western blotting and IF. I also would like to thank all the members of Dr. Ian Ganley's group for the discussions and the great working environment but also for the drinks, the dinners, the retreat and the Christmas party: Marianna Longo, Lambert Montava Garriga, Alice Nardin, Francois Singh, Christina Vrahnas, Lea Wilhelm, Maria Zachari, Jin-Feng Zhao.

It has been a pleasure to collaborate with Dr. Isabelle Landrieu and Dr. Joao Neves from the CNRS in Lille, France. Thank you for performing the protein NMR experiments. Many thanks as well to the PhD students of the TASPPi consortium: Blaz Andlovic, Alice Ballone, Francesco Bosica, Federica Centorrino, Leire Iralde Lorrente, Dominico Lentini Santo, Marianna Longo, Joao Neves, Lorenzo Soini,

Sonja Srdanov, Dario Valenti, Madita Wolter, and their PIs: Prof. Maurizio Botta, Dr. Jeremy Davis, Dr. Jan Eickhoff, Dr. Thorsten Genski, Dr. Isabelle Landrieu, Prof. Carol MacKintosh, Dr. Gavin O'Mahony, Prof. Tomáš Obšil, Dr. Christian Ottmann, Prof. Andrew Wilson. Thank you for your fruitful discussions and strong support. I was always very much looking forward to meeting you at our TASPPI meetings across Europe.

I would like to thank the old-members and members of the team I was part of at AZ: Dr. Stefan von Berg, Susanne Berglund, Jesper Malmberg, Dr. Beatrice Ranieri, Dr. Tove Slagbrand, Victoria Ullah, and my former line manager and line manager: Dr. Magnus Nilsson and Annika Wellner. Thank you for our discussions about chemistry and life, your insightful advice to discover Sweden and most importantly for the great fun, jokes and laughs! I also would like to deeply thank the former R&I MedChem department head and the R&I MedChem department head: Dr. Peter Sjö and Dr. Werngard Czechtizky for generous support of the project.

A big thank you to all the students, postdocs, graduates I met at AZ and the scientists from the KK building. Many of you became true friends and thanks to all of you I fell in Sweden at home.

A special thanks to Anais, my big sister in Sweden. Thank you for your constant support, your numerous advice, our never-ending conversations about everything and for feeding me with frozen food from Picard. Be sure that I am going to use this bedroom you keep for me in your house!

I would like to thank my landlords Angelica, David and their kids Neo, Melvin and Ludwig. Thank you for offering me to stay in your converted garage during these last four years 😊. Thank you for introducing me to the Swedish culture and mostly, thank you for considering me as one of your family members. Please keep calling me "Hello" I love this nickname.

Finally, I would not have enough words to thank my family for your unconditional and loving support. Mamounette, papounet, bubu, fort loup and Nocky, je n'aurais littéralement pas pu finir cette thèse sans vous. Maman, merci de m'avoir toujours écoutée et de toujours trouver les bons mots pour me remotiver. Merci pour les petits colis remplis de nourriture et de vêtements, je les ai ouverts à chaque fois avec tellement d'excitation ! Merci papa pour tes séances de motivation et tes conseils toujours justes. Tu es vraiment un mentor pour moi ! Merci Bubu tu es bien plus que ma sœur, tu es ma confidente, ma « Partner in crime » et ma meilleure amie pour la vie. Juju, merci d'avoir été tellement patient, je suis d'accord 4 ans c'est long. J'ai hâte de te retrouver. Je t'aime.